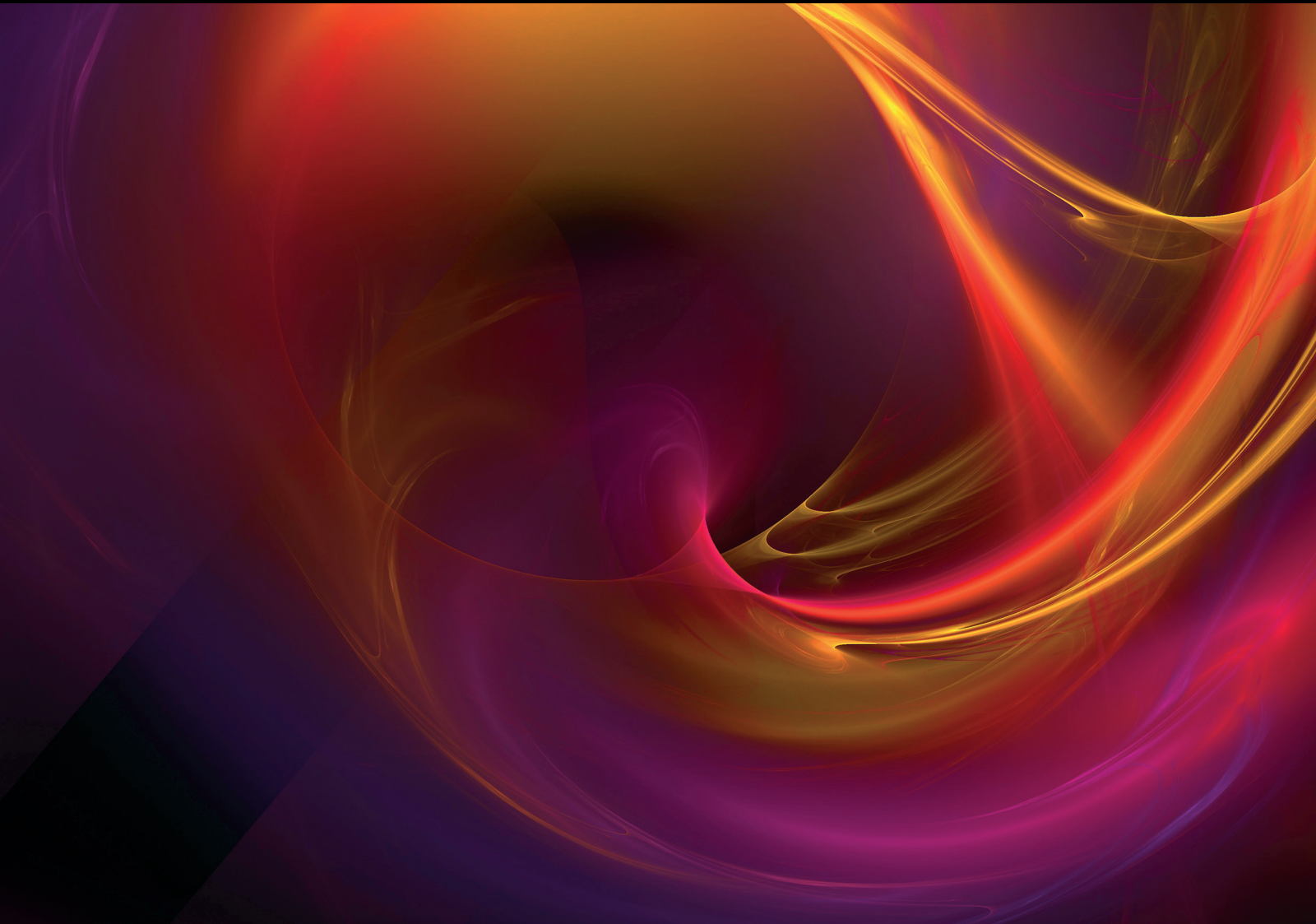# Open Challenges on the Stability of Complex Systems: Insights of Nonlinear Phenomena with or without Delay

Lead Guest Editor: Baltazar Aguirre-Hernandez
Guest Editors: Eric Campos-Canton, Raúl Villafuerte-Segura,
Carlos Vázquez-Aguilera, and Carlos-Arturo Loredo-Villalobos

Open Challenges on the Stability of Complex Systems: Insights of Nonlinear Phenomena with or without Delay

Open Challenges on the Stability of Complex Systems: Insights of Nonlinear Phenomena with or without Delay

Lead Guest Editor: Baltazar Aguirre-Hernandez
Guest Editors: Eric Campos-Canton, Raúl Villafuerte-Segura, Carlos Vázquez-Aguilera, and Carlos-Arturo Loredo-Villalobos

Editorial Board

Contents

Editorial

Open Challenges on the Stability of Complex Systems: Insights of Nonlinear Phenomena with or without Delay

Baltazar Aguirre-Hernández [iD],[1] **Eric Campos-Cantón** [iD],[2] **Raúl Villafuerte-Segura** [iD],[3] **Carlos Vázquez-Aguilera** [iD],[4] **and Carlos-Arturo Loredo-Villalobos** [iD][1]

[1]*Departamento de Matemáticas, Universidad Autónoma Metropolitana – Iztapalapa, San Rafael Atlixco 186, CDMX México 09340, Mexico*
[2]*División de Matemáticas Aplicadas, IPICyT, SLP, 78216, Mexico*
[3]*Centro de Investigación en Tecnologías de Información y Sistemas, Universidad Autónoma del Estado de Hidalgo, Hidalgo, Mexico*
[4]*Umea Universitet, Umea, Sweden*

Correspondence should be addressed to Baltazar Aguirre-Hernández; bahe@xanum.uam.mx

Received 11 March 2019; Accepted 11 March 2019; Published 15 April 2019

New developments and applications of science and industry demand no conventional modeling approaches where the increase of complexity is a common denominator. Due to nonlinear dynamics, many of the resulting mathematical models are complex systems. For example, the inherent nonlinear dynamics of physical systems make it difficult to analyze a large majority of these complex systems, giving them a wide variety of dynamic behavior. Another well-known example is the delay phenomena where the information on the state of the system in past events can be very valuable for prediction and control. In recent years, the study to determine stability and stabilization of nonlinear phenomena has had a great research interest, developing novel methods. Thus, some of these methods have been implemented to study controls for systems with delay. In this special issue new insights into the stabilization of particular nonlinear systems and systems with delay are introduced. We are sure that the selected manuscripts will be useful for the reader, providing valuable contributions, novel methods, and overall good proposals.

In the paper "Implementation of a Controller to Eliminate the Limit Cycle in the Inverted Pendulum on a Cart", M. Antonio-Cruz et al. discuss a frequency response-based linear controller. The main aim of this paper is to study a control strategy to eliminate limit cycle in the inverted pendulum on a cart generated by the dead-zone, induced by static friction.

The paper "Dynamics induced by delay in a nutrient-phytoplankton model with multiple delays" by C. Dai et al. studies a nitrogen-phosphorus-phytoplankton model described by a couple of delay differential equations to study the effect of delay on the nutrient-phytoplankton dynamics. The authors prove that the positive equilibrium is always globally asymptotically stable when there are no delays and the model may undergo a Hopf bifurcation as the delays are varied.

The paper "Simulation and Analysis of the Complex Behavior of Supply Chain Inventory System Based on Third-Party Logistics Management Inventory Model with No Accumulating of Unsatisfied Demand" by Z. Zhang et al. is a study based on third-party logistics management inventory models. The authors construct a dynamic model and they give conditions on the parameters for obtaining stability and getting useful conclusions; for example, a reasonable decision can make the inventory of the warehouse distribution system stable to a small interval.

The paper "Stability of the Evolutionary Game System and Control Strategies of Behavior Instability in Coal Mine Safety Management" by X. Wang et al. analyzes the stability of a dynamical game system with flexible and inflexible costs and penalties. The analysis carried out provides a theoretical basis for a more reasonable and effective safety management policy, in coal mine safety system. From such analysis, the authors conclude that combined mechanisms of incentive rewards

and flexible penalties can optimize and control the instability of the behavior strategy selection in the safety supervision model.

The paper "Synchronization Control in Reaction-Diffusion Systems: Application to Lengyel-Epstein System" by A. Ouannas et al. considers the complete synchronization of a large class of reaction-diffusion coupled systems. The class of systems considered is very general: the nonlinear term only requires continuity in order to attain complete synchronization with nonlinear controllers, and the continuity plus a boundedness condition in order to attain it with linear controllers. The authors study a model derived from a chemical-physics system, i.e., the Lengyel-Epstein system. The complete synchronization is in both cases (linear and nonlinear) verified via Lyapunov stability theory.

The paper "Hybrid Functions Direct Approach and State Feedback Optimal Solutions for a Class of Nonlinear Polynomial Time-Delay Systems", by M. K. Bouafoura and N. B. Braiek, presents an approximate method to determine the optimal open loop solution and nonlinear delay-dependent state feedback suboptimal control for a class of nonlinear polynomial time-delay systems by transforming the dynamical optimal control problem into a static optimization problem. In the proposed numerical method, Legendre polynomials are used.

In the paper "Consensus of Multiagent Systems Described by Various Noninteger Derivatives", G. Nava-Antonio et al. analyze recent developments in Lyapunov stability theory to determine the asymptotic stability of particular fractional dynamical systems. The results are applied to study the consensus of a fractional multiagent system with linear and nonlinear dynamics.

In the paper "New Results on the Control for a Kind of Uncertain Chaotic Systems Based on Fuzzy Logic", B. Wang and L. L. Chen analyze a single-dimensional controller, based on fuzzy logic and Lyapunov theory, to control uncertain nonlinear chaotic systems. The effectiveness of the designer controller is discussed trough typical numerical simulations.

A systematic study of the local and the global stability of traveling wave solutions to the Lotka-Volterra diffusive model is investigated in "Stability of Traveling Waves to the Lotka-Volterra Competition Model" by A. Alhasanat and C. Ou. The local stability is given using the method of spectrum analysis. However, for global stability, the authors construct an upper and a lower solution to the Lotka-Volterra system and prove their convergence to the traveling wave.

The paper "New Results on Stability Analysis of Uncertain Neutral-Type Lur'e Systems Derived from a Modified Lyapunov-Krasovskii Functional" by W. Duan et al. is concerned with the problem of the absolute and robustly absolute stability for the uncertain neutral-type Lur'e system with time-varying delays. Here, the quadratic generalized free-weighting matrix inequality technique is used to reduce the conservatism of the stability conditions. Unlike previous results, the matrix inequalities of the stability criteria proposed in this paper are converted to LMIs via the properties of quadratic functions application, which can be solved easily by Matlab LMI-toolbox.

The paper "Parameter Identification and Adaptive Control of Uncertain Goodwin Oscillator Networks with Disturbances" by J. Zhang et al. studies a drive-response system based on a differential equation model of mammals' circadian rhythms, where the suprachiasmatic nucleus (SCN) of the hypothalamus was modeled by a Goodwin oscillator and the vasoactive intestinal polypeptides (VIP) were modeled by a Van der Pol oscillator. Outer synchronization in a drive-response system has been achieved by considering effective parameter updating laws to identify the unknown parameters and designing adaptive control strategies. This paper has designed a targeted adaptive controllers to synchronize a drive-response system based on Goodwin oscillator network.

Conflicts of Interest

The editors declare that they have no conflicts of interest regarding the publication of this special issue.

Acknowledgments

Baltazar Aguirre-Hernández
Eric Campos-Cantón
Raúl Villafuerte-Segura
Carlos Vázquez-Aguilera
Carlos-Arturo Loredo-Villalobos

Research Article

New Results on Stability Analysis of Uncertain Neutral-Type Lur'e Systems Derived from a Modified Lyapunov-Krasovskii Functional

Wenyong Duan [iD],[1,2] **Yan Li,**[3] **Jian Chen,**[1] **and Lin Jiang**[2]

[1]*School of Electrical Engineering, Yancheng Institute of Technology, Yancheng Jiangsu, China*
[2]*Department of Electrical Engineering and Electronics, University of Liverpool, Liverpool, L69 3GJ, UK*
[3]*Undergraduate Office, Yancheng Biological Engineering Higher Vocational Technology School, Yancheng Jiangsu, China*

Correspondence should be addressed to Wenyong Duan; dwy1985@126.com

This paper is concerned with the problem of the absolute and robustly absolute stability for the uncertain neutral-type Lur'e system with time-varying delays. By introducing a modified Lyapunov-Krasovskii functional (LKF) related to a delay-product-type function and two delay-dependent matrices, some new delay-dependent robustly absolute stability criteria are proposed, which can be expressed as convex linear matrix inequality (LMI) framework. The criteria proposed in this paper are less conservative than some recent previous ones. Finally, some numerical examples are presented to show the effectiveness of the proposed approach.

1. Introduction

In many real systems, time delay is often considered as the main cause of poor performance and even instability. The stability of time-delay systems is always a hot topic for researchers. As a result, to obtain stability criteria of time-delayed systems by using the Lyapunov theorem, the main efforts are concentrated on the following several directions; one is finding an appropriate positive definite functional with a negative definite time derivative along the trajectory of system, for example, LKF with delay partitioning approach [1, 2], LKF with augmented terms [3], LKF with triple-integral and quadruple-integral terms [4, 5], and so on. The other is reducing the upper bounds of the time derivative of LKF as much as possible by developing various inequality techniques, such as Jensen inequality [6], Wirtinger-based inequality [7], auxiliary function based inequality [8], and Bessel-Legendre inequality [9]. Besides, further to increase the freedom of solving LMIs, there are some other methods, for instance, the generalized zero equality [10, 11], the one- or second-order reciprocally convex combinations [12–15], the free-weighting-matrix approach [16], and so on.

In practical engineering applications, most systems are nonlinear. As is known to all, Lur'e system, which is composed of the feedback connection of the linear dynamical system and the nonlinearity satisfying the sector-bounded condition, can represent many deterministic nonlinear systems, for example, Chua's Circuit and the Lorenz system [17]. Therefore, the study on the stability of Lur'e systems becomes more and more popular [18–21]. Moreover, the paper [22] pointed out that many practical systems can be modeled as neutral time-delayed systems, in which not only the system states or outputs contain time delays, but also the derivative of the system states. Due to the theoretical and practical significance, the analysis of the robust stability of the time-delayed neutral-type Lur'e systems has attached great importance by many scholars [23–29], where many important robust stability criteria were given. However, the main improvement of stability criteria depends on the development of LKF and the update of inequality techniques based on linear systems. For example, recently, [29] improved the stability results of some previous ones by combining the extended double integral with Wirtinger-based inequalities technique; however, the range of delay with nonzero lower bound and

the lower bound of the delay derivative are not involved; in [30], some less conservative stability criteria than some recent previous ones were derived for time-delayed Lur'e system via the second-order Bessel-Legendre inequality approach, a novel inequality technique; in [21], some improved stability criteria for time-delayed neutral-type Lur'e system were given by constructing a novel LKF consisting of a quadratic term and integral terms for the time-varying delays and the nonlinearities, and so on. Recently, C. Zhang [31] considered the effect of the LKFs while discussing the relationship between the tightness of inequalities and the conservatism of criteria for linear systems. The results illustrate the integral inequality that makes the upper bound closer to the true value does not always deduce a less conservative stability condition if the LKF is not properly constructed. Particularly, another novel LKF was proposed by C. Zhang et al. [31, 32] with delay-product-type terms $h(t)P_1$ and $(h - h(t))P_2$. Compared with the general LKF, P_1 and P_2 were just symmetrical, not always positive definite, which can lead to a less conservative stability condition by extending the freedom for checking the feasibility of stable conditions based on LMI. Recently, to fully utilize the information of delay derivative, a new LKF was constructed by W. Kwon et al. [33] with delay-dependent Lyapunov matrices $Q_1(t)$ and $Q_2(t)$. W. Kwon et al. point that the stability conditions based on an LKF with delay-dependent matrices are less conservative than those based on the LKF without delay-dependent matrices. As mentioned above, the two types of LKFs only improve one class of Lyapunov matrices, respectively, that is, only for the Lyapunov matrix P or the Lyapunov matrix Q. It is natural to wonder about whether can both classes of Lyapunov matrices be improved, simultaneously.

Inspired by the above analysis, the following ideas of reducing the conservation of the previous proposed stability criteria should be addressed:

(i) A modified LKF with the above both classes of Lyapunov matrices, that is delay-product-type and delay-dependent matrices, is constructed. Compared with the general LKFs in some previous published papers, such as [21, 28, 30], the Lyapunov matrices of the nonintegral item are just symmetrical, not always positive definite, which can extend the freedom for checking the feasibility of stable conditions based on LMI. And the delay-dependent matrices of the single-integral items are utilized, which can also further improve the utilization of time delay and its derivative information. In addition, the results proposed by [31–33] can be improved via the LKF modified in this paper due to the combination of the two types of LKFs.

(ii) The double integral items of the modified LKF in this paper are decomposed into two subintervals, that is $[0, h(t)]$ and $[h(t), h]$, instead of being considered directly in [33], which further make full use of the information of time-varying delays $h(t)$, $h - h(t)$ and their derivative $\dot{h}(t)$. And the quadratic generalized free-weighting matrix inequality (QGFMI) technique can be used fully in each subinterval, which can

further reduce the conservatism of the stability conditions.

(iii) To deal with the delay-derivative-dependent single-integral items feasibly, another double integral items of $V_4(t)$ are also added to the LKF under the above two subintervals, instead of introducing a positive integral item, which is actually difficult to estimate, to the derivative of the LKF like [33].

(iv) Indeed, the main result of [33] was not LMI due to the terms with $h^2(t)$ even $h^3(t)$. The matrix inequalities of the stability criteria proposed in this paper are converted to LMIs via the properties of quadratic functions application, which can be solved easily by Matlab LMI-toolbox. In conclusion, it is interesting and still challenging problem to address the above issues, which offers motivation to derive less conservative stability criteria for the time-delayed neutral-type Lur'e systems.

This paper mainly analyzes and studies the stability of uncertain neutral-type Lur'e systems with mixed time-varying delays. Some less conservative delay-dependent absolute stability criteria and robust absolute stability criteria than some previous ones are derived via a modified LKF application. In the end, four popular numerical examples are given to illustrate that this method improves some existing methods and achieves good results in stability. The structure of this paper is as follows: *Section 1* describes the research background and research topic status and defines the scope of the study of this article; *Section 2* describes the main research questions, including some necessary definitions, assumptions, and lemmas; *Section 3* presents the main results, including theorems and corollaries; in *Section 4* the discussions and simulations based on numerical examples are given; *Section 5* summarizes the whole thesis.

Notation. $P > 0 (< 0)$ represents a positive (negative) definite matrix. I and 0 represent an identity matrix and a zero matrix with the corresponding dimensions, respectively. $*$ denotes the symmetric terms in a block matrix and diag$\{\cdots\}$ denotes a block-diagonal matrix. e_i $(i = 1, \ldots, m)$ are block entry matrices with $e_2^T = [0 \quad I \quad \underbrace{0 \cdots 0}_{m-2}]$, where m is the dimension of the vector ξ. $F_{[\alpha(t), \beta(t)]}$ denotes F is the function of $\alpha(t)$ and $\beta(t)$. sym$\{B\} = B + B^T$.

2. Problem Formulation

Consider the following neutral-type Lur'e system with mixed time-varying delays:

$$\dot{x}(t) - C\dot{x}(t - \tau(t)) = [A + \Delta A(t)] x(t)$$
$$+ [A_1 + \Delta A_1(t)] x(t - h(t))$$
$$+ [B + \Delta B(t)] f(\sigma(t)),$$

$$\sigma(t) = H^T x(t), \quad \forall t \geq 0,$$

$$x(s) = \varphi(s),$$

$$\dot{x}(s) = \dot{\varphi}(s),$$

$$s \in [-\max(h_2, \tau), 0], \quad h(t) \in \textbf{C.1}$$

$$s \in [-\max(h, \tau), 0], \quad h(t) \in \textbf{C.2},$$

$$(1)$$

where $x(t) \in \mathbb{R}^n$ and $\sigma(t) \in \mathbb{R}^m$ are the state and output vectors of the system, respectively. A, A_1, B, C, and H are real constant matrices with appropriate dimensions; $\varphi(s)$ is an $\mathbb{R}^n$-valued continuous initial functional specified on $[-\max(h, \tau), 0]$ or $[-\max(h_2, \tau), 0]$ with known positive scalars h, h_2, and τ. $f(\sigma(t)) \in \mathbb{R}^m$ is the nonlinear functional in the feedback path. The time-varying delays $h(t)$ and $\tau(t)$ are continuous-time functional and satisfy the following two types of conditions:

C. 1.

$$0 \leq \tau(t) \leq \tau,$$

$$\dot{\tau}(t) \leq \tau_d < 1,$$

$$h_1 \leq h(t) \leq h_2, \tag{2}$$

$$\mu_1 \leq \dot{h}(t) \leq \mu_2$$

$$\forall t \geq 0,$$

C. 2.

$$0 \leq \tau(t) \leq \tau,$$

$$\dot{\tau}(t) \leq \tau_d < 1,$$

$$0 \leq h(t) \leq h, \tag{3}$$

$$\mu_1 \leq \dot{h}(t) \leq \mu_2,$$

$$\forall t \geq 0,$$

where $\tau \geq 0$, $\tau_d < 1$, $h_1 \geq 0$, $h_2 \geq 0$, $h \geq 0$, μ_1 and $\mu_2 < 1$ are constants.

The nonlinear functional $f(\sigma(t))$ in the feedback path is given by

$$f(\sigma(t)) = [f_1(\sigma_1(t)) \ f_2(\sigma_2(t)) \ \cdots \ f_m(\sigma_m(t))]^T \tag{4}$$

satisfying the finite sector condition:

$$f_i(\sigma_i(t)) \in \textbf{K}_{[0,k_i]} = \{f_i(\sigma_i(t)) \mid f_i(0) = 0, \ 0$$

$$< \sigma_i(t) f_i(\sigma_i(t)) \leq k_i \sigma_i(t)^2, \ \sigma_i(t) \neq 0\} \tag{5}$$

or the infinite sector condition:

$$f_i(\sigma_i(t)) \in \textbf{K}_{[0,\infty)} = \{f_i(\sigma_i(t)) \mid f_i(0)$$

$$= 0, \ \sigma_i(t) f_i(\sigma_i(t)) > 0, \ \sigma_i(t) \neq 0\}, \tag{6}$$

where $K = \text{diag}\{k_1, k_2, \ldots, k_m\}$.

$\Delta A(t)$, $\Delta A_1(t)$, and $\Delta B(t)$ denote real-valued matrix functions representing parameter uncertainties, which are assumed to satisfy

$$[\Delta A(t) \ \Delta B(t) \ \Delta A_1(t)] = DF(t) [E_a \ E_b \ E_{a1}], \tag{7}$$

where D, E_a, E_b, and E_{a1} are known constant matrices with appropriate dimensions, and $F(t)$ is an unknown matrix with Lebesgue-measurable elements and satisfies

$$F^T(t) F(t) \leq I, \quad \forall t \geq 0. \tag{8}$$

This paper mainly analyzes and studies the stability of uncertain neutral-type Lur'e system (1) under conditions (2), (3), (5), (6), (7), and (8) based on Lyapunov stability theory. For neutral-type systems, the assumption that $\rho(C) < 1$ [41] is required, where $\rho(\cdot)$ denotes the spectral radius of C. To obtain the main results of this paper, the following definition and lemmas are important.

Definition 1 (robustly absolute stability). The uncertain neutral-type Lur'e system described by (1) is said to be robustly absolutely stable in the sector $[0, K]$ (or $[0, \infty)$), if the system is asymptotically stable for any nonlinear function $f(\sigma(t))$ satisfying (5) (or (6)) and all admissible uncertainties.

Lemma 2 (see [15]). *For given vectors α_1, α_2 and positive real scalars λ satisfying $0 < \lambda < 1$, symmetric positive definite matrix $R_1, R_2 \in \mathbb{R}^{n \times n}$, and any matrix $U_{01}, U_{02} \in \mathbb{R}^{n \times n}$, the following inequality holds*

$$\frac{\alpha_1^T R_1 \alpha_1}{\lambda} + \frac{\alpha_2^T R_2 \alpha_2}{1 - \lambda} \geq \begin{bmatrix} \alpha_1 \\ \alpha_2 \end{bmatrix}^T$$

$$\cdot \begin{bmatrix} R_1 + (1 - \lambda) T_1 & (1 - \lambda) U_{01} + \lambda U_{02} \\ * & R_2 + \lambda T_2 \end{bmatrix} \begin{bmatrix} \alpha_1 \\ \alpha_2 \end{bmatrix}, \tag{9}$$

where $T_1 = R_1 - U_{02} R_2^{-1} U_{02}^T$, $T_2 = R_2 - U_{01}^T R_1^{-1} U_{01}$.

Lemma 3 (QGFMI [33]). *For any given matrices X, Y, a positive definite matrix R and a continuous differentiable function $\{\omega(s) \mid s \in [a, b]\}$, the following inequality holds*

$$-\int_a^b \omega^T(s) R\omega(s) ds \leq \begin{bmatrix} \eta_0 \\ \eta_1 \end{bmatrix}^T$$

$$\cdot \begin{bmatrix} (b - a) XR^{-1} X^T & X[I \ 0] \\ * & \frac{b - a}{3} YR^{-1} Y^T + \text{sym}\{Y[-I \ 2I]\} \end{bmatrix} \begin{bmatrix} \eta_0 \\ \eta_1 \end{bmatrix}, \tag{10}$$

where η_0 is an any vector, and $\eta_1^T = \left[\int_a^b \omega^T(s)ds \ \ (1/(b-a)) \int_a^b \int_\theta^b \omega^T(s)ds \, d\theta\right]$.

Lemma 4 (see [42]). *For a given quadratic function $l(s) = a_2 s^2 + a_1 s + a_0$, where $a_i \in \textbf{R}$ ($i = 0, 1, 2$), $h_{12} = h_2 - h_1$, if the following inequalities hold*

$$(i) \ l(h_1) < 0;$$

$$(ii) \ l(h_2) < 0; \tag{11}$$

$$(iii) \ -h_{12}^2 a_2 + l(h_1) < 0,$$

one has $l(s) < 0$, for all $s \in [h_1, h_2]$.

$$
\begin{aligned}
&h_{1t} = h(t) - h_1, \ h_{2t} = h_2 - h(t), \ h_{12} = h_2 - h_1, \\
&h_d = 1 - \dot{h}(t), \ \overline{\mu}_1 = |\mu_1| + \dot{h}(t), \ \gamma^T(s) = \left[x^T(s) \ \dot{x}^T(s)\right], \\
&v_1(t) = \int_{t-h_1}^{t} \frac{x^T(s)}{h_1} ds, \ v_2(t) = \int_{t-h(t)}^{t-h_1} \frac{x^T(s)}{h_{1t}} ds, \ v_3(t) = \int_{t-h_2}^{t-h(t)} \frac{x^T(s)}{h_{2t}} ds, \\
&\omega_1(t) = h_1 v_1(t), \ \omega_2(t) = h_{1t} v_2(t), \ \omega_3(t) = h_{2t} v_3(t), \\
&\zeta^T(t) = \left[x^T(t) \ x^T(t-h_1) \ x^T(t-h(t)) \ x^T(t-h_2) \ \omega_1(t) \ \omega_2(t) \ \omega_3(t)\right], \\
&\zeta_1^T(t) = \left[x^T(t) \ x^T(t-h_1) \ x^T(t-h(t)) \ x^T(t-h_2) \ v_2(t)\right], \\
&\zeta_2^T(t) = \left[x^T(t) \ x^T(t-h_1) \ x^T(t-h(t)) \ x^T(t-h_2) \ v_3(t)\right], \\
&\Delta^T(t) = \left[\omega_2^T(t) \ x^T(t-h_1) - x^T(t-h(t)) \ \omega_3^T(t) \ x^T(t-h(t)) - x^T(t-h_2)\right], \\
&\xi^T(t) = [x^T(t) \ x^T(t-h_1) \ x^T(t-h(t)) \ x^T(t-h_2) \ \dot{x}^T(t) \ \dot{x}^T(t-h_1) \ \dot{x}^T(t-h(t)) \ \dot{x}^T(t-h_2) \ v_1(t) \ v_2(t) \ v_3(t) \\
&\qquad \int_{t-h_1}^{t}\int_{u}^{t}\left(x^T(s)/h_1\right) du \, ds \ \int_{t-h(t)}^{t-h_1}\int_{u}^{t-h_1}\left(x^T(s)/h_{1t}\right) du \, ds \ \int_{t-h_2}^{t-h(t)}\int_{u}^{t-h(t)}\left(x^T(s)/h_{2t}\right) du \, ds \ \dot{x}^T(t-\tau(t)) \ f^T(\sigma(t))], \\
&\eta_1(t) = \begin{bmatrix} \omega_2(t) \\ x(t-h_1) - x(t-h(t)) \end{bmatrix}, \ \eta_2(t) = \begin{bmatrix} \omega_3(t) \\ x(t-h(t)) - x(t-h_2) \end{bmatrix}.
\end{aligned}
$$

Box 1: Notations of several symbols and matrices in Theorems 8 and 14.

Proof. The proof is similar to lemma 2 of [42]. First, in the case of $a_2 \geq 0$, l is a convex function. So, (i) and (ii) guarantee $l(s) < 0$, $\forall s \in [h_1, h_2]$. Next, for $a_2 < 0$, l is a concave function. So, $l(s) \leq \dot{l}(h_2)(s-h_2)+l(h_2) = (2a_2 h_2 + a_1)s - a_2 h_2^2 + a_0 := g(s)$. Then $g(h_1) = -a_2 h_{12}^2 + a_2 h_1^2 + a_1 h_1 + a_0 = -a_2 h_{12}^2 + l(h_1) < 0$ from (iii) and $g(h_2) = l(h_2) < 0$ from (ii) guarantee that $l(s) < 0$, for all $l \in [h_1, h_2]$. This completes the proof. □

Remark 5. It is interesting to note that, in Lemma 4, when $h_1 = 0$, inequalities (11) can be rewritten in those of lemma 2 in [42]. Hence the established Lemma 4 covers the lemma in [42].

Lemma 6 (see [43]). *Given matrices Γ, Ξ, and $\Omega = \Omega^T$, the following inequality*

$$
\Omega + \Gamma F(\sigma) \Xi + \Xi^T F^T(\sigma) \Gamma^T < 0 \tag{12}
$$

holds for any $F(\sigma)$ satisfying $F^T(\sigma)F(\sigma) \leq I$, if and only if there exists a scalar $\varepsilon > 0$ such that

$$
\Omega + \varepsilon^{-1} \Gamma\Gamma^T + \varepsilon \Xi^T \Xi < 0. \tag{13}
$$

Remark 7. Recently, [29] improved the stability results of the uncertain neutral-type Lur'e system (1) by combining the extended double integral with Wirtinger-based inequalities technique. In practice, it is known that the range of delay with nonzero lower bound is often encountered, and such systems are referred to as interval time-delay systems. So, both the range of delay with zero lower bound and that with nonzero lower bound are considered in this paper. In addition, the lower bound of the delay derivative is also involved in this paper, which is not mentioned in [29].

3. Main Results

3.1. Absolute Stability Criteria for Nominal Form.
In this section, we will investigate the robustly absolute stability problem of the system (1). First, we give an absolute stability criterion for nominal form of system (1) without uncertainties described as

$$
\begin{aligned}
\dot{x}(t) - C\dot{x}(t - \tau(t)) &= Ax(t) + A_1 x(t - h(t)) \\
&\quad + Bf(\sigma(t)), \\
\sigma(t) &= H^T x(t), \quad \forall t \geq 0, \\
x(s) &= \varphi(s), \\
\dot{x}(s) &= \dot{\varphi}(s), \\
s &\in [-\max(h_2, \tau), 0], \ h(t) \in \mathbf{C.1} \\
s &\in [-\max(h, \tau), 0], \ h(t) \in \mathbf{C.2}.
\end{aligned} \tag{14}
$$

For the sake of simplicity on matrix representation, the notations of several symbols and matrices are defined as Box 1 of Appendix A. The following theorem will give an absolute stability criterion for Lur'e system (14) satisfying the conditions **C. 1** and (5).

Theorem 8. *The system (14) satisfying the conditions (2) and (5) is absolutely stable for given values of $h_2 \geq h_1 \geq 0$, $\mu_1, \mu_2 < 1, \tau_d < 1$ and $k_j > 0$ $(j = 1, 2, \ldots, m)$, if there exist symmetric matrices $P \in \mathbb{R}^{7n \times 7n}$, $(P_a, P_b \in \mathbb{R}^{5n \times 5n})$, $(Q_a, Q_b, R_{0a}, R_a, R_b \in \mathbb{R}^{n \times n})$, positive definite matrices $(Q_2 \in \mathbb{R}^{n \times n})$, $(Q_1, R_0, R_1, R_2, Q_1(t), Q_2(t) \in \mathbb{R}^{2n \times 2n})$, $S = \text{diag}\{s_1, s_2, \ldots, s_m\}$, $\Lambda = \text{diag}\{\lambda_1, \lambda_2, \ldots, \lambda_m\}$ and any matrices $(U_{01}, U_{02} \in \mathbb{R}^{2n \times 2n}, \overline{U} \in \mathbb{R}^{(3n+m) \times n})$, $X_0 \in \mathbb{R}^{3n \times 2n}$, $X_i \in \mathbb{R}^{5n \times 2n}, Y_\lambda \in \mathbb{R}^{4n \times 2n}$ $(i = 1, \ldots, 4; \lambda = 0, \ldots, 4)$ such that the following LMIs hold for $[h(t), \dot{h}(t)] \in \{[h_1, h_2] \times [\mu_1, \mu_2]\}$:*

$$
\begin{aligned}
\overline{Q}_a &> 0, \\
\overline{Q}_b &> 0, \\
\overline{R}_{0a} &> 0,
\end{aligned}
$$

$$\overline{R}_a > 0,$$
$$\overline{R}_b > 0,$$
$$\Omega_{1[h(t)]} > 0,$$
$$\Omega_{2[h(t)]} > 0,$$

$$(15)$$

$$\begin{bmatrix} \Omega_{4[h_1]} + \dfrac{1}{h_{12}} J^T \Omega_{3[h_1]} J & E_1 U_{02} \\ * & h_{12}\Omega_{2[h_1]} \end{bmatrix} > 0,$$

$$(16)$$

$$\begin{bmatrix} \Omega_{4[h_2]} + \dfrac{1}{h_{12}} J^T \Omega_{3[h_2]} J & E_2 U_{01}^T \\ * & h_{12}\Omega_{1[h_2]} \end{bmatrix} > 0,$$

$$l\left(h_1, \dot{h}(t), \alpha\right) = \begin{bmatrix} \Pi_{[h_1,\dot{h}(t)]} & \Omega_{01} & \Omega_{02} & \Omega_{a[1,4]} & \overline{\mu_1}\Omega_{a[1,2]} & h_d\Omega^{[h_1]}_{b[2,1,3]} & \Omega^{[h_1]}_{b[2,1,1]} \\ * & -h_1\overline{R}_{0a} & 0 & 0 & 0 & 0 & 0 \\ * & * & -3h_1\overline{R}_{0a} & 0 & 0 & 0 & 0 \\ * & * & * & -h_{12}\overline{R}_b & 0 & 0 & 0 \\ * & * & * & * & -\overline{\mu_1}h_{12}\overline{Q}_b & 0 & 0 \\ * & * & * & * & * & -3h_dh_{12}\overline{R}_a & 0 \\ * & * & * & * & * & * & -3h_{12}\overline{Q}_a \end{bmatrix} < 0, \quad (17)$$

$$l\left(h_1, \dot{h}(t), 1-\alpha\right) = \begin{bmatrix} \Pi_{[h_1,\dot{h}(t)]} & \Omega_{01} & \Omega_{02} & \Omega_{a[1,4]} & \overline{\mu_1}\Omega_{a[1,2]} & \Omega^{[h_1]}_{b[3,2,4]} & \overline{\mu_1}\Omega^{[h_1]}_{b[3,2,2]} \\ * & -h_1\overline{R}_{0a} & 0 & 0 & 0 & 0 & 0 \\ * & * & -3h_1\overline{R}_{0a} & 0 & 0 & 0 & 0 \\ * & * & * & -h_{12}\overline{R}_b & 0 & 0 & 0 \\ * & * & * & * & -\overline{\mu_1}h_{12}\overline{Q}_b & 0 & 0 \\ * & * & * & * & * & -3h_{12}\overline{R}_b & 0 \\ * & * & * & * & * & * & -3\overline{\mu_1}h_{12}\overline{Q}_b \end{bmatrix} < 0, \quad (18)$$

$$l\left(h_2, \dot{h}(t), \alpha\right) = \begin{bmatrix} \Pi_{[h_2,\dot{h}(t)]} & \Omega_{01} & \Omega_{02} & h_d\Omega_{a[1,3]} & \Omega_{a[1,1]} & h_d\Omega^{[h_2]}_{b[2,1,3]} & \Omega^{[h_2]}_{b[2,1,1]} \\ * & -h_1\overline{R}_{0a} & 0 & 0 & 0 & 0 & 0 \\ * & * & -3h_1\overline{R}_{0a} & 0 & 0 & 0 & 0 \\ * & * & * & -h_dh_{12}\overline{R}_a & 0 & 0 & 0 \\ * & * & * & * & -h_{12}\overline{Q}_a & 0 & 0 \\ * & * & * & * & * & -3h_dh_{12}\overline{R}_a & 0 \\ * & * & * & * & * & * & -3h_{12}\overline{Q}_a \end{bmatrix} < 0, \quad (19)$$

$$l\left(h_2, \dot{h}(t), 1-\alpha\right) = \begin{bmatrix} \Pi_{[h_2,\dot{h}(t)]} & \Omega_{01} & \Omega_{02} & h_d\Omega_{a[1,3]} & \Omega_{a[1,1]} & \Omega^{[h_2]}_{b[3,2,4]} & \overline{\mu_1}\Omega^{[h_2]}_{b[3,2,2]} \\ * & -h_1\overline{R}_{0a} & 0 & 0 & 0 & 0 & 0 \\ * & * & -3h_1\overline{R}_{0a} & 0 & 0 & 0 & 0 \\ * & * & * & -h_dh_{12}\overline{R}_a & 0 & 0 & 0 \\ * & * & * & * & -h_{12}\overline{Q}_a & 0 & 0 \\ * & * & * & * & * & -3h_{12}\overline{R}_b & 0 \\ * & * & * & * & * & * & -3\overline{\mu_1}h_{12}\overline{Q}_b \end{bmatrix} < 0, \quad (20)$$

$$-a_2 h_{12}^2 + l\left(h_1, \dot{h}(t), \alpha\right) < 0,$$

$$-a_2 h_{12}^2 + l\left(h_1, \dot{h}(t), 1 - \alpha\right) < 0,$$

$$(21)$$

where the related notations are defined in Box 3 of Appendix B.

Proof. Construct an *LKF* candidate as

$$V(t) = \sum_{i=1}^{5} V_i(t) \tag{22}$$

with

$$V_1(t) = \zeta^T(t) P \zeta(t) + h_{1t} \zeta_1^T(t) P_a \zeta_1(t)$$

$$+ h_{2t} \zeta_2^T(t) P_b \zeta_2(t),$$

$$V_2(t) = \int_{t-h(t)}^{t-h_1} \gamma^T(s) Q_1(t) \gamma(s) \, ds$$

$$+ \int_{t-h_2}^{t-h(t)} \gamma^T(s) Q_2(t) \gamma(s) \, ds,$$

$$V_3(t) = \int_{t-h_1}^{t} \gamma^T(s) Q_1 \gamma(s) \, ds$$

$$+ \int_{t-\tau(t)}^{t} \dot{x}^T(s) Q_2 \dot{x}(s) \, ds$$

$$+ 2 \sum_{i=1}^{m} \lambda_i \int_0^{\sigma_i} f_i(\sigma_i) \, d\sigma_i, \tag{23}$$

$$V_4(t) = \int_{t-h(t)}^{t-h_1} \int_{\theta}^{t-h_1} \gamma^T(s) \overline{Q}_a \gamma(s) \, ds \, d\theta$$

$$+ |\mu_1| \int_{t-h_2}^{t-h(t)} \int_{\theta}^{t-h(t)} \gamma^T(s) \overline{Q}_b \gamma(s) \, ds \, d\theta$$

$$V_5(t) = \int_{t-h_1}^{t} \int_{\theta}^{t} \gamma^T(s) R_0 \gamma(s) \, ds \, d\theta$$

$$+ \int_{t-h(t)}^{t-h_1} \int_{\theta}^{t-h_1} \gamma^T(s) R_1 \gamma(s) \, ds \, d\theta$$

$$+ \int_{t-h_2}^{t-h(t)} \int_{\theta}^{t-h(t)} \gamma^T(s) R_2 \gamma(s) \, ds \, d\theta,$$

where notations of several symbols and matrices can be found in Boxes 1 and 3 of Appendixes A and B.

First step, because the positive definiteness of the Lyapunov matrices P, P_a, and P_b is not required, the positive definiteness of the LKF (22) should be proved. The P_a- and P_b- dependent terms can be rewritten as

$$h_{1t} \zeta_1^T(t) P_a \zeta_1(t) + h_{2t} \zeta_2^T(t) P_b \zeta_2(t)$$

$$= \begin{bmatrix} x(t) \\ x(t-h_1) \\ x(t-h(t)) \\ x(t-h_2) \\ 0 \end{bmatrix}^T [h_{1t} P_a + h_{2t} P_b] \begin{bmatrix} x(t) \\ x(t-h_1) \\ x(t-h(t)) \\ x(t-h_2) \\ 0 \end{bmatrix}$$

$$+ 2 \begin{bmatrix} x(t) \\ x(t-h_1) \\ x(t-h(t)) \\ x(t-h_2) \\ 0 \end{bmatrix}^T \tag{24}$$

$$\cdot \left\{ P_a \begin{bmatrix} 0 \\ 0 \\ 0 \\ 0 \\ \omega_2(t) \end{bmatrix} + P_b \begin{bmatrix} 0 \\ 0 \\ 0 \\ 0 \\ \omega_3(t) \end{bmatrix} \right\}$$

$$+ \frac{\omega_2^T(t) E P_a E^T \omega_2(t)}{h_{1t}} + \frac{\omega_3^T(t) E P_b E^T \omega_3(t)}{h_{2t}},$$

where $E = [0 \ 0 \ 0 \ 0 \ I]$.

Based on $Q_1(t) > 0$, $Q_2(t) > 0$ and Jensen's inequality, the $V_2(t)$ term can be estimated as

$$V_2(t) \geq \frac{\eta_1^T(t) Q_1(t) \eta_1(t)}{h_{1t}} + \frac{\eta_2^T(t) Q_2(t) \eta_2(t)}{h_{2t}}. \tag{25}$$

According to $\Omega_{i[h(t)]} > 0$ $(i = 1, 2)$ and Lemma 2, we can obtain the following inequality from (24) and (25)

$$V_2(t) + \frac{\omega_2^T(t) E P_a E^T \omega_2(t)}{h_{1t}} + \frac{\omega_3^T(t) E P_b E^T \omega_3(t)}{h_{2t}}$$

$$\geq \frac{\eta_1^T(t) \left(\begin{bmatrix} E P_a E^T & 0 \\ 0 & 0 \end{bmatrix} + Q_1(t) \right) \eta_1(t)}{h_{1t}}$$

$$+ \frac{\eta_2^T(t) \left(\begin{bmatrix} E P_b E^T & 0 \\ 0 & 0 \end{bmatrix} + Q_2(t) \right) \eta_2(t)}{h_{2t}}$$

$$\geq \Delta^T (t) \frac{\Omega_{3[h(t)]}}{h_{12}} \Delta (t)$$

$$- \frac{(1-\alpha)}{h_{12}} \eta_1^T (t) U_{02} \Omega_{2[h(t)]}^{-1} U_{02}^T \eta_1 (t)$$

$$- \frac{\alpha}{h_{12}} \eta_2^T (t) U_{01}^T \Omega_{1[h(t)]}^{-1} U_{01} \eta_2 (t). \tag{26}$$

It follows from (15)-(16), (22), (24), (25), and (26) and $Q_1 > 0$, $Q_2 > 0$, $R_i > 0$ $(i = 0, 1, 2)$ that

$$V (t) > 0. \tag{27}$$

Thus, the LKF (22) is positive definite.

Second step, the time derivative of $V(t)$ with respect to time along the trajectory of the system (14) is as follows:

$$\dot{V}_1 (t) = \dot{h} (t) \zeta_1^T (t) P_a \zeta_1 (t) - \dot{h} (t) \zeta_2^T (t) P_b \zeta_2 (t)$$

$$+ 2\zeta^T (t) P \dot{\zeta} (t) + 2h_{1t} \zeta_1^T (t) P_a \dot{\zeta}_1 (t) + 2h_{2t} \zeta_2^T (t)$$

$$\cdot P_b \dot{\zeta}_2 (t) = \dot{h} (t) \zeta_1^T (t) P_a \zeta_1 (t) - \dot{h} (t) \zeta_2^T (t) P_b \zeta_2 (t)$$

$$+ 2\zeta^T (t) P \begin{bmatrix} \dot{x} (t) \\ \dot{x} (t - h_1) \\ h_d \dot{x} (t - h (t)) \\ \dot{x} (t - h_2) \\ x (t) - x (t - h_1) \\ x (t - h_1) - h_d x (t - h (t)) \\ h_d x (t - h (t)) - x (t - h_2) \end{bmatrix}$$

$$+ 2h_{1t} \zeta_1^T (t)$$

$$\cdot P_a \begin{bmatrix} \dot{x} (t) \\ \dot{x} (t - h_1) \\ h_d \dot{x} (t - h (t)) \\ \dot{x} (t - h_2) \\ \dfrac{x (t - h_1) - h_d x (t - h (t)) - \dot{h} (t) v_2 (t)}{h_{1t}} \end{bmatrix}$$

$$+ 2h_{2t} \zeta_2^T (t)$$

$$\cdot P_b \begin{bmatrix} \dot{x} (t) \\ \dot{x} (t - h_1) \\ h_d \dot{x} (t - h (t)) \\ \dot{x} (t - h_2) \\ \dfrac{h_d x (t - h (t)) - x (t - h_2) + \dot{h} (t) v_3 (t)}{h_{2t}} \end{bmatrix}, \tag{28}$$

$$\dot{V}_2 (t) = \gamma^T (t - h_1) Q_1 (t) \gamma (t - h_1) + h_d \gamma^T (t - h (t))$$

$$\cdot [Q_2 (t) - Q_1 (t)] \gamma (t - h (t)) - \gamma^T (t - h_2) Q_2 (t)$$

$$\cdot \gamma (t - h_2) - \dot{h} (t) \int_{t-h(t)}^{t-h_1} \gamma^T (s) Q_{11} \gamma (s) ds - \dot{h} (t) \tag{29}$$

$$\cdot \int_{t-h_2}^{t-h(t)} \gamma^T (s) Q_{21} \gamma (s) ds,$$

$$\dot{V}_3 (t) \leq \gamma^T (t) Q_1 \gamma (t) - \gamma^T (t - h_1) Q_1 \gamma (t - h_1)$$

$$+ \dot{x}^T (t) Q_2 \dot{x} (t) - (1 - \tau_d) \dot{x}^T (t - \tau (t)) \tag{30}$$

$$\cdot Q_2 \dot{x} (t - \tau (t)) + 2f^T (\sigma (t)) \Lambda H^T \dot{x} (t),$$

$$\dot{V}_4 (t) = h_{1t} \gamma^T (t - h_1) \overline{Q}_a \gamma (t - h_1) + |\mu_1|$$

$$\cdot h_d h_{2t} \gamma^T (t - h (t)) \overline{Q}_b \gamma (t - h (t))$$

$$- h_d \int_{t-h(t)}^{t-h_1} \gamma^T (s) \overline{Q}_a \gamma (s) ds - |\mu_1| \tag{31}$$

$$\cdot \int_{t-h_2}^{t-h(t)} \gamma^T (s) \overline{Q}_b \gamma (s) ds,$$

$$\dot{V}_5 (t) = h_1 \gamma^T (t) R_0 \gamma (t) + h_{1t} \gamma^T (t - h_1) R_1 \gamma (t - h_1)$$

$$+ h_d h_{2t} \gamma^T (t - h (t)) R_2 \gamma (t - h (t))$$

$$- \int_{t-h_1}^{t} \gamma^T (s) R_0 \gamma (s) ds \tag{32}$$

$$- h_d \int_{t-h(t)}^{t-h_1} \gamma^T (s) R_1 \gamma (s) ds$$

$$- \int_{t-h_2}^{t-h(t)} \gamma^T (s) R_2 \gamma (s) ds.$$

For additional symmetric matrices Q_a, Q_b, R_{0a}, R_a, and R_b the following zero equations are satisfied

$$0 = \dot{h} (t) \left[x^T (t - h_1) Q_a x (t - h_1) \right.$$

$$- x^T (t - h (t)) Q_a x (t - h (t))$$

$$- 2 \int_{t-h(t)}^{t-h_1} x^T (s) Q_a \dot{x} (s) ds$$

$$+ x^T (t - h (t)) Q_b x (t - h (t)) \tag{33}$$

$$- x^T (t - h_2) Q_b x (t - h_2)$$

$$\left. - 2 \int_{t-h_2}^{t-h(t)} x^T (s) Q_b \dot{x} (s) ds \right],$$

$$0 = x^T(t) R_{0a} x(t) - x^T(t-h_1) R_{0a} x(t-h_1)$$
$$- 2 \int_{t-h_1}^{t} x^T(s) R_{0a} \dot{x}(s) ds, \tag{34}$$

$$0 = h_d \left[x^T(t-h_1) R_a x(t-h_1) \right.$$
$$- x^T(t-h(t)) R_a x(t-h(t))$$
$$- 2 \int_{t-h(t)}^{t-h_1} x^T(s) R_a \dot{x}(s) ds \right] + x^T(t-h(t)) R_b x(t \tag{35}$$
$$- h(t)) - x^T(t-h_2) R_b x(t-h_2)$$
$$- 2 \int_{t-h_2}^{t-h(t)} x^T(s) R_b \dot{x}(s) ds.$$

Taking the zero inequalities in $\dot{V}_2$ and $\dot{V}_4$, we have the following integral terms.

$$\varphi = - \int_{t-h(t)}^{t-h_1} \gamma^T(s) \overline{Q}_a \gamma(s) ds$$
$$- \left(|\mu_1| + \dot{h}(t) \right) \int_{t-h_2}^{t-h(t)} \gamma^T(s) \overline{Q}_b \gamma(s) ds$$
$$- \int_{t-h_1}^{t} \gamma^T(s) \overline{R}_{0a} \gamma(s) ds \tag{36}$$
$$- h_d \int_{t-h(t)}^{t-h_1} \gamma^T(s) \overline{R}_a \gamma(s) ds$$
$$- \int_{t-h_2}^{t-h(t)} \gamma^T(s) \overline{R}_b \gamma(s) ds.$$

It follows from Lemma 3 with an augmented vector $\gamma(s)$ that

$$- \int_{t-h_1}^{t} \gamma^T(s) \overline{R}_{0a} \gamma(s) ds \leq \begin{bmatrix} W_{01}^T \\ W_{02}^T \end{bmatrix}^T \begin{bmatrix} h_1 X_0 \overline{R}_{0a}^{-1} X_0^T & X_0 H_{01} \\ * & \frac{h_1}{3} G_0 Y_0 \overline{R}_{0a}^{-1} Y_0^T G_0 + \text{sym}\{G_0 Y_0 H_{02}\} \end{bmatrix} \begin{bmatrix} W_{01}^T \\ W_{02}^T \end{bmatrix}, \tag{37}$$

$$- \int_{t-h(t)}^{t-h_1} \gamma^T(s) \overline{Q}_a \gamma(s) ds \leq \begin{bmatrix} W_1^T \\ W_2^T \end{bmatrix}^T \begin{bmatrix} h_{1t} X_1 \overline{Q}_a^{-1} X_1^T & X_1 H_1 \\ * & \frac{h_{1t}}{3} G_1 Y_1 \overline{Q}_a^{-1} Y_1^T G_1 + \text{sym}\{G_1 Y_1 H_3\} \end{bmatrix} \begin{bmatrix} W_1^T \\ W_2^T \end{bmatrix}, \tag{38}$$

$$-\overline{\mu}_1 \int_{t-h_2}^{t-h(t)} \gamma^T(s) \overline{Q}_b \gamma(s) ds \leq \overline{\mu}_1 \begin{bmatrix} W_1^T \\ W_3^T \end{bmatrix}^T \begin{bmatrix} h_{2t} X_2 \overline{Q}_b^{-1} X_2^T & X_2 H_2 \\ * & \frac{h_{2t}}{3} G_2 Y_2 \overline{Q}_b^{-1} Y_2^T G_2 + \text{sym}\{G_2 Y_2 H_4\} \end{bmatrix} \begin{bmatrix} W_1^T \\ W_3^T \end{bmatrix}, \tag{39}$$

$$-h_d \int_{t-h(t)}^{t-h_1} \gamma^T(s) \overline{R}_a \gamma(s) ds \leq h_d \begin{bmatrix} W_1^T \\ W_2^T \end{bmatrix}^T \begin{bmatrix} h_{1t} X_3 \overline{R}_a^{-1} X_3^T & X_3 H_1 \\ * & \frac{h_{1t}}{3} G_1 Y_3 \overline{R}_a^{-1} Y_3^T G_1 + \text{sym}\{G_1 Y_3 H_3\} \end{bmatrix} \begin{bmatrix} W_1^T \\ W_2^T \end{bmatrix}, \tag{40}$$

$$- \int_{t-h_2}^{t-h(t)} \gamma^T(s) \overline{R}_b \gamma(s) ds \begin{bmatrix} W_1^T \\ W_3^T \end{bmatrix}^T \begin{bmatrix} h_{2t} X_4 \overline{R}_b^{-1} X_4^T & X_4 H_2 \\ * & \frac{h_{2t}}{3} G_2 Y_4 \overline{R}_b^{-1} Y_4^T G_2 + \text{sym}\{G_2 Y_4 H_4\} \end{bmatrix} \begin{bmatrix} W_1^T \\ W_3^T \end{bmatrix}. \tag{41}$$

For any appropriately dimensioned matrices $\overline{U} = [U_1^T \ U_2^T \ U_3^T \ U_4^T]^T$, it is true that

$$0 = 2 \left[x^T(t) \ \dot{x}^T(t) \ \dot{x}^T(t-\tau(t)) \ f^T(\sigma(t)) \right]$$
$$\cdot \overline{U} \left[Ax(t) + A_1 x(t-h(t)) + Bf(\sigma(t)) \tag{42} \right.$$
$$+ C\dot{x}(t-\tau(t)) - \dot{x}(t) \right].$$

Letting $S = \text{diag}\{s_1, s_2, \ldots, s_m\} > 0$, it follows from (5) that

$$2 f^T(\sigma(t)) S \left[KH^T x(t) - f^T(\sigma(t)) \right] \geq 0. \tag{43}$$

Finally, from the above derivation, we have

$$\dot{V}(t) \leq \xi^T(t) \left\{ \Pi_{[h(t), \dot{h}(t)]} + h_1 \left[W_{01} X_0 \overline{R}_{0a}^{-1} X_0^T W_{01}^T \right. \right.$$
$$+ \frac{1}{3} W_{02} G_0 Y_0 \overline{R}_{0a}^{-1} Y_0^T G_0 W_{02}^T \right]$$
$$+ h_{1t} \left[h_d W_1 X_3 \overline{R}_a^{-1} X_3^T W_1^T + W_1 X_1 \overline{Q}_a^{-1} X_1^T W_1^T \right]$$
$$+ h_{2t} \left[W_1 X_4 \overline{R}_b^{-1} X_4^T W_1^T + \overline{\mu}_1 W_1 X_2 \overline{Q}_b^{-1} X_2^T W_1^T \right]$$
$$+ h_{1t} \left[\frac{h_d}{3} W_2 G_1 Y_3 \overline{R}_a^{-1} Y_3^T G_1 W_2^T \right.$$

$$+ \frac{1}{3} W_2 G_1 Y_1 \overline{Q}_a^{-1} Y_1^T G_1 W_2^T \Big]$$

$$+ h_{2t} \Big[\frac{1}{3} W_3 G_2 Y_4 \overline{R}_b^{-1} Y_4^T G_2 W_3^T$$

$$+ \frac{\overline{\mu}_1}{3} W_3 G_2 Y_2 \overline{Q}_b^{-1} Y_2^T G_2 W_3^T \Big] \Big\} \xi(t)$$

$$= \xi^T(t) \Big\{ \Pi_{[h(t),\dot{h}(t)]} + h_1 \Big[W_{01} X_0 \overline{R}_{0a}^{-1} X_0^T W_{01}^T$$

$$+ \frac{1}{3} W_{02} G_0 Y_0 \overline{R}_{0a}^{-1} Y_0^T G_0 W_{02}^T \Big]$$

$$+ h_{1t} \Big[h_d W_1 X_3 \overline{R}_a^{-1} X_3^T W_1^T + W_1 X_1 \overline{Q}_a^{-1} X_1^T W_1^T \Big]$$

$$+ h_{2t} \Big[W_1 X_4 \overline{R}_b^{-1} X_4^T W_1^T + \overline{\mu}_1 W_1 X_2 \overline{Q}_b^{-1} X_2^T W_1^T \Big]$$

$$+ \alpha h_{12} \Big[\frac{h_d}{3} W_2 G_1 Y_3 \overline{R}_a^{-1} Y_3^T G_1 W_2^T$$

$$+ \frac{1}{3} W_2 G_1 Y_1 \overline{Q}_a^{-1} Y_1^T G_1 W_2^T \Big] + (1 - \alpha)$$

$$\cdot h_{12} \Big[\frac{1}{3} W_3 G_2 Y_4 \overline{R}_b^{-1} Y_4^T G_2 W_3^T$$

$$+ \frac{\overline{\mu}_1}{3} W_3 G_2 Y_2 \overline{Q}_b^{-1} Y_2^T G_2 W_3^T \Big] \Big\} \xi(t) \tag{44}$$

with $\alpha = (h(t) - h_1)/h_{12} \geq 0$, $1 - \alpha = (h_2 - h(t))/h_{12} \geq 0$.

Therefore, LMIs (17)–(21) hold, which together with *Schur complement equivalence*, Lemma 4 and the convex function theory imply that $\dot{V}(t) < 0$. Hence, it follows from the Lyapunov stability theory that the nominal system (14) is absolutely stable for any nonlinear function $f(\sigma(t))$ satisfying (5). From Definition 1, this completes the proof. □

The following theorem will give an absolute stability criterion for the Lure system (14) satisfying the conditions **C. 2** and (5).

Corollary 9. *The system (14) satisfying the conditions (3) and (5) is absolutely stable for given values of $h \geq 0$, $\mu_1, \mu_2 < 1$, $\tau_d < 1$, and $k_j > 0$ ($j = 1, 2, \ldots, m$), if there exist symmetric matrices $P \in \mathbb{R}^{5n \times 5n}$, $(P_a, P_b \in \mathbb{R}^{4n \times 4n})$, $(Q_a, Q_b, R_a, R_b \in \mathbb{R}^{n \times n})$, positive definite matrices $(Q_2 \in \mathbb{R}^{n \times n})$, $(R_1, R_2, Q_1(t), Q_2(t) \in \mathbb{R}^{2n \times 2n})$, $S = \mathrm{diag}\{s_1, s_2, \ldots, s_m\}$, $\Lambda = \mathrm{diag}\{\lambda_1, \lambda_2, \ldots, \lambda_m\}$ and any matrices $(U_{01}, U_{02} \in \mathbb{R}^{2n \times 2n}, \overline{U} \in \mathbb{R}^{(3n+m) \times n})$, $X_i \in \mathbb{R}^{5n \times 2n}$, $Y_i \in \mathbb{R}^{4n \times 2n}$ ($i = 1, \ldots, 4$) such that LMIs (15) and (16) and the following LMIs hold for $[h(t), \dot{h}(t)] \in \{[0, h] \times [\mu_1, \mu_2]\}$:*

$$l(0, \dot{h}(t), \alpha)$$

$$= \begin{bmatrix} \Pi_{[0,\dot{h}(t)]} & \Omega_{a[1,4]} & \overline{\mu}_1 \Omega_{a[1,2]} & h_d \Omega_{b[2,1,3]}^{[0]} & \Omega_{b[2,1,1]}^{[0]} \\ * & -h\overline{R}_b & 0 & 0 & 0 \\ * & * & -\overline{\mu}_1 h\overline{Q}_b & 0 & 0 \\ * & * & * & -3h_d h\overline{R}_a & 0 \\ * & * & * & * & -3h\overline{Q}_a \end{bmatrix}$$

$$< 0, \tag{45}$$

$$l(0, \dot{h}(t), 1 - \alpha)$$

$$= \begin{bmatrix} \Pi_{[0,\dot{h}(t)]} & \Omega_{a[1,4]} & \overline{\mu}_1 \Omega_{a[1,2]} & \Omega_{b[3,2,4]}^{[0]} & \overline{\mu}_1 \Omega_{b[3,2,2]}^{[0]} \\ * & -h\overline{R}_b & 0 & 0 & 0 \\ * & * & -\overline{\mu}_1 h\overline{Q}_b & 0 & 0 \\ * & * & * & -3h\overline{R}_b & 0 \\ * & * & * & * & -3\overline{\mu}_1 h\overline{Q}_b \end{bmatrix} \tag{46}$$

$$< 0,$$

$$l(h, \dot{h}(t), \alpha)$$

$$= \begin{bmatrix} \Pi_{[h,\dot{h}(t)]} & h_d \Omega_{a[1,3]} & \Omega_{a[1,1]} & h_d \Omega_{b[2,1,3]}^{[h]} & \Omega_{b[2,1,1]}^{[h]} \\ * & -h_d h\overline{R}_a & 0 & 0 & 0 \\ * & * & -h\overline{Q}_a & 0 & 0 \\ * & * & * & -3h_d h\overline{R}_a & 0 \\ * & * & * & * & -3h\overline{Q}_a \end{bmatrix} \tag{47}$$

$$< 0,$$

$$l(h, \dot{h}(t), 1 - \alpha)$$

$$= \begin{bmatrix} \Pi_{[h,\dot{h}(t)]} & h_d \Omega_{a[1,3]} & \Omega_{a[1,1]} & \Omega_{b[3,2,4]}^{[h]} & \overline{\mu}_1 \Omega_{b[3,2,2]}^{[h]} \\ * & -h_d h\overline{R}_a & 0 & 0 & 0 \\ * & * & -h\overline{Q}_a & 0 & 0 \\ * & * & * & -3h\overline{R}_b & 0 \\ * & * & * & * & -3\overline{\mu}_1 h\overline{Q}_b \end{bmatrix} \tag{48}$$

$$< 0,$$

$$-a_2 h^2 + l(0, \dot{h}(t), \alpha) < 0,$$

$$-a_2 h^2 + l(0, \dot{h}(t), 1 - \alpha) < 0, \tag{49}$$

where the related notations are defined in Box 4 of Appendix C.

Proof. The *LKF* (22) can be reduced to the following one by taking $h_1 = 0$, $h_2 = h$, $Q_1 = 0$, and $R_0 = 0$:

$$\widetilde{V}(t) = \sum_{i=1}^{4} \widetilde{V}_i(t) \tag{50}$$

with

$$\widetilde{V}_1(t) = \zeta^T(t) P \zeta(t) + h(t) \zeta_1^T(t) P_a \zeta_1(t)$$
$$+ (h - h(t)) \zeta_2^T(t) P_b \zeta_2(t),$$

$$\widetilde{V}_2(t) = \int_{t-h(t)}^{t} \gamma^T(s) Q_1(t) \gamma(s) \, ds$$
$$+ \int_{t-h}^{t-h(t)} \gamma^T(s) Q_2(t) \gamma(s) \, ds,$$

$$\widetilde{V}_3(t) = \int_{t-\tau(t)}^{t} \dot{x}^T(s) Q_2 \dot{x}(s) \, ds$$
$$+ 2 \sum_{i=1}^{m} \lambda_i \int_0^{\sigma_i} f_i(\sigma_i) \, d\sigma_i, \qquad (51)$$

$$\widetilde{V}_4(t) = \int_{t-h(t)}^{t} \int_{\theta}^{t} \gamma^T(s) \overline{Q}_a \gamma(s) \, ds \, d\theta$$
$$+ |\mu_1| \int_{t-h}^{t-h(t)} \int_{\theta}^{t-h(t)} \gamma^T(s) \overline{Q}_b \gamma(s) \, ds \, d\theta$$

$$\widetilde{V}_5(t) = \int_{t-h(t)}^{t} \int_{\theta}^{t} \gamma^T(s) R_1 \gamma(s) \, ds \, d\theta$$
$$+ \int_{t-h}^{t-h(t)} \int_{\theta}^{t-h(t)} \gamma^T(s) R_2 \gamma(s) \, ds \, d\theta,$$

where notations of several symbols and matrices can be found in Boxes 2 and 4 of Appendixes A and C. The proof of Corollary 9 is omitted because of the similarity to Theorem 8. □

Remark 10. Theorem 8 and Corollary 9 can reduce the conservatism of stability conditions based LMI via the LKFs (22) and (50) application. For nonintegral item $V_1(t)$, the matrices P, P_a, and P_b are just symmetrical, not always positive definite, and $Q_1(t)$ and $Q_2(t)$ of the single-integral item $V_2(t)$ are delay-dependent matrices which can also further improve the utilization of time delay and its derivative information. When proving $V(t) > 0$, we calculate $V_1(t)$ and $V_2(t)$ as a whole applying Lemma 2, which may expand the feasible regions of LMIs (15) and (16). When bounded the derivative of the LKFs, three additional zero equations (33)–(35) and Lemma 3 have been used to narrow the gap between the upper bound and the true value, which may be another contribution of reducing the conservatism of stability conditions.

Remark 11. It is worth noting that the delay-product-type item was introduced firstly by C. Zhang et al. [31, 44]; another novel LKF with delay-dependent matrix was constructed by W. Kwon et al. [33], where some improved stability conditions for linear systems with time-varying delay were given. C. Zhang and W. Kwon et al. pointed that the LKFs with delay-product-type item or delay-dependent matrix may reduce the conservatism of stability conditions based on the same inequality scaling technique. The LKFs (22) and (50) constructed in this paper, which combine the advantage of

the delay-product-type item and delay-dependent matrix, are more general than those given in [31, 33]. In fact, letting $Q_{11} = Q_{21} = 0$, $Q_{20} = \mathrm{diag}\{Q_2, 0\}$, $\overline{Q}_a = \overline{Q}_b = 0$, and $R_1 = R_2$, the LKF (50) can be reduced to the LKF (18) of [31]. And taking $P_a = P_b = 0$, $\overline{Q}_a = \overline{Q}_b = 0$, and $R_1 = R_2$ the LKF (50) can be reduced to the LKF (16) of [33]. However, the derivation method of [31, 33] cannot be applied directly. The positive definiteness of the LKF and negative definiteness of the LKF's derivative are proved in Theorem 8.

Remark 12. It is worth noting that in [33], to bound the integral item for $-\mu \leq \dot{h}(t) \leq \mu$, $(\mu > 0)$

$$-\dot{h}(t) \int_{t-h(t)}^{t} \gamma^T \overline{Q}_a \gamma \, ds - \dot{h}(t) \int_{t-h}^{t-h(t)} \gamma^T \overline{Q}_b \gamma \, ds \qquad (52)$$

via the QGFMI technique, the following addition zero equation was introduced

$$0 = \mu \int_{t-h(t)}^{t} \gamma^T(s) \overline{Q}_a \gamma(s) \, ds$$
$$- \mu \int_{t-h(t)}^{t} \gamma^T(s) \overline{Q}_a \gamma(s) \, ds$$
$$+ \mu \int_{t-h}^{t-h(t)} \gamma^T(s) \overline{Q}_b \gamma(s) \, ds \qquad (53)$$
$$- \mu \int_{t-h}^{t-h(t)} \gamma^T(s) \overline{Q}_b \gamma(s) \, ds.$$

Then, the above integral item can be rewritten as the following form:

$$\widetilde{\varphi} = -\left(\mu + \dot{h}(t)\right) \int_{t-h(t)}^{t} \gamma^T \overline{Q}_a \gamma \, ds$$
$$- \left(\mu + \dot{h}(t)\right) \int_{t-h}^{t-h(t)} \gamma^T \overline{Q}_b \gamma \, ds \qquad (54)$$
$$+ \mu \int_{t-h(t)}^{t} \gamma^T \overline{Q}_a \gamma \, ds + \mu \int_{t-h}^{t-h(t)} \gamma^T \overline{Q}_b \gamma \, ds.$$

The first two items on the right can be bounded via the QGFMI technique like (39) of this paper; however, there are fewer proper techniques for obtaining a tight upper bound of the integral terms $\mu \int_{t-h(t)}^{t} \gamma^T(s) \overline{Q}_a \gamma(s) ds$ and $\mu \int_{t-h}^{t-h(t)} \gamma^T(s) \overline{Q}_b \gamma(s) ds$ due to their positive definiteness. Thus, to avoid introducing the two positive define integral terms, we give the modified LKF (22) with a double integral item $V_4(t)$.

Remark 13. In addition, the main result of [33] was not LMI due to the terms $h^2(t)$ even $h^3(t)$. In this paper, all matrices inequations of Theorem 8 and Corollary 9 are LMI via Lemma 4 application, which can be solved easily by using Matlab LMI-toolbox. Moreover, the double integral items $V_4(t)$ and $V_5(t)$ of the LKF (22) divide the time-delay interval $[h_1, h_2]$ into two subintervals, that is, $[h_1, h(t)]$ and $[h(t), h_2]$,

$$h_d = 1 - \dot{h}(t), \ \gamma^T(s) = \left[x^T(s) \ \dot{x}^T(s) \right], \ \overline{\mu}_1 = |\mu_1| + \dot{h}(t),$$

$$v_1(t) = \int_{t-h(t)}^t \frac{x^T(s)}{h(t)} ds, \ v_2(t) = \int_{t-h}^{t-h(t)} \frac{x^T(s)}{h-h(t)} ds,$$

$$\omega_1(t) = h(t) v_1(t), \ \omega_2(t) = (h - h(t)) v_2(t), \ \zeta^T(t) = \left[x^T(t) \ x^T(t - h(t)) \ x^T(t - h) \ \omega_1(t) \ \omega_2(t) \right],$$

$$\zeta_1^T(t) = \left[x^T(t) \ x^T(t - h(t)) \ x^T(t - h) \ v_1(t) \right], \ \zeta_2^T(t) = \left[x^T(t) \ x^T(t - h(t)) \ x^T(t - h) \ v_2(t) \right],$$

$$\Delta^T(t) = \left[\omega_1^T(t) \ x^T(t) - x^T(t - h(t)) \ \omega_2^T(t) \ x^T(t - h(t)) - x^T(t - h) \right],$$

$$\xi^T(t) = [x^T(t) \ x^T(t - h(t)) \ x^T(t - h) \ \dot{x}^T(t) \ \dot{x}^T(t - h(t)) \ \dot{x}^T(t - h) \ v_1(t) \ v_2(t),$$

$$\int_{t-h(t)}^t \int_u^t \left(x^T(s)/h(t) \right) du \, ds \ \int_{t-h}^{t-h(t)} \int_u^{t-h(t)} \left(x^T(s)/(h - h(t)) \right) du \, ds \ \dot{x}^T(t - \tau(t)) \ f^T(\sigma(t))],$$

$$\eta_1(t) = \begin{bmatrix} \omega_1(t) \\ x(t) - x(t - h(t)) \end{bmatrix}, \ \eta_2(t) = \begin{bmatrix} \omega_2(t) \\ x(t - h(t)) - x(t - h) \end{bmatrix}.$$

Box 2: Notations of several symbols and matrices in Corollaries 9 and 15.

instead of using the item $\int_{t-h}^t \gamma^T(s) R \gamma(s) ds$ directly, which further make full use of the information of time-varying delays $h(t) - h_1$, $h_2 - h(t)$ and their derivative $\dot{h}(t)$. Thus, the QGFMI technique can be used fully in each subinterval, which can further reduce the conservatism of the stability conditions.

3.2. Robustly Absolute Stability Criteria for Uncertain Form.
Next, we extend the obtained absolute stability conditions to robustly absolute stability problem for the uncertain neutral-type Lur'e system (1) with time-varying parameter uncertainties satisfying (7) and (8).

Theorem 14. *The system (1) satisfying the conditions (2), (5), (7), and (8) is robustly absolutely stable for given values of $h_2 \geq h_1 \geq 0$, $\mu_1, \mu_2 < 1$, $\tau_d < 1$, and $k_j > 0$ ($j = 1, 2, \ldots, m$), if there exist symmetric matrices $P \in \mathbb{R}^{7n \times 7n}$, $(P_a, P_b \in \mathbb{R}^{5n \times 5n})$, $(Q_a, Q_b, R_{0a}, R_a, R_b \in \mathbb{R}^{n \times n})$, positive definite matrices $(Q_2 \in \mathbb{R}^{n \times n})$, $(Q_1, R_0, R_1, R_2, Q_1(t), Q_2(t) \in \mathbb{R}^{2n \times 2n})$, $S = \mathrm{diag}\{s_1, s_2, \ldots, s_m\}$, $\Lambda = \mathrm{diag}\{\lambda_1, \lambda_2, \ldots, \lambda_m\}$, any matrices $(U_{01}, U_{02} \in \mathbb{R}^{2n \times 2n}, \overline{U} \in \mathbb{R}^{(3n+m) \times n})$, $X_0 \in \mathbb{R}^{3n \times 2n}$, $X_i \in \mathbb{R}^{5n \times 2n}$, $Y_\lambda \in \mathbb{R}^{4n \times 2n}$ ($i = 1, \ldots, 4; \lambda = 0, \ldots, 4$) and $\varepsilon > 0$ such that LMIs (15)-(16) and the following LMIs hold for $[h(t), \dot{h}(t)] \in \{[h_1, h_2] \times [\mu_1, \mu_2]\}$:*

$$J_1 l \left(h_1, \dot{h}(t), \alpha \right) J_1^T + \varepsilon J_2 \Phi_1^T \Phi_1 J_2^T + \mathrm{sym} \left\{ J_2 \Phi_2^T J_3^T \right\}$$
$$- \varepsilon J_3 J_3^T < 0, \tag{55}$$

$$J_1 l \left(h_1, \dot{h}(t), 1 - \alpha \right) J_1^T + \varepsilon J_2 \Phi_1^T \Phi_1 J_2^T$$
$$+ \mathrm{sym} \left\{ J_2 \Phi_2^T J_3^T \right\} - \varepsilon J_3 J_3^T < 0, \tag{56}$$

$$J_1 l \left(h_2, \dot{h}(t), \alpha \right) J_1^T + \varepsilon J_2 \Phi_1^T \Phi_1 J_2^T + \mathrm{sym} \left\{ J_2 \Phi_2^T J_3^T \right\}$$
$$- \varepsilon J_3 J_3^T < 0, \tag{57}$$

$$J_1 l \left(h_2, \dot{h}(t), 1 - \alpha \right) J_1^T + \varepsilon J_2 \Phi_1^T \Phi_1 J_2^T$$
$$+ \mathrm{sym} \left\{ J_2 \Phi_2^T J_3^T \right\} - \varepsilon J_3 J_3^T < 0, \tag{58}$$

$$- a_2 h_{12}^2 + J_1 l \left(h_1, \dot{h}(t), \alpha \right) J_1^T + \varepsilon J_2 \Phi_1^T \Phi_1 J_2^T$$
$$+ \mathrm{sym} \left\{ J_2 \Phi_2^T J_3^T \right\} - \varepsilon J_3 J_3^T < 0, \tag{59}$$

$$- a_2 h_{12}^2 + J_1 l \left(h_1, \dot{h}(t), 1 - \alpha \right) J_1^T + \varepsilon J_2 \Phi_1^T \Phi_1 J_2^T$$
$$+ \mathrm{sym} \left\{ J_2 \Phi_2^T J_3^T \right\} - \varepsilon J_3 J_3^T < 0, \tag{60}$$

where

$$\Phi_1 = \left[e_1 E_a^T + e_2 E_{a1}^T + e_{16} E_b^T \right]^T,$$

$$\Phi_2 = \left[e_1 U_1 D + e_5 U_2 D + e_{15} U_3 D + e_{16} U_4 D \right]^T,$$

$$J_1^T = \left[I \ I \ I \ I \ I \ I \ I \ 0 \right], \tag{61}$$

$$J_2^T = \left[I \ 0 \ 0 \ 0 \ 0 \ 0 \ 0 \ 0 \right],$$

$$J_3^T = \left[0 \ 0 \ 0 \ 0 \ 0 \ 0 \ 0 \ I \right].$$

Proof. If we replace A, A_1, and B in LMIs (17)–(21) with $A + DF(t)E_a$, $A_1 + DF(t)E_{a1}$, $B + DF(t)E_b$, respectively, Theorem 14 can be proved based on Lemma 6 easily. $\square$

The following corollary will give the robustly absolute stability criterion for the Lur'e system (1) satisfying the condition **C. 2**.

Corollary 15. *System (1) satisfying the conditions (3) and (5), (7), and (8) is robustly absolutely stable for given values of $h \geq 0$, $\mu_1, \mu_2 < 1$, $\tau_d < 1$, and $k_j > 0$ ($j = 1, 2, \ldots, m$), if there exist symmetric matrices $P \in \mathbb{R}^{5n \times 5n}$, $(P_a, P_b \in \mathbb{R}^{4n \times 4n})$, $(Q_a, Q_b, R_a, R_b \in \mathbb{R}^{n \times n})$, positive definite matrices $(Q_2 \in \mathbb{R}^{n \times n})$, $(R_1, R_2, Q_1(t), Q_2(t) \in \mathbb{R}^{2n \times 2n})$, $S = \mathrm{diag}\{s_1, s_2, \ldots, s_m\}$, $\Lambda = \mathrm{diag}\{\lambda_1, \lambda_2, \ldots, \lambda_m\}$, any matrices $(U_{01}, U_{02} \in \mathbb{R}^{2n \times 2n}, \overline{U} \in \mathbb{R}^{(3n+m) \times n})$, $X_i \in \mathbb{R}^{5n \times 2n}$, $Y_i \in \mathbb{R}^{4n \times 2n}$ ($i = 1, \ldots, 4$) and $\varepsilon > 0$ such that LMIs (15)-(16) and the following LMIs hold for $[h(t), \dot{h}(t)] \in \{[h_1, h_2] \times [\mu_1, \mu_2]\}$:*

$$\widetilde{J}_1 l \left(0, \dot{h}(t), \alpha \right) \widetilde{J}_1^T + \varepsilon \widetilde{J}_2 \widetilde{\Phi}_1^T \widetilde{\Phi}_1 \widetilde{J}_2^T + \mathrm{sym} \left\{ \widetilde{J}_2 \widetilde{\Phi}_2^T \widetilde{J}_3^T \right\}$$
$$- \varepsilon \widetilde{J}_3 \widetilde{J}_3^T < 0, \tag{62}$$

$$\tilde{J}_1 l\left(0,\dot{h}(t),1-\alpha\right)\tilde{J}_1^T + \varepsilon\tilde{J}_2\widetilde{\Phi}_1^T\widetilde{\Phi}_1\tilde{J}_2^T + \mathrm{sym}\left\{\tilde{J}_2\widetilde{\Phi}_2^T\tilde{J}_3^T\right\}$$
$$- \varepsilon\tilde{J}_3\tilde{J}_3^T < 0, \tag{63}$$

$$\tilde{J}_1 l\left(h,\dot{h}(t),\alpha\right)\tilde{J}_1^T + \varepsilon\tilde{J}_2\widetilde{\Phi}_1^T\widetilde{\Phi}_1\tilde{J}_2^T + \mathrm{sym}\left\{\tilde{J}_2\widetilde{\Phi}_2^T\tilde{J}_3^T\right\}$$
$$- \varepsilon\tilde{J}_3\tilde{J}_3^T < 0, \tag{64}$$

$$\tilde{J}_1 l\left(h,\dot{h}(t),1-\alpha\right)\tilde{J}_1^T + \varepsilon\tilde{J}_2\widetilde{\Phi}_1^T\widetilde{\Phi}_1\tilde{J}_2^T + \mathrm{sym}\left\{\tilde{J}_2\widetilde{\Phi}_2^T\tilde{J}_3^T\right\}$$
$$- \varepsilon\tilde{J}_3\tilde{J}_3^T < 0, \tag{65}$$

$$- a_2 h^2 + \tilde{J}_1 l\left(0,\dot{h}(t),\alpha\right)\tilde{J}_1^T + \varepsilon\tilde{J}_2\widetilde{\Phi}_1^T\widetilde{\Phi}_1\tilde{J}_2^T$$
$$+ \mathrm{sym}\left\{\tilde{J}_2\widetilde{\Phi}_2^T\tilde{J}_3^T\right\} - \varepsilon\tilde{J}_3\tilde{J}_3^T < 0, \tag{66}$$

$$- a_2 h^2 + \tilde{J}_1 l\left(0,\dot{h}(t),1-\alpha\right)\tilde{J}_1^T + \varepsilon\tilde{J}_2\widetilde{\Phi}_1^T\widetilde{\Phi}_1\tilde{J}_2^T$$
$$+ \mathrm{sym}\left\{\tilde{J}_2\widetilde{\Phi}_2^T\tilde{J}_3^T\right\} - \varepsilon\tilde{J}_3\tilde{J}_3^T < 0, \tag{67}$$

where

$$\widetilde{\Phi}_1 = \left[e_1 E_a^T + e_2 E_{a1}^T + e_{12} E_b^T\right]^T,$$
$$\widetilde{\Phi}_2 = \left[e_1 U_1 D + e_4 U_2 D + e_{11} U_3 D + e_{12} U_4 D\right]^T,$$
$$\tilde{J}_1^T = \left[I \ \ I \ \ I \ \ I \ \ I \ \ 0\right], \tag{68}$$
$$\tilde{J}_2^T = \left[I \ \ 0 \ \ 0 \ \ 0 \ \ 0 \ \ 0\right],$$
$$\tilde{J}_3^T = \left[0 \ \ 0 \ \ 0 \ \ 0 \ \ 0 \ \ I\right].$$

Remark 16. If the nonlinear function $f(\sigma)$ in the feedback path satisfies the infinite sector conditions (6), for any $s_i \geq 0$, $i = 1, 2, \ldots, m$, it follows from (6) that

$$s_i f_i\left(\sigma_i\right) h_i^T x(t) \geq 0, \tag{69}$$

which is equivalent to

$$2x^T(t) HSf(\sigma) \geq 0, \tag{70}$$

where $S = \mathrm{diag}\{s_1, s_2, \ldots, s_m\}$.

Therefore, the corresponding absolute and robustly absolute stability criteria can be obtained by replacing the matrix Θ_1 of Theorems 8 and 14 and Corollaries 9 and 15 with $\Theta_2 = e_1 HSe_{16}^T$ and $\widetilde{\Theta}_2 = e_1 HSe_{12}^T$, respectively.

Remark 17. For one special case, in the absence of the nonlinear function, that is, in case of $B = 0$, the system (1) is simply written as the following linear neutral system

$$\dot{x}(t) - C\dot{x}(t - \tau(t)) = (A + \Delta A) x(t)$$
$$+ \left(A_1 + \Delta A_1\right) x(t - h(t)),$$
$$x(s) = \varphi(s), \tag{71}$$
$$\dot{x}(s) = \dot{\varphi}(s),$$

$$s \in \left[-\max\left(h_2, \tau\right), 0\right], \ h(t) \in \mathbf{C.1}$$
$$s \in \left[-\max\left(h, \tau\right), 0\right], \ h(t) \in \mathbf{C.2}, \tag{72}$$

and for another special case, in the absence of the nonlinear function and neutral-type item, that is, in case of $B = 0$ and $C = 0$, the system (1) is simply written as the following linear time-delayed system:

$$\dot{x}(t) = (A + \Delta A) x(t) + \left(A_1 + \Delta A_1\right) x(t - h(t)),$$
$$x(s) = \varphi(s), \tag{73}$$
$$s \in \left[-\max\left(h_2, \tau\right), 0\right], \ h(t) \in \mathbf{C.1}$$
$$s \in \left[-\max\left(h, \tau\right), 0\right], \ h(t) \in \mathbf{C.2}.$$

Obviously, take Theorem 8 as an example. Only letting $\Theta_1 = 0, \Pi_4 = [e_1 U_1 + e_5 U_2 + e_{15} U_3]$ and $\Pi_5 = [Ae_1^T + A_1 e_2^T + Ce_{15}^T - e_5^T]$, the stability criteria proposed in this paper are also applied to this linear neutral system (71) with time-varying delays; taking $\Theta_1 = 0, Q_2 = 0, \Pi_4 = [e_1 U_1 + e_5 U_2]$ and $\Pi_5 = [Ae_1^T + A_1 e_2^T]$, the stability criteria proposed in this paper are also applied to this linear system (73) with time-varying delays. We will not elaborate here due to the limited space available. However, some results of detailed comparisons will be given in the next section directly.

Remark 18. It is worth pointing out that in this paper, the upper and lower bounds constraints of the time-delay derivative are $\mu_1 \leq \dot{h}(t) \leq \mu_2$, where $\tau_d < 1, \mu_2 < 1$ due to the diagonal entry $-(1 - \dot{\tau}(t))Q_2, -(1 - \dot{h}(t))\dot{x}^T(t - h(t))(Q_1(t) - Q_2(t))\dot{x}(t - h(t))$ in $\Pi_{[h(t),\dot{h}(t)]}$, and $-(1 - \dot{h}(t))\int_{t-h(t)}^t \gamma^T(s)R_1\gamma(s)ds$ in $\dot{V}_5(t)$. Similar to Remark 5 of [45], one can establish a stability criterion for system (1) in the case $\tau_d \geq 1$ and $\mu_2 \geq 1$ if $\xi(t), \zeta(t), \zeta_1(t), \zeta_2(t), \gamma(s)$ and $V_5(t)$ are replaced with

$$\bar{\xi}^T(t)$$
$$= \left[x^T(t) \ x^T(t - h_1) \ x^T(t - h(t)) \ x^T(t - h_2) \ \dot{x}^T(t) \ \dot{x}^T(t - h_1) \ \dot{x}^T(t - h_2) \ v_1(t) \ v_2(t) \ v_3(t) \ \int_{t-h_1}^t \int_u^t \frac{x^T(s)}{h_1}du\,ds \ \int_{t-h(t)}^{t-h_1} \int_u^{t-h_1} \frac{x^T(s)}{h_{1t}}du\,ds \ \int_{t-h_2}^{t-h(t)} \int_u^{t-h(t)} \frac{x^T(s)}{h_{2t}}du\,ds \ f^T(\sigma(t))\right],$$
$$\bar{\zeta}^T(t) = \left[x^T(t) \ x^T(t - h_1) \ x^T(t - h_2) \ \omega_1(t) \ \omega_2(t) \ \omega_3(t)\right],$$
$$\bar{\zeta}_1^T(t) = \left[x^T(t) \ x^T(t - h_1) \ x^T(t - h_2) \ v_2(t)\right],$$
$$\bar{\zeta}_2^T(t) = \left[x^T(t) \ x^T(t - h_1) \ x^T(t - h_2) \ v_3(t)\right],$$
$$\bar{\gamma}^T(s) = x^T(s),$$
$$Q_2 = 0,$$
$$\bar{V}_5(t) = \int_{t-h_1}^t \int_\theta^{t-h_1} x^T(s) R_0 x(s)\,ds\,d\theta + \int_{t-h_2}^{t-h_1} \int_\theta^{t-h_1} x^T(s) R_1 x(s)\,ds\,d\theta. \tag{74}$$

Due to page limitation, this result is omitted.

4. Numerical Examples

In this section, we give three types of examples, including the Lur'e system, the linear neutral system, and two linear systems, to show the effectiveness of the criteria proposed in this paper. Moreover, the conservatism of the criteria is checked based on the calculated maximal admissible delay upper bounds (MADUBs). And the index of the number of decision variables (NoVs) is applied to show the complexity of criteria. The stability criteria proposed in this paper are just dependent on τ_d, h, μ_1, and μ_2, however, independent on τ and $\tau(t)$. So, only τ_d of the information of the neutral-type time delay $\tau(t)$ is given for Examples 1 and 3. For the sake of simplicity, let $-\mu_1 = \mu_2 = \mu$.

Example 1. Consider the nominal neutral-type Lur'e system (14) with the time-varying delays satisfying **C.2** and the nonlinearity satisfying (6), and the system parameters are described as

$$
A = \begin{bmatrix} -2 & 0.5 \\ 0 & -1 \end{bmatrix},
$$

$$
A_1 = \begin{pmatrix} 1 & 0.4 \\ 0.4 & -1 \end{pmatrix},
$$

$$
B = \begin{pmatrix} -0.5 \\ -0.75 \end{pmatrix}, \quad (75)
$$

$$
C = \begin{pmatrix} 0.2 & 0.1 \\ 0.1 & 0.2 \end{pmatrix},
$$

$$
H = \begin{pmatrix} 0.2 \\ 0.6 \end{pmatrix}.
$$

Let the nonlinearity $f(\sigma(t)) = \sigma^3(t)$, where $\sigma(t) = H^T x(t) = 0.2x_1(t) + 0.6x_2(t)$. Then, it follows from the infinite sector condition (6) and $f_i(\sigma_i(t))/\sigma_i(t) = f(\sigma_i(t))/\sigma(t) = \sigma^2(t) > 0$, that is $f_i(\sigma_i(t)) \in K_{[0,\infty)}$. Under the condition **C. 2**, in Table 1, the MADUBs h of the Lur'e system (14) for $\tau_d = 0.1$ and different μ by using Remark 16 and recent methods in [26, 27, 29, 34] are compared. From the table, notwithstanding the NoVs of our criteria are bigger than those of the criteria [26, 27, 29, 34], only [29] is less conservative than Remark 16 under $\mu = 0.2$. However our results become better and better with the increasing of μ. Figure 1 displays the responses of system states $x(t)$ for $h(t) = 2.8490/2 + (2.8490/2)\sin(0.8t/2.8490)$, $\tau(t) = 0.5 + |\sin(0.1t)|$ and initial condition $x(0) = [0.2 \quad -0.2]^T$. It is possible to see that, for this realization, the trajectory converges to the origin, as expected.

Remark 2. The MADUBs h of the Lur'e system (14) for $\tau_d = 0.1$ and different μ by using our results are less than those of [21] because the slope restrictions for nonlinearity and the lower bound of the derivative of the neutral-type delay $\dot{\tau}(t)$ were considered in [21], where these restrictions are more strict than those of this paper. Thus, the related results of [21] were not compared with the ones of this paper.
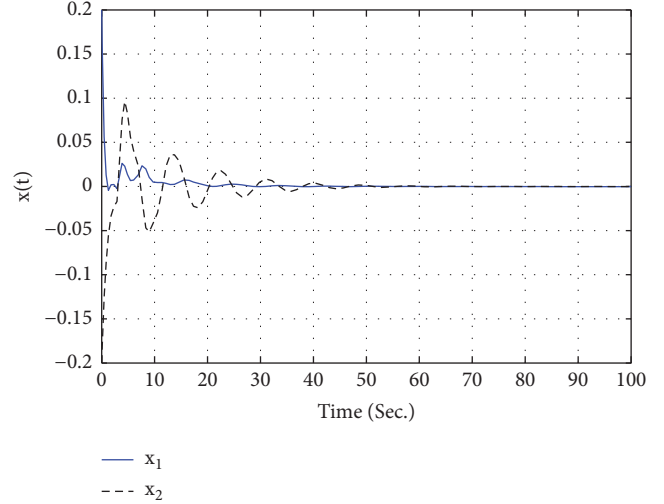
FIGURE 1: The state responses for Example 1.

In addition, the construction of the LKF with delay-dependent matrices is the main reason to reduce the conservatism of the stability criterion in [29], and another one is that the lower bound of the delay derivative is also involved in this paper, which is not mentioned in [29].

Example 2. Consider the following Chua's circuit

$$
\begin{aligned}
\dot{x} &= \alpha(y - g(x)) \\
\dot{y} &= x - y + z \quad (76) \\
\dot{z} &= -\beta y,
\end{aligned}
$$

where $m_0 = -1/7$, $m_1 = 2/7$, $\alpha = 9$, $\beta = 14.28$, and $c = 1$, and the nonlinear function $g(x)$ is given by $g(x) = m_1\theta_1 + 0.5(m_0 - m_1)(|x + c| - |x - c|)$. This Chua's circuit can be expressed as a Lur'e-type system.

In [19], a master-slave synchronization scheme through a time-delayed state error feedback control is devised for the Chua's circuit (76), which is given as

$$
Master: \begin{cases} \dot{x}(t) = Ax(t) + Bf(Cx(t)) \\ p(t) = Wx(t), \end{cases}
$$

$$
Slave: \begin{cases} \dot{y}(t) = Ay(t) + Bf(Cy(t)) + u(t) \\ q(t) = Wy(t), \end{cases} \quad (77)
$$

$$
Controller: \; u(t) = -K_a(x(t) - y(t))
$$

$$
+ K_b(p(t - h(t)) - q(t - h(t))),
$$

where $f(\theta) = 0.5(|\theta + 1| - |\theta - 1|) \in [0, 1]$, $C = W = [1 \quad 0 \quad 0]$ and

TABLE 1: MADUBs h for different μ (Example 1).

τ_d	Methods\\μ	0.2	0.4	0.6	0.8	NoVs
	[26]	2.9962	2.1316	1.7138	1.3204	75
	[27]	3.1743	2.1789	1.7467	1.7153	96
0.1	[34]	3.4880	2.3787	1.8062	1.4625	93
	[29]	3.8557	2.8490	2.4014	2.2130	117
	Remark 16	3.6076	2.8490	2.5501	2.4526	705

TABLE 2: MADUBs h for different μ (Example 2).

Methods\\μ	0	0.3	0.6	0.9	NoVs
[19]	0.1622	0.1591	0.1566	0.1527	10
[23]	0.1745	0.1698	0.1698	0.1698	160
[24]	0.1747	0.1710	0.1703	0.1703	140
[27]	0.1771	0.1721	0.1715	0.1715	194
[21]	0.1894	0.1894	0.1894	0.1893	627
[30]	0.2638	0.2578	0.2540	0.2510	809
Corollary 9	0.2707	0.2700	0.2545	0.2544	1548

$$
A = \begin{bmatrix} -\alpha m_1 & \alpha & 0 \\ 1 & -1 & 1 \\ 0 & -\beta & 0 \end{bmatrix},
$$

$$
B = \begin{bmatrix} -\alpha\left(m_0 - m_1\right) \\ 0 \\ 0 \end{bmatrix}. \tag{78}
$$

Letting $e = x - y$, then the resultant error system is given by

$$
\dot{e}(t) = \left(A + K_a\right)e(t) - K_b We(t - h(t)) + B\varphi\left(Ce(t)\right). \tag{79}
$$

Suppose the synchronization controller gains are designed by [18]

$$
K_a = \begin{bmatrix} -1 & 0 & 0 \\ 0 & -1 & 0 \\ 0 & 0 & -1 \end{bmatrix},
$$

$$
K_b = \begin{bmatrix} 6.0029 \\ 1.3367 \\ -2.1264 \end{bmatrix}. \tag{80}
$$

In Table 2, we calculate the MADUBs h of the error system (79) for different μ and the condition **C. 2** by using our results and methods in [18, 19, 21, 23, 27, 30] are compared. From the table, it is found that notwithstanding the NoVs of Corollary 9 are bigger than those of the criteria [19, 23, 24, 27], the MADUBs computed by Corollary 9 are larger. Compared with the criteria in [21, 30], Corollary 9 obtains less conservative MADUBs but requires less computation complexity. Moreover, for $h(t) = 0.2707$ and initial condition $e(0) = [-0.1 \ 0.4 \ -0.3]^T$, Figure 2 depicts the error state responses for the error system (79) under control of the
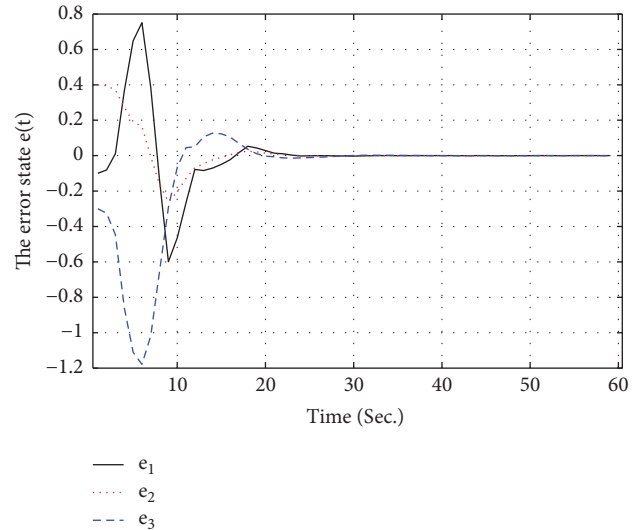
FIGURE 2: The error state responses for Example 2.

synchronization controller. Thus, one can see that the error system is asymptotically stable for the time-varying delay $h(t)$ less than 0.2707.

Remark 3. In Example 2, the purpose of this paper is to enlarge the MADUBs under the same controller to [19]. At this point, the error system (79) can be seen as a new Lure system within the given gain matrices $A + K_a$, $-K_b W$ and B proposed by [19]. The MADUBs of are calculated by solving the LMIs in Theorem 8. For an example, an MADUB $h = 0.2700$ is obtained for $\mu = 0.3$ by Theorem 8, then the stability of the error system (79) must be guaranteed by Theorem 8 under the same controller to [19] for $0 \leq h(t) \leq h$ and $|\mu| \leq 0.3$. In other words, this paper does not design any controllers, but analyzes the stability. The same controller gains of [19] are seen as the known system matrices of the error system

TABLE 3: MADUBs h for $\tau_d = 0.6$ and different μ_1 and μ_2 (Example 3).

μ_1	Methods\μ_2	0.5	0.9	NoVs
	[25]	1.5572	1.5572	10
Ignore μ_1	[27]	1.6635	1.5742	160
	[35]	1.5812	1.5745	140
-0.5	[28]	1.8763	1.7352	120
	Remark 17	2.0555	1.9357	518
-0.2	[28]	1.8780	1.7453	120
	Remark 17	2.0671	1.9558	518

TABLE 4: MADUBs h for different μ (Example 4).

Methods\μ	0.1	0.2	0.5	0.8	NoVs
[36]	6.6103	4.0034	1.6875	1.0287	$23n^2 + 4n$
[37]	7.1672	4.5179	2.4158	1.8384	$142n^2 + 18n$
[38]	7.1765	4.5438	2.4963	1.9225	$114n^2 + 18n$
[39]	7.2030	4.5126	2.3860	1.8476	$203n^2 + 9n$
[40]	7.1905	4.5275	2.4473	1.8562	$70n^2 + 12n$
[30]	7.2734	4.6213	2.6505	2.0612	$185.5n^2 + 21.5n$
[3]	7.4001	4.7954	2.7175	2.0894	$108n^2 + 12n$
[33]	8.6565	5.8907	3.1754	2.3953	$91.5n^2 + 4.5n$
Remark 17	8.9647	7.1866	4.9390	3.8477	$165.5n^2 + 19.5n$
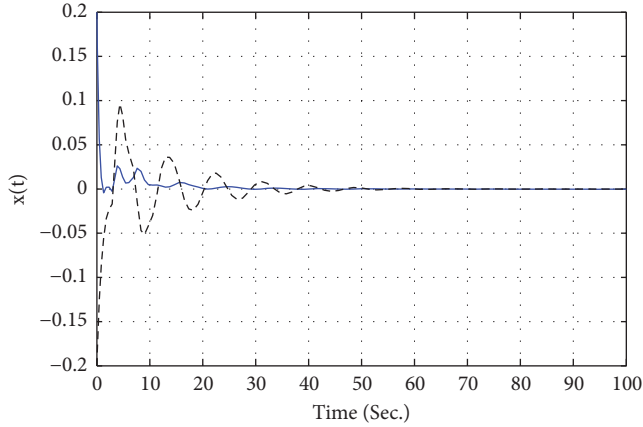
FIGURE 3: The state responses for Example 3.

(79). Therefore, the controller gains obtained in [19] will also stabilize the system considered in Example 2 under a bounds of $h(t)$ obtained by Theorem 8.

Example 3. Consider the linear neutral-type system (71) with the time-varying delays satisfying **C.2**, and the system parameters are described as

$$A = \begin{pmatrix} -1 & 1 \\ 0 & -1 \end{pmatrix},$$

$$A_1 = \begin{pmatrix} 0.5 & 0 \\ 0.5 & -0.5 \end{pmatrix},$$

$$C = \begin{pmatrix} 0.4 & 0 \\ 0 & 0.4 \end{pmatrix},$$

$$D = \text{diag}\{1, 1\},$$

$$E_a = \text{diag}\{0.05, 0.05\},$$

$$E_{a1} = \text{diag}\{0.1, 0.1\}. \tag{81}$$

Under the condition **C. 2**, in Table 3, we calculate the MADUBs h of the linear neutral-type system (71) for $\tau_d = 0.6$ and different μ_1, μ_2 by using Remark 16 and methods in [25, 27, 28, 35] are compared. From the table, it is found that notwithstanding the NoVs of our criteria are bigger than those of the criteria [25, 27, 28, 35], the MADUBs computed by our criteria are larger. Figure 3 displays the responses of system states $x(t)$ for $h(t) = 2.0555/2 + (2.0555/2)\sin(t/2.0555)$, $\tau(t) = 1.2|\sin(0.5t)|$ and initial condition $x(0) = [-0.2 \quad 0.2]^T$. It is possible to see that, for this realization, the trajectory converges to the origin, as expected.

Example 4. Consider the linear systems (73) with time-varying delays, where the system parameters are described as

$$A = \begin{bmatrix} 0 & 1 \\ -1 & -2 \end{bmatrix},$$

$$A_1 = \begin{bmatrix} 0 & 0 \\ -1 & 1 \end{bmatrix}. \tag{82}$$

As a special case pointed out by Remark 16, Corollary 9 removed some redundant terms which can be used to check the stability of the linear systems with time-varying delays. In order to make a comparison with some existing stability criteria, the MADUBs under the condition **C. 2** are listed in Table 4, which shows that notwithstanding the NoVs of Corollary 9 are bigger than those of the criteria [3, 33, 36, 38, 40], the MADUBs computed by Corollary 9 are larger. Compared with the criteria in [30, 37, 39], Corollary 9 obtains less conservative MADUBs but requires less computation complexity.

5. Conclusion

In this paper, some improved absolute and robustly absolute stability criteria are proposed for the uncertain neutral-type Lurė systems with mixed time-varying delays and sector-bounded nonlinearities via a novel LKF combining the delay-product-type function and the delay-dependent matrix. An effective technique, QGFMI, is applied to further reduce the conservatism of the proposed criteria from some existing results. Finally, some numerical examples are used to illustrate the effectiveness of the proposed approaches.

Appendix

A. Boxes 1 and 2

See Boxes 1 and 2.

B. Box 3

$$\Omega_{1[h(t)]} = \begin{bmatrix} EP_aE^T & 0 \\ 0 & 0 \end{bmatrix} + Q_1(t),$$

$$\Omega_{2[h(t)]} = \begin{bmatrix} EP_bE^T & 0 \\ 0 & 0 \end{bmatrix} + Q_2(t),$$

$$\Omega_{3[h(t)]} = \begin{bmatrix} (2-\alpha)\,\Omega_{1[h(t)]} & (1-\alpha)\,U_{01} + \alpha U_{02} \\ * & (1+\alpha)\,\Omega_{2[h(t)]} \end{bmatrix},$$

$$\Omega_{4[h(t)]} = P + \begin{bmatrix} \tilde{e}_1^T \\ \tilde{e}_2^T \\ \tilde{e}_3^T \\ \tilde{e}_4^T \\ 0 \end{bmatrix}^T [h_{1t}P_a + h_{2t}P_b] \begin{bmatrix} \tilde{e}_1^T \\ \tilde{e}_2^T \\ \tilde{e}_3^T \\ \tilde{e}_4^T \\ 0 \end{bmatrix}$$

$$+ \text{sym} \left\{ \begin{bmatrix} \tilde{e}_1^T \\ \tilde{e}_2^T \\ \tilde{e}_3^T \\ \tilde{e}_4^T \\ 0 \end{bmatrix}^T \right.$$

$$\left. \cdot \left(P_a \begin{bmatrix} 0 \\ 0 \\ 0 \\ 0 \\ \tilde{e}_6^T \end{bmatrix} + P_b \begin{bmatrix} 0 \\ 0 \\ 0 \\ 0 \\ \tilde{e}_7^T \end{bmatrix} \right) \right\},$$

$$\alpha = \frac{h(t) - h_1}{h_{12}},$$

$$J^T = [E_1 \quad E_2],$$

$$E_1 = [\tilde{e}_6 \ \tilde{e}_2 - \tilde{e}_3]$$

$$E_2 = [\tilde{e}_7 \ \tilde{e}_3 - \tilde{e}_4],$$

$$\Pi_{[h(t),\dot{h}(t)]} = \text{sym}\left\{\Pi_{1[h(t),\dot{h}(t)]} + \Pi_{3[h(t),\dot{h}(t)]}\right\}$$

$$\quad + \Pi_{2[h(t),\dot{h}(t)]},$$

$$\Pi_{1[h(t),\dot{h}(t)]} = \Gamma_{[h(t)]}P\Psi_{[h(t)]}^T$$

$$+ [e_1 \ e_2 \ e_3 \ e_4 \ e_{10}]\,P_a\,[h_{1t}e_5 \ h_{1t}e_6 \ h_{1t}h_de_7 \ h_{1t}e_8 \ e_2$$

$$- h_de_3 - \dot{h}(t)\,e_{10}]^T$$

$$+ [e_1 \ e_2 \ e_3 \ e_4 \ e_{11}]\,P_b\,[h_{2t}e_5 \ h_{2t}e_6 \ h_{2t}h_de_7 \ h_{2t}e_8 \ h_de_3$$

$$- e_4 + \dot{h}(t)\,e_{11}]^T + \Theta_1 + \widetilde{\Theta}_1 + \Pi_4\Pi_5,$$

$$\Pi_{2[h(t),\dot{h}(t)]} = [e_1 \ e_5]\,[Q_1 + h_1R_0]\,[e_1 \ e_5]^T$$

$$+ [e_2 \ e_6]\,[Q_1(t) - Q_1]\,[e_2 \ e_6]^T$$

$$+ h_d\,[e_3 \ e_7]\,[Q_2(t) - Q_1(t)]\,[e_3 \ e_7]^T - [e_4 \ e_8]\,Q_2(t)\,[e_4 \ e_8]^T$$

$$+ e_1R_{0a}e_1^T + e_2\,[h_dR_a - R_{0a} + \dot{h}(t)\,Q_a]\,e_2^T$$

$$+ e_3\,[R_b - h_dR_a + \dot{h}(t)$$

$$\cdot (Q_b - Q_a)]\,e_3^T - e_4\,[R_b + \dot{h}(t)\,Q_b]\,e_4^T + e_5Q_2e_5^T$$

$$- (1 - \tau_d)\,e_{15}Q_2e_{15}^T$$

$$+ h_{1t}\,[e_2 \ e_6]\,(\overline{Q}_a + R_1)\,[e_2 \ e_6]^T$$

$$+ |\mu_1|$$

$$\cdot h_dh_{2t}\,[e_3 \ e_7]\,\overline{Q}_b\,[e_3 \ e_7]^T$$

$$+ h_dh_{2t}\,[e_3 \ e_7]\,R_2\,[e_3 \ e_7]^T + \dot{h}(t)\,\Pi_6P_a\Pi_6^T$$

$$- \dot{h}(t)\,\Pi_7P_b\Pi_7^T,$$

$$\Pi_{3[h(t),\dot{h}(t)]} = W_{01}X_0H_{01}W_{02}^T + W_{02}G_0Y_0H_{02}W_{02}^T$$

$$+ h_dW_1X_3H_1W_2^T + h_dW_2G_1Y_3H_3W_2^T$$

$$+ W_1X_4H_2W_3^T + W_3G_2Y_4H_4W_3^T + W_1X_1H_1W_2^T$$

$$+ W_2G_1Y_1H_3W_2^T + \overline{\mu}_1W_1X_2H_2W_3^T$$

$$+ \overline{\mu}_1 W_3 G_2 Y_2 H_4 W_3^T,$$

$$\Omega_{01} = h_1 W_{01} X_0,$$

$$\Omega_{02} = h_1 W_{02} G_0 Y_0,$$

$$\Omega_{a[k,j]} = h_{12} W_k X_j,$$

$$\Omega_{b[k,r,j]}^{[h(t)]} = h_{12} W_k G_r Y_j,$$

$$k \in [1, 2, 3], \ j \in [1, 2, 3, 4], \ r \in [1, 2],$$

$$\Gamma_{[h(t)]} = [e_1 \ e_2 \ e_3 \ e_4 \ h_1 e_9 \ h_{1t} e_{10} \ h_{2t} e_{11}],$$

$$\Psi_{[h(t)]} = [e_5 \ e_6 \ h_d e_7 \ e_8 \ e_1 - e_2 \ e_2 - h_d e_3 \ h_d e_3 - e_4],$$

$$W_{01} = [e_1 \ e_2 \ e_9],$$

$$W_{02} = [h_1 e_9 \ e_1 - e_2 \ e_{12} \ e_1 - e_9],$$

$$W_1 = [e_2 \ e_3 \ e_4 \ e_{10} \ e_{11}],$$

$$G_0 = \mathrm{diag}\{h_1, \ 0, \ 0, \ 0\},$$

$$G_1 = \mathrm{diag}\{h(t) - h_1, \ 0, \ 0, \ 0\},$$

$$G_2 = \mathrm{diag}\{h_2 - h(t), \ 0, \ 0, \ 0\},$$

$$W_2 = [e_{10} \ e_2 - e_3 \ e_{13} \ e_2 - e_{10}],$$

$$W_3 = [e_{11} \ e_3 - e_4 \ e_{14} \ e_3 - e_{11}],$$

$$a_2$$
$$= \mathrm{sym}\left\{e_{10} \overline{E}^T (Y_1 \right.$$
$$\left. + h_d Y_3) F e_{10}^T + e_{11} \overline{E}^T (\overline{\mu}_1 Y_2 + Y_4) F e_{11}^T\right\},$$

$$\overline{E}^T = [I \ 0 \ 0 \ 0],$$

$$F^T = [I \ 0],$$

$$Q_1(t) = Q_{10} - h(t) Q_{11},$$

$$Q_2(t) = Q_{20} + (h - h(t)) Q_{21},$$

$$\overline{Q}_a = Q_{11} + \begin{bmatrix} 0 & Q_a \\ Q_a & 0 \end{bmatrix},$$

$$\overline{Q}_b = Q_{21} + \begin{bmatrix} 0 & Q_b \\ Q_b & 0 \end{bmatrix},$$

$$\overline{R}_{0a} = R_0 + \begin{bmatrix} 0 & R_{0a} \\ R_{0a} & 0 \end{bmatrix},$$

$$\overline{R}_a = R_1 + \begin{bmatrix} 0 & R_a \\ R_a & 0 \end{bmatrix},$$

$$\overline{R}_b = R_2 + \begin{bmatrix} 0 & R_b \\ R_b & 0 \end{bmatrix},$$

$$H_{01} = \begin{bmatrix} I & 0 & 0 & 0 \\ 0 & I & 0 & 0 \end{bmatrix},$$

$$H_{02} = \begin{bmatrix} -I & 0 & 2I & 0 \\ 0 & -I & 0 & 2I \end{bmatrix},$$

$$H_1 = \begin{bmatrix} h_{1t} I & 0 & 0 & 0 \\ 0 & I & 0 & 0 \end{bmatrix},$$

$$H_2 = \begin{bmatrix} h_{2t} I & 0 & 0 & 0 \\ 0 & I & 0 & 0 \end{bmatrix},$$

$$H_3 = \begin{bmatrix} -h_{1t} I & 0 & 2I & 0 \\ 0 & -I & 0 & 2I \end{bmatrix},$$

$$H_4 = \begin{bmatrix} -h_{2t} I & 0 & 2I & 0 \\ 0 & -I & 0 & 2I \end{bmatrix},$$

$$\Theta_1 = e_1 HKS e_{16}^T - e_{16} S e_{16}^T,$$

$$\widetilde{\Theta}_1 = 2 e_5 H \Lambda e_{16}^T,$$

$$\Pi_4 = [e_1 U_1 + e_5 U_2 + e_{15} U_3 + e_{16} U_4],$$

$$\Pi_5 = [A e_1^T + A_1 e_3^T + C e_{15}^T + B e_{16}^T - e_5^T],$$

$$\Pi_6 = [e_1 \ e_2 \ e_3 \ e_4 \ e_{10}],$$

$$\Pi_7 = [e_1 \ e_2 \ e_3 \ e_4 \ e_{11}].$$

$$(B.1)$$

C. Box 4

$$\Omega_{4[h(t)]} = P + \begin{bmatrix} \widetilde{e}_1^T \\ \widetilde{e}_2^T \\ \widetilde{e}_3^T \\ 0 \end{bmatrix}^T [h(t) P_a + (h - h(t)) P_b] \begin{bmatrix} \widetilde{e}_1^T \\ \widetilde{e}_2^T \\ \widetilde{e}_3^T \\ 0 \end{bmatrix}$$

$$+ \mathrm{sym}\left\{ \begin{bmatrix} \widetilde{e}_1^T \\ \widetilde{e}_2^T \\ \widetilde{e}_3^T \\ 0 \end{bmatrix}^T \left(P_a \begin{bmatrix} 0 \\ 0 \\ 0 \\ \widetilde{e}_4^T \end{bmatrix} + P_b \begin{bmatrix} 0 \\ 0 \\ 0 \\ \widetilde{e}_5^T \end{bmatrix} \right) \right\},$$

$$\alpha = \frac{h(t)}{h},$$

$$J^T = [E_1 \ E_2],$$

$$E_1 = [\widetilde{e}_4 \ \widetilde{e}_1 - \widetilde{e}_2]$$

$$E_2 = [\widetilde{e}_5 \ \widetilde{e}_2 - \widetilde{e}_3],$$

$$\Pi_{[h(t), \dot{h}(t)]} = \mathrm{sym}\left\{\Pi_{1[h(t), \dot{h}(t)]} + \Pi_{3[h(t), \dot{h}(t)]}\right\}$$
$$+ \Pi_{2[h(t), \dot{h}(t)]},$$

$$\Pi_{1[h(t), \dot{h}(t)]} = \Gamma_{[h(t)]} P \Psi_{[\dot{h}(t)]}^T + [e_1 \ e_2 \ e_3 \ e_7] P_a [h(t)$$
$$\cdot e_4 \ h(t) h_d e_5 \ h(t) e_6 \ e_1 - h_d e_2 - \dot{h}(t) e_7]^T$$
$$+ [e_1 \ e_2 \ e_3 \ e_8] P_b [(h - h(t)) e_4 \ (h - h(t))$$
$$\cdot h_d e_5 \ (h - h(t)) e_6 \ h_d e_2 - e_3 + \dot{h}(t) e_8]^T + \Theta_2$$
$$+ \widetilde{\Theta}_2 + \Pi_4 \Pi_5,$$

$$\Pi_{2[h(t), \dot{h}(t)]} = [e_1 \ e_4] Q_1(t) [e_1 \ e_4]^T$$
$$+ h_d [e_2 \ e_5] [Q_2(t) - Q_1(t)] [e_2 \ e_5]^T$$

$$- [e_3 \ e_6] Q_2(t) [e_3 \ e_6]^T + e_1 [h_d R_a + \dot{h}(t) Q_a] e_1^T$$

$$+ e_2 [R_b - h_d R_a + \dot{h}(t)(Q_b - Q_a)] e_2^T - e_3 [R_b$$

$$+ \dot{h}(t) Q_b] e_3^T + e_4 Q_2 e_4^T - (1 - \tau_d) e_{11} Q_2 e_{11}^T$$

$$+ h(t) [e_1 \ e_4] (\overline{Q}_a + R_1) [e_1 \ e_4]^T + |\mu_1|$$

$$\cdot h_d h [e_2 \ e_5] \overline{Q}_b [e_2 \ e_5]^T$$

$$+ h_d h [e_2 \ e_5] R_2 [e_2 \ e_5]^T + \dot{h}(t) \Pi_6 P_a \Pi_6^T$$

$$- \dot{h}(t) \Pi_7 P_b \Pi_7^T,$$

$$\Pi_{3[h(t),\dot{h}(t)]} = h_d W_1 X_3 H_1 W_2^T + h_d W_2 G_1 Y_3 H_3 W_2^T$$

$$+ W_1 X_4 H_2 W_3^T + W_3 G_2 Y_4 H_4 W_3^T + W_1 X_1 H_1 W_2^T$$

$$+ W_2 G_1 Y_1 H_3 W_2^T + \overline{\mu}_1 W_1 X_2 H_2 W_3^T$$

$$+ \overline{\mu}_1 W_3 G_2 Y_2 H_4 W_3^T,$$

$$\Omega_{a[k,j]} = h W_k X_j,$$

$$\Omega_{b[k,r,j]}^{[h(t)]} = h W_k G_r Y_j,$$

$$k \in [1,2,3], \quad j \in [1,2,3,4], \quad r \in [1,2],$$

$$\Gamma_{[h(t)]} = [e_1 \ e_2 \ e_3 \ h(t) e_7 \ (h - h(t)) e_8],$$

$$\Psi_{[\dot{h}(t)]} = [e_4 \ h_d e_5 \ e_6 \ e_1 - h_d e_2 \ h_d e_2 - e_3],$$

$$W_1 = [e_1 \ e_2 \ e_3 \ e_7 \ e_8],$$

$$W_2 = [e_7 \ e_1 - e_2 \ e_9 \ e_1 - e_7],$$

$$W_3 = [e_8 \ e_2 - e_3 \ e_{10} \ e_2 - e_8],$$

$$G_1 = \text{diag}\{h(t), 0, 0, 0\},$$

$$G_2 = \text{diag}\{h - h(t), 0, 0, 0\},$$

$$H_1 = \begin{bmatrix} h(t) I & 0 & 0 & 0 \\ 0 & I & 0 & 0 \end{bmatrix},$$

$$H_2 = \begin{bmatrix} (h - h(t)) I & 0 & 0 & 0 \\ 0 & I & 0 & 0 \end{bmatrix},$$

$$H_3 = \begin{bmatrix} -h(t) I & 0 & 2I & 0 \\ 0 & -I & 0 & 2I \end{bmatrix},$$

$$H_4 = \begin{bmatrix} -(h - h(t)) I & 0 & 2I & 0 \\ 0 & -I & 0 & 2I \end{bmatrix},$$

$$\Theta_2 = e_1 H K S e_{12}^T - e_{12} S e_{12}^T,$$

$$\widetilde{\Theta}_2 = 2 e_4 H \Lambda e_{12}^T$$

$$\Pi_4 = [e_1 U_1 + e_4 U_2 + e_{11} U_3 + e_{12} U_4],$$

$$\Pi_5 = [A e_1^T + A_1 e_2^T + C e_{11}^T + B e_{12}^T - e_4^T],$$

$$\Pi_6 = [e_1 \ e_2 \ e_3 \ e_7],$$

$$\Pi_7 = [e_1 \ e_2 \ e_3 \ e_8].$$

$$a_2 = \text{sym}\left\{ e_7 \overline{E}^T (Y_1 + h_d Y_3) F e_7^T + e_8 \overline{E}^T (\overline{\mu}_1 Y_2 + Y_4) \right.$$

$$\left. \cdot F e_8^T \right\}$$

(C.1)

Data Availability

The data used to support the findings of this study are available from the corresponding author upon request.

Conflicts of Interest

The authors declare that they have no conflicts of interest.

Acknowledgments

References

[1] Z. Feng, J. Lam, and G.-H. Yang, "Optimal partitioning method for stability analysis of continuous/discrete delay systems," *International Journal of Robust and Nonlinear Control*, vol. 25, no. 4, pp. 559–574, 2013.

[2] L. Ding, Y. He, M. Wu, and Z. Zhang, "A novel delay partitioning method for stability analysis of interval time-varying delay systems," *Journal of The Franklin Institute*, vol. 354, no. 2, pp. 1209–1219, 2017.

[3] J. Chen, J. H. Park, and S. Xu, "Stability analysis of continuous-time systems with time-varying delay using new Lyapunov–Krasovskii functionals," *Journal of The Franklin Institute*, vol. 355, no. 13, pp. 5957–5967, 2018.

[4] J. Sun, Q.-L. Han, J. Chen, and G.-P. Liu, "Less conservative stability criteria for linear systems with interval time-varying delays," *International Journal of Robust and Nonlinear Control*, vol. 25, no. 4, pp. 475–485, 2015.

[5] W. Qian, M. Yuan, L. Wang, X. Bu, and J. Yang, "Stabilization of systems with interval time-varying delay based on delay decompsing approach," *ISA Transactions*, vol. 70, pp. 1–6, 2017.

[6] K. Gu, "An integral inequality in the stability problem of time-delay systems," in *Proceedings of the Conference of the IEEE Industrial Electronics*, Sydney, Australia, 2010.

[7] A. Seuret and F. Gouaisbaut, "Wirtinger-based integral inequality: application to time-delay systems," *Automatica*, vol. 49, no. 9, pp. 2860–2866, 2013.

[8] P. Park, W. I. Lee, and S. Y. Lee, "Auxiliary function-based integral inequalities for quadratic functions and their applications to time-delay systems," *Journal of The Franklin Institute*, vol. 352, no. 4, pp. 1378–1396, 2015.

[9] A. Seuret and F. Gouaisbaut, "Hierarchy of LMI conditions for the stability analysis of time-delay systems," *Systems & Control Letters*, vol. 81, pp. 1–7, 2015.

[10] S. Y. Lee, W. I. Lee, and P. Park, "Improved stability criteria for linear systems with interval time-varying delays: generalized zero equalities approach," *Applied Mathematics and Computation*, vol. 292, pp. 336–348, 2017.

[11] C.-K. Zhang, Y. He, L. Jiang, Q.-G. Wang, and M. Wu, "Stability analysis of discrete-time neural networks with time-varying delay via an extended reciprocally convex matrix inequality," *IEEE Transactions on Cybernetics*, vol. 47, no. 10, pp. 3040–3049, 2017.

[12] W. Qian, L. Wang, and M. Chen, "Local consensus of nonlinear multiagent systems with varying delay coupling," *IEEE transactions on systems, man, and cybernetics. Part B, Cybernetics*, 2017.

[13] W. I. Lee, S. Y. Lee, and P. Park, "A combined first- and second-order reciprocal convexity approach for stability analysis of systems with interval time-varying delays," *Journal of The Franklin Institute*, vol. 353, no. 9, pp. 2104–2116, 2016.

[14] C.-K. Zhang, Y. He, L. Jiang, and M. Wu, "An improved summation inequality to discrete-time systems with time-varying delay," *Automatica*, vol. 74, pp. 10–15, 2016.

[15] C. Zhang, Y. He, L. Jiang, M. Wu, and Q. Wang, "An extended reciprocally convex matrix inequality for stability analysis of systems with time-varying delay," *Automatica*, vol. 85, pp. 481–485, 2017.

[16] H.-B. Zeng, Y. He, M. Wu, and J. She, "Free-matrix-based integral inequality for stability analysis of systems with time-varying delay," *IEEE Transactions on Automatic Control*, vol. 60, no. 10, pp. 2768–2772, 2015.

[17] A. Lurie, *Some Nonlinear Problem in the Theory of Automatic Control*, H. M. Stationary Office, London, UK, 1957.

[18] H. Huang, H. Li, and J. Zhong, "Master-slave synchronization of general Lur'e systems with time-varying delay and parameter uncertainty," *International Journal of Bifurcation and Chaos*, vol. 16, pp. 281–294, 2006.

[19] Q. Han, "On designing time-varying delay feedback controllers for master-slave synchronization of Lure systems," *IEEE Transactions on Circuits and Systems I: Regular Paper*, vol. 54, no. 7, pp. 1573–1583, 2007.

[20] S. Xiao, X. Liu, C. Zhang, and H. Zeng, "Further results on absolute stability of Lure systems with a time-varying delay," *Neurocomputing*, vol. 207, pp. 823–827, 2016.

[21] J. Park, S. Y. Lee, and P. Park, "An improved stability criteria for neutral-type Lur'e systems with time-varying delays," *Journal of The Franklin Institute*, vol. 355, no. 12, pp. 5291–5309, 2018.

[22] A. Bellen, N. Guglielmi, and A. E. Ruehli, "Methods for linear systems of circuit delay differential equations of neutral type," *IEEE Transactions on Circuits and Systems I: Fundamental Theory and Applications*, vol. 46, no. 1, pp. 212–216, 1999.

[23] K. Ramakrishnan and G. Ray, "An improved delay-dependent stability criterion for a class of Lur'e systems of neutral-type," *Journal of Dynamic Systems, Measurement, and Control*, vol. 134, no. 1, Article ID 011008, 2012.

[24] W. Duan, B. Du, Z. Liu, and Y. Zou, "Improved stability criteria for uncertain neutral-type Lur'e systems with time-varying delays," *Journal of The Franklin Institute*, vol. 351, no. 9, pp. 4538–4554, 2014.

[25] R. Q. Lu, H. Y. Wu, and J. J. Bai, "New delay-dependent robust stability criteria for uncertain neutral systems with mixed delays," *Journal of The Franklin Institute*, vol. 351, no. 3, pp. 1386–1399, 2014.

[26] W. Duan, B. Du, J. You, and Y. Zou, "Improved robust stability criteria for a class of Lure systems with interval time-varying delays and sector-bounded nonlinearity," *International Journal of Systems Science*, vol. 46, no. 5, pp. 944–954, 2015.

[27] Y. Wang, Y. Xue, and X. Zhang, "Less conservative robust absolute stability criteria for uncertain neutral-type Lur'e systems with time-varying delays," *Journal of The Franklin Institute*, vol. 353, no. 4, pp. 816–833, 2016.

[28] T. Wang, T. Li, G. Zhang, and S. Fei, "New Lyapunov–Krasovskii functional for mixed-delay-dependent stability of uncertain linear neutral systems," *Circuits, Systems and Signal Processing*, vol. 37, no. 5, pp. 1825–1845, 2018.

[29] W. Duan, B. Du, Y. Li et al., "Improved sufficient LMI conditions for the robust stability of time-delayed neutral-type Lur'e systems," *International Journal of Control, Automation, and Systems*, vol. 16, no. 5, pp. 2343–2353, 2018.

[30] B. Liu and X.-C. Jia, "New absolute stability criteria for uncertain Lur'e systems with time-varying delays," *Journal of The Franklin Institute*, vol. 355, no. 9, pp. 4015–4031, 2018.

[31] C. Zhang, Y. He, L. Jiang, and M. Wu, "Notes on stability of time-delay systems: bounding inequalities and augmented lyapunov-krasovskii functionals," *IEEE Transactions on Automatic Control*, vol. 62, no. 10, pp. 5331–5336, 2017.

[32] H. Xu, C. Zhang, L. Jiang, and J. Smith, "Stability analysis of linear systems with two additive time-varying delays via delay-product-type Lyapunov functional," *Applied Mathematical Modelling*, vol. 45, pp. 955–964, 2017.

[33] W. Kwon, B. Koo, and S. Lee, "Novel Lyapunov–Krasovskii functional with delay-dependent matrix for stability of time-varying delay systems," *Applied Mathematics and Computation*, vol. 320, pp. 149–157, 2018.

[34] Y. Wang, L. Xiong, Y. Li, H. Zhang, and C. Peng, "Novel stability analysis for uncertain neutral-type Lur'e systems with time-varying delays using new inequality," *Mathematical Problems in Engineering*, vol. 2017, Article ID 5731325, 13 pages, 2017.

[35] Y. Liu, S. Lee, O. Kwon, and J. Park, "Robust delay-dependent stability criteria for time-varying delayed Lur'e systems of neutral type," *Circuits, Systems and Signal Processing*, vol. 5, no. 34, pp. 1481–1497, 2015.

[36] C.-K. Zhang, Y. He, L. Jiang, M. Wu, and H.-B. Zeng, "Stability analysis of systems with time-varying delay via relaxed integral inequalities," *Systems & Control Letters*, vol. 92, pp. 52–61, 2016.

[37] T. H. Lee, J. H. Park, and S. Xu, "Relaxed conditions for stability of time-varying delay systems," *Automatica*, vol. 75, pp. 11–15, 2017.

[38] T. H. Lee and J. H. Park, "A novel Lyapunov functional for stability of time-varying delay systems via matrix-refined-function," *Automatica*, vol. 80, pp. 239–242, 2017.

[39] M. Park, O. Kwon, and J. Ryu, "Advanced stability criteria for linear systems with time-varying delays," *Journal of The Franklin Institute*, vol. 355, no. 1, pp. 520–543, 2018.

[40] T. H. Lee and J. H. Park, "Improved stability conditions of time-varying delay systems based on new Lyapunov functionals," *Journal of The Franklin Institute*, vol. 355, no. 3, pp. 1176–1191, 2018.

[41] D. Yue and Q.-L. Han, "A delay-dependent stability criterion of neutral systems and its application to partial element equivalent circuit model," *IEEE Transactions on Circuits and Systems II: Express Briefs*, vol. 51, no. 12, pp. 685–689, 2004.

[42] J.-H. Kim, "Further improvement of Jensen inequality and application to stability of time-delayed systems," *Automatica*, vol. 64, pp. 121–125, 2016.

[43] I. R. Petersen, "A stabilization algorithm for a class of uncertain linear systems," *Systems & Control Letters*, vol. 8, no. 4, pp. 351–357, 1987.

[44] C. Zhang, Y. He, L. Jiang, M. Wu, and H. Zeng, "delay-variation-dependent stability of delayed discrete-time systems," *IEEE Transactions on Automatic Control*, vol. 61, no. 9, pp. 2663–2669, 2016.

[45] X.-M. Zhang, Q.-L. Han, A. Seuret, and F. Gouaisbaut, "An improved reciprocally convex inequality and an augmented Lyapunov-Krasovskii functional for stability of linear systems with time-varying delay," *Automatica*, vol. 84, pp. 221–226, 2017.

Research Article

Hybrid Functions Direct Approach and State Feedback Optimal Solutions for a Class of Nonlinear Polynomial Time Delay Systems

Mohamed Karim Bouafoura [ID] **and Naceur Benhadj Braiek**

Ecole Polytechnique de Tunisie, BP 743, La Marsa, Tunisia

Correspondence should be addressed to Mohamed Karim Bouafoura; mohamed.bouafoura@ept.rnu.tn

The aim of this paper is to determine the optimal open loop solution and a nonlinear delay-dependent state feedback suboptimal control for a class of nonlinear polynomial time delay systems. The proposed method uses a hybrid of block pulse functions and Legendre polynomials as an orthogonal base for system's states and input expansion. Hence, the complex dynamic optimization problem is then reduced, with the help of operational properties of the hybrid basis and Kronecker tensor product lemmas, to a nonlinear programming problem that could be solved with available NLP solvers. A practical nonlinear feedback controller gains are deduced with respect to a least square formalism based on the optimal open loop control results. Simulation results show efficiency of the proposed numerical optimal approach.

1. Introduction

Time delays affect systems dynamics in many engineering applications like chemical control systems, biology, and medicine [1, 2]. Delays are also encountered in communication and information technologies like high-speed communication networks [3]. It should be noted that time delay may be, in some applications like communication lines, a source of instability and performance degradation [4]. Time delay system is therefore a very important class of processes whose stabilization [5] and optimization [6, 7] have been of interest to many researchers.

Particularly, many attempts have been made in literature to solve optimal control problems for many classes of linear [8–11] and nonlinear [6, 12, 13] time delay systems. Among them, we recall the application of Pontryagins maximum principle to the optimization of control systems with time delays which was firstly proposed by [14]. It had been shown that it results in a system of coupled two-point boundary-value (TPBV) problem involving both delay and advance terms whose exact solution, except in very special cases, is

very difficult to determine (see [15]). Perhaps one of the most effective techniques is dynamic programming approaches (see [2]) for overcoming the complexity of the nonlinear time delay systems in optimal control problems. Of course, application of dynamic programming methods has some difficulties due to the need to provide an appropriate level model and also to define recursive relationships for each case problem. Also a computational algorithm considering a linear approximation of the original system which is defined about a nominal trajectory is offered by [16]. Clearly, using the linear approximation is not reliable and may lead to large errors. Reference [7] proposed an approach based on discretization techniques and necessary conditions to obtain approximate optimal control and the state for optimal control problems with nonlinear delay systems. Despite the good performance of this method, achieving the necessary conditions in some problems and the implementation of approach may be faced with difficulties. So different numerical methods have been proposed to avoid the problems arising from the applications of analytical methods. It is then straightforward that many of the numerical methods dedicated to solving

classical optimal control problems have been extended to handle optimal control problems governed by time delay systems.

Typically, direct methods are based on converting the dynamical optimal control problem into static optimization problem. Among direct methods, parametrization technique [17–19] is known to minimize decision variables compared to the discretization of the problem [7]. It is worth noting that parametrization relies basically on orthogonal functions or wavelets [20–22]; however that tool have been used to solve various other problems of dynamic systems like identification (see [8]), tracking control (see [23]), observer based control (see [24]), or minimum time control (see [25]). The main characteristic of this pseudo-spectral technique is that it allows transforming complex dynamic optimization problems to solving a set of algebraic equations in the least square sense in the linear systems case [26, 27] or permits formulating an equivalent nonlinear static programming problem for problems related to nonlinear systems [13, 28, 29].

In recent years, a growing interest has been appeared toward the application of hybrid functions, which is a combination of block pulse and an orthogonal polynomials basis [26]. In the nonlinear time delay optimal control problems context, an approach using hybrid functions which consist of block pulse functions and orthonormal Taylor series (see [15, 29]) had been proposed, where authors propose to solve the necessary and sufficient condition equations for stationary emanating from the Hamiltonian based on state and control coefficients over the basis. Similarly, [28] propose a direct approach based on a hybrid of block pulse functions and Lagrange interpolating polynomials in order to convert the original optimal problem containing multiple delay into a mathematical programming one, where the resulting optimization problem is solved numerically by the Lagrange multipliers method. Reference [27] proposed similar approach based on hybrid functions of block pulse and Bernouilli polynomials, while [30] uses biorthogonal cubic Hermite spline multiwavelets in addition to block pulse functions to constitute the hybrid basis. Although above contributions treat some nonlinear delayed optimal control problem, they do not propose any general nonlinear programming problem that could handle all examples depicted in their works. In fact, for each considered nonlinear system, a nonlinear optimization problem is formulated and then solved with an NLP solver. Furthermore, only open loop control solutions are investigated therein, which is not of great interest in practice.

In the present paper, we introduce a direct method to solve forwardly the finite time quadratic optimal control problem of polynomial systems with delayed state, by the use of hybrid functions of block pulse and Legendre polynomials. The operational matrices of delay and Kronecker product specific to that basis are recalled. At first, the open loop solution of the nonlinear time delay optimal control problem is investigated. Secondly, a suboptimal nonlinear state feedback is determined based on the first part results. Hence, the main contributions in this work could be summarized as follows:

(a) expressing the constraint of the formulated NLP problem properly for the class of polynomial systems; thus the proposed formulation could handle a wide range of nonlinear analytic nonlinear systems. Then, a unified development is carried for that class of systems,

(b) deriving a nonlinear polynomial delay-dependent nonlinear suboptimal state feedback that reproduce the optimal state trajectories determined in the open loop framework,

(c) using an hybrid basis with reduced number of elementary functions, which makes open loop synthesis faster, with a good enough accuracy compared to other approaches, and closed loop solution within a simpler formulation and resolution.

The remainder of the paper is organised as follows. In the second section, hybrid functions and their properties are introduced. In the third section, the open loop numerical solution of the nonlinear time delay optimal control problem is detailed. The suboptimal closed loop framework is presented in the fourth section. In the fifth section, computational results are depicted. Finally, concluding remarks and future works are presented.

2. Hybrid Functions

Hybrid functions $h_{ij}(t)$, $i = 1, 2, \cdots N$, $j = 0, 1 \cdots M - 1$, have three arguments; i and j are the order of block pulse functions and Legendre polynomials, respectively, and t is the normalized time. They are defined on the interval $t = [0, t_f]$ as [26]

$$h_{ij}(t)$$
$$= \begin{cases} L_j\left(\dfrac{2N}{t_f}t - 2i + 1\right), & t \in \left[\left(\dfrac{i-1}{N}\right)t_f, \dfrac{i}{N}t_f\right), \\ 0 & otherwise. \end{cases} \quad (1)$$

Here, $L_j(t)$ are the well-known Legendre polynomials of order M which constitute the base $\mathbf{L}(t)$ and satisfy the following recursive formula:

$$L_0(t) = 1,$$
$$L_1(t) = t,$$
$$L_{j+1}(t) = \left(\dfrac{2j+1}{j+1}\right)tL_j(t) - \left(\dfrac{j}{j+1}\right)L_{j-1}(t), \quad (2)$$
$$j = 1, 2, 3, \cdots$$

We define $\mathbf{\Phi}(t)$ the vector of N block pulse functions $\phi_i(t)$, $i = 0, 1, \cdots N - 1$, as follows:

$$\phi_i(t) = \begin{cases} 1, & \forall t \in \left[\dfrac{i-1}{N}t_f, \dfrac{i}{N}t_f\right), \\ 0, & otherwise. \end{cases} \quad (3)$$

Since $h_{ij}(t)$ is the combination of Legendre polynomials and block pulse functions which are both complete and orthogonal, then the set of hybrid functions is a complete orthogonal system.

In the rest of the paper we notate $w = NM$ the dimension of the hybrid basis.

2.1. Operational Matrix of Integration.

The integration of $\mathbf{h}(t)$ can be approximated by [26]

$$\int_0^t \mathbf{h}(\nu)\, d\nu \cong P\mathbf{h}(t) \tag{4}$$

where P is the integration operational matrix of order $w \times w$

$$P_{(w \times w)} = \begin{bmatrix} T & H & H & \cdots & H \\ 0 & T & H & \cdots & H \\ 0 & 0 & T & \cdots & H \\ \vdots & \vdots & \vdots & \ddots & \vdots \\ 0 & 0 & 0 & \cdots & T \end{bmatrix} \tag{5}$$

where

$$H_{(M \times M)} = \frac{t_f}{N} \begin{bmatrix} 1 & 0 & 0 & \cdots & 0 \\ 0 & 0 & 0 & \cdots & 0 \\ 0 & 0 & 0 & \cdots & 0 \\ \vdots & \vdots & \vdots & \vdots & \vdots \\ 0 & 0 & 0 & \cdots & 0 \end{bmatrix} \tag{6}$$

and

$$T_{(M \times M)} = \frac{t_f}{2N}.$$

$$\begin{bmatrix} 1 & 1 & 0 & 0 & \cdots & 0 & 0 & 0 \\ \dfrac{-1}{3} & 0 & \dfrac{1}{3} & 0 & \cdots & 0 & 0 & 0 \\ 0 & \dfrac{-1}{5} & 0 & \dfrac{1}{5} & \cdots & 0 & 0 & 0 \\ \vdots & \vdots & \vdots & \vdots & \vdots & \vdots & \vdots & \vdots \\ 0 & 0 & 0 & 0 & \cdots & \dfrac{-1}{2N-3} & 0 & \dfrac{1}{2N-3} \\ 0 & 0 & 0 & 0 & \cdots & 0 & \dfrac{-1}{2N-1} & 0 \end{bmatrix} \tag{7}$$

2.2. Delay Modeling with Hybrid Functions.

A vector function $g(t)$ of r dimensional components which are square integrable in $[0, t_f]$ can be approximated by a block pulse series as

$$g(t) \cong \sum_{i=1}^{N} g_i \phi_i(t) = G^T \Phi(t) \tag{8}$$

where $G = [g_1, g_2, \ldots, g_N]^T$.

For an r component delay vector variable $g(t-\tau)$ with

$$g(t) = \zeta(t) \quad \forall t \in [-\tau, 0] \tag{9}$$

the block pulse series approximation of $g(t-\tau)$ may be defined as [31]

$$g(t-\tau) \cong \sum_{i=1}^{N} g^*(\tau)\phi_i(t) = G^*(\tau)\Phi(t) \tag{10}$$

where

$$g_i^*(\tau) = \frac{N}{T} \int_{it_f/N}^{(i+1)t_f/N} g(t-\tau)\, dt$$

$$= \begin{cases} \zeta_i(\tau) & \text{for } i < \mu \\ g_{i-\mu} & \text{for } i \geq \mu \end{cases} \tag{11}$$

with

$$\zeta_i(\tau) = \frac{N}{T} \int_{it_f/N}^{(i+1)t_f/N} \zeta(t-\tau)\, dt \quad \text{for } i < \mu \tag{12}$$

and μ is the number of block pulse functions considered over $0 \leq t \leq \tau$, and $G^*(\tau) = [g_1^*(\tau), g_2^*(\tau), \ldots, g_N^*(\tau)]^T$.

Let

$$\zeta_\mu(\tau) = \left[\zeta_1^*(\tau), \zeta_2^*(\tau), \ldots, \zeta_{\mu-1}^*(\tau) \right]^T \tag{13}$$

Then, it comes [31]

$$vec\left(G^*(\tau)\right) = E(r,\mu)\, vec\left(\zeta_\mu(\tau)\right) + D(r,\mu)\, vec(G) \tag{14}$$

$E(r,\mu)$ and $D(r,\mu)$ are called the shift operational matrices, given by

$$E(r,\mu) = \begin{bmatrix} I_{r\mu \times r\mu} \\ \cdots \\ 0_{r(N-\mu) \times r\mu} \end{bmatrix} \tag{15}$$

and

$$D(r,\mu) = \begin{bmatrix} 0_{r\mu \times r(N-\mu)} & \vdots & 0_{r\mu \times r\mu} \\ \cdots & \vdots & \cdots \\ I_{r(N-\mu) \times r(N-\mu)} & \vdots & 0_{r(N-\mu) \times r\mu} \end{bmatrix} \tag{16}$$

It is worth noticing that the Shift operational matrices of hybrid functions could be derived forwardly from those of block pulse functions by

$$E_h = I_M \otimes E(r,\mu)$$
$$D_h = I_M \otimes D(r,\mu) \tag{17}$$

where $\otimes$ stands for the Kronecker product.

However, it should be noticed that block pulse functions are fundamental for delay modeling. The choice of N depends on τ and t_f, which issue had been addressed in [26]. In this framework, we propose to choose N as follows:

$$N = a.nint\left(\frac{t_f}{\tau}\right), \quad a \in \mathbb{N}^* \tag{18}$$

where a is a nonnegative integer, to be chosen bigger than one if possible in order to improve approximation and $nint(.)$ denotes the nearest integer function [22] (implemented by $round$ routine in MATLAB).

2.3. The Integration of the Cross Product. The integration of the cross product of two hybrid functions vectors $\mathbf{h}(t)$ can be obtained as [26]

$$C = \int_0^{t_f} \mathbf{h}(t)\,\mathbf{h}^T(t)\,dt = \begin{bmatrix} L & 0_M & \cdots & 0_M \\ 0_M & L & \cdots & 0_M \\ \vdots & \vdots & \ddots & \vdots \\ 0_M & 0_M & \cdots & L \end{bmatrix} \quad (19)$$

where C is an $w \times w$ matrix. 0_M stands for the zero $M \times M$ matrix and L is an $M \times M$ diagonal matrix that is given by

$$L = \frac{t_f}{N} \begin{bmatrix} 1 & 0 & \cdots & 0 \\ 0 & \frac{1}{3} & \cdots & 0 \\ \vdots & \vdots & \ddots & \vdots \\ 0 & 0 & \cdots & \frac{1}{2M-1} \end{bmatrix} \quad (20)$$

2.4. Kronecker Product Operational Matrix. It would be interesting, for bilinear systems, as it will be proven later, to investigate the Kronecker product operational matrix for hybrid functions. This particular matrix operator derivation, as it is the case for the integration, cross product, and delay operators, is highly inspired of the Kronecker operational matrix of both Legendre polynomials and block pulse functions.

For the block pulse functions, we can state

$$\boldsymbol{\Phi}(t) \otimes \boldsymbol{\Phi}(t) = \begin{bmatrix} \phi_1(t)\,\boldsymbol{\Phi}(t) \\ \phi_2(t)\,\boldsymbol{\Phi}(t) \\ \vdots \\ \phi_N(t)\,\boldsymbol{\Phi}(t) \end{bmatrix} = K_\Phi \boldsymbol{\Phi}(t) \quad (21)$$

with

$$K_\Phi = \begin{bmatrix} E_{1,1}^{N \times N} \\ E_{2,2}^{N \times N} \\ \vdots \\ E_{N,N}^{N \times N} \end{bmatrix} \quad (22)$$

where $K_\Phi \in \mathbb{R}^{N^2 \times N}$ is the Kronecker product operational matrix of block pulse functions and the matrix $E_{i,j}^{N \times N}$ is defined in Appendix.

On the other hand, the product of two Shifted Legendre Polynomials $L_i(t)$ and $L_j(t)$ can be expressed by

$$L_i(t)\,L_j(t) \cong \sum_{k=0}^{M-1} \psi_{ijk} L_k(t) \quad (23)$$

with

$$\psi_{ijk} = \frac{2k+1}{t_f} \int_0^{t_f} L_i(t)\,L_j(t)\,L_k(t)\,dt \quad (24)$$

A practical implementation of the latter scalar products is given in [19].

Then, we may write

$$L_j(t)\,\mathbf{L}(t) = \begin{bmatrix} \psi_{i00} \\ \psi_{i11} \\ \vdots \\ \psi_{i(M-1)(M-1)} \end{bmatrix} = K_L^i \mathbf{L}(t) \quad (25)$$

where K_L^i is a $M \times M$ square matrix.

Then it comes

$$\mathbf{L}(t) \otimes \mathbf{L}(t) = \begin{bmatrix} K_L^0 \\ K_L^1 \\ \vdots \\ K_L^{M-1} \end{bmatrix} = K_{\mathbf{L}} \mathbf{L}(t) \quad (26)$$

where $K_{\mathbf{L}} \in \mathbb{R}^{M^2 \times M}$ is the Kronecker product operational matrix of Legendre polynomials.

Based on relations (26) and (23), we define

$$\mathbf{h}(t) \otimes \mathbf{h}(t) = \begin{bmatrix} K_L^0 \otimes E_{1,1}^{N \times N} \\ K_L^1 \otimes E_{1,1}^{N \times N} \\ \vdots \\ K_L^{M-1} \otimes E_{1,1}^{N \times N} \\ \cdots \\ K_L^0 \otimes E_{2,2}^{N \times N} \\ K_L^1 \otimes E_{2,2}^{N \times N} \\ \vdots \\ K_L^{M-1} \otimes E_{2,2}^{N \times N} \\ \cdots \\ \vdots \\ \cdots \\ K_L^0 \otimes E_{N,N}^{N \times N} \\ K_L^1 \otimes E_{N,N}^{N \times N} \\ \vdots \\ K_L^{M-1} \otimes E_{N,N}^{N \times N} \end{bmatrix} = K_{\mathbf{h}} \mathbf{h}(t) \quad (27)$$

where $K_{\mathbf{h}} \in \mathbb{R}^{w^2 \times w}$ is the Kronecker product operational matrix of hybrid functions.

3. Numerical Solution of the Nonlinear Time Delay Optimal Control Problem

3.1. Description of the Studied System. We consider the nonlinear continuous system which can be represented by the following state space representation:

$$\dot{x}(t) = f(x(t,\tau)) + g(x(t,\tau))u(t)$$
$$x(t-\tau) = x_0, \quad \forall t \in [0,\tau] \tag{28}$$

where $x(t) \in \mathbb{R}^n$ is the state vector, $x(t-\tau) \in \mathbb{R}^n$ is the delayed state where τ denotes the time delay, $u(t) \in \mathbb{R}^m$ is the control vector, and $f(x(t,\tau))$ from $\mathbb{R}^n$ into $\mathbb{R}^n$ and $g(x(t,\tau))$ from $\mathbb{R}^n$ into $\mathbb{R}^{n \times m}$ are nonlinear analytic functions of $x(t)$ and $x(t-\tau)$.

Note that, any functions $f(x(t,\tau))$ and $g(x(t,\tau))$ could be approached using truncated series of the Kronecker power of $x(t)$ and $x(t-\tau)$ as follows:

$$f(x(t,\tau)) \approx \sum_{i=1}^{p} F_i x^{[i]}(t) + \sum_{j=1}^{q} \overline{F}_j x^{[j]}(t-\tau)$$
$$+ \sum_{i=1}^{p} \sum_{j=1}^{q} \Gamma_{ij}\left(x^{[i]}(t) \otimes x^{[j]}(t-\tau)\right) \tag{29}$$

where $F_i \in \mathbb{R}^{n \times n^j}$, $\overline{F}_j \in \mathbb{R}^{n \times n^j}$ and $\Gamma_{ij} \in \mathbb{R}^{n \times n^{i+j}}$ are constant matrices. $x^{[i]}(t)$ denotes the ith Kronecker power of the state vector (see Appendix).

And

$$g(x(t,\tau))$$
$$= \left[g_1(x(t,\tau)) \vdots g_2(x(t,\tau)) \vdots \cdots \vdots g_m(x(t,\tau)) \right] \tag{30}$$

where $g_k(x(t,\tau)) \in \mathbb{R}^n$, for $k = 1, \ldots, m$, are defined by

$$g_k(x(t,\tau)) \approx \sum_{i=0}^{r} G_{ki} x^{[i]}(t) + \sum_{j=1}^{s} \overline{G}_{kj} x^{[j]}(t-\tau)$$
$$+ \sum_{i=1}^{r} \sum_{j=1}^{s} \Upsilon_{kij}\left(x^{[i]}(t) \otimes x^{[j]}(t-\tau)\right) \tag{31}$$

where $G_{ki} \in \mathbb{R}^{n \times n^j}$, $\overline{G}_{kj} \in \mathbb{R}^{n \times n^j}$, and $\Upsilon_{kij} \in \mathbb{R}^{n \times n^{i+j}}$ are constant matrices.

Notice that $g(x(t,\tau))$ is composed of three terms, the first is a function of $x^{[i]}(t)$, the second depends on $x^{[j]}(t-\tau)$, and the third is a function of $x^{[i]}(t) \otimes x^{[j]}(t-\tau)$. Consider the first term of $g(x(t,\tau))$; we note it $g(x(t))$. It could be written as follows:

$$g(x(t)) = \sum_{i=0}^{r} \left[G_{1i} x^{[i]}(t) \vdots G_{2i} x^{[i]}(t) \vdots \cdots \vdots G_{mi} x^{[i]}(t) \right]$$

$$= \sum_{i=0}^{r} \underbrace{\left[G_{1i} \vdots G_{2i} \vdots \cdots \vdots G_{mi} \right]}_{G_i}$$

$$\cdot \underbrace{\begin{bmatrix} x^{[i]}(t) & & & 0 \\ & x^{[i]}(t) & & \\ & & \ddots & \\ 0 & & & x^{[i]}(t) \end{bmatrix}}_{I_m \otimes x^{[i]}(t)} \tag{32}$$

Then $g(x(t,\tau))$ could be generalized to the following expression:

$$g(x(t,\tau)) = \sum_{i=0}^{r} G_i \left(I_m \otimes x^{[i]}(t) \right)$$
$$+ \sum_{j=1}^{s} \overline{G}_j \left(I_m \otimes x^{[j]}(t-\tau) \right) \tag{33}$$
$$+ \sum_{i=1}^{r} \sum_{j=1}^{s} \Upsilon_{ij} \left(I_m \otimes x^{[i]}(t) \otimes x^{[j]}(t-\tau) \right)$$

3.2. Statement of the Problem. Consider the system defined by (28), (29), and (33) with an initial condition $x(0) = x_0$. Our objective is firstly to find the optimal open loop control $u^*(t)$, which minimizes the performance index:

$$J = \frac{1}{2} x^T(t_f) Sx(t_f) + \frac{1}{2} \int_0^{t_f} \left(x^T Q x + u^T R u \right) dt \tag{34}$$

where Q and S are positive semidefinite matrices and R is symmetric positive definite with appropriate dimensions.

The direct approach presented in this paper is based on expanding system equations (28), (29), and (33) as well as objective function (34) to be minimized over an hybrid functions basis. Hence, the main purpose is to transform the optimal control problem under dynamic constraints to a nonlinear programming problem. To this end, each of the state and control variables is approximated by a finite length of unknown parameters as follows:

$$x(t) \approx X^T \mathbf{h}(t)$$
$$u(t) \approx U^T \mathbf{h}(t) \tag{35}$$

where X and U are unknown state and control parameters, respectively. Applying the *vec* operator (see Appendix) and related Kronecker product property [32] yields

$$vec(x(t)) \approx \left(\mathbf{h}^T(t) \otimes I_n \right) vec\left(X^T \right)$$

$$vec\left(u\left(t\right)\right) \approx \left(\mathbf{h}^T\left(t\right) \otimes I_m\right) vec\left(U^T\right)$$
(36)

where I_n and I_m are $n \times n$ and $m \times m$ identity matrices.

Moreover, at the initial time, $t_0 = 0$, the initial state could be written

$$x\left(0\right) \cong X_0^T h\left(t\right)$$
(37)

where

X_0^T

$$= \left[\underbrace{x_0 \ 0 \ \cdots \ 0}_{M} \ \underbrace{x_0 \ 0 \ \cdots \ 0}_{M} \ \cdots \ \underbrace{x_0 \ 0 \ \cdots \ 0}_{M} \right]$$
(38)

is an w constant vector.

For clarity purpose, let us denote z as the whole unknown parameters vector. $z_x = vec(X^T)$ and $z_u = vec(U^T)$ are, respectively, the state parameters and the control ones, such that

$$z = \begin{bmatrix} z_x \\ z_u \end{bmatrix}$$
(39)

and $z_{x0} = vec(X_0^T)$.

According to (14) and (17), the delayed state coefficients are given by

$$vec\left(X^{*T}\left(\tau\right)\right) = E_h z_{x0} + D_h z_x$$
(40)

3.3. Optimal Control Problem Reformulation Using Hybrid Functions.

The cost function (33) is composed of two parts. The first is the terminal penalty of the state, while the second is known to be the running cost.

3.3.1. Cost of the Final State Approximation.

At the final time, t_f, the state approximation could be written

$$x\left(t_f\right) \approx X^T h\left(t_f\right)$$
(41)

It is important to mention here that hybrid functions inherit an important property from Legendre polynomials($L_i(t_f) = 1, \quad \forall i = 0, \ldots, M-1$). In fact, the subset $h_{Nj}(t)$ verifies

$$h_{Nj}\left(t_f\right) = 1, \quad \forall j = 0, 1, \cdots M-1$$
(42)

The rest of hybrid functions are null at $t = t_f$.

The cross product of two hybrid functions at the final time is given by

$$\mathbf{h}\left(t_f\right)\mathbf{h}^T\left(t_f\right) = Q_f = \begin{bmatrix} 0_M & 0_M & \cdots & 0_M \\ 0_M & \ddots & \ddots & \vdots \\ \vdots & \ddots & 0_M & 0_M \\ 0_M & \cdots & 0_M & 1_M \end{bmatrix}$$
(43)

where Q_f is $NM \times NM$ matrix. 1_M stands for the all-ones $M \times M$ matrix.

Hence, the terminal penalty of the state could be approximated as follows:

$$x^T\left(t_f\right)Sx\left(t_f\right)$$
$$\approx z_x^T\left(\mathbf{h}\left(t_f\right) \otimes I_n\right)S\left(\mathbf{h}^T\left(t_f\right) \otimes I_n\right)z_x$$
(44)
$$\approx z_x^T\left(Q_f \otimes S\right)z_x$$

3.3.2. Cost of the State Trajectory Approximation.

The integral term $\int_0^{t_f} x^T(t)Qx(t) + u^T(t)Ru(t)dt$ in the criterion is approached now as

$$\int_0^{t_f} \left[z_x^T\left(\mathbf{h}\left(t\right) \otimes I_n\right)Q\left(\mathbf{h}^T\left(t\right) \otimes I_n\right)z_x \right.$$
$$\left. + z_u^T\left(\mathbf{h}\left(t\right) \otimes I_m\right)R\left(h^T\left(t\right) \otimes I_m\right)z_u \right]dt$$
(45)

which is equivalent to

$$\int_0^{t_f} \left[z_x^T\left(\mathbf{h}\left(t\right)\mathbf{h}^T\left(t\right) \otimes Q\right)z_x \right.$$
$$\left. + z_u^T\left(\mathbf{h}\left(t\right)\mathbf{h}^T\left(t\right) \otimes R\right)z_u \right]dt$$
(46)

Using the integral of the cross operational matrix C, it reduces to

$$z_x^T\left(C \otimes Q\right)z_x + z_u^T\left(C \otimes R\right)z_u$$
(47)

3.3.3. System Path Approximation.

The expansion of the system state over a hybrid basis requires the development of functions $f(x(t, \tau))$ and $g(x(t, \tau))$ over that basis. To this end, several preliminary lemmas need to be introduced.

Lemma 1. *The development of the ith Kronecker power of the state vector over a hybrid basis $\mathbf{h}(t)$ gives*

$$x^{[i]}\left(t\right) = X_{[i]}^T.\mathbf{h}\left(t\right)$$
(48)

where

$$X_{[i]}^T = X^{T[i]}.\kappa_{[i]}$$
(49)

with

$$\kappa_{[i]} = \left(\kappa_{[i-1]} \otimes I_w\right).\mathbf{K}_h, \quad for \ i = 3, 4, \ldots$$
(50)

and

$$\kappa_{[2]} = \mathbf{K}_h,$$
$$\kappa_{[1]} = \kappa_{[0]} = 1$$
(51)

We recall that $X^{T[i]}$ denotes the ith Kronecker power of the state coefficients X^T, with $\mathbf{K}_h$ being the operational matrix of the Kronecker product.

Proof. The proof of this lemma needs only a few manipulations. $\square$

Notice that results of Lemma 1 could be applied to the jth Kronecker power of the delayed state coefficients (i.e., $x^{[j]}(t-\tau) = X_{[j]}^{*T}.\mathbf{h}(t)$) and express it in terms of decision variable z_x by the mean of relation (32):

$$X_{[j]}^{*T} = X^{*T[j]}.\kappa_{[j]} \tag{52}$$

Expansion of $f(x(t,\tau))$ over the Hybrid Basis. The third term of (29) could be developed over the hybrid basis as follows:

$$x^{[i]}(t) \otimes x^{[j]}(t-\tau) \simeq \left(X^{T[i]} \otimes X^{*T[j]}\right)\kappa_{[i,j]}K_h.\mathbf{h}(t),$$
$$\forall i = 1,2,\ldots \tag{53}$$

where we notate $\kappa_{[i,j]} = \kappa_{[i]} \otimes \kappa_{[j]}$.

Now, $f(x(t,\tau))$ could be approached as follows:

$$f(x(t,\tau)) \simeq F^T.h(t) \tag{54}$$

where

$$F^T = \sum_{i=1}^{p} F_i X^{T[i]}\kappa_{[i]} + \sum_{j=1}^{q} \overline{F}_j X^{*T[j]}\kappa_{[j]}$$
$$+ \sum_{i=1}^{p}\sum_{j=1}^{q}\Gamma_{ij}\left(X^{T[i]} \otimes X^{*T[j]}\right)\kappa_{[i,j]}K_h \tag{55}$$

Expansion of $g(x(t,\tau))u(t)$ over the Hybrid Basis. Notice that the first term of $g(x(t,\tau))u(t)$ under the sum could be expanded over the hybrid basis as follows:

$$\left(I_m \otimes x^{[i]}(t)\right)u(t) \simeq \left(U^T \otimes X^{T[i]}\kappa_{[i]}\right)K_h h(t)$$
$$\simeq \left(U^T \otimes X^{T[i]}\right)\left(I_w \otimes \kappa_{[i]}\right)K_h h(t), \quad \forall i = 1,2,\ldots \tag{56}$$

while the second one could be derived similarly.

The third term could be approached as

$$\left(I_m \otimes x^{[i]}(t) \otimes x^{[j]}(t-\tau)\right)u(t)$$
$$\simeq \left(U^T \otimes \left[\left(X^{T[i]} \otimes X^{*T[j]}\right)\kappa_{[i,j]}K_h\right]\right).K_h h(t) \tag{57}$$
$$\simeq \left(U^T \otimes \left(X^{T[i]} \otimes X^{*T[j]}\right)\right)\left(I_w \otimes \kappa_{[i,j]}K_h\right)K_h h(t)$$

where i and j belong to $\mathbb{N}^*$. Then it comes

$$g(x(t,\tau))u(t) \simeq G^T.h(t) \tag{58}$$

with

$$G^T = G_0 U^T + \sum_{i=1}^{r} G_i\left(U^T \otimes X^{T[i]}\right)\left(I_w \otimes \kappa_{[i]}\right)K_h$$
$$+ \sum_{j=1}^{s}\overline{G}_j\left(U^T \otimes X^{*T[j]}\right)\left(I_w \otimes \kappa_{[j]}\right)K_h \tag{59}$$
$$+ \sum_{i=1}^{r}\sum_{j=1}^{s}\Upsilon_{ij}\left(U^T \otimes \left(X^{T[i]} \otimes X^{*T[j]}\right)\right)\left(I_w \otimes \kappa_{[i,j]}K_h\right)$$
$$\cdot K_h$$

Expansion of System Equation over the Hybrid Basis. The integration of the system equation by introducing the operational matrix of integration P with respect to notations (58) and (54) gives

$$X^T - X_0^T = F^T P + G^T P \tag{60}$$

Our objective is to express the constraint (60) in terms of decision variables z_x and z_u; to this end we apply the *vec* operator to (60). That allows us to state

$$z_x - z_{x0} = vec\left(\sum_{i=1}^{p} F_i X^{T[i]}\kappa_{[i]}P + \sum_{j=1}^{q}\overline{F}_j X^{*T[j]}\kappa_{[j]}P\right.$$
$$+ \sum_{i=1}^{p}\sum_{j=1}^{q}\Gamma_{ij}\left(X^{T[i]} \otimes X^{*T[j]}\right)\kappa_{[i,j]}K_h P + G_0 U^T P$$
$$+ \sum_{i=1}^{r} G_i\left(U^T \otimes X^{T[i]}\kappa_{[i]}\right).K_h P + \sum_{j=1}^{s}\overline{G}_j\left(U^T\right.$$
$$\otimes X^{*T[j]}\right)\left(I_w \otimes \kappa_{[j]}\right)K_h P \tag{61}$$
$$+ \sum_{i=1}^{r}\sum_{j=1}^{s}\Upsilon_{ij}\left(U^T \otimes \left(X^{T[i]} \otimes X^{*T[j]}\right)\right)\left(I_w \otimes \kappa_{[i,j]}K_h\right)$$
$$\left.\cdot K_h P\right)$$

Using the linearity property of the *vec* operator it comes

$$z_x - z_{x0} = \sum_{i=1}^{p} vec\left(F_i X^{T[i]}\kappa_{[i]}P\right)$$
$$+ \sum_{j=1}^{q} vec\left(\overline{F}_j X^{*T[j]}\kappa_{[j]}P\right)$$
$$+ \sum_{i=1}^{p}\sum_{j=1}^{q} vec\left(\Gamma_{ij}\left(X^{T[i]} \otimes X^{*T[j]}\right)\kappa_{[i,j]}K_h P\right)$$
$$+ G_0 U^T P + \sum_{i=1}^{r} vec\left(G_i\left(U^T \otimes X^{T[i]}\right)\left(I_w \otimes \kappa_{[i]}\right)\right. \tag{62}$$
$$\left.\cdot K_h P\right) + \sum_{j=1}^{s} vec\left(\overline{G}_j\left(U^T \otimes X^{*T[j]}\left(I_w \otimes \kappa_{[j]}\right)\right.\right.$$
$$\left.\cdot K_h P\right) + \sum_{i=1}^{r}\sum_{j=1}^{s} vec\left(\Upsilon_{ij}\left(U^T \otimes \left(X^{T[i]} \otimes X^{*T[j]}\right)\right)\right.$$
$$\left.\cdot \left(I_w \otimes \kappa_{[i,j]}K_h\right)K_h P\right)$$

which is equivalent to

$$z_x - z_{x0} = \sum_{i=1}^{p}\left(P^T\kappa_{[i]}^T \otimes F_i\right)vec\left(X^{T[i]}\right) + \sum_{j=1}^{q}\left(P^T\kappa_{[j]}^T\right.$$
$$\left.\otimes \overline{F}_j\right)vec\left(X^{*T[j]}\right) + \sum_{i=1}^{p}\sum_{j=1}^{q}\left(P^T K_h^T\kappa_{[i,j]}^T \otimes \Gamma_{ij}\right)$$

$$\cdot vec\left(X^{T[i]} \otimes X^{*T[j]}\right) + G_0 U^T P$$

$$+ \sum_{i=1}^{r} \left(P^T K_h^T \left(I_w \otimes \kappa_{[i]}^T\right) \otimes G_i\right) vec\left(U^T \otimes X^{T[i]}\right)$$

$$+ \sum_{j=1}^{s} \left(P^T K_h^T \left(I_w \otimes \kappa_{[i]}^T\right) \otimes \overline{G}_j\right) vec\left(U^T \otimes X^{*T[j]}\right)$$

$$+ \sum_{i=1}^{r}\sum_{j=1}^{s} \left(P^T K_h^T \left(I_w \otimes K_h^T \kappa_{[i,j]}^T\right) \otimes \Upsilon_{ij}\right)$$

$$\cdot vec\left(U^T \otimes \left(X^{T[i]} \otimes X^{*T[j]}\right)\right)$$

$$(63)$$

Lemma 2.

$$vec\left(X^{T[i]}\right) = \Pi_{(n^{i-1}, w^{i-1})}\left(mat\left(z_x\right)\right).$$

$$\Pi_{(n^{i-2}, w^{i-2})}\left(mat\left(z_x\right)\right)\ldots\Pi_{(n,w)}\left(mat\left(z_x\right)\right).z_x \qquad (64)$$

$$= \Delta_i\left(z_x\right), \quad for \; i = 2, 3, \ldots$$

where the matrix $\Pi_{(.,.)}$ *is defined in Appendix.*

Proof. The proof of this lemma needs only a few manipulations. □

Notice that results of Lemma 2 could be applied to the jth Kronecker power of the delayed state coefficients (i.e., $X^{*T[j]}$) and express it in terms of decision variable z_x by the mean of relation (42). We note

$$vec\left(X^{*T[i]}\right) = \Delta_i^*\left(z_x\right) \qquad (65)$$

Applying the *vec* operator to $\left(X^{T[i]} \otimes X^{*T[j]}\right)$ yields

$$vec\left(X^{T[i]} \otimes X^{*T[j]}\right)$$

$$= \Pi_{(n^j, w^j)}\left(mat\left(vec\left(X^{T[i]}\right)\right)\right).vec\left(X^{*T[j]}\right) \qquad (66)$$

$$= \Pi_{(n^j, w^j)}\left(mat\left(\Delta_i\left(z_x\right)\right)\Delta_j^*\left(z_x\right)\right)$$

Similarly

$$vec\left(U^T \otimes X^{T[i]}\right) = \Pi_{(n^i, w^i)}\left(mat\left(z_u\right)\right).vec\left(X^{T[i]}\right)$$
$$= \Pi_{(n^i, w^i)}\left(mat\left(z_u\right)\right)\Delta_i\left(z_x\right) \qquad (67)$$

Finally, the system path constraint could be implemented using the following equation:

$$z_x - z_{x0} = \sum_{i=1}^{p} \left(P^T \kappa_{[i]}^T \otimes F_i\right)\Delta_i\left(z_x\right) + \sum_{j=1}^{q} \left(P^T \kappa_{[j]}^T\right.$$

$$\left. \otimes \overline{F}_j\right)\Delta_i^*\left(z_x\right) + \sum_{i=1}^{p}\sum_{j=1}^{q} \left(P^T K_h^T \kappa_{[i,j]}^T \otimes \Gamma_{ij}\right)$$

$$\cdot \Pi_{(n^i, w^i)}\left(mat\left(\Delta_i\left(z_x\right)\right)\Delta_j^*\left(z_x\right)\right) + \left(P^T \otimes G_0\right)z_u$$

$$+ \sum_{i=1}^{r} \left(P^T K_h^T \left(I_w \otimes \kappa_{[i]}^T\right) \otimes G_i\right)\Pi_{(n^i, w^i)}\left(mat\left(z_u\right)\right)$$

$$\cdot \Delta_i\left(z_x\right) + \sum_{j=1}^{s} \left(P^T K_h^T \left(I_w \otimes \kappa_{[i]}^T\right) \otimes \overline{G}_j\right)$$

$$\cdot \Pi_{(n^j, w^j)}\left(mat\left(z_u\right)\right)\Delta_j^*\left(z_x\right)$$

$$+ \sum_{i=1}^{r}\sum_{j=1}^{s} \left(P^T K_h^T \left(I_w \otimes K_h^T \kappa_{[i,j]}^T\right) \otimes \Upsilon_{ij}\right)$$

$$\cdot \Pi_{(n^{i+j}, w^{i+j})}\left(mat\left(z_u\right)\right)$$

$$\cdot \Pi_{(n^i, w^i)}\left(mat\left(\Delta_i\left(z_x\right)\right)\Delta_j^*\left(z_x\right)\right)$$

$$(68)$$

Now, it could be noticed that the system path constraint is expressed properly in terms of unknown parameters z_x and z_u.

3.4. The Nonlinear Programming Problem. The optimal control problem has been approximated by a nonlinear programming problem and is given by the following: find the optimal vector z of the unknown parameters z_x and z_u that minimizes

$$\frac{1}{2}z^T \Omega z \qquad (69)$$

subject to (68).
One has

$$\Omega = \begin{bmatrix} Q_f + Q & 0_{nNM \times mNM} \\ 0_{mNM \times nNM} & R \end{bmatrix} \qquad (70)$$

The mathematical programming problem can be solved by using available nonlinear programming solvers like IPOPT or the routine *fmincon* of the MATLAB Toolbox.

After solving the latter nonlinear programming problem and determining the optimal value of the unknown parameters vector z, these parameters are substituted back into (28) to determine the optimal state vector and the optimal control.

4. Suboptimal Feedback Control

Once the optimal open loop results are obtained by solving the nonlinear programming problem given by (69)-(68), let us note

$$z^* = \begin{bmatrix} z_x^* \\ z_u^* \end{bmatrix}, \qquad (71)$$

the optimal state and control coefficients.

We are interested now, based on previous results, to synthesize the following nonlinear state feedback control law:

$$u(t) = -\sum_{i=1}^{l} K_i x^{[i]}(t) - \sum_{j=1}^{v} \overline{K}_j x^{[j]}(t - \tau) \qquad (72)$$

The idea is to find control matrices K_i and $\overline{K}_j$ such that the optimal vector (71) verifies the control equation (72).

Expanding (72) over the hybrid basis yields

$$U^T = -\sum_{i=1}^{l} K_i X^{T[i]} \kappa_{[i]} - \sum_{j=1}^{v} \overline{K}_j X^{*T[j]} \kappa_{[j]} \quad (73)$$

Substituting the control and state coefficients with their optimal values and applying the *vec* operator give

$$z_u^* = -\sum_{i=1}^{l} \alpha_i vec\left(K_i\right) - \sum_{j=1}^{v} \beta_j vec\left(\overline{K}_j\right) \quad (74)$$

with $\alpha_i = (\kappa_{[i]}^T (mat(z_x^*))^{[i]T} \otimes I_m)$ and $\beta_j = (\kappa_{[j]}^T (mat(E_h z_{x0} + D_h z_x^*))^{[j]T} \otimes I_m)$.

Finding control parameters could be then reduced to solving, in the least square sense, the following problem:

$$\mathcal{A}.\theta = \mathcal{B} \quad (75)$$

where

$$\mathcal{A} = \left[\alpha_1 \vdots \alpha_2 \vdots \cdots \vdots \alpha_l \vdots \beta_1 \vdots \beta_2 \vdots \cdots \vdots \beta_v\right],$$

$$\mathcal{B} = -z_u^*,$$

$$\theta = \begin{bmatrix} vec\left(K_1\right) \\ vec\left(K_2\right) \\ \vdots \\ vec\left(K_l\right) \\ vec\left(\overline{K}_1\right) \\ vec\left(\overline{K}_2\right) \\ \vdots \\ vec\left(\overline{K}_v\right) \end{bmatrix} \quad (76)$$

5. Computational Results

5.1. Example 1. Consider the system [33]

$$\dot{x}_1(t) = x_1(t) x_2(t) + 2x_1(t-\tau) x_2(t) - x_1(t-\tau)$$
$$+ u(t) \quad (77)$$
$$\dot{x}_2(t) = -x_1(t) + x_2(t-\tau)$$

When $u = 0$, the above system has two equilibria, one which is at the origin and the other one at $(1/3, 1/3)$.

In this example, we aim to minimize the following criterion $\int_0^{10} (x_1^2(t) + x_2^2(t) + u^2(t))dt$ in order to find optimal states and open loop control, $x^*(t)$ and $u^*(t)$, then a suboptimal control $u(t) = -Kx(t) - \overline{K}x(t-\tau)$ is characterized.

TABLE 1: Hybrid functions and block pulse functions direct approach performance analysis for Example 1.

Method	Parameters	J
Hybrid Functions	N=5, M=5	1.9955
Block Pulse Functions	N=25	2.1679
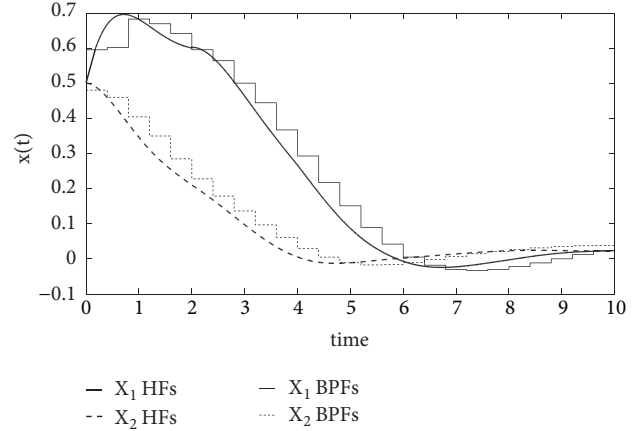
FIGURE 1: Optimal states trajectories with hybrid functions (HFs) and block pulse functions (BPFs).

Nonlinear system (77) could be written under a polynomial form (28), (29), and (32) with

$$F1 = \begin{bmatrix} 0 & 0 \\ -1 & 0 \end{bmatrix},$$

$$\overline{F}_1 = \begin{bmatrix} -1 & 0 \\ 0 & -1 \end{bmatrix},$$

$$G_0 = \begin{bmatrix} 1 \\ 0 \end{bmatrix}, \quad (78)$$

$$F_2 = \begin{bmatrix} 0 & 1 & 0 & 0 \\ 0 & 0 & 0 & 0 \end{bmatrix},$$

$$\Gamma_{11} = \begin{bmatrix} 0 & 0 & 2 & 0 \\ 0 & 0 & 0 & 0 \end{bmatrix}$$

The time delay is considered as $\tau = 2$.

5.1.1. Open Loop Study. The development presented above is implemented in this subsection by using both hybrid functions (HFs) and block pulse functions (BPFs).

Table 1 summarizes considered parameters for simulations below and obtained performances indexes with the different bases. It is then clear that hybrid basis is superior over the piecewise constant one, both with the same number of elementary functions.

Simulation results for the above open loop controlled system initialized with $(0.5, 0, 5)$ are given in Figures 1 and 2 based on hybrid and block pulse functions.
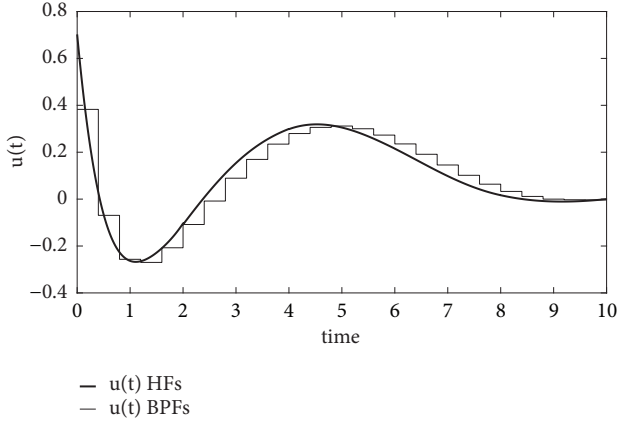
FIGURE 2: Optimal control signals with hybrid functions (HFs) and block pulse functions (BPFs).
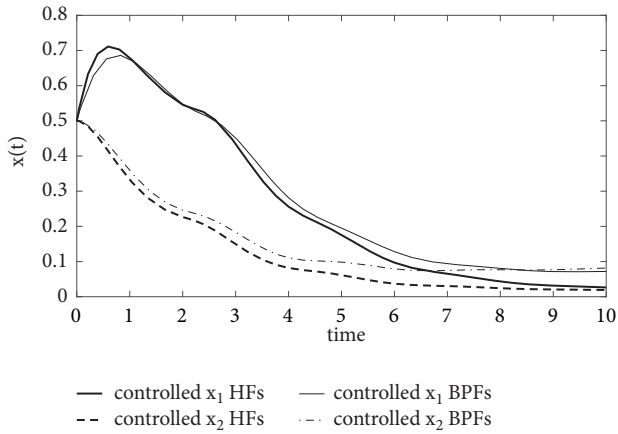
FIGURE 3: Closed loop states trajectories with hybrid functions (HFs) and block pulse functions (BPFs).

5.1.2. *Closed Loop Framework.* The state feedback control gains designed based on hybrid and block pulse open loop frameworks are as follows:

$$
\begin{aligned}
K_{HFs} &= \begin{bmatrix} 3.0813 & -1.3873 \end{bmatrix}, \\
\overline{K}_{HFs} &= \begin{bmatrix} -1.1017 & -1.7575 \end{bmatrix} \\
K_{BPFs} &= \begin{bmatrix} 2.9425 & -0.6949 \end{bmatrix} \\
\overline{K}_{BPFs} &= \begin{bmatrix} -0.9131 & -2.1364 \end{bmatrix}
\end{aligned}
\tag{79}
$$

Controlled state trajectories, obtained with determined gains, are depicted in Figure 3. It is shown that the hybrid functions technique is also better in closed loop.

Figure 4 shows the optimal states trajectories obtained by minimizing the formulated NLP problem, by using the hybrid of block pulse and Legendre polynomials basis, over a finite horizon $t_f = 10$. Controlled states with obtained suboptimal feedback are drawn on the same figure over a simulation time 20s. It could be seen that system states converge to the origin equilibrium with respect to imposed criterion.
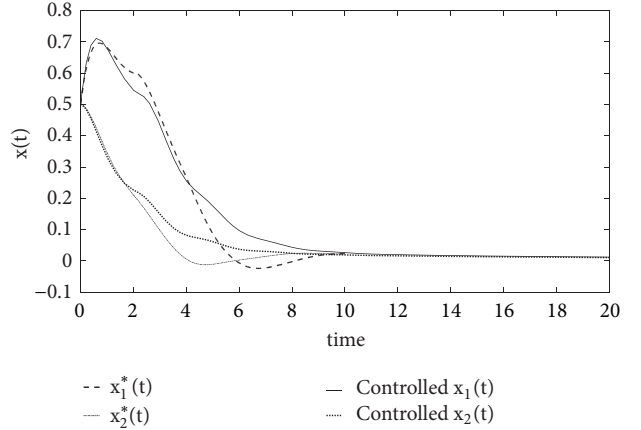
FIGURE 4: Optimal and suboptimal states trajectories.
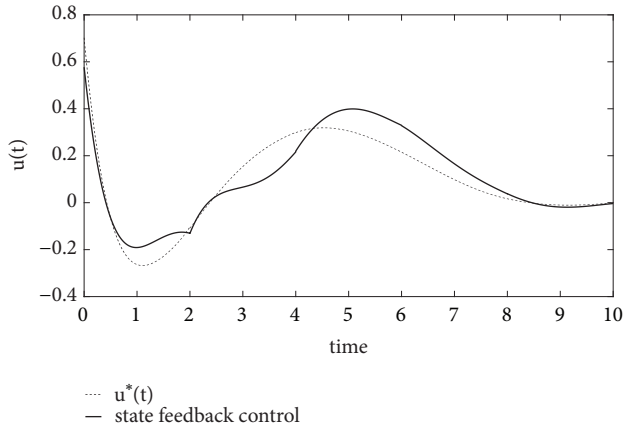
FIGURE 5: Optimal and suboptimal control signals.

Figure 5 exposes optimal control and suboptimal state feedback control signals using HFs.

5.2. *Example 2: A Two-Stage Chemical Reactor.* In this section, we consider a cascade chemical system with two reactors [34]

$$
\begin{aligned}
\dot{x}_1(t) &= -k_1 x_1(t) - \frac{1}{\theta_1} x_1(t) - \frac{1}{\theta_1} x_1(t-d) \\
&\quad + \frac{1-R_2}{V_1} x_2(t) + \delta_1\left(x_1(t-d)\right) \\
\dot{x}_2(t) &= -k_2 x_2(t) - \frac{1}{\theta_2} x_2^2(t) + \frac{R_1}{V_2} x_1(t-d) \\
&\quad - \frac{1}{\theta_2} x_2(t) + \frac{R_2}{V_2} x_2(t-d) + \frac{F}{V_2} u(t) \\
&\quad + \delta_2\left(x_2(t-d)\right)
\end{aligned}
\tag{80}
$$

where $x_i, i = 1, 2$, are the compositions, d is a known time delay, R_i are the recycle flow rates, θ_i are the reactor residence times, k_i are the reaction constants, F is the feed rate, V_i are reactor volumes, and δ_i are nonlinear functions for describing

TABLE 2: Hybrid functions and block pulse functions open loop and closed loop results for Example 2.

Method	Parameters	J	State feedback gains
Hybrid Functions	N=6, M=5	57.9349	$K_1 = [47.8366 \quad 10.7607]$,
			$K_2 = [-65.4651 \quad -26.375 \quad 0 \quad -6.0281]$,
			$\overline{K}_1 = \quad -17.7816 \quad 0.5511]$,
			$\overline{K}_2 = [9.6281 \quad 0 \quad -2.1138 \quad -0.7305]$
Block Pulse Functions	N=30	69.2999	$K_1 = [90.9235 \quad -1.9396]$,
			$K_2 = [-131.5504 \quad 0 \quad -30.3858 \quad -8.1110]$,
			$\overline{K}_1 = \quad -36.3910 \quad -9.3258]$,
			$\overline{K}_2 = [22.8197 \quad 14.7181 \quad 0 \quad 2.3220]$

the system uncertainties and external disturbances. Note that (80) is the transformed reactor model given by [34]. The original one may have a nonzero equilibrium point and the compositions x_i actually denote the deviations from the equilibrium point.

Let $R_i = 0.5$, $V_i = 0.5$, $d = 0.5$, $k_i = 0.5$, and $F = 0.5$. The uncertainties δ_i are the functions $\delta_1(x_1(t-d)) = \theta_3 x_1(t-d)$ and $\delta_2(x_2(t-d)) = 0.5\theta_4 x_2^2(t-d)$, respectively, with $\theta_i = 1$.

The simulation is done by taking $(x_1(t_0), x_2(t_0)) = (1, -2)$ for $t_0 \in [-0.5, 0]$ and results are given in Figures 3 and 4.

We consider in this example the criterion $\int_0^3 (100x_1^2(t) + 100x_2^2(t) + u^2(t))dt$ in order to find optimal states and open loop control, $x^*(t)$ and $u^*(t)$, then suboptimal control gains such that $u(t) = -K_1x(t) - K_2x^{[2]}(t) - \overline{K}_1x(t-\tau) - \overline{K}_2x^{[2]}(t-\tau)$ are investigated.

Nonlinear system (80) could be written under a polynomial form (28), (29), and (32) with

$$F1 = \begin{bmatrix} -k_1 - \dfrac{1}{\theta_1} & \dfrac{1-R_2}{V_1} \\ 0 & -k_2 - \dfrac{1}{\theta_2} \end{bmatrix},$$

$$\overline{F}_1 = \begin{bmatrix} -\dfrac{1}{\theta_1} + \theta_3 & 0 \\ \dfrac{R_1}{V_2} & \dfrac{R_2}{V_2} \end{bmatrix},$$

$$G_0 = \begin{bmatrix} 0 \\ \dfrac{F}{V_2} \end{bmatrix}, \tag{81}$$

$$F_2 = \begin{bmatrix} 0 & 0 & 0 & 0 \\ 0 & 0 & 0 & -\dfrac{1}{\theta_2} \end{bmatrix},$$

$$\overline{F}_2 = \begin{bmatrix} 0 & 0 & 2 & 0 \\ 0 & 0 & 0 & 0.5\dfrac{1}{\theta_2} \end{bmatrix}$$

Table 2 gives simulations parameters and obtained Performances indexes with the two bases utilized in Example 1. Also, state feedback gains are included.

It is worth noting that for this particular system, control gains determined by the mean of block pulse functions are not
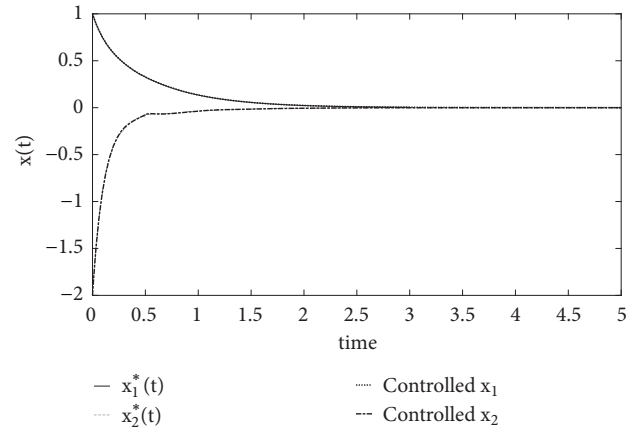
FIGURE 6: Optimal and suboptimal states trajectories of the chemical reactor.
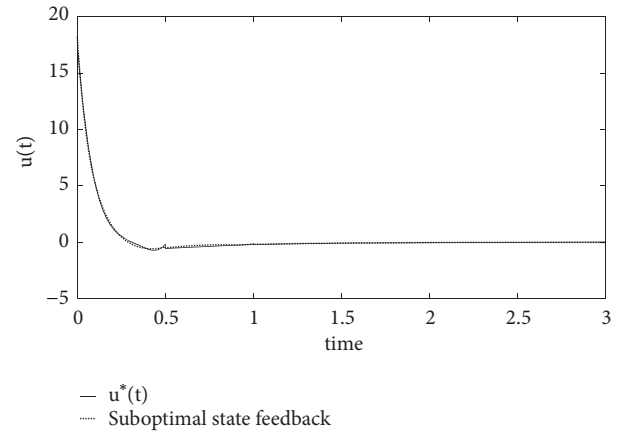
FIGURE 7: Optimal and suboptimal control signals for the chemical reactor.

stabilizing. While hybrid functions results are illustrated on Figures 6 and 7, controlled states with obtained suboptimal feedback designed over a finite horizon $t_f = 3s$ are drawn on the same figure over a simulation time $5s$. It could be seen that suboptimal system states coincide perfectly with optimal solution.

Figure 7 exposes optimal control and suggested suboptimal nonlinear state feedback control signals. The proposed

nonlinear feedback reproduces sharply the optimal open loop control.

6. Conclusion

In this paper a practical approach is developed to solve the problem of finite time quadratic optimal control for polynomial time delay systems. The proposed method is based on the expansion of the system model on a complete set of orthogonal hybrid of block pulse and Legendre polynomials. Two types of optimal control laws have been investigated. In the first step, the method focuses on the determination of the open loop optimal control law. Thus, by defining a general NLP problem for the considered system class, in the second step, a nonlinear delay-depending state feedback control law has been derived in order to meet the optimal states trajectories. The developed results have been illustrated on different examples of nonlinear time delay systems; namely, a two-stage chemical reactor and the obtained results are significant. Note that the proposed method may be enhanced, by decreasing the polynomial system matrices order when introducing the nonredundant form. In addition, if the state information is not completely available, the output feedback is a good choice. The method is feasible for the output feedback control and could be even extended to handle dynamic nonlinear state/output feedback synthesis. Moreover, the presented development is limited to some class of analytical nonlinear systems. In future work, we intend to apply the presented method to the class of switched systems, where the used hybrid functions seems to be convenient to treat that models which are a mixture of smooth functions and piecewise constant signals.

Appendix

A.

A.1. Kronecker Product and **vec**(.) *Function Properties.* The Kronecker power of order i, $X^{[i]} \in \mathbb{R}^{n^i}$ of the vector $X \in \mathbb{R}^n$ is defined by

$$X^{[0]} = 1$$
$$X^{[i]} = X^{[i-1]} \otimes X = X \otimes X^{[i-1]}, \quad for\ i = 1, 2, \ldots \tag{A.1}$$

For any matrices X, Y, and Z having appropriate dimensions, the following property of the Kronecker product is given [32]:

$$vec(XYZ) = \left(Z^T \otimes X\right) vec(Y) \tag{A.2}$$

where *vec* denotes the vectorization operator of a matrix [32].

Letting A, B, C, and D matrices with appropriate dimensions, we recall the following properties [32]:

$$(A \otimes B)(C \otimes D) = AC \otimes BD \tag{A.3}$$

$$(A \otimes B)^T = A^T \otimes B^T \tag{A.4}$$

A.2. **mat**(.) *Function.* An important matrix-valued linear function of a vector, denoted as $mat(n, m)$, is defined as follows.

If V is a vector of dimension $p = nm$, then $M = mat_{(n,m)}(V)$ is the $(n \times m)$ matrix verifying

$$V = vec(M) \tag{A.5}$$

A.3. $\Pi_{(.,.)}(.)$ *Definition.* We note e_i^p, the p dimensional unit vector which has 1 in the $i - th$ element and zeros elsewhere. The elementary matrix of dimension $(p \times q)$ could be defined by [32]

$$E_{i,j}^{p \times q} = e_i^p \left(e_j^q\right)^T \tag{A.6}$$

It has 1 on the element of coordinates (i, j) and zeros elsewhere.

Let $A = [a_{ij}] \in \mathbb{R}^{m \times n}$ and $B \in \mathbb{R}^{p \times q}$; we have

$$vec(A \otimes B) = vec\left(\left(\sum_{i=1}^m \sum_{j=1}^n a_{ij} E_{i,j}^{m \times n}\right) \otimes B\right)$$
$$= \Pi_{(m,n)}(B) vec(A) \tag{A.7}$$

where

$$\Pi_{(m,n)}(B) = \left[vec\left(E_{1,1}^{m \times n} \otimes B\right) \cdots vec\left(E_{m,1}^{m \times n} \otimes B\right) \right.$$
$$\vdots vec\left(E_{1,2}^{m \times n} \otimes B\right) \cdots vec\left(E_{m,2}^{m \times n} \otimes B\right) \tag{A.8}$$
$$\left. \vdots \cdots \vdots vec\left(E_{1,n}^{m \times n} \otimes B\right) \cdots vec\left(E_{m,n}^{m \times n} \otimes B\right) \right]$$

The matrix $\Pi_{(.,.)}$, with respect to dimensions, could be also used as follows:

$$vec(A \otimes B) = vec\left(\left(\sum_{i=1}^p \sum_{j=1}^q b_{ij} E_{i,j}^{p \times q}\right) \otimes B\right)$$
$$= \Pi_{(p,q)}(A) vec(B) \tag{A.9}$$

where

$$\Pi_{(p,q)}(A) = \left[vec\left(A \otimes E_{1,1}^{p \times q}\right) \cdots vec\left(A \otimes E_{m,1}^{p \times q}\right) \right.$$
$$\vdots vec\left(A \otimes E_{1,2}^{p \times q}\right) \cdots vec\left(A \otimes E_{m,2}^{p \times q}\right) \tag{A.10}$$
$$\left. \vdots \cdots \vdots vec\left(A \otimes E_{1,n}^{p \times q}\right) \cdots vec\left(A \otimes E_{m,n}^{p \times q}\right) \right]$$

Data Availability

The data used to support the findings of this study are included within the article.

Conflicts of Interest

The authors declare that there are no conflicts of interest regarding the publication of this paper.

References

[1] V. Kolmanovskii and A. Myshkis, *Applied Theory of Functional Differential Equations*, Kluwer Academic, Dordrecht, Netherlands, 1999.

[2] L. Göllmann and H. Maurer, "Theory and applications of optimal control problems with multiple time-delays," *Journal of Industrial and Management Optimization*, vol. 10, no. 2, pp. 413–441, 2014.

[3] C. Hua, S. Wu, X. Yang, and X. Guan, "Stability analysis of time-delay systems via free-matrix-based double integral inequality," *International Journal of Systems Science*, vol. 48, no. 2, pp. 257–263, 2017.

[4] K. Kobayashi, A. Minohara, and Y. Uchimura, "Network-based control with state prediction for time-delayed system," in *Proceedings of the 2018 IEEE 27th International Symposium on Industrial Electronics (ISIE)*, pp. 982–987, Cairns, QLD, Australia, June 2018.

[5] O. Naifar, A. Ben Makhlouf, M. Hammami, and A. Ouali, "State feedback control law for a class of nonlinear time-varying system under unknown time-varying delay," *Nonlinear Dynamics*, vol. 82, no. 1-2, pp. 349–355, 2015.

[6] A. J. Koshkouei, M. H. Farahi, and K. J. Burnham, "An almost optimal control design method for nonlinear time-delay systems," *International Journal of Control*, vol. 85, no. 2, pp. 147–158, 2012.

[7] L. Göllmann, D. Kern, and H. Maurer, "Optimal control problems with delays in state and control variables subject to mixed control-state constraints," *Optimal Control Applications & Methods*, vol. 30, no. 4, pp. 341–365, 2008.

[8] F. Khellat, "Optimal control of linear time-delayed systems by linear Legendre multiwavelets," *Journal of Optimization Theory and Applications*, vol. 143, no. 1, pp. 107–121, 2009.

[9] H. R. Marzban, "Optimal control of linear multi-delay systems based on a multi-interval decomposition scheme," *Optimal Control Applications and Methods*, vol. 37, no. 1, pp. 190–211, 2016.

[10] H. R. Marzban and S. M. Hoseini, "Solution of linear optimal control problems with time delay using a composite Chebyshev finite difference method," *Optimal Control Applications and Methods*, vol. 34, no. 3, pp. 253–274, 2013.

[11] H. R. Sharif, M. A. Vali, M. Samavat, and A. A. Gharavisi, "A new algorithm for optimal control of time-delay systems," *Applied Mathematical Sciences*, vol. 5, no. 9-12, pp. 595–606, 2011.

[12] C. Yu, Q. Lin, R. Loxton, K. L. Teo, and G. Wang, "A hybrid time-scaling transformation for time-delay optimal control problems," *Journal of Optimization Theory and Applications*, vol. 169, no. 3, pp. 876–901, 2016.

[13] H. R. Marzban and S. M. Hoseini, "An efficient discretization scheme for solving nonlinear optimal control problems with multiple time delays," *Optimal Control Applications and Methods*, vol. 37, no. 4, pp. 682–707, 2016.

[14] G. L. Kharatishvili, "The maximum principle in the theory of optimal process with time-lags," *Doklady Akademii Nauk SSSR*, vol. 136, pp. 39–42, 1961.

[15] M. Dadkhah and M. H. Farahi, "Optimal control of time delay systems via hybrid of block-pulse functions and orthonormal Taylor series," *International Journal of Applied and Computational Mathematics*, vol. 2, no. 1, pp. 137–152, 2016.

[16] M. Jamshidi and C. M. Wang, "A computational algorithm for large-scale nonlinear time-delay systems," *IEEE Transactions on Systems, Man, and Cybernetics*, vol. 14, no. 1, pp. 2–9, 1984.

[17] C. J. Goh and K. L. Teo, "Control parametrization: a unified approach to optimal control problems with general constraints," *Automatica*, vol. 24, no. 1, pp. 3–18, 1988.

[18] H. Jaddu and E. Shimemura, "Computation of optimal control trajectories using Chebyshev polynomials: parameterization, and quadratic programming," *Optimal Control Applications and Methods*, vol. 20, no. 1, pp. 21–42, 1999.

[19] Z. Rafiei, B. Kafash, and S. M. Karbassi, "State-control parameterization method based on using hybrid functions of block-pulse and Legendre polynomials for optimal control of linear time delay systems," *Applied Mathematical Modelling: Simulation and Computation for Engineering and Environmental Systems*, vol. 45, pp. 1008–1019, 2017.

[20] M. Mortezaee and A. Nazemi, "Solving infinite horizon optimal control problems of nonlinear interconnected large scale dyncmaic systems via a Haar wavelet collocation scheme," *Iranian J Operations Research*, vol. 6, no. 2, pp. 19–35, 2015.

[21] A. Nazemi and M. Mansoori, "Solving optimal control problems of the time-delayed systems by Haar wavelet," *Journal of Vibration and Control*, vol. 21, no. 11, pp. 2657–2670, 2016.

[22] I. Malmir, "Optimal control of linear time-varying systems with state and input delays by Chebyshev wavelets," *Statistics, Optimization & Information Computing*, vol. 5, no. 4, pp. 302–324, 2017.

[23] B. Iben Warrad, M. K. Bouafoura, and N. Benhadj Braiek, "Static output tracking control for non-linear polynomial time-delay systems via block-pulse functions," *Journal of the Chinese Institute of Engineers*, vol. 41, no. 3, pp. 194–205, 2018.

[24] B. I. Warrad, M. K. Bouafoura, and N. Benhadj Braiek, "Observer based output tracking control for bounded linear time variant systems," *Nonlinear Dynamics and Systems Theory. An International Journal of Research and Surveys*, vol. 15, no. 4, pp. 428–440, 2015.

[25] S. Bichiou, M. K. Bouafoura, and N. Benhadj Braiek, "Time optimal control laws for bilinear systems," *Mathematical Problems in Engineering*, vol. 2018, Article ID 5217427, 10 pages, 2018.

[26] H. R. Marzban and M. Razzaghi, "Optimal control of linear delay systems via hybrid of block-pulse and Legendre polynomials," *Journal of The Franklin Institute*, vol. 341, no. 3, pp. 279–293, 2004.

[27] N. Haddadi, Y. Ordokhani, and M. Razzaghi, "Optimal control of delay systems by using a hybrid functions approximation," *Journal of Optimization Theory and Applications*, vol. 153, no. 2, pp. 338–356, 2012.

[28] H. R. Marzban and H. Pirmoradian, "A novel approach for the numerical investigation of optimal control problems containing multiple delays," *Optimal Control Applications and Methods*, vol. 39, no. 1, pp. 302–325, 2018.

[29] M. Dadkhah, M. H. Farahi, and A. Heydari, "Optimal control of a class of non-linear time-delay systems via hybrid functions," *IMA Journal of Mathematical Control and Information*, vol. 34, no. 1, pp. 255–270, 2017.

[30] R. Mohammadzadeh and M. Lakestani, "Optimal control of linear time-delay systems by a hybrid of block-pulse functions

and biorthogonal cubic Hermite spline multiwavelets," *Optimal Control Applications and Methods*, vol. 39, no. 1, pp. 357–376, 2018.

[31] B. M. Mohan and S. Kumar Kar, "Orthogonal functions approach to optimal control of delay systems with reverse time terms," *Journal of The Franklin Institute*, vol. 347, no. 9, pp. 1723–1739, 2010.

[32] J. W. Brewer, "Kronecker products and matrix calculus in system theory," *IEEE Transactions on Circuits and Systems II: Express Briefs*, vol. 25, no. 9, pp. 772–781, 1978.

[33] A. Papachristodoulou, "Robust stabilization of nonlinear time delay systems using convex optimization," in *Proceedings of the 44th IEEE Conference on Decision and Control, and the European Control Conference, CDC-ECC '05*, pp. 5788–5793, Sevilla, Spain, December 2005.

[34] C. Hua, P. X. Liu, and X. Guan, "Backstepping control for nonlinear systems with time delays and applications to chemical reactor systems," *IEEE Transactions on Industrial Electronics*, vol. 56, no. 9, pp. 3723–3732, 2009.

Research Article

New Results on the Control for a Kind of Uncertain Chaotic Systems Based on Fuzzy Logic

Bo Wang [ID] [1,2] **and L. L. Chen** [1]

[1] *School of Electrical Engineering and Electronic Information, Xihua University, Chengdu 610039, China*
[2] *School of Applied Mathematics, University Electronic Science and Technology of China, Chengdu 610054, China*

Correspondence should be addressed to Bo Wang; coolbie@163.com

In this paper, the problem of the control for an uncertain nonlinear chaotic system has been studied; based on fuzzy logic, a kind of single-dimensional controller is constructed for the control of the chaotic systems in the situation that uncertainties and unknowns exist; at last some typical numerical simulations are carried out, and corresponding results illuminate the effectiveness of the controller.

1. Introduction

Nonlinear systems exist in real engineering widely. Since the pioneering work from Lurie in 1944, the research on nonlinear system control has become the challenging issue, and many techniques, such as differential geometry technique [1, 2], sliding mode technique [3–6] and so on, have been proposed to deal with this problem. It can be noted that these approaches are based on multidimensional control. However, in some cases, the single-dimensional controller is more cherished for its simpler structure and more convenient application in practice.

As an important branch of nonlinear systems, chaotic system and its control received many attentions, and a lot of related results have been reported so far [7–14]. For instance, in [7], based on output feedback control strategy, a method was presented to realize the control for unified chaotic systems; in [8], the synchronization control for Lü systems with unknown parameters was investigated; in [9], the adaptive control for the synchronization of hyperchaotic systems was studied; in [10], the fuzzy control for Arneodo chaotic system is discussed. However most of these researches focused on just one typical chaotic system. In addition, it is well known that there exist many kinds of uncertainties in

practical control system, and the following chaotic system model is studied.

$$
\begin{aligned}
\dot{x}_i &= (b_i + \Delta b_i)\, x_{i+1} + f_i\left(\overline{x}_i\right), \quad 1 \le i \le n-1 \\
\dot{x}_n &= h_n(x) + \Delta h_n(x) + f_n(x) + b_n u \\
y &= x_1
\end{aligned}
\tag{1}
$$

where $x = [x_1, x_2, \cdots, x_n]^{\mathrm{T}} \in \mathbf{R}^n, \overline{x}_i = [x_1, x_2, \cdots, x_i]^{\mathrm{T}} \in \mathbf{R}^i, b_i$ are the known system parameters and satisfy $0 < b_{im} \le |b_i| \le b_{iM}$, where b_{im} and b_{iM} are the positive scalars, $f_n(x)$ and $f_i(\overline{x}_i)$ are the unknown terms, Δb_i and Δh_n are the uncertainties, h_n is the known term, b_n is the control parameter, y is the system output, and u is the single-dimensional control input. A lot of chaotic systems can be transformed into the system with the form (1) through topological mapping.

As an important technique, fuzzy techniques are very suitable for the research of nonlinear and complex systems (see [15–23] and references therein), and they will be introduced to design the single-dimensional controller for system (1) in this paper. Some simulations will be included to illuminate the effectiveness of the constructed controller.

2. Model Description and Preliminaries

It is well known that fuzzy logic system can approximate the nonlinear function. Let $f(x)$ denote the smooth function and $\varphi(x)$ denote the fuzzy logic system. There exists the optimal parameter $\theta^* = \arg\min_{\theta \in \Omega_0}[\sup_{x \in \Omega}|f(x) - \varphi(x)|]$ for the least approximation error, where Ω_0 and Ω are bounded sets of θ and x.

Define fuzzy rules as

$$\text{IF } x_1 \text{ is F}_1^j \text{ and} \ldots \text{and } x_n \text{ is F}_n^j,$$
$$\text{then } \varphi(x) \text{ is B}^j \quad (j = 1, 2, \cdots, N) \tag{2}$$

Define the following fuzzy logic system [16]

$$\varphi(x) = \frac{\sum_{j=1}^{N} \theta_j \prod_{i=1}^{n} \mu_{F_i^j}(x_i)}{\sum_{j=1}^{N} \prod_{i=1}^{n} \mu_{F_i^j}(x_i)} \tag{3}$$

where $x = [x_1, x_2, \cdots, x_n]^T \in \mathbf{R}^n$, $\mu_{F_i^j}(x_i)$ is the fuzzy membership function, $\theta_j = \max_{\varphi(x) \in \mathbf{R}} B^j(\varphi(x))$.

Let $\xi(x) = [\xi_1(x), \xi_2(x), \cdots, \xi_N(x)]^T$ and $\theta = [\theta_1, \theta_2, \cdots, \theta_N]^T$; one can get $\varphi(x) = \xi^T(x)\theta$.

Hence, if $\overline{f}_k$ is the continuous function from a compact set, $\varphi_k(\overline{x}_k)$ can approximate $\overline{f}_k$, which means that there exist $\theta_k = [\theta_1^k, \theta_2^k, \cdots, \theta_N^k]^T$ and $\varepsilon_k > 0$, such that

$$\left|\overline{f}_k(\overline{x}_k) - \xi_k^T(\overline{x}_k)\theta_k\right| \le \varepsilon_k, \quad k = 1, 2, \cdots, n. \tag{4}$$

where $\overline{x}_k = [x_1, x_2, \cdots, x_k]^T, k = 1, 2, \cdots, n$.
In the paper, the following lemmas are concerned.

Lemma 1 (see [24]). *If $f(t) \in L_\infty \cap L_2$ and $\dot{f}(t) \in L_\infty$, one has*

$$\lim_{t \longrightarrow +\infty} f(t) = 0 \tag{5}$$

3. Main Results

For convenience, let $\Delta g_i(\overline{x}_{i+1}) = \Delta b_i x_{i+1}$, $1 \le i \le n-1$, and $\Delta g_n = \Delta h_n(x)$.

Step 1. Define the tracking error $e_1 = y - y_d$; y_d is the desired trajectory.

For the first subsystem of system (1), the virtual variable α_1 is introduced, such that

$$\dot{e}_1 = \dot{x}_1 - \dot{y}_d$$
$$= b_1 x_2 - b_1 \alpha_1 + b_1 \alpha_1 + f_1(\overline{x}_1) + \Delta g_1(\overline{x}_2) - \dot{y}_d \tag{6}$$
$$= b_1 e_2 + b_1 \alpha_1 + f_1(\overline{x}_1) + \Delta g_1(\overline{x}_2) - \dot{y}_d$$

where $e_2 = x_2 - \alpha_1$.

Step 2. For the second subsystem of system (1), the virtual variable α_2 is introduced, such that

$$\dot{e}_2 = \dot{x}_2 - \dot{\alpha}_1$$
$$= b_2 x_3 - b_2 \alpha_2 + b_2 \alpha_2 - \dot{\alpha}_1 + f_2(\overline{x}_2) + \Delta g_2(\overline{x}_3) \tag{7}$$
$$= b_2 e_3 + b_2 \alpha_2 - \dot{\alpha}_1 + f_2(\overline{x}_2) + \Delta g_2(\overline{x}_3)$$

where $e_3 = x_3 - \alpha_2$.

Step k ($k < n$). For k-th subsystem of system (1), the virtual variable α_k is introduced, such that

$$\dot{e}_k = \dot{x}_k - \dot{\alpha}_{k-1}$$
$$= b_k x_{k+1} - b_k \alpha_k + b_k \alpha_k - \dot{\alpha}_{k-1} + f_k(\overline{x}_k)$$
$$+ \Delta g_k(\overline{x}_{k+1}) \tag{8}$$
$$= b_k e_{k+1} + b_k \alpha_k - \dot{\alpha}_{k-1} + f_k(\overline{x}_k) + \Delta g_k(\overline{x}_{k+1})$$

where $e_{k+1} = x_{k+1} - \alpha_k$

Step n. For the n-th subsystem of system (1), one can get

$$\dot{e}_n = \dot{x}_n - \dot{\alpha}_{n-1}$$
$$= b_n u + h_n(x) + f_n(x) + \Delta g_n(x) - \dot{\alpha}_{n-1} \tag{9}$$

where $e_n = x_n - \alpha_{n-1}$

Then, the following tracking error dynamic system can be derived

$$\dot{e}_i = b_i e_{i+1} + b_i \alpha_i - \dot{\alpha}_{i-1} + f_i(\overline{x}_i) + \Delta g_i(\overline{x}_{i+1}(t)),$$
$$1 \le i \le n-1 \tag{10}$$

$$\dot{e}_n = -\dot{\alpha}_{n-1} + h_n(x) + f_n(x) + \Delta g_n(x) + b_n u$$

where $\alpha_0 = y_d$

The object of this paper is to design a controller, such that

$$\lim_{t \longrightarrow +\infty} e(t) = 0 \tag{11}$$

Choose the first Lyapunov function as

$$V_1 = \frac{1}{2b_1} e_1^2 \tag{12}$$

then

$$\dot{V}_1 = \frac{1}{b_1} e_1 \dot{e}_1 = \frac{1}{b_1} e_1 (b_1 e_2 + b_1 \alpha_1 + f_1 + \Delta g_1 - \dot{y}_d)$$
$$= e_1 (e_2 + \alpha_1) + \frac{1}{b_1} e_1 (f_1 + \Delta g_1 - \dot{y}_d) \tag{13}$$
$$= e_1 (e_2 + \alpha_1 + \overline{f}_1)$$

where

$$\overline{f}_1 = \frac{f_1 + \Delta g_1 - \dot{y}_d}{b_1}. \tag{14}$$

Let $\alpha_1 = -\lambda_1 e_1 - \varphi_1, \lambda_1 > 0$, where $\varphi_1 = \xi_1^T(\overline{x}_2)\theta_1$ is used to approximate the nonlinear function $\overline{f}_1$, then

$$\dot{V}_1 = -\lambda_1 e_1^2 + e_1 e_2 + e_1 \left(\overline{f}_1 - \varphi_1 \right) \tag{15}$$

Choose the second Lyapunov function as

$$V_2 = V_1 + \frac{1}{2b_2} e_2^2 \tag{16}$$

Let $\alpha_2 = -\lambda_2 e_2 - e_1 - \varphi_2$, $\lambda_2 > 0$, where $\varphi_2 = \xi_2^{\mathrm{T}}(\overline{x}_3)\theta_2$ is used to approximate the nonlinear function $\overline{f}_2$, then

$$\begin{aligned}
\dot{V}_2 &= \dot{V}_1 + \frac{1}{b_2} e_2 \dot{e}_2 \\
&= \dot{V}_1 + e_2 \left(e_3 + \alpha_2 + \frac{f_2 + \Delta g_2 - \dot{\alpha}_1}{b_2} \right) \\
&= -\lambda_1 e_1^2 + e_2 \left(e_1 + e_3 + \alpha_2 + \overline{f}_2 \right) + e_1 \left(\overline{f}_1 - \varphi_1 \right) \\
&= -\lambda_1 e_1^2 + e_2 e_3 - \lambda_2 e_2^2 + e_1 \left(\overline{f}_1 - \varphi_1 \right) \\
&\quad + e_2 \left(\overline{f}_2 - \varphi_2 \right) \\
&= -\sum_{i=1}^{2} \lambda_i e_i^2 + \sum_{i=1}^{2} e_i \left(\overline{f}_i - \varphi_i \right) + e_2 e_3
\end{aligned} \tag{17}$$

where

$$\overline{f}_2 = \frac{f_2 + \Delta g_2 - \dot{\alpha}_1}{b_2}. \tag{18}$$

Let $\alpha_{k-1} = -\lambda_{k-1} e_{k-1} - e_{k-2} - \varphi_{k-1}$, $\lambda_{k-1} > 0$, where $\varphi_{k-1} = \xi_{k-1}^{\mathrm{T}}(\overline{x}_k)\theta_{k-1}$ is used to approximate the nonlinear function $\overline{f}_{k-1}$, then

$$\dot{V}_{k-1} = -\sum_{i=1}^{k-1} \lambda_i e_i^2 + \sum_{i=1}^{k-1} e_i \left(\overline{f}_i - \varphi_i \right) + e_{k-1} e_k \tag{19}$$

Choose the k-th Lyapunov function ($k < n$) as

$$V_k = V_{k-1} + \frac{1}{2b_k} e_k^2 \tag{20}$$

Hence

$$\begin{aligned}
\dot{V}_k &= \dot{V}_{k-1} + \frac{1}{b_k} e_k \dot{e}_k \\
&= \dot{V}_{k-1} + e_k \left(e_{k+1} + \alpha_k + \frac{1}{b_k} \left(f_k + \Delta g_k - \dot{\alpha}_{k-1} \right) \right) \\
&= -\sum_{i=1}^{k-1} \lambda_i e_i^2 + \sum_{i=1}^{k-1} e_i \left(\overline{f}_i - \varphi_i \right) \\
&\quad + e_k \left(e_{k+1} + \alpha_k + e_{k-1} + \frac{1}{b_k} \left(f_k + \Delta g_k - \dot{\alpha}_{k-1} \right) \right) \\
&= -\sum_{i=1}^{k-1} \lambda_i e_i^2 + \sum_{i=1}^{k-1} e_i \left(\overline{f}_i - \varphi_i \right) \\
&\quad + e_k \left(e_{k+1} + \alpha_k + e_{k-1} + \overline{f}_k \right)
\end{aligned} \tag{21}$$

where

$$\overline{f}_k = \frac{1}{b_k} \left(f_k + \Delta g_k - \dot{\alpha}_{k-1} \right). \tag{22}$$

Let $\alpha_k = -\lambda_k e_k - e_{k-1} - \varphi_k$, $\lambda_k > 0$, where $\varphi_k = \xi_k^{\mathrm{T}}(\overline{x}_{k+1})\theta_k$ is used to approximate the nonlinear function $\overline{f}_k$, then

$$\dot{V}_k = -\sum_{i=1}^{k} \lambda_i e_i^2 + \sum_{i=1}^{k} e_i \left(\overline{f}_i - \varphi_i \right) + e_k e_{k+1} \tag{23}$$

It is consistent with our notation that $\alpha_{n-1} = -\lambda_{n-1} e_{n-1} - e_{n-2} - \varphi_{n-1}$, $\lambda_{n-1} > 0$, where $\varphi_{n-1} = \xi_{n-1}^{\mathrm{T}}(\overline{x}_n)\theta_{n-1}$ is used to approximate the nonlinear function $\overline{f}_{n-1}$, then

$$\dot{V}_{n-1} = -\sum_{i=1}^{n-1} \lambda_i e_i^2 + \sum_{i=1}^{n-1} e_i \left(\overline{f}_i - \varphi_i \right) + e_{n-1} e_n \tag{24}$$

Choose the n-th Lyapunov function as

$$V_n = V_{n-1} + \frac{1}{2b_n} e_n^2 \tag{25}$$

Hence

$$\begin{aligned}
\dot{V}_n &= \dot{V}_{n-1} + e_n \left(u + \frac{1}{b_n} \left(\overline{f}_n - \dot{\alpha}_{n-1} \right) \right) \\
&= -\sum_{i=1}^{n-1} \lambda_i e_i^2 + \sum_{i=1}^{n-1} e_i \left(\overline{f}_i - \varphi_i \right) + e_{n-1} e_n \\
&\quad + e_n \left(u + \frac{1}{b_n} \left(f_n + \Delta g_n - \dot{\alpha}_{n-1} \right) \right) \\
&= -\sum_{i=1}^{n-1} \lambda_i e_i^2 + \sum_{i=1}^{n-1} e_i \left(\overline{f}_i - \varphi_i \right) \\
&\quad + e_n \left(u + e_{n-1} + \frac{1}{b_n} \left(f_n + \Delta g_n - \dot{\alpha}_{n-1} \right) \right)
\end{aligned} \tag{26}$$

where

$$\overline{f}_n = \frac{1}{b_n} \left(f_n + \Delta g_n - \dot{\alpha}_{n-1} \right) \tag{27}$$

Suppose that $\varphi_n = \xi_n^{\mathrm{T}}(x)\theta_n$ approximate the nonlinear function $\overline{f}_n$ and that is based on Lyapunov theory, then the following theoretical result can be obtained.

Theorem 2. *For $\lambda_n > 0$, $r_i > 0$ and $k_i > 0$, based on the controller*

$$u = -\lambda_n e_n - e_{n-1} - \frac{h_n(x)}{b_n} - \xi_n^{\mathrm{T}}(x)\theta_n \tag{28}$$

and the adaptive law

$$\dot{\theta}_i = r_i e_i \xi_i - 2k_i \theta_i, \quad i = 1, 2, \cdots, n \tag{29}$$

then the output of chaotic system (10) can track the desired trajectory.

Proof. Based on (25), construct Lyapunov function as

$$V = V_n + \sum_{i=1}^{n} \frac{1}{2r_i} \overline{\theta}_i^{\mathrm{T}} \overline{\theta}_i \tag{30}$$

where $\overline{\theta}_i = \theta_i^* - \theta_i$.

Combined with (28), it can be concluded that

$$
\begin{aligned}
\dot{V} &= -\sum_{i=1}^{n} \lambda_i e_i^2 + \sum_{i=1}^{n} e_i \left(\overline{f}_i - \varphi_i \right) - \sum_{i=1}^{n} \frac{1}{r_i} \overline{\theta}_i^{\mathrm{T}} \dot{\theta}_i \\
&= -\sum_{i=1}^{n} \lambda_i e_i^2 + \sum_{i=1}^{n} e_i \left(\overline{f}_i - \theta_i^{*\mathrm{T}} \xi_i \right) \\
&\quad + \sum_{i=1}^{n} e_i \left(\theta_i^{*\mathrm{T}} \xi_i - \theta_i^{\mathrm{T}} \xi_i \right) - \sum_{i=1}^{n} \frac{1}{r_i} \overline{\theta}_i^{\mathrm{T}} \dot{\theta}_i \\
&= -\sum_{i=1}^{n} \lambda_i e_i^2 + \sum_{i=1}^{n} e_i \left(\overline{f}_i - \theta_i^{*\mathrm{T}} \xi_i \right) + \sum_{i=1}^{n} e_i \overline{\theta}_i^{\mathrm{T}} \xi_i \\
&\quad - \sum_{i=1}^{n} \frac{1}{r_i} \overline{\theta}_i^{\mathrm{T}} \dot{\theta}_i \\
&\leq -\sum_{i=1}^{n} \lambda_i e_i^2 + \sum_{i=1}^{n} \overline{\theta}_i^{\mathrm{T}} \left(e_i \xi_i - \frac{1}{r_i} \dot{\theta}_i \right) + \sum_{i=1}^{n} |e_i \varepsilon_i|
\end{aligned} \tag{31}
$$

Define

$$S = -\sum_{i=1}^{n} \lambda_i e_i^2 + \sum_{i=1}^{n} \overline{\theta}_i^{\mathrm{T}} \left(e_i \xi_i - \frac{1}{r_i} \dot{\theta}_i \right) + \sum_{i=1}^{n} |e_i \varepsilon_i| \tag{32}$$

Supposing that $a_i = \lambda_i - 1/2$, it can be derived

$$\lambda_i = a_i + \frac{1}{2} \tag{33}$$

Hence

$$S = -\sum_{i=1}^{n} a_i e_i^2 - \frac{1}{2} \sum_{i=1}^{n} e_i^2 + \sum_{i=1}^{n} \overline{\theta}_i^{\mathrm{T}} \left(e_i \xi_i - \frac{1}{r_i} \dot{\theta}_i \right) + \sum_{i=1}^{n} |e_i \varepsilon_i| \tag{34}$$

Consider

$$-\frac{1}{2} \sum_{i=1}^{n} e_i^2 + \sum_{i=1}^{n} |e_i \varepsilon_i| \leq -\frac{1}{2} \sum_{i=1}^{n} \varepsilon_i^2 \tag{35}$$

and with adaptive law (29), one can get

$$
\begin{aligned}
S &\leq -\sum_{i=1}^{n} a_i e_i^2 + \sum_{i=1}^{n} \overline{\theta}_i^{\mathrm{T}} \left(e_i \xi_i - \frac{1}{r_i} \left(r_i e_i \xi_i - 2k_i \theta_i \right) \right) \\
&\quad + \frac{1}{2} \sum_{i=1}^{n} \varepsilon_i^2 \\
&= -\sum_{i=1}^{n} a_i e_i^2 + \sum_{i=1}^{n} \frac{2k_i}{r_i} \left(\theta_i^* - \theta_i \right)^{\mathrm{T}} \theta_i + \frac{1}{2} \sum_{i=1}^{n} \varepsilon_i^2 \\
&= -\sum_{i=1}^{n} a_i e_i^2 + \sum_{i=1}^{n} \frac{k_i}{r_i} \left(2\theta_i^{*\mathrm{T}} \theta_i - 2\theta_i^{\mathrm{T}} \theta_i \right) + \frac{1}{2} \sum_{i=1}^{n} \varepsilon_i^2
\end{aligned} \tag{36}
$$

Consider

$$\theta_i^{*\mathrm{T}} \theta_i^* + \theta_i^{\mathrm{T}} \theta_i \geq 2\theta_i^{*\mathrm{T}} \theta_i \tag{37}$$

Then

$$2\theta_i^{*\mathrm{T}} \theta_i - 2\theta_i^{\mathrm{T}} \theta_i \leq \theta_i^{*\mathrm{T}} \theta_i^* - \theta_i^{\mathrm{T}} \theta_i \tag{38}$$

One can derive

$$
\begin{aligned}
\dot{V} &\leq -\sum_{i=1}^{n} a_i e_i^2 + \sum_{i=1}^{n} \frac{k_i}{r_i} \left(-\theta_i^{\mathrm{T}} \theta_i + \theta_i^{*\mathrm{T}} \theta_i^* \right) + \frac{1}{2} \sum_{i=1}^{n} \varepsilon_i^2 \\
&= -\sum_{i=1}^{n} a_i e_i^2 + \sum_{i=1}^{n} \frac{k_i}{r_i} \left(-\theta_i^{\mathrm{T}} \theta_i - \theta_i^{*\mathrm{T}} \theta_i^* \right) + \sum_{i=1}^{n} \frac{2k_i}{r_i} \theta_i^{*\mathrm{T}} \theta_i^* \\
&\quad + \frac{1}{2} \sum_{i=1}^{n} \varepsilon_i^2
\end{aligned} \tag{39}
$$

Consider

$$
\begin{aligned}
\overline{\theta}_i^{\mathrm{T}} \overline{\theta}_i &= \left(\theta_i^* - \theta_i \right)^{\mathrm{T}} \left(\theta_i^* - \theta_i \right) = \theta_i^{*\mathrm{T}} \theta_i^* - 2\theta_i^{*\mathrm{T}} \theta_i + \theta_i^{\mathrm{T}} \theta_i \\
&\leq 2\theta_i^{*\mathrm{T}} \theta_i^* + 2\theta_i^{\mathrm{T}} \theta_i
\end{aligned} \tag{40}
$$

Then

$$-\frac{1}{2} \overline{\theta}_i^{\mathrm{T}} \overline{\theta}_i \geq -\theta_i^{\mathrm{T}} \theta_i - \theta_i^{*\mathrm{T}} \theta_i^* \tag{41}$$

One can derive

$$
\begin{aligned}
\dot{V} &\leq -\sum_{i=1}^{n} a_i e_i^2 - \sum_{i=1}^{n} \frac{k_i}{2r_i} \overline{\theta}_i^{\mathrm{T}} \overline{\theta}_i + \sum_{i=1}^{n} \frac{2k_i}{r_i} \theta_i^{*\mathrm{T}} \theta_i^* + \frac{1}{2} \sum_{i=1}^{n} \varepsilon_i^2 \\
&\leq -\sum_{i=1}^{n} a_i \frac{2b_{im}}{2b_i} e_i^2 - \sum_{i=1}^{n} \frac{k_i}{2r_i} \overline{\theta}_i^{\mathrm{T}} \overline{\theta}_i + \sum_{i=1}^{n} \frac{2k_i}{r_i} \theta_i^{*\mathrm{T}} \theta_i^* \\
&\quad + \frac{1}{2} \sum_{i=1}^{n} \varepsilon_i^2
\end{aligned} \tag{42}
$$

Choosing $\lambda_i > 1/2$, one can obtain $a_i > 0$.

Let

$$
\begin{aligned}
a_0 &= \min \left\{ 2b_{im} a_i, k_i : i = 1, 2, \cdots, n \right\} \\
b_0 &= \sum_{i=1}^{n} \frac{2k_i}{r_i} \theta_i^{*\mathrm{T}} \theta_i^* + \frac{1}{2} \sum_{i=1}^{n} \varepsilon_i^2
\end{aligned} \tag{43}
$$

Then

$$\dot{V} \leq -a_0 \left(\sum_{i=1}^{n} \frac{1}{2b_i} e_i^2 + \sum_{i=1}^{n} \frac{1}{2r_i} \overline{\theta}_i^{\mathrm{T}} \overline{\theta}_i \right) + b_0 = -a_0 V + b_0 \tag{44}$$

The solution of differential equation $\dot{V} = -a_0 V + b_0$ is

$$
\begin{aligned}
V(t) &= V(0) \exp\left(-a_0 t \right) \\
&\quad + b_0 \exp\left(-a_0 t \right) \frac{\exp\left(a_0 t \right) - 1}{a_0}
\end{aligned} \tag{45}
$$

Considering (44), it can be derived that

$$V(t) \leq \left(V(0) - \frac{b_0}{a_0}\right) \exp(-a_0 t) + \frac{b_0}{a_0}$$

$$\leq V(0) \exp(-a_0 t) + \frac{b_0}{a_0} \leq V(0) + \frac{b_0}{a_0} \tag{46}$$

Define

$$d_0 = \min\{a_i : i = 1, 2, \cdots, n\}. \tag{47}$$

From (42), one can obtain

$$\dot{V} \leq -\sum_{i=1}^{n} a_i e_i^2 - \sum_{i=1}^{n} \frac{k_i}{2r_i} \overline{\theta}_i^{\mathrm{T}} \overline{\theta}_i + \sum_{i=1}^{n} \frac{2k_i}{r_i} \theta_i^{*\mathrm{T}} \theta_i^* + \frac{1}{2} \sum_{i=1}^{n} \varepsilon_i^2$$

$$\leq -\min\{a_i\} \sum_{i=1}^{n} e_i^2 + \sum_{i=1}^{n} \frac{2k_i}{r_i} \theta_i^{*\mathrm{T}} \theta_i^* + \frac{1}{2} \sum_{i=1}^{n} \varepsilon_i^2 \tag{48}$$

$$= -d_0 \sum_{i=1}^{n} e_i^2 + b_0$$

Hence, when $\|e\| > (b_0/d_0)^{1/2}$, one can get $\dot{V} < 0$, which means $e(t) \in L_\infty$.

Integrating both sides of inequality (48) from 0 to T, one can get

$$\int_0^T \dot{V}(t) \, dt \leq -\int_0^T d_0 \sum_{i=1}^{n} e_i^2(s) \, ds + T b_0 \tag{49}$$

Consider

$$\int_0^T \dot{V}(t) \, dt = V(T) - V(0) \tag{50}$$

One can get

$$V(T) - V(0) \leq -d_0 \sum_{i=1}^{n} \int_0^T e_i^2(s) \, ds + T b_0 \tag{51}$$

Hence

$$\sum_{i=1}^{n} \int_0^T e_i^2(s) \, ds \leq \frac{1}{d_0} \left(V(0) - V(T) + T b_0\right) \tag{52}$$

which means $e(t) \in L_2$. From error dynamic system (10), it can be concluded that $\dot{e}(t) \in L_\infty$. Accordingly based on Lemma 1, one can get $\lim_{t \to +\infty} e(t) = 0$, which means the achievement of the track control. The proof of Theorem 2 is thus completed. □

4. Numerical Simulation

First the following uncertain Arneodo system is considered.

$$\dot{x}_1 = b_1 x_2 + f_1$$

$$\dot{x}_2 = (b_2 + \Delta b_2) x_3 + f_2 \tag{53}$$

$$\dot{x}_3 = h_3 + \Delta h_3 + f_3 + b_3 u$$

where

$$b_1 = 1,$$

$$f_1 = 0.3 \sin x_1,$$

$$b_2 = 1,$$

$$\Delta b_2 = 0.02,$$

$$f_2 = 0.1 \cos(x_1 x_2),$$

$$h_3 = c_3 x_1^3 - c_0 x_1 - c_1 x_2 - c_2 x_3,$$

$$\Delta h_3 = 0.1 x_1,$$

$$f_3 = 0.2 \cos(x_1) \sin(x_3),$$

$$b_3 = 5,$$

$$c_0 = -5.4,$$

$$c_1 = 3.5,$$

$$c_2 = 1,$$

$$c_3 = -1,$$

$$k_1 = 1,$$

$$k_2 = 1.5,$$

$$k_3 = 1.5,$$

$$r_1 = 1.5,$$

$$r_2 = 2,$$

$$r_3 = 2,$$

$$\lambda_1 = 2.5,$$

$$\lambda_2 = 5,$$

$$\lambda_3 = 5,$$

$$\alpha_1 = -\lambda_1 (x_1 - y_d) + \dot{y}_d,$$

$$\alpha_2 = -\lambda_2 (x_2 - \alpha_1) - (x_1 - y_d) - \xi_2^{\mathrm{T}}(\overline{x}_2) \theta,$$

$$u = -\lambda_3 (x_3 - \alpha_2) - (x_2 - \alpha_1) - \xi_3^{\mathrm{T}}(\overline{x}_3) \theta,$$

$$\xi_{1j}(\overline{x}_1) = \frac{\mu F_1^j(x_1)}{\sum_{j=1}^{9} \mu F_1^j(x_1)},$$

$$\xi_{2j}(\overline{x}_2) = \frac{\mu F_1^j(x_1) \mu F_2^j(x_2)}{\sum_{j=1}^{9} \mu F_1^j(x_1) \mu F_2^j(x_2)},$$

$$\xi_{3j}(x) = \frac{\mu F_1^j(x_1) \mu F_2^j(x_2) \mu F_3^j(x_3)}{\sum_{j=1}^{9} \mu F_1^j(x_1) \mu F_2^j(x_2) \mu F_3^j(x_3)},$$

$$\mu F_i^1(x_i) = \exp\left(-0.5(x_i + 2)^2\right),$$

$$\mu F_i^2(x_i) = \exp\left(-0.5(x_i + 1.5)^2\right),$$

$$\mu F_i^3(x_i) = \exp\left(-0.5(x_i + 1)^2\right),$$

$$\mu F_i^4(x_i) = \exp\left(-0.5(x_i + 0.5)^2\right),$$

$$\mu F_i^5(x_i) = \exp\left(-0.5 x_i^2\right)],$$

$$\mu F_i^6(x_i) = \exp\left(-0.5(x_i - 0.5)^2\right),$$

$$\mu F_i^7(x_i) = \exp\left(-0.5(x_i - 1)^2\right),$$

$$\mu F_i^8(x_i) = \exp\left(-0.5(x_i - 1.5)^2\right),$$
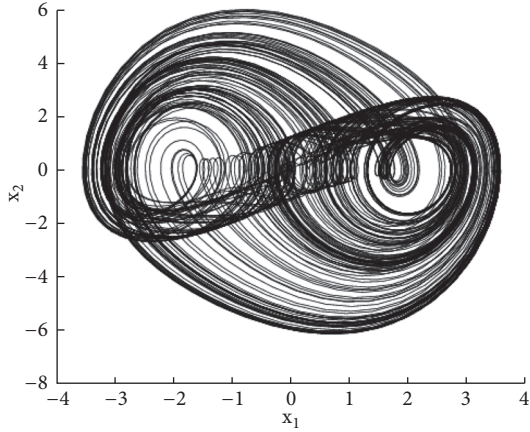
FIGURE 1: Chaotic attractor of Arneodo system.
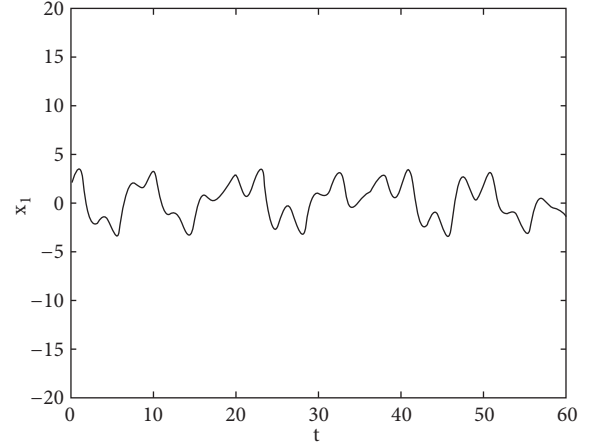
FIGURE 2: State response of x_1 of Arneodo system.

$$\mu F_i^9(x_i) = \exp\left(-0.5(x_i - 2)^2\right),$$

$$\xi_1(\overline{x}_1) = \left[\xi_{11}(\overline{x}_1), \xi_{12}(\overline{x}_1), \cdots, \xi_{19}(\overline{x}_1)\right]^T,$$

$$\xi_2(\overline{x}_2) = \left[\xi_{21}(\overline{x}_2), \xi_{22}(\overline{x}_2), \cdots, \xi_{29}(\overline{x}_2)\right]^T,$$

$$\xi_3(\overline{x}_3) = \left[\xi_{31}(\overline{x}_3), \xi_{32}(\overline{x}_3), \cdots, \xi_{39}(\overline{x}_3)\right]^T.$$

$$(54)$$

Let desired trajectory $y_d = \sin 2\pi t$, initial value $x(0) = [2, 0, 0]^T$, and the simulation results are displayed in Figures 1–7.

Remark 3. Figure 1 displays the chaotic attractor of Arneodo system. Figure 2 displays the state response of x_1 of Arneodo system. From Figures 1 and 2, it can be seen that Arneodo system has the complicated dynamical behavior. Figure 3 displays the state response of variable x_1 of uncertain Arneodo system. It can be seen that the existence of unknowns and uncertainties makes Arneodo system unstable.

Remark 4. Figure 4 displays the fuzzy membership function. Figure 5 displays the state response of control input. Figure 6 displays the state response of y_d and y. Figure 7 displays the state response of position tracking error. From Figures 4–7, it can be seen that for uncertain Arneodo system, the position tracking can be achieved during 0.5 second based on the designed controller.

5. Conclusion

In this paper, based on fuzzy logic, a single-dimensional controller has been constructed for the control of a kind of uncertain chaotic systems. Some typical examples have been employed and corresponding simulation results have illuminated the effectiveness of proposed controller.
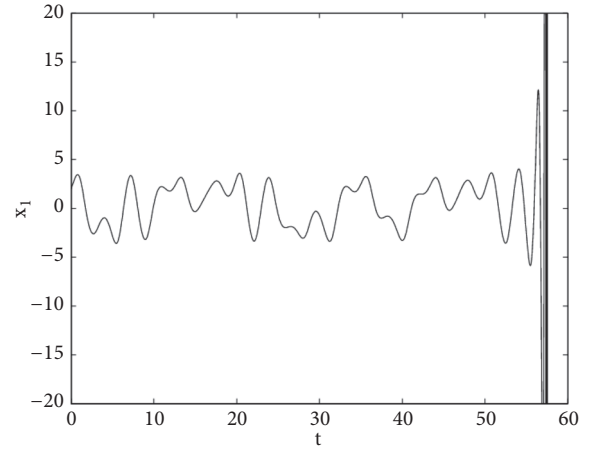
FIGURE 3: State response of x_1 of uncertain Arneodo system.
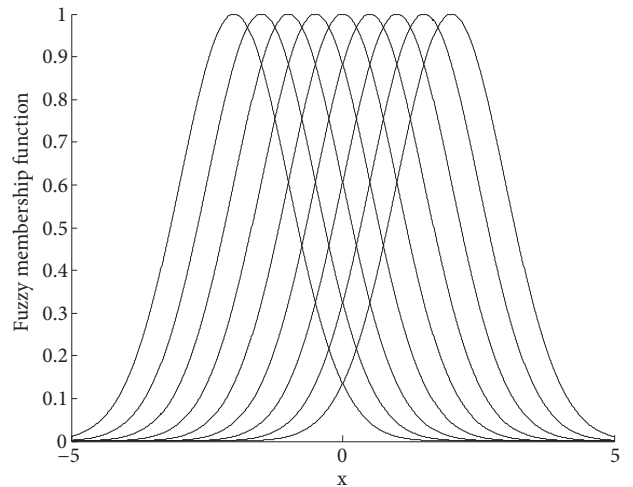
FIGURE 4: Fuzzy membership function.
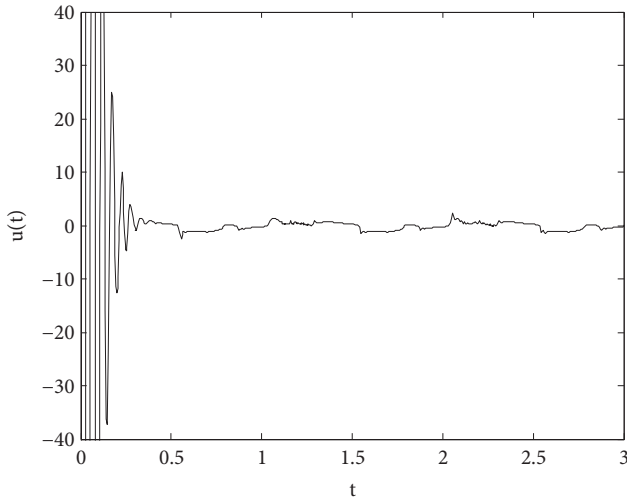
FIGURE 5: State response of control input.

y_d
y
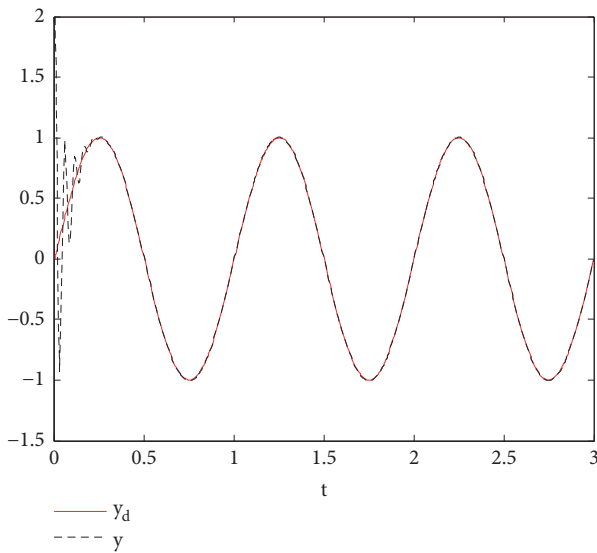
FIGURE 6: State response of y_d and y.
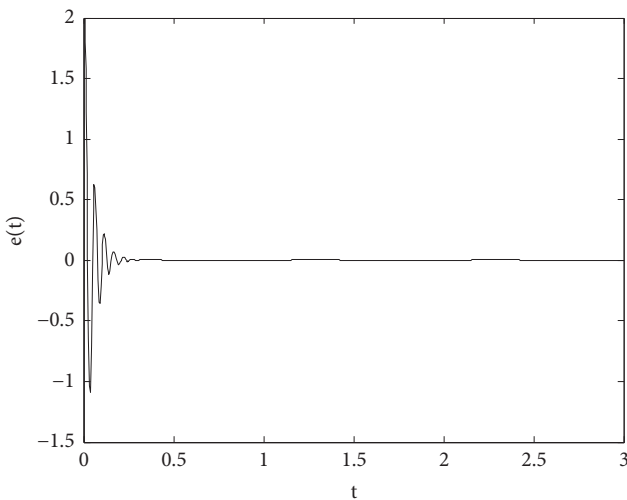
FIGURE 7: State response of position tracking error.

Data Availability

The data used to support the findings of this study are included within the article.

Conflicts of Interest

The authors declare that there are no conflicts of interest regarding the publication of this paper.

Acknowledgments

References

[1] T.-L. Chien, C.-C. Chen, and C.-Y. Hsu, "Tracking control of nonlinear automobile idle-speed time-delay system via differential geometry approach," *Journal of The Franklin Institute*, vol. 342, no. 7, pp. 760–775, 2005.

[2] R. Yu and Y. Xie, "Investigation on cubic chua's circuit via differential geometry," *Physics Procedia*, vol. 24, pp. 412–417, 2012.

[3] A. Levant and M. Livne, "Weighted homogeneity and robustness of sliding mode control," *Automatica*, vol. 72, pp. 186–193, 2016.

[4] Z. Liu, C. Gao, and Y. Kao, "Robust H-infinity control for a kind of neutral-type systems via sliding mode observer," *Applied Mathematics and Computation*, vol. 271, pp. 669–681, 2015.

[5] J. Hua, L.-X. An, and Y.-M. Li, "Bionic fuzzy sliding mode control and robustness analysis," *Applied Mathematical Modelling: Simulation and Computation for Engineering and Environmental Systems*, vol. 39, no. 15, pp. 4482–4493, 2015.

[6] J. Xu, M. Wang, and L. Qiao, "Dynamical sliding mode control for the trajectory tracking of underactuated unmanned underwater vehicles," *Ocean Engineering*, vol. 105, pp. 54–63, 2015.

[7] Z. Shen and J. Li, "Chaos control for a unified chaotic system using output feedback controllers," *Mathematics and Computers in Simulation*, vol. 132, pp. 208–219, 2017.

[8] H. Tirandaz and A. Hajipour, "Adaptive synchronization and anti-synchronization of TSUCS and Lü unified chaotic systems with unknown parameters," *Optik - International Journal for Light and Electron Optics*, vol. 130, pp. 543–549, 2017.

[9] B. Wang, P. Shi, H. R. Karimi, Y. Song, and J. Wang, "Robust H-infinity synchronization of a hyper-chaotic system with disturbance," *Nonlinear Analysis: Real World Applications*, vol. 14, no. 3, pp. 1487–1495, 2013.

[10] W. Wang and Y. Fan, "Synchronization of Arneodo chaotic system via backstepping fuzzy adaptive control," *Optik - International Journal for Light and Electron Optics*, vol. 126, no. 20, pp. 2679–2683, 2015.

[11] B. Wang, L. Chen, and Y. Liu, "New results on contrast enhancement for infrared images," *Optik - International Journal for Light and Electron Optics*, vol. 178, pp. 1264–1269, 2019.

[12] C. Ge, H. Wang, Y. Liu, and J. H. Park, "Stabilization of chaotic systems under variable sampling and state quantized controller," *Fuzzy Sets and Systems*, vol. 344, pp. 129–144, 2018.

[13] B. Wang, L. Chen, and Z. Zhang, "A novel method on the edge detection of infrared image," *Optik - International Journal for Light and Electron Optics*, vol. 180, pp. 610–614, 2019.

[14] B. Wang, X. Zhang, and X. Dong, "Novel secure communication based on chaos synchronization," *IEICE Transactions on Fundamentals of Electronics, Communications and Computer Sciences*, vol. E101A, no. 7, pp. 1132–1135, 2018.

[15] Y. Zheng, "Fuzzy prediction-based feedback control of fractional order chaotic systems," *Optik - International Journal for Light and Electron Optics*, vol. 126, no. 24, pp. 5645–5649, 2015.

[16] B. Wang and L. L. Chen, "New results on fuzzy synchronization for a kind of disturbed memristive chaotic system," *Complexity*, vol. 2018, Article ID 3079108, 9 pages, 2018.

[17] B. Wang, J. Cheng, and S. M. Zhong, "Bounded input bounded output stability for Lurie system with time-varying delay," *Advances in Difference Equations*, Paper No. 57, 13 pages, 2018.

[18] B. Wang, J. Cheng, and F. Zou, "Stochastic finite-time H∞ filtering for nonlinear Markovian jump systems with partly known transition probabilities," *Proceedings of the Institution of Mechanical Engineers, Part I: Journal of Systems and Control Engineering*, vol. 233, no. 1, pp. 31–43, 2018.

[19] G. Lai, Z. Liu, Y. Zhang, and C. L. Philip Chen, "Adaptive fuzzy tracking control of nonlinear systems with asymmetric actuator backlash based on a new smooth inverse," *IEEE Transactions on Cybernetics*, vol. 46, no. 6, pp. 1250–1262, 2016.

[20] B. Wang, "Results on a novel piecewise-linear memristor-based chaotic system," *Complexity*, vol. 2019, Article ID 8948656, 6 pages, 2019.

[21] V. Nazari and B. Surgenor, "Improved position tracking performance of a pneumatic actuator using a fuzzy logic controller with velocity, system lag and friction compensation," *International Journal of Control, Automation, and Systems*, vol. 14, no. 5, pp. 1376–1388, 2016.

[22] B. Wang, D. Zhang, J. Cheng, and J. H. Park, "Fuzzy model-based nonfragile control of switched discrete-time systems," *Nonlinear Dynamics*, vol. 93, no. 4, pp. 2461–2471, 2018.

[23] L. X. Wang, *Adaptive Fuzzy Systems and Control*, Prentice Hall, Englewood Cliffs, NJ, USA, 1994.

[24] K. Narendra and A. Annaswamy, *Stable Adaptive Systems*, Prentice-Hall, Englewood Cliffs, NJ, USA, 1989.

Research Article

Consensus of Multiagent Systems Described by Various Noninteger Derivatives

G. Nava-Antonio (ID),[1] **G. Fernández-Anaya,**[1] **E. G. Hernández-Martínez** (ID),[2]
J. J. Flores-Godoy (ID),[3] **and E. D. Ferreira-Vázquez** (ID)[4]

[1]*Departamento de Física y Matemáticas, Universidad Iberoamericana, México City, Mexico*
[2]*Departamento de Estudios en Ingeniería para la Innovación, Universidad Iberoamericana, México City, Mexico*
[3]*Departamento de Matemática, Universidad Católica del Uruguay, Montevideo, Uruguay*
[4]*Departamento de Ingeniería Eléctrica, Universidad Católica del Uruguay, Montevideo, Uruguay*

Correspondence should be addressed to J. J. Flores-Godoy; jose.flores@ucu.edu.uy

In this paper, we unify and extend recent developments in Lyapunov stability theory to present techniques to determine the asymptotic stability of six types of fractional dynamical systems. These differ by being modeled with one of the following fractional derivatives: the Caputo derivative, the Caputo distributed order derivative, the variable order derivative, the conformable derivative, the local fractional derivative, or the distributed order conformable derivative (the latter defined in this work). Additionally, we apply these results to study the consensus of a fractional multiagent system, considering all of the aforementioned fractional operators. Our analysis covers multiagent systems with linear and nonlinear dynamics, affected by bounded external disturbances and described by fixed directed graphs. Lastly, examples, which are solved analytically and numerically, are presented to validate our contributions.

1. Introduction

The concept of fractional calculus arose more than three centuries ago, thanks to a question posed by L'Hôpital to Leibniz where the meaning of derivatives of order 1/2 was asked [1]. However, this discipline has gained popularity only in the last decades, in which new methods to solve and analyze fractional differential equations have appeared and researchers have made great efforts to study real phenomena using these tools. This modern boom has occurred mainly because of the capability of fractional order calculus to model certain systems more accurately in comparison with traditional integer order calculus. This greater precision is due to the liberty that fractional calculus gives us to consider noninteger orders for the differential and integral operators.

Throughout the life of this branch of mathematics, various definitions for the fractional derivative have been

proposed. A survey of the most common of these can be found in Kilbas, Srivastava, and Trujillo [2]; Petráš [3]; Podlubny [4], along with a rich overview of interesting applications and simulation techniques. In this paper, we will focus on six different fractional derivatives. The first of them is the Caputo fractional derivative which is widely studied in the already-mentioned references and is preferred by many because the Caputo derivative of a constant is zero (which is not true for all fractional derivatives) and the initial conditions of a Caputo fractional system have the same physical interpretation as the integer order case.

The rest of the fractional derivatives addressed in this work are of more recent origin. In the fractional variable-order (also known as time-varying order) derivative, introduced in Samko and Ross [5], the orders of differentiation can be functions of the independent variable or even of other parameters. In Sun, Chen, Wei, and Chen [6] it is argued

that variable-order calculus allows to better describe certain systems with memory properties that change, for example, with time or position.

The Caputo distributed order derivative, originally presented in Caputo [7], acquired relevance in problems with ultra-slow diffusion, where it has been applied with physical justification, for instance, in Chechkin, Klafter, and Sokolov [8]; Naber [9]. Regarding its meaning, a possible conceptual interpretation for this fractional derivative is suggested in Lorenzo and Hartley [10]: in systems where nonhomogenous or anisotropic properties are involved, it might be appropriate to consider that each differential element of the system should have its own differentiation order.

The fractional derivatives discussed in the above lines do not satisfy the product or the chain rules. Furthermore, the monotonicity of a function is not specified by the sign of those derivatives. The conformable derivative emerged in response to these inconveniences, as explained in Khalil, Al Horani, Yousef, and Sababheh [11]; nevertheless, this fractional operator, which is defined as a limit, loses the memory properties and global character of the others, which are built with integrals. A very similar but more general fractional derivative was proposed in Almeida, Guzowska, and Odzijewicz [12]. That operator is characterized by a kernel function that can be tuned to better represent a given physical system. In the same spirit of the Caputo distributed derivative, in this article we introduce the distributed conformable derivative, a further generalization of the fractional differential operator defined in Khalil et al. [11].

The broad variety of applications that the aforementioned fractional derivatives have had is remarkable: from quantum mechanics, Laskin [13], to control theory, Baleanu, Machado, and Luo [14], and study of human memory and emotions, Tabatabaei, Yazdanpanah, Jafari, and Sprott [15]. In general, these and other problems involving differential equations of fractional order are complicated to approach and in many cases there are no analytical or numerical schemes to solve them. Consequently, the qualitative theory of fractional dynamical systems has become an important line of research. Within this field, the Lyapunov direct method is a tool that allows us to determine the stability and long-term behavior of a certain system, without the need of solving it.

In recent years, Lyapunov stability theory has integrated to fractional calculus; see Li, Chen, and Podlubny [16]; Souahi, Makhlouf, and Hammami [17]; Tabatabaei, Talebi, and Tavakoli [18]; Taghavian and Tavazoei [19]; Wang and Li [20]. One of the objectives of the present article is to take advantage of the similarities between those papers and unify them into a generalized fractional Lyapunov method, useful for systems of differential equations with the fractional derivatives mentioned in the above paragraphs. As an application of this— and with the purpose of comparing the performance of different fractional derivatives in the same problem— we also study in this article the consensus problem of a generalized fractional multiagent system.

A multiagent system is an arrangement of various agents that are organized to accomplish group objectives by means of their local interactions. A multiagent system is said to achieve consensus when the dynamics of the agents converge to a certain desired value. We can appreciate the relevance of this concept by noticing its multiple applications, including: the study of the formation of multivehicle systems [21], the synchronization of coupled oscillators [22], or the distributed sensor fusion in sensor networks [23].

The consensus of multiagent systems has been mostly investigated under the framework of integer order calculus. Extensive introductory reviews of this topic can be found in W. Ren and Beard [21]; W. Ren and Cao [24]. Some of the ideas presented in those references have been generalized for fractional order systems, solely using the Caputo fractional derivative, for example: in Yu, Jiang, Hu, and Yu [25], an adaptive pinning control is used to realize leader-following consensus in a fractional multiagent system; Yin, Yue, and Hu [26] studied the consensus problem for fractional heterogeneous systems, made up of agents with different dynamics; Song, Cao, and Liu [27] proposed a distributed protocol to accomplish robust consensus, based on the information of second-order neighbors; Nava-Antonio et al. [28] present sufficient conditions for consensus of multiagent systems with distributed fractional order; and G. Ren and Yu [29] gave conditions for fractional multiagent systems to achieve robust consensus, via Mittag-Leffler stability methods. That last article is the main inspiration of the second half of this paper, where we will extend the results of G. Ren and Yu [29] to be used in multiagent systems with five other fractional differentiation orders, with linear or nonlinear dynamics, and in the presence of external perturbations.

The order of this text is described next. In Section 2, fundamental preliminary concepts are introduced. Section 3 contains, in two parts, our main results: firstly, we present the generalized fractional Lyapunov direct method and, then, we apply it to study the consensus of multiagent systems modeled with different fractional derivatives. Afterwards, Section 4 gives examples where we verify the validity of the developed theory. Lastly, Section 5 contains the conclusions of the present work.

2. Preliminary Concepts

In the following section, we present the definitions of various fractional derivatives and discuss certain properties of systems of equations with these operators. All the definitions below are given considering orders of differentiation $\alpha \in (0, 1)$.

Definition 1 (Aguila-Camacho, Duarte-Mermoud, and Gallegos [30]). The Caputo fractional derivative of order α is defined as

$$T_1^\alpha x(t) = \frac{1}{\Gamma(1-\alpha)} \int_{t_0}^t \frac{x'(\tau)}{(t-\tau)^\alpha} d\tau, \quad t > t_0, \tag{1}$$

where $x'(t)$ is the integer derivative of $x(t)$. We suppose that $x(t)$ is a differentiable function for all $t \geq t_0$ and for all operators in this work.

Definition 2 (Tabatabaei et al. [18]). The modified initialized Caputo fractional derivative of time-varying order $\alpha(t)$ is defined as follows:

$$T_2^{\alpha} x(t) = \frac{1}{\Gamma(1 - \alpha(t))} \int_0^t \frac{x'(\zeta)}{(t - \zeta)^{\alpha(t)}} d\zeta + \Psi_c^x(t),$$ (2)

$$\forall t \geq 0,$$

where $\Psi_c^x(t) = (1/\Gamma(1 - \alpha(t))) \int_{-c}^0 (t - \zeta)^{-\alpha(t)} x'(\zeta) d\zeta$ captures the behavior of x before $t = 0$, assuming that x begins from $-c < 0$. Since we will focus in this paper on systems which are at rest at $t < 0$, $\Psi_c^x(t) = 0$.

Definition 3 (Jiao, Chen, and Podlubny [31]). The distributed order fractional derivative in the Caputo sense with respect to the density function $c : [\mu, 1] \longrightarrow [0, +\infty)$ for some $1 > \mu > 0$, such that $\int_\mu^1 c(\alpha) d\alpha \neq 0$, is defined as follows:

$$T_3^{\alpha} x(t) = \int_\mu^1 c(\alpha) T_1^{\alpha} x(t) d\alpha.$$ (3)

The Laplace transform of a distributed order derivative, which will appear in the derivation of our main results, is

$$\mathcal{L}\{T_3^{\alpha} x(t)\} = C(s) X(s) - \frac{1}{s} C(s) x(0^+),$$ (4)

where $C(s) = \int_{m-1}^m c(\alpha) s^{\alpha} d\alpha$.

Definition 4 (Souahi et al. [17]). The conformable fractional derivative starting from a of a function x defined on $[a, \infty)$ is

$$T_4^{\alpha} x(t) = \lim_{\epsilon \longrightarrow 0} \frac{x(t + \epsilon(t - a)^{1-\alpha}) - x(t)}{\epsilon},$$ (5)

for all $t > a$. If $\lim_{t \longrightarrow a^+} T_4^{\alpha} x(t)$ exists, then

$$T_4^{\alpha} x(a) = \lim_{t \longrightarrow a^+} T_4^{\alpha} x(t).$$ (6)

Definition 5 (Almeida et al. [12]). Let $k : [a, b] \longrightarrow \mathbb{R}$ be a continuous nonnegative map such that $k(t) \neq 0$, whenever $t > a$ and $x : [a, b] \longrightarrow \mathbb{R}$. By definition, x is α-differentiable at $t > a$, with respect to kernel k, if the limit

$$T_5^{\alpha} x(t) = \lim_{\epsilon \longrightarrow 0} \frac{x(t + \epsilon k(t)^{1-\alpha}) - x(t)}{\epsilon}$$ (7)

exists. The local fractional derivative at $t = a$ is defined by

$$T_5^{\alpha} x(a) = \lim_{t \longrightarrow a^+} T_5^{\alpha} x(t),$$ (8)

if the limit exists.

Definition 6. Let k and x be functions as in Definition 5 and c a density function as in Definition 3. The distributed conformable fractional derivative is defined as

$$T_6^{\alpha} x(t) = \int_0^1 c(\alpha) T_5^{\alpha} x(t) d\alpha.$$ (9)

Theorem 7 (Almeida et al. [12]). *A function $x : [a, b] \longrightarrow \mathbb{R}$ is α-differentiable at $t > a$ if and only if it is differentiable at t. In that case, we have the relation*

$$T_5^{\alpha} x(t) = k(t)^{1-\alpha} x'(t), \quad t > a.$$ (10)

Notice that Definition 5 is a particular case of Definition 6. Then by Theorem 7 if we take $k(t) = t - a$ we obtain

$$T_4^{\alpha} x(t) = (t - a)^{1-\alpha} x'(t), \quad t > a.$$ (11)

In a similar form by substituting (10) in (9) we have

$$T_6^{\alpha} x(t) = x'(t) \int_0^1 c(\alpha) k(t)^{1-\alpha} d\alpha.$$ (12)

Consider the generalized system of fractional differential equations of order $\alpha \in (0, 1)$:

$$T_j^{\alpha} x = f(t, x(t)), \quad j = 1, 2, 3, 4, 5, \text{or } 6,$$ (13)

where $x \in \mathbb{R}^n$, $x(t_0) = x_0$, and $f : \mathbb{R}_+ \times \mathbb{R}^n \longrightarrow \mathbb{R}^n$ is a given nonlinear function is Lipzchitz with respect to the second argument. For simplicity and without loss of generality, we will consider that the equilibrium points of the systems analyzed hereafter are at the origin, i.e., $f(t, 0) = 0$, $\forall t \geq 0$.

Throughout this paper, we will assume that the studied systems have unique solutions. The existence and uniqueness of the solution of system (13) is discussed in Podlubny [4], Xu and He [32], Ford and Morgado [33], and Bayour and Torres [34], for the cases $j = 1, 2, 3$, and 4, respectively. The theory of existence and uniqueness of solutions when $j = 5$ or 6 can be easily generalized from Bayour and Torres [34], by taking into account (11) and (12).

The Final Value Theorem and an important Laplace transform associated with fractional calculus, both used in the following sections of this article, are presented next.

Theorem 8 (Duffy [35]). *Let $F(s) = \mathcal{L}\{f(t)\}$. If all poles of $sF(s)$ are in the open left-half complex plane, then*

$$\lim_{t \longrightarrow \infty} f(t) = \lim_{s \longrightarrow 0} sF(s).$$ (14)

Definition 9 (Podlubny [4]). A two-parameter function of the Mittag-Leffler type is defined by

$$E_{\alpha, \beta}(z) = \sum_{k=0}^{\infty} \frac{z^k}{\Gamma(\alpha k + \beta)}, \quad \alpha > 0, \ \beta > 0$$ (15)

Lemma 10 (Podlubny [4]). *The Mittag-Leffler function of two parameters satisfies the following relationship:*

$$\mathcal{L}^{-1} \left[\frac{s^{-(\alpha-\beta)}}{s^\beta - a} \right] = t^{\alpha-1} E_{\beta, \alpha}(at^\beta), \quad |s^\beta - a| < 1.$$ (16)

3. Lyapunov Stability for Generalized Fractional Systems

The two Theorems in this section summarize the known results for Lyapunov stability theory for nonlinear systems

of (A) Li et al. [16] and Wang and Li [20] (Definition 1); (B) Souahi et al. [17] (Definition 2); (C) Tabatabaei et al. [18] (Definition 3); (D) Taghavian and Tavazoei [19] (Definition 4); (E) Almeida et al. [12] (Definition 5) and also extends the Lyapunov stability theory for nonlinear systems defined by operators introduced in Definitions 5 and 6. Specifically, in (A) the Lyapunov direct method for standard Caputo fractional system (13) with $j = 1$ is proved and the definition of Mittag-Leffler stability is introduced. In (B) the same result for the case of the modified initialized Caputo fractional derivative of time-varying order $\alpha(t)$ with $j = 2$ is proved. For the case of distributed fractional systems (13) the mentioned result in (C) for $j = 3$ is proved. In the case of conformal fractional systems in (D), it is shown that (13) is fractional exponentially stable which implies asymptotic stability for $j = 4$. For the case of Definitions 5 and 6 we show that the proofs are very similar to the one for the case $j = 4$. In consequence, Theorems 12 and 16 extend the Lyapunov direct method for generalized fractional systems defined in (13).

Assumption 11. For $j = 2$, system (13) is autonomous, i.e., $f(t, x(t)) = f(x(t))$.

Theorem 12. *Consider system (13) with $j = 1, 2, 3, 4, 5$ or 6. Let $V(t, x(t))$ be a continuously differentiable function such that*

$$\gamma_1 \|x(t)\|^l \leq V(t, x(t)) \leq \gamma_2 \|x(t)\|^{lm}, \qquad (17)$$

$$T_j^\alpha V(t, x(t)) \leq -\gamma_3 \|x(t)\|^{lm}, \qquad (18)$$

where $t \geq 0$, γ_i ($i = 1, 2, 3$), and l and m are arbitrary positive constants. If Assumption 11 is fulfilled, then the origin of system (13) is asymptotically stable.

Proof.

(i) For $j = 1$, (13) is a standard Caputo fractional system. For this system, the proof is the same as the one of Theorem 5.1 of Li et al. [16]. There, it is shown that (13) is Mittag-Leffler stable, which implies asymptotic stability.

(ii) For $j = 2$, (13) is a fractional system of time-varying order. This proof follows from Theorem 1 of Tabatabaei et al. [18]. That result requires the weaker hypotheses $V(t, x(t)) \geq 0$, $V(t, x(t)) = 0 \iff x = 0$ (which are implied by (17)) and $T_2^\alpha V(t, x(t)) < 0$ in $D - \{0\}$ (which is implied by (18)).

(iii) For $j = 3$, (13) is a distributed fractional system. In this case, the proof can be found in Theorem 4.1 of Taghavian and Tavazoei [19].

(iv) For $j = 4$, (13) is a conformable fractional system. This proof is the same as the one of Theorem 1 of Souahi et al. [17], where it is shown that (13) is fractional exponentially stable. That kind of stability also implies asymptotic stability.

(v) For $j = 5$ or 6, (13) is a system with local fractional derivatives or a distributed conformable fractional

system, respectively. In these instances, the proofs are very similar to the one of the previous case ($j = 4$). That proof depends on two facts about the conformable derivative: that it satisfies the product rule in the traditional sense and that the sign of $T_4^\alpha x(t)$ determines the monotonicity of $x(t)$. Note, from (8) and (12), that these features are also true for the operators T_5^α and T_6^α. □

The next result is a partial generalization of Theorem 12, being more permissive with the Lyapunov function and its fractional derivative, but requiring a couple of additional hypotheses.

Assumption 13. For $j = 3$ in (13), the Lyapunov function of Theorem 16 has a nonzero initial value, i.e., $V(0, x(0)) \neq 0$.

Definition 14 (Teel and Praly [36]). A function $h : [0, \infty) \longrightarrow [0, \infty)$ is said to belong to class $\mathcal{K}$ if it is continuous, zero at zero, and strictly increasing.

Assumption 15. For $j = 4, 5$, and 6 in (13), the class $\mathcal{K}$ functions h_i ($i = 1, 2, 3$) satisfy $\lim_{t \to \infty} h_i(t) = \infty$.

Theorem 16. *Consider system (13) with $j = 1, 2, 3, 4, 5$ or 6. Suppose that there exist class $\mathcal{K}$ functions h_i ($i = 1, 2, 3$) and a continuously differentiable function $V(t, x(t))$ such that*

$$h_1(\|x(t)\|) \leq V(t, x(t)) \leq h_2(\|x(t)\|), \qquad (19)$$

$$T_j^\alpha V(t, x(t)) \leq -h_3(\|x(t)\|). \qquad (20)$$

If Assumptions 11, 13, and 15 are fulfilled, then the origin of system (13) is asymptotically stable.

Proof.

(i) For $j = 1$, the proof can be found on Theorem 6.2 of Li et al. [16].

(ii) For $j = 2$, the proof is presented in Tabatabaei et al. [18], as explained in item (ii) of Theorem 12 proof.

(iii) For $j = 3$, the proof is the same as the one of Theorem 4.2 of Taghavian and Tavazoei [19].

(iv) For $j = 4$, proof can be found in Theorem 3 of Souahi et al. [17].

(v) For $j = 5$ or 6, considering the argument stated in (v) of Theorem 12 proof, we can readily generalize the result of $j = 4$ to cases of the distributed conformable and local fractional derivatives. □

We now know that Theorem 16 is valid also for Riemann-Liouville-like fractional difference equations (see Theorem 3.6 in Wu, Baleanu, and Luo [37]). So we conjecture that Theorem 16 can be valid for a larger family of operators.

The following lemma contains a property of the generalized fractional differential operator which is useful when putting into practice the previous Lyapunov Stability Theorems.

Lemma 17. *Let* $x : \mathbb{R} \longrightarrow \mathbb{R}$ *be a continuous differentiable function. Then, for* $j = 1, 2, 3, 4, 5$ *or* 6*, the following relationship holds:*

$$\frac{1}{2} T_j^\alpha \left[x^T(t) P x(t) \right] \leq x^T(t) P T_j^\alpha [x(t)], \qquad (21)$$

where P is a Hermitian positive definite matrix.

Proof. The proof for the cases $j = 1, 2, 4$ can be found in Aguila-Camacho et al. [30]; Souahi et al. [17]; Tabatabaei et al. [18], respectively. If $j = 3$, a proof for when $P = I$ is presented in Fernández-Anaya, Nava-Antonio, Jamous-Galante, Muñoz-Vega, and Hernández-Martínez [38]. To obtain the more general version, consider inequality (21) with $j = 1$, multiply it by the distribution function $c(\alpha) \geq 0$, and integrate

$$\int_0^1 \frac{1}{2} c(\alpha) T_1^\alpha \left[x^T(t) P x(t) \right] d\alpha = \frac{1}{2} T_3^\alpha \left[x^T(t) P x(t) \right]$$

$$\leq \ldots \qquad (22)$$

$$\ldots \leq \int_0^1 x^T(t) P c(\alpha) T_1^\alpha [x(t)] d\alpha$$

$$= x^T(t) P T_3^\alpha [x(t)].$$

We can follow a similar reasoning to prove this lemma for $j = 5$ or 6, by multiplying (21) with $j = 4$ and $\alpha = 1$ (that is, the traditional integer order derivative) by $k(t)^{1-\alpha}$ or $\int_0^1 c(\alpha) k(t)^{1-\alpha} d\alpha$ and using properties (8) or (12), respectively. □

4. Application to the Consensus of Multiagent Systems of Generalized Fractional Order

In this section, we will investigate the problem of consensus for generalized multiagent systems. First, we will consider systems with nonlinear dynamics and then we will present the linear simplification of that analysis.

4.1. Graph Theory Fundamentals. We can describe the interaction topology of a multagent system with the help of graph theory. A graph $\mathcal{G}$ is characterized by its vertices $\mathcal{V} = \{v_1, v_2, \ldots, v_n\}$ (which represent the agents of the system) and its edges $\mathcal{W} \subseteq \mathcal{V}^2$ (which correspond to the agents' relationships). In this paper, we will focus on directed graphs, where each edge is an ordered pair (v_i, v_j); this means that agent j receives information from agent i. A graph can be represented by its adjacency matrix $A = [a_{ij}] \in \mathbb{R}^{n \times n}$, where $a_{ij} = 1$ if $(v_i, v_j) \in \mathcal{W}$ and $a_{ij} = 0$ if $(v_i, v_j) \notin \mathcal{W}$, or by its Laplacian matrix $L = [l_{ij}] \in \mathbb{R}^{n \times n}$, where $l_{ii} = \sum_{j \in N_i} a_{ij}$ and $l_{ij} = -a_{ij}$ for $i \neq j$ with N_i the number of connected nodes to node i.

The following lemmas will be used in the proofs of our main results to gain insight into the graphs associated with the multiagent systems of our interest.

Lemma 18 (W. Ren and Cao [24]). *If a graph has a directed spanning tree, then the Laplacian matrix L has a simple zero eigenvalue and all its other eigenvalues have positive real parts. Moreover, all eigenvalues of* $H = L + B$ *will have positive real parts, where* $B = \text{diag}\{b_1, b_2, \ldots, b_n\}$ *and* $b_i \geq 0$ *is not all 0.*

Lemma 19 (Zhang and Tian [39]). *Let* $E = [1_{n-1}, -I_{n-1}] \in \mathbb{R}^{(n-1) \times n}$ *and* $F = \begin{pmatrix} 0_{n-1}^T \\ -I_{n-1} \end{pmatrix} \in \mathbb{R}^{n \times (n-1)}$*, where* 1_{n-1} *is the column vector of ones,* I_{n-1} *is the identity matrix, and* 0_{n-1} *is the zero column vector, and each of them is of size* $n-1$*. Then,* $C = -ELF$ *is Hurwitz, where L is the Laplacian matrix, if and only if the associated interaction graph has a directed spanning tree.*

The notion of consensus that will be considered throughout this paper is presented next.

Definition 20. A multiagent system accomplishes consensus if it fulfills the following condition:

$$\lim_{t \to \infty} \|x_i(t) - x_k(t)\| \leq 0,$$

$$\forall i, k \in \{1, 2, \ldots, n\}, \ i \neq k, \qquad (23)$$

where $x_k(t)$ is the state of the k-th agent.

Hereinafter, we will suppose, for simplicity, that all agents are in a one-dimensional space. All our results can be easily generalized for m dimensions by means of the Kronecker product. Moreover, in this work we will consider the matrix norm:

$$\|A\| = \sqrt{\sum_{i=1}^n \sum_{j=1}^m a_{ij}^2}, \qquad (24)$$

with $A = (a_{ij}) \in \mathbb{R}^{n \times m}$. And for any matrix $Q \in \mathbb{R}^{n \times n}$, $\lambda_{\max}(Q)$, and $\lambda_{\min}(Q)$ denote the largest and smallest eigenvalues, respectively.

4.2. Robust Consensus of Nonlinear Generalized Fractional Multiagent Systems. A generalized nonlinear fractional multi-agent system can be represented by

$$T_j^\alpha x_i(t) = f(t, x_i(t)) + u_i(t) + w_i(t),$$

$$i \in \{1, 2, \ldots, n\}, \qquad (25)$$

where $j = 1, 2, 3, 4, 5$ or 6 and $x_i(t), f(t, x_i(t)), u_i(t)$, and $w_i(t)$ are the state, nonlinear dynamics, control input, and external disturbances of the i-th agent, respectively.

As an auxiliary element, we will consider a virtual leader, which is an isolated agent that designates objectives for the states of all other agents. The behavior of the virtual leader is characterized by

$$T_j^\alpha x_r(t) = f(t, x_r(t)), \qquad (26)$$

where $x_r(t)$ is the state of the virtual leader. To accomplish consensus in system (25), we will use the following control input:

$$u_i(t)$$
$$= -\beta \left[\sum_{k=1}^n a_{ik}\left(x_i(t) - x_k(t)\right) + b_i\left(x_i(t) - x_r(t)\right) \right], \quad (27)$$

where a_{ik}, for $i, k \in \{1, 2, \ldots, n\}$ with $i \neq k$, is the (i, k)-th entry of the adjacency matrix $A \in \mathbb{R}^{n \times n}$ associated with the undirected graph describing the interaction of the agents, and $\beta \geq 0$ and b_i, for $(i = 1, 2, \ldots, n)$, are positive constants to be chosen as mentioned in Theorem 23.

We will require that the following assumptions hold.

Assumption 21. The disturbance signal $w_i(t)$ satisfies $\|w_i(t)\| \leq l < \infty \ \forall i \in \{1, 2, \ldots, n\}$.

Assumption 22. For the multiagent system (25) with $j = 3$, the distribution function $c(\alpha)$ is such that

$$\mathscr{L}^{-1} \left\{ \frac{1}{C(s) + \mu/\lambda_{\max}(Q)} \right\} \geq 0, \quad (28)$$

where $C(s)$ is defined in terms of $c(\alpha)$ as in (4).

Theorem 23. *Consider the generalized fractional nonlinear multiagent system (25) with the virtual leader (26) and the controller (27). Assume that the nonlinear function $f(t, x(t))$ is Lipschitz (with respect to x and with Lipschitz constant θ) and that the associated fixed directed graph has a directed spanning tree.*

(1) *For $j = 1, 2, 3, 4, 5$ or 6: if $w_i(t) = 0$, $\forall i$, Assumption 11 is satisfied and*

$$\frac{\sqrt{2}\beta}{\theta} \geq \|Q\|, \quad (29)$$

where $Q > 0$ is the solution of the Lyapunov equation $H^T Q + QH = 3I_n$, and then robust consensus is achieved.

(2) *For $j = 1$ or 3 if $\exists\ w_i(t) \neq 0$, Assumptions 21 and 22 are satisfied, and*

$$\frac{\beta}{\theta} \geq \|Q\|, \quad (30)$$

where $Q > 0$ is the solution of the Lyapunov equation $H^T Q + QH = 3I_n$, and then the steady-state errors of any two agent will converge as $t \longrightarrow \infty$ to the region M_1, where

$$M_1 = \left\{ \left|x_i(t) - x_y(t)\right| \leq \sqrt{\frac{2n\lambda_{\max}(Q)}{\beta\mu\lambda_{\min}(Q)}} \|Q\| l \right\}, \quad (31)$$

and $\mu = \beta - \|Q\|^2 \theta^2/\beta$.

Proof. By substituting (27) in system (25), we can write

$$T_j^\alpha X(t) = F(X(t)) - \beta \left[LX(t) + B\left(X(t) - x_r 1_n\right) \right] + W(t), \quad (32)$$

where $F(X(t)) = [f(x_1(t)), \ldots, f(x_n(t))]^T$. Subtracting $T_j^\alpha[1_n x_r(t)]$ from both sides of (32) and using the change of variables $z_i(t) = x_i(t) - x_r(t)$, $i \in \{1, 2, \ldots, n\}$ yields

$$T_j^\alpha Z(t) = -\beta HZ(t) + \Delta F(Z(t)) + W(t), \quad (33)$$

where H is defined as in Lemma 18, $Z(t) = [z_1(t), \ldots, z_n(t)]^T$ and $\Delta F(Z(t)) = [f(z_1(t) + x_r(t)) - f(x_r(t)), \ldots, f(z_n(t) + x_r(t)) - f(x_r(t))]^T$. Consider the following Lyapunov candidate function for system (33):

$$V(t) = Z^T Q Z(t). \quad (34)$$

Applying Lemma 17 and substituting (33), we can analyze $T_j^\alpha V(t)$:

$$T_j^\alpha V(t) \leq \beta Z^T(t) \left[-QH - H^T Q \right] Z(t) + 2Z^T(t) \left[Q\Delta F(Z(t)) + QW(t) \right]. \quad (35)$$

Using Lemma 18 we can conclude that all the eigenvalues of H have positive real parts, so that $-H$ is Hurwitz. Thus, there exists a matrix $Q = Q^T > 0$ that satisfies $-H^T Q - QH = -3I_n$. Applying in (35) this identity along with the property $\xi^T \zeta + \zeta^T \xi \leq \kappa\ \xi^T \xi + (1/\kappa)\zeta^T \zeta$, which is valid for any $\xi, \zeta \in \mathbb{R}^m$, we obtain

$$T_j^\alpha V(t) \leq -3\beta \|Z(t)\|^2 + \beta \|Z(t)\|^2 + \frac{1}{\beta} \|QW(t)\|^2 + \beta \|Z(t)\|^2 + \frac{1}{\beta} \|Q\|^2 \|\Delta F(t, Z(t))\|^2. \quad (36)$$

Since $f(t, x(t))$ is Lipschitz with respect to $x(t)$, we can simplify (36) as follows:

$$T_j^\alpha V(t)$$
$$\leq -\beta \|Z(t)\|^2 + \frac{nl^2 \|Q\|^2}{\beta}$$
$$\quad + \frac{\|Q\|^2}{\beta} \sum_{i=1}^n \left(f(t, z_i(t) + x_r(t)) - f(t, x_r(t)) \right)^2 \quad (37)$$
$$\leq -\beta \|Z(t)\|^2 + \frac{nl^2 \|Q\|^2}{\beta} + \frac{\|Q\|^2 \theta^2}{\beta} \|Z(t)\|^2$$
$$\leq -\mu \|Z(t)\|^2 + \frac{nl^2 \|Q\|^2}{\beta}$$

where $\mu = 2\beta - \|Q\|^2 \theta^2/\beta > 0$ by (29).

(1) In the following, we will use Theorem 12 to prove that system (33) is asymptotically stable at its origin.

If $w_i(t) = 0$, $\forall i$, then $l = 0$. As consequence, (37) turns into $T_j^\alpha V(t) \leq -\mu\|Z(t)\|^2$, so that (18) is satisfied for $\alpha_3 = \mu$. Additionally, noting that $\lambda_{\min}(Q)Z^T(t)Z(t) \leq V(t) \leq \lambda_{\max}(Q)Z^T(t)Z(t)$, it is clear that $V(t)$ satisfies (17) for $\alpha_1 = \lambda_{\min}(Q)$ and $\alpha_2 = \lambda_{\max}(Q)$. By Theorem 12 we can conclude that system (33) is asymptotically stable at $Y(t) = 0_{n-1}$. This means, according to the definition of $Z(t)$, that $\lim_{t\to\infty}\|x_1(t) - x_i(t)\| = 0$, $\forall i \in \{1, 2, \ldots, n\}$, and hence the multiagent system (25) achieves robust consensus.

(2) Using the inequality $Z^T(t)PZ(t) \leq \lambda_{\max}(Q)\|Z(t)\|^2$ in (34) yields $V(t)/\lambda_{\max}(Q) \leq \|Z(t)\|^2$. Hence

$$T_j^\alpha V(t) \leq -\frac{\mu}{\lambda_{\max}(Q)}V(t) + \frac{nl^2\|Q\|^2}{\beta}. \qquad (38)$$

Let $u(t) = V(t) - nl^2\|Q\|^2\lambda_{\max}(Q)/\mu\beta$. The generalized fractional derivative of $u(t)$ can be analyzed as follows:

$$\begin{aligned} T_j^\alpha u(t) &\leq -\frac{\mu}{\lambda_{\max}(Q)}V(t) + \frac{nl^2\|Q\|^2}{\beta} \\ &\leq -\frac{\mu}{\lambda_{\max}(Q)}u(t). \end{aligned} \qquad (39)$$

There exists a nonnegative function $m(t)$ satisfying

$$T_j^\alpha u(t) + m(t) = -\frac{\mu}{\lambda_{\max}(Q)}u(t). \qquad (40)$$

From this point, we will only consider $j = 3$ and then we will obtain the same result for $j = 1$ as a particular case. Taking the Laplace transform of (40) produces

$$B(s)\left[U(s) - \frac{u(0)}{s}\right] + M(s) = -\frac{\mu}{\lambda_{\max}(Q)}U(s), \qquad (41)$$

where $B(s)$ is defined as in (4), and $U(s)$ and $M(s)$ are the Laplace transforms of $u(t)$ and $m(t)$, respectively. Solving for $U(s)$ we obtain

$$U(s) = \frac{(B(s)/s)u(0)}{B(s) + \mu/\lambda_{\max}(Q)} - \frac{M(s)}{B(s) + \mu/\lambda_{\max}(Q)}. \qquad (42)$$

Note that the inverse Laplace Transform of the second term of the right-hand side of (42) is nonnegative, since $m(t)$, $\mathcal{L}^{-1}\{1/(B(s) + \mu/\lambda_{\max}(Q))\} \geq 0$. Considering this, we can turn (42) into

$$u(t) \leq \mathcal{L}^{-1}\left\{\frac{(B(s)/s)u(0)}{B(s) + \mu/\lambda_{\max}(Q)}\right\}. \qquad (43)$$

Substituting the definition of $u(t)$ into (43) yields

$$\begin{aligned} V(t) &- \frac{nl^2\lambda_{\max}(Q)\|Q\|^2}{\beta\mu} \\ &\leq \mathcal{L}^{-1}\left\{\frac{B(s)u(0)}{s(B(s) + \mu/\lambda_{\max}(Q))}\right\}. \end{aligned} \qquad (44)$$

By using Theorem 8 we can calculate the limit of (44) as $t \to \infty$. Note that $\lim_{s\to0}B(s) = 0$. Then

$$\begin{aligned} \lim_{t\to\infty} &\left\{V(t) - \frac{nl^2\lambda_{\max}(Q)\|Q\|^2}{\beta\mu}\right\} \\ &\leq \lim_{s\to0}\frac{B(s)u(0)}{B(s) + \beta/\lambda_{\max}(Q)} = 0. \end{aligned} \qquad (45)$$

Considering that $\lambda_{\min}(Q)\|Z(t)\|^2 \leq V(t)$, it follows from (45) that

$$\lim_{t\to\infty}\|Z(t)\| \leq \frac{\sqrt{n\lambda_{\max}(Q)/\lambda_{\min}(Q)}\|Q\|l}{\sqrt{\beta\mu}}. \qquad (46)$$

According to the definition of $Z(t)$ and using inequality properties, we obtain

$$\begin{aligned} \left|x_i(t) - x_y(t)\right| &\leq \left|x_r(t) - x_i(t)\right| + \left|x_r(t) - x_y(t)\right| \\ &\leq \left|z_i(t)\right| + \left|z_y(t)\right| \\ &\leq \sqrt{2\left(\left|z_i(t)\right|^2 + \left|z_y(t)\right|^2\right)} \\ &\leq \sqrt{2}\|Z(t)\|, \end{aligned} \qquad (47)$$

$\forall i, y \in \{1, 2, \ldots, n\}$. Combining (46) and (47), we can analyze the limit as $t \to \infty$ of the difference between any pair of agents:

$$\lim_{t\to\infty}\left|x_i(t) - x_y(t)\right| \leq \frac{\sqrt{2n\lambda_{\max}(Q)/\lambda_{\min}(Q)}\|Q\|l}{\sqrt{\beta\mu}} \qquad (48)$$

$\forall i, y \in \{1, 2, \ldots, n\}$, which proves that the steady-state errors between the agents converge to M_1.

We can prove this theorem with $j = 1$ by considering the case $j = 3$ and setting the distribution function of T_3^α as $c(\alpha) = \delta(\alpha - a)$, which turns this operator into the standard Caputo fractional derivative of order a. Furthermore, notice that

$$\begin{aligned} \mathcal{L}^{-1}&\left\{\frac{1}{C(s) + \mu/\lambda_{\max}(Q)}\right\} \\ &= \mathcal{L}^{-1}\left\{\frac{1}{s^\beta + \mu/\lambda_{\max}(Q)}\right\} \\ &= t^{\beta-1}E_{\beta,\beta}\left(-\frac{\mu}{\lambda_{\max}(Q)}t^\beta\right) \geq 0, \end{aligned} \qquad (49)$$

where we have used Lemma 10. This means that Assumption 22 is satisfied. Alternatively, the case $j = 1$ is derived in Theorem 2 of G. Ren and Yu [29]. □

4.3. Robust Consensus of Linear of Generalized Fractional Multiagent Systems.

A linear generalized fractional multiagent system with external disturbances can be described as a particular case of (25), with $f(t, x_i) = 0$:

$$T_i^\alpha x_i(t) = u_i(t) + w_i(t), \quad i \in \{1, 2, \ldots, n\}, \qquad (50)$$

where $x_i(t)$, $u_i(t)$, and $w_i(t)$ are the state, control input, and external disturbances of the ith agent, respectively.

In order to accomplish robust consensus we can use as simpler controller than (27)

$$u_i(t) = -\beta \sum_{k=1}^{n} a_{ij} \left(x_i(t) - x_k(t) \right), \tag{51}$$

where $\beta \geq 0$ and a_{ik} $(i, k = 1, 2, \ldots, n;\ i \neq k)$ is the (i, k)-th element of the adjacency matrix $A \in \mathbb{R}^{n \times n}$ associated with the directed graph describing the interaction of the agents. By following a procedure completely analogous to the one done in the previous section, the following theorem can be readily proved.

Theorem 24. *Consider the generalized fractional nonlinear multiagent system (50) with the control input (51). Suppose that the associated fixed directed graph has a directed spanning tree.*

(1) *For $j = 1, 2, 3, 4, 5$ or 6: if $w_i(t) = 0$, $\forall i$, then system (50) achieves robust consensus.*

(2) *For $j = 1$ or 3: if $\exists\ w_i(t) \neq 0$ and Assumptions 11, 21, and 22 are satisfied, then the steady-state errors of any two agents will converge to the region M_2, defined as*

$$M_2 = \left\{ \left| x_i(t) - x_y(t) \right| \leq \frac{\sqrt{2n\lambda_{\max}(P)}\,\|PE\|\,l}{\beta\sqrt{\lambda_{\min}(P)}} \right\}, \tag{52}$$

where $\lambda_{\max}(P)$ and $\lambda_{\min}(P)$ are the maximum and minimum eigenvalues of the matrix $P > 0$, which is the solution of the Lyapunov equation $C^T P + PC = -2I_{n-1}$, and E, C are defined as in Lemma 19.

5. Examples

Example 1. Consider a group of 3 undisturbed agents described by (50) with $w_i(t) = 0$, $\forall i$, under the influence of

controller (51), with the interaction graph shown in Figure 1. The Laplacian matrix associated with this system is

$$L = \begin{bmatrix} 2 & -1 & -1 \\ -1 & 2 & -1 \\ -1 & -1 & 2 \end{bmatrix}. \tag{53}$$

From Figure 1, it is clear that this graph has a directed spanning tree. Therefore, by Theorem 24, this system accomplishes consensus. In order to verify our prediction, we solved this problem for the six types of fractional derivatives addressed in this text. To this end, we considered the initial conditions $x_1(0) = 0.7996$, $x_2(0) = 3.9978$, $x_3(0) = -4.7974$ and the parameter $\beta = 1$. Additionally, we used the differentiation orders given in Table 1.

The cases $j = 1$ and $j = 2$ were analyzed numerically with the aid of the MATLAB functions developed in Petráš [40] and Valério [41]; Valério, Vinagre, Domingues, and Da Costa [42]. Taking advantage of (10) and (12), the cases $j = 4$, $j = 5$, and $j = 6$ were worked out with MATLAB's standard ODE Solver. Given the limitations of the existing computational methods to study fractional distributed order equations, we solved the case $j = 3$ analytically, as it is shown next.

We can rewrite the system in vector and obtain

$$T_3^\alpha X(t) = -\beta L X(t). \tag{54}$$

By taking the Laplace transform of (54) and solving for $\mathbb{X}(s)$, we get

$$\mathbb{X}(s) = [C(s)I + L]^{-1} \left[\frac{C(s)}{s} X(0) \right]$$

$$= \frac{1}{s(B(s) + 3)} \begin{bmatrix} B(s)x_1(0) + q \\ B(s)x_2(0) + q \\ B(s)x_3(0) + q \end{bmatrix}, \tag{55}$$

where $q = \sum_{i=1}^{3} x_i(0)$. Substituting $B(s) = s^\beta + 4s^{\beta/2}$, decomposing the right hand side of (55) into partial fractions, and taking their inverse Laplace transforms yields

$$X(t) = \begin{bmatrix} x_1(0) + \dfrac{q - 3x_1(0)}{2} t^{1/2} E_{1/2, 3/2}\left(-t^{1/2}\right) + \dfrac{3x_1(0) - q}{2} t^{1/2} E_{1/2, 3/2}\left(-3t^{1/2}\right) \\ x_2(0) + \dfrac{q - 3x_2(0)}{2} t^{1/2} E_{1/2, 3/2}\left(-t^{1/2}\right) + \dfrac{3x_2(0) - q}{2} t^{1/2} E_{1/2, 3/2}\left(-3t^{1/2}\right) \\ x_3(0) + \dfrac{q - 3x_3(0)}{2} t^{1/2} E_{1/2, 3/2}\left(-t^{1/2}\right) + \dfrac{3x_3(0) - q}{2} t^{1/2} E_{1/2, 3/2}\left(-3t^{1/2}\right) \end{bmatrix}. \tag{56}$$

which are the expressions shown in Figure 4.

In Figures 2–7 we can see the behavior of the error between the states of the multiagents. In all the cases these errors converge to zero as expected and depending on the characteristics of the operator T_j^α this rate of convergence varies.

Example 2. Consider again system (54), with the same interaction topology as in Example 1, $\beta = 1$, but this time with the disturbances $w_i(t) = \gamma_i + a_i e^{-c_i t}$, where $\gamma_i, a_i, c_i \in \mathbb{R}$, $\forall i \in \{1, 2, 3\}$. Let the differentiation orders be $\alpha = 0.5$ and $c(\alpha) = \delta(\alpha - 2/3) + 4\delta(\alpha - 1/3)$ for $j = 1$ and $j = 3$, respectively. Assumption 21 is fulfilled, since the external disturbances are
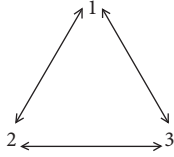
FIGURE 1: Interaction graph for the 3 agents of Examples 1, 2, and 3.
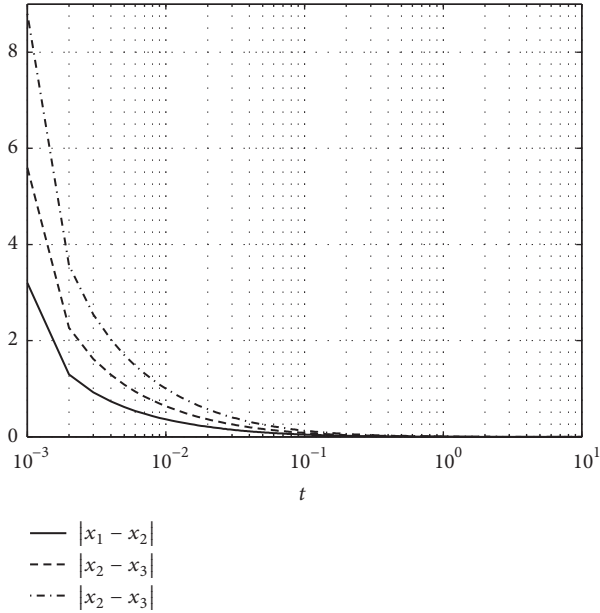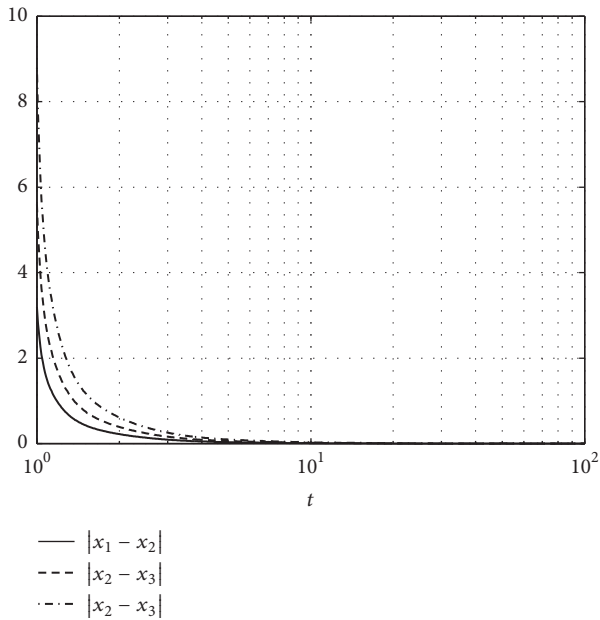
TABLE 1: Differential orders for simulations.

j	Parameters
1	$\alpha = 0.5$
2	$\alpha(t) = 1 - \dfrac{\exp(-t/50)}{2}$
3	$c(\alpha) = \delta(\alpha - \nu) + 4\delta\left(\alpha - \dfrac{\nu}{2}\right), \nu = \dfrac{2}{3}$
4	$a = 0, \alpha = 0.5$
5	$k(t) = 1 + 0.4\log(t+1)$
6	$c(\alpha) = \delta(\alpha - \nu) + 4\delta\left(\alpha - \dfrac{\nu}{2}\right), \nu = \dfrac{2}{3}, k(t) = 1 + 0.4\log(t+1)$

FIGURE 2: Linear case, $j = 1$.

— $|x_1 - x_2|$
--- $|x_2 - x_3|$
-·- $|x_2 - x_3|$

FIGURE 4: Linear case, $j = 3$.

— $|x_1 - x_2|$
--- $|x_2 - x_3|$
-·- $|x_2 - x_3|$
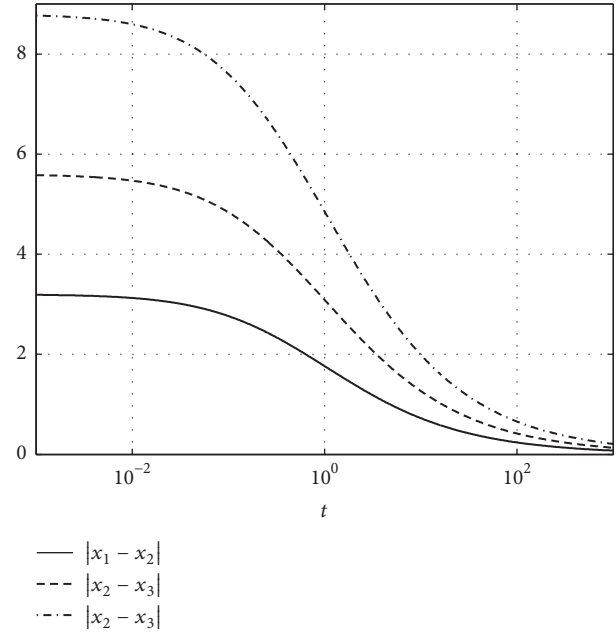
FIGURE 3: Linear case, $j = 2$.

— $|x_1 - x_2|$
--- $|x_2 - x_3|$
-·- $|x_2 - x_3|$

bounded by $\max_{i\in\{1,2,3\}}\{\|\gamma_i + a_i\|\}$. Hence, we only need to show that Assumption 22 is also satisfied in order to apply Theorem 24. In this specific problem, the left-hand side of (28) is

$$
\begin{aligned}
\mathscr{L}^{-1}\left\{\frac{1}{C(s) + \beta/\lambda_{\max}(P)}\right\} &= \mathscr{L}^{-1}\left\{\frac{1}{s^{2/3} + 4s^{1/3} + 3}\right\} \\
&= \mathscr{L}^{-1}\left\{\frac{1}{s^{1/3} + 3}\right\} * \mathscr{L}^{-1}\left\{\frac{1}{s^{1/3} + 1}\right\} \\
&= \left[t^{-2/3}E_{1/3,1/3}\left(-3t^{1/3}\right)\right] * \left[t^{-2/3}E_{1/3,1/3}\left(-3t^{1/3}\right)\right] \\
&= \int_{-\infty}^{+\infty}(t-\tau)^{-2/3}E_{1/3,1/3}\left(-3(t-\tau)^{1/3}\right) \\
&\quad \cdot t^{-2/3}E_{1/3,1/3}\left(-3t^{1/3}\right)d\tau,
\end{aligned}
\tag{57}
$$

where we have used Theorems 8 and 16. Considering that all the factors inside the integral in (57) are nonnegative, we can conclude that Assumption 22 is fulfilled and, therefore, the steady-state errors between the agents will converge asymptotically to M_1. Solving the equation $C^T P + PC =$
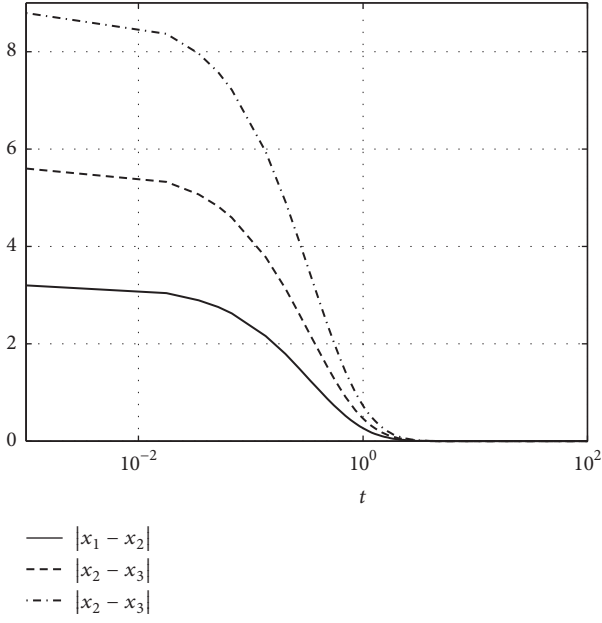
FIGURE 5: Linear case, $j = 4$.
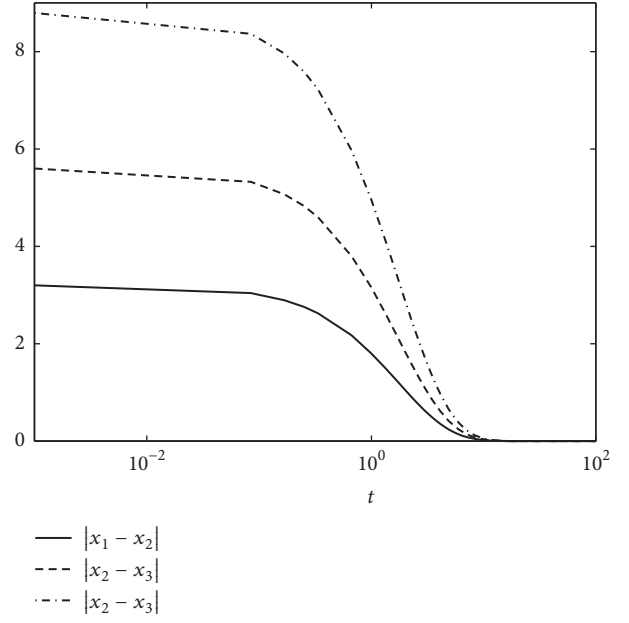
FIGURE 7: Linear case, $j = 6$.
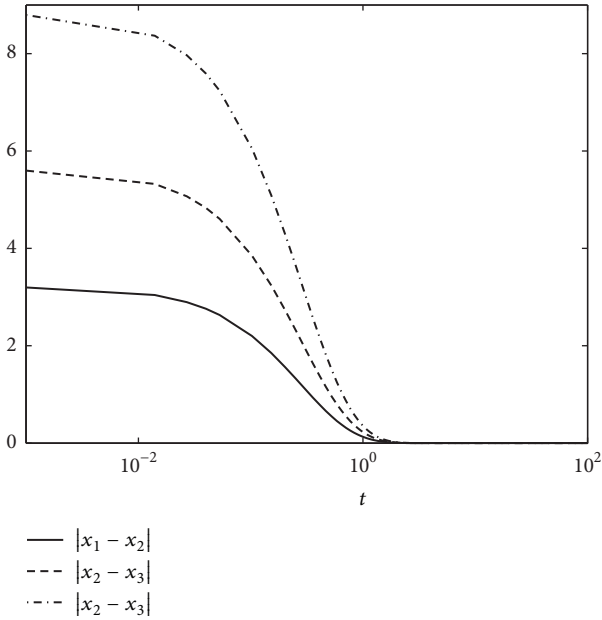
FIGURE 6: Linear case, $j = 5$.

$-2I_{n-1}$ yields $P = (1/3)I$, so that $\lambda_{\max}(P) = \lambda_{\min}(P) = 1/3$. Moreover, $\|PE\| = \max_{1 \le j \le 3}\{\sum_{i=1}^{2} |(PE)_{ij}|\} = 2/3$. By setting the parameters $\gamma_1 = -2$, $\gamma_2 = 1$, $\gamma_3 = 2$, $a_1 = 1$, $a_2 = 2$, $a_3 = -1$, $c_1 = 2$, $c_2 = 1.5$, and $c_3 = 1.7$, one can calculate that the disturbances are bounded by $l = 3$. Substituting these values in the definition of M_1 produces

$$M_1 = \left\{ \left| x_i(t) - x_j(t) \right| \le 2\sqrt{6} \approx 4.8989 \right\}. \tag{58}$$

To verify this analysis, we solved this system numerically, for $j = 1$ (using the MATLAB functions of Petráš [40]), and analytically, for $j = 3$ (since there are no suitable numerical methods). For the case $j = 3$, we can take the Laplace transform of (54) and solve for $\mathbb{X}(s)$:

$$\mathbb{X}(s) = [C(s)I + L]^{-1} \left[\mathbb{W}(s) + \frac{C(s)}{s}X(0) \right]$$

$$= \frac{1}{sC(s)(C(s) + 3)}$$

$$\times \begin{bmatrix} C(s)sw_1(s) + C^2(s)x_1(0) + s\sum_{i=1}^{3} w_i(s) \\ C(s)sw_2(s) + C^2(s)x_2(0) + s\sum_{i=1}^{3} w_i(s) \\ C(s)sw_3(s) + C^2(s)x_3(0) + s\sum_{i=1}^{3} w_i(s) \end{bmatrix}, \tag{59}$$

where $\mathscr{L}^{-1}\{W(t)\} = \mathbb{W}(s)$, and, for simplicity, we have considered $x_1(0) + x_2(0) + x_3(0) = 0$. Substituting $C(s) = s^{2/3} + 4s^{1/3}$ and $w_i(s) = \gamma_i/s + a_i/(s + c_i)$, one can decompose the right hand side of (59) into partial fractions and take their inverse Laplace transforms. After extensive calculations, we obtain

$$X(t) = G(t) + H(t) + f(t)X(0), \tag{60}$$

where $f(t)$, $G = [g_1(t), g_2(t), g_3(t)]^T$, $H = h(t)[1, 1, 1]^T$ are defined as follows:

$$f(t) = \frac{12t^{-1/3}}{9\Gamma(2/3)} - \frac{39t^{-2/3}}{27\Gamma(1/3)} + \frac{3t^{-2/3}E_{1/3,1/3}\left(-t^{1/3}\right)}{2}$$

$$- \frac{3t^{-2/3}E_{1/3,1/3}\left(-3t^{1/3}\right)}{54}, \tag{61}$$

$$g_i(t) = \gamma_i \left\{ \frac{1}{3} - \frac{4t^{-1/3}}{9\Gamma(2/3)} + \frac{13t^{-2/3}}{27\Gamma(1/3)} \right\}$$

$$+ \frac{a_i}{c_i^2 - 28c_i + 27} \left\{ (9 + 4c_i)e^{-c_i t} \right.$$

$$+ 13t^{-2/3}E_{1,1/3}\left(-c_i t\right) - (12 + c_i)t^{-1/3}E_{1,2/3}\left(-c_i t\right) \Big\} \tag{62}$$

$$+ t^{-2/3} \left[\left(\frac{a_i}{2(c_i - 1)} - \frac{\gamma_i}{2} \right) E_{1/3,1/3}\left(-t^{1/3}\right) \right.$$

$$+ \left(\frac{\gamma_i}{54} - \frac{a_i}{2(c_i - 27)} \right) E_{1/3,1/3}\left(-3t^{1/3}\right) \Bigg],$$

$\forall i \in \{1, 2, 3\}$ and

$$h(t) = \sum_{i=1}^{3} \left\{ \gamma_i \left[\frac{t^{1/3}}{12\Gamma(4/3)} - \frac{19}{144} + \frac{265t^{-1/3}}{1728\Gamma(2/3)} \right] \right.$$

$$+ \frac{t^{-2/3}}{\Gamma(1/3)} \left(\frac{a_i}{12c_i} - \frac{3355\gamma_i}{20736} \right)$$

$$+ t^{-2/3} \left[E_{1/3,1/3}\left(-t^{1/3}\right) \left(\frac{\gamma_i}{6} - \frac{a_i}{6(c_i - 1)} \right) \right.$$

$$+ E_{1/3,1/3}\left(-3t^{1/3}\right) \left(\frac{a_i}{6(c_i - 27)} - \frac{\gamma_i}{162} \right) \tag{63}$$

$$+ E_{1/3,1/3}\left(-4t^{1/3}\right) \left(\frac{\gamma_i}{768} - \frac{a_i}{12(c_i - 64)} \right) \Bigg]$$

$$+ \frac{a_i}{c_i(c_i^3 - 92c_i^2 + 1819c_i - 1728)} \times \left[228c_i \right.$$

$$+ 45c_i^2 e^{-c_i t} - \left(8c_i^2 + 265c_i \right) t^{-1/3}E_{1,2/3}\left(-c_i t\right)$$

$$+ \left(c_i^2 + 128c_i + 144 \right) t^{-2/3}E_{1,1/3}\left(-c_i t\right) \Big] \Bigg\}.$$

For both cases $j = 1$ and $j = 3$, Figure 8 depicts the states of the agents and Figure 9 the errors between them. To plot our results, we used the initial conditions $x_1(0) = -30$, $x_2(0) = 10$, $x_3(0) = 20$. From these figures, we can confirm that the steady-state errors of the agents converge to the calculated region.

Example 3. Consider the nonlinear system described by the interaction graph shown in Figure 1 and (25) and (26), where $f(t, x(t)) = \arctan(x(t))$, for which we can take its Lipschitz constant as $\theta = 1$. For this system, one can calculate $\|Q\| =$
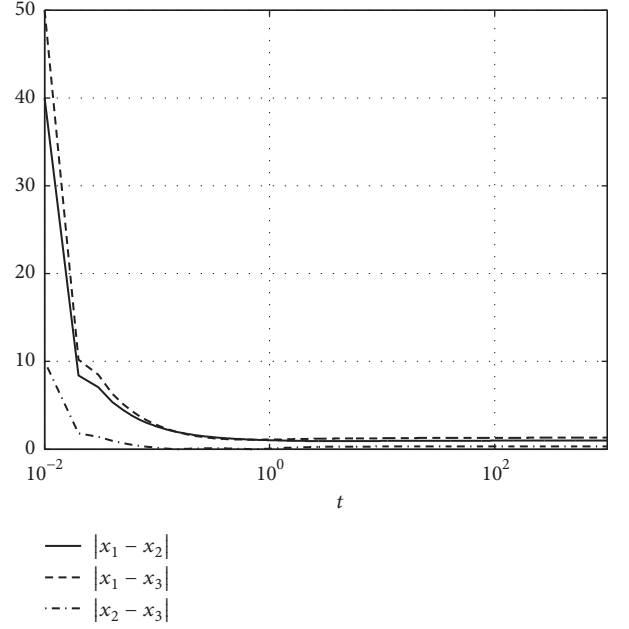
FIGURE 8: Linear case with perturbation, $j = 1$.
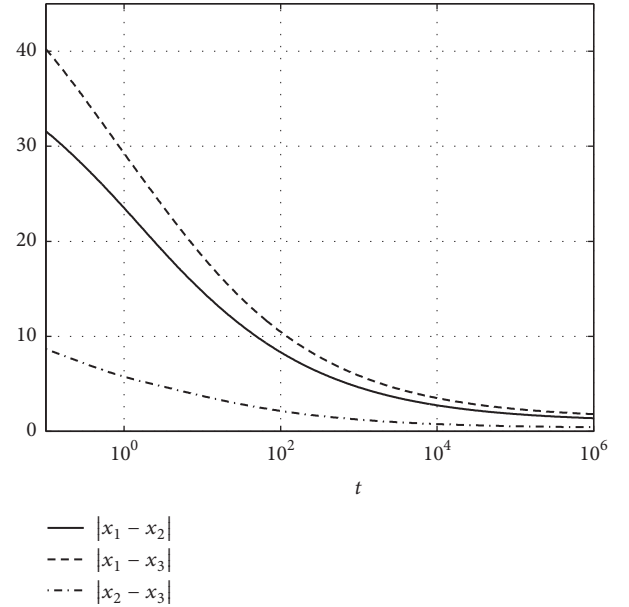
FIGURE 9: Linear case with perturbation, $j = 3$.

$3\sqrt{26}/23$. Setting the parameters of the controller as $\beta = 1$, $b_1 = 1$, $b_2 = 2$, and $b_3 = 3$ allows us to fulfill inequality (29) and, thus, according to Theorem 23, this system achieves consensus.

All the simulations start with zero initial conditions and constant input such that the agents evolve with different trajectories; at time $t = 3$ the agents start using the control law given by (27). The simulation for the different operators are shown in Figures 10–14 where we plotted the errors between states of the different agents for $j = 1, 2, 4, 5,$ and 6 (see
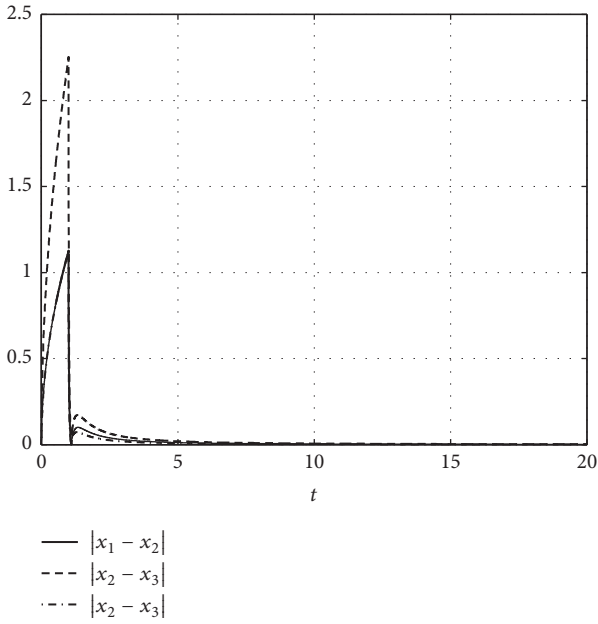
FIGURE 10: No-linear case, $j = 1$.
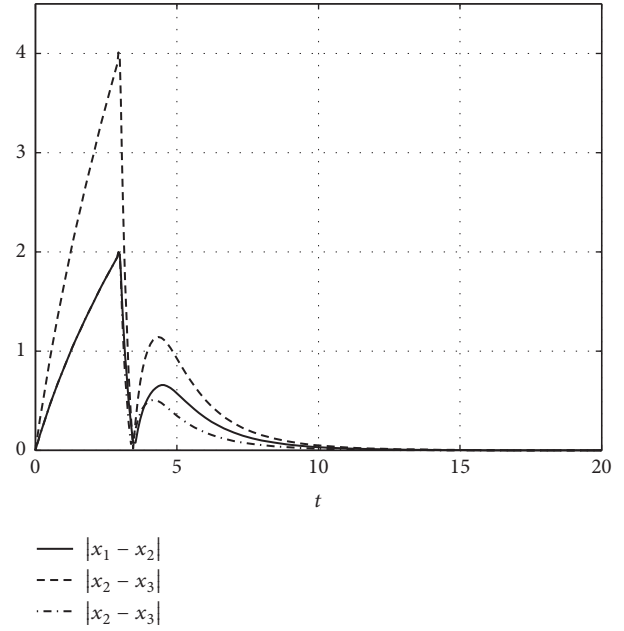
FIGURE 12: No-linear case, $j = 4$.
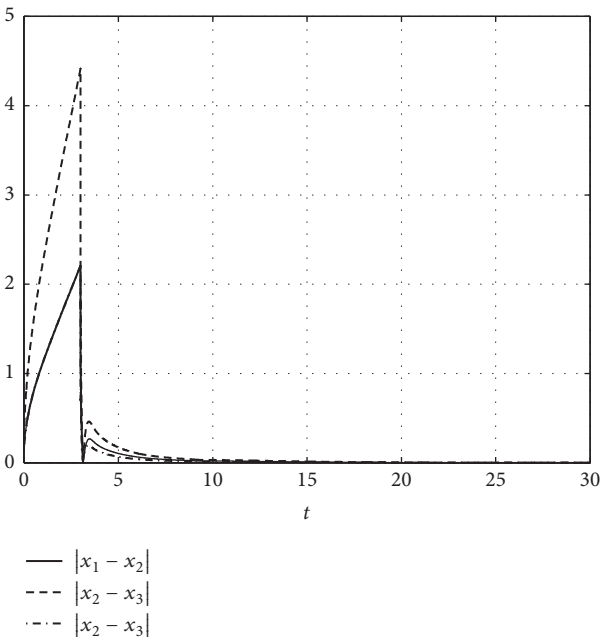
FIGURE 11: No-linear case, $j = 2$.
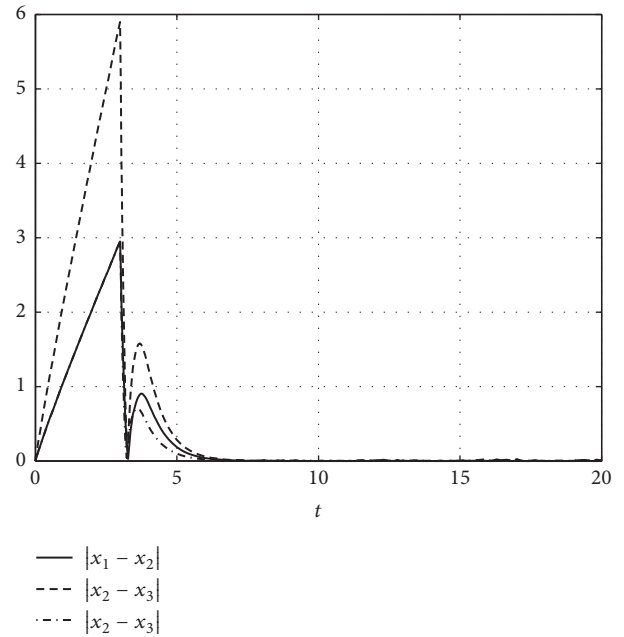
FIGURE 13: No-linear case, $j = 5$.

Table 1), with the computational tools already mentioned. We do not present the solution of this system for $j = 3$ since neither the available numerical methods for distributed order systems nor the Laplace transform technique used in the previous examples are applicable for the nonlinear case.

In all the simulation we can see that while $t < 3$ the error between the agents increases and once the controller is engaged after $t \geq 3$ the errors converge to zero; the rate of convergence depend on the nature of the operators.

6. Conclusions

We introduced the distributed conformable derivative, which preserves the product and chain rules. For this and five other fractional derivatives, we unified the Lyapunov direct method. That result was presented in two theorems; the first bounds the Lyapunov function and its fractional derivative by powers of the norm of the states and the second by class $\mathcal{K}$ functions. Moreover, we employed this generalized fractional Lyapunov method to prove whether linear and nonlinear
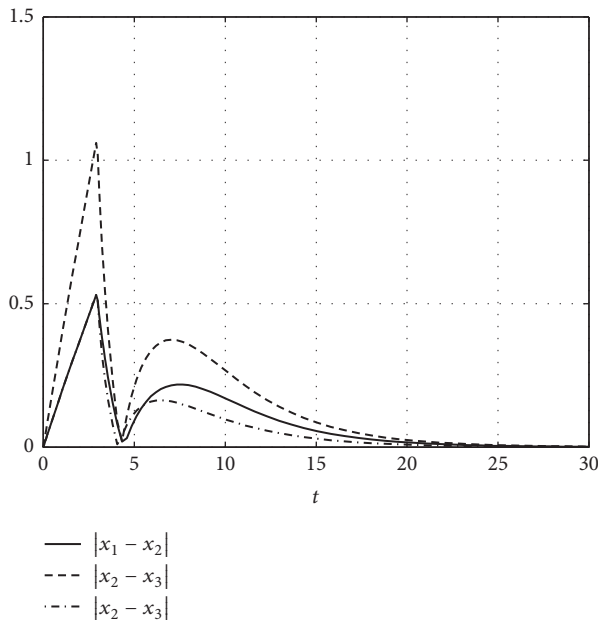
FIGURE 14: No-linear case, $j = 6$.

multiagent systems, modeled with different fractional derivatives, accomplish consensus. We found that if the system is undisturbed, the agents converge asymptotically and if there are external disturbances, the steady-state errors evolve towards a region which diminishes linearly in size as the gain of the controller is increased. It is worth noticing that same control inputs are effective for all the differentiation orders considered in this paper.

In the light of these results, potential future objectives would be to carry out a similar analysis in the presence of time delays or to study the finite-time consensus problem for fractional multiagent systems, possibly employing different controllers.

Data Availability

The data used to support the findings of this study are available from the corresponding author upon request.

Conflicts of Interest

The authors declare that there are no conflicts of interest regarding the publication of this paper.

Acknowledgments

References

[1] G. W. F. Von Leibniz, *Mathematische Schriften*, vol. 1, Asher, 1849.

[2] A. Kilbas, H. M. Srivastava, and J. J. Trujillo, *Theory and Applications of Fractional Differential Equations*, New York, NY, USA, Elsevier, 2006.

[3] I. Petráš, *Fractional-Order Nonlinear Systems: Modeling, Analysis and Simulation*, Springer Science & Business Media, 2011.

[4] I. Podlubny, *Fractional Differential Equations*, Academic Press, London, 1999.

[5] S. G. Samko and B. Ross, "Integration and differentiation to a variable fractional order," *Integral Transforms and Special Functions*, vol. 1, no. 4, pp. 277–300, 1993.

[6] H. G. Sun, W. Chen, H. Wei, and Y. Q. Chen, "A comparative study of constant-order and variable-order fractional models in characterizing memory property of systems," *The European Physical Journal Special Topics*, vol. 193, article no. 185, no. 1, 2011.

[7] M. Caputo, *Elasticitá E Dissipazione*, Zanichelli, Bologna, Italy, 1969.

[8] A. V. Chechkin, J. Klafter, and I. M. Sokolov, "Fractional Fokker-Planck equation for ultraslow kinetics," *EPL (Europhysics Letters)*, vol. 63, no. 3, article no. 326, 2003.

[9] M. Naber, "Distributed order fractional sub-diffusion," *Fractals*, vol. 12, no. 1, pp. 23–32, 2004.

[10] C. F. Lorenzo and T. T. Hartley, "Variable order and distributed order fractional operators," *Nonlinear Dynamics*, vol. 29, no. 1–4, pp. 57–98, 2002.

[11] R. Khalil, M. Al Horani, A. Yousef, and M. Sababheh, "A new definition of fractional derivative," *Journal of Computational and Applied Mathematics*, vol. 264, pp. 65–70, 2014.

[12] R. Almeida, M. Guzowska, and T. Odzijewicz, "A remark on local fractional calculus and ordinary derivatives," *Open Mathematics*, vol. 14, pp. 1122–1124, 2016.

[13] N. Laskin, *Fractional Quantum Mechanics*, World Scientific, 2018.

[14] D. Baleanu, J. A. T. Machado, and A. C. J. Luo, *Fractional Dynamics and Control*, Springer, New York, NY, USA, 2012.

[15] S. S. Tabatabaei, M. J. Yazdanpanah, S. Jafari, and J. C. Sprott, "Extensions in dynamic models of happiness: Effect of memory," *International Journal of Happiness and Development*, vol. 1, no. 4, pp. 344–356, 2014.

[16] Y. Li, Y. Chen, and I. Podlubny, "Stability of fractional-order nonlinear dynamic systems: Lyapunov direct method and generalized Mittag–Leffler stability," *Computers & Mathematics with Applications*, vol. 59, no. 5, pp. 1810–1821, 2010.

[17] A. Souahi, A. B. Makhlouf, and M. A. Hammami, "Stability analysis of conformable fractional-order nonlinear systems," *Indagationes Mathematicae*, vol. 28, no. 6, pp. 1265–1274, 2017.

[18] S. S. Tabatabaei, H. A. Talebi, and M. Tavakoli, "An adaptive order/state estimator for linear systems with non-integer time-varying order," *Automatica*, vol. 84, pp. 1–9, 2017.

[19] H. Taghavian and M. S. Tavazoei, "Stability analysis of distributed-order nonlinear dynamic systems," *International Journal of Systems Science*, vol. 49, no. 3, pp. 523–536, 2018.

[20] Y. Wang and T. Li, "Stability analysis of fractional-order nonlinear systems with delay," *Mathematical Problems in Engineering*, vol. 2014, Article ID 301235, 8 pages, 2014.

[21] W. Ren and R. W. Beard, *Distributed Consensus in Multi-Vehicle Cooperative Control*, Springer, 2008.

[22] A. Jadbabaie, N. Motee, and M. Barahona, "On the stability of the Kuramoto model of coupled nonlinear oscillators," in *Proceedings of the American Control Conference (AAC)*, pp. 4296–4301, IEEE, Boston, MA, USA, 2004.

[23] R. Olfati-Saber and J. S. Shamma, "Consensus filters for sensor networks and distributed sensor fusion," in *Proceedings of the 44th IEEE Conference on Decision and Control, and the European Control Conference (CDC-ECC)*, pp. 6698–6703, IEEE, Seville, Spain, 2005.

[24] W. Ren and Y. Cao, *Distributed Coordination of Multi-Agent Networks: Emergent Problems, Models, And Issues*, Springer Science & Business Media, 2010.

[25] Z. Yu, H. Jiang, C. Hu, and J. Yu, "Leader-following consensus of fractional-order multi-agent systems via adaptive pinning control," *International Journal of Control*, vol. 88, no. 9, pp. 1746–1756, 2015.

[26] X. Yin, D. Yue, and S. Hu, "Consensus of fractional-order heterogeneous multi-agent systems," *IET Control Theory & Applications*, vol. 7, no. 2, pp. 314–322, 2013.

[27] C. Song, J. Cao, and Y. Liu, "Robust consensus of fractional-order multi-agent systems with positive real uncertainty via second-order neighbors information," *Neurocomputing*, vol. 165, pp. 293–299, 2015.

[28] G. Nava-Antonio, G. Fernandez-Anaya, E. G. Hernandez-Martinez, J. Jamous-Galante, E. D. Ferreira-Vazquez, and J. J. Flores-Godoy, "Consensus of multi-agent systems with distributed fractional order dynamics," in *Proceedings of the 14th International Workshop on Complex Systems and Networks (IWCSN)*, pp. 190–197, IEEE, Doha, Qatar, 2017.

[29] G. Ren and Y. Yu, "Robust consensus of fractional multi-agent systems with external disturbances," *Neurocomputing*, vol. 218, pp. 339–345, 2016.

[30] N. Aguila-Camacho, M. A. Duarte-Mermoud, and J. A. Gallegos, "Lyapunov functions for fractional order systems," *Communications in Nonlinear Science and Numerical Simulation*, vol. 19, no. 9, pp. 2951–2957, 2014.

[31] Z. Jiao, Y. Chen, and I. Podlubny, *Distributed-Order Dynamic Systems Stability, Simulation, Applications and Perspectives*, Springer Briefs in Electrical and Computer Engineering, Springer, 2012.

[32] Y. Xu and Z. He, "Existence and uniqueness results for Cauchy problem of variable-order fractional differential equations," *Journal of Applied Mathematics and Computing*, vol. 43, no. 1-2, pp. 295–306, 2013.

[33] N. J. Ford and M. L. Morgado, "Distributed order equations as boundary value problems," *Computers & Mathematics with Applications*, vol. 64, no. 10, pp. 2973–2981, 2012.

[34] B. Bayour and D. F. M. Torres, "Existence of solution to a local fractional nonlinear differential equation," *Journal of Computational and Applied Mathematics*, vol. 312, pp. 127–133, 2017.

[35] D. G. Duffy, *Transform Methods for Solving Partial Differential Equations*, Symbolic & Numeric Computation, CRC press, 2nd edition, 2004.

[36] A. R. Teel and L. Praly, "A smooth Lyapunov function from a class-KL estimate involving two positive semidefinite functions," *ESAIM: Control, Optimisation and Calculus of Variations*, vol. 5, pp. 313–367, 2000.

[37] G.-C. Wu, D. Baleanu, and W.-H. Luo, "Lyapunov functions for Riemann-Liouville-like fractional difference equations," *Applied Mathematics and Computation*, vol. 314, pp. 228–236, 2017.

[38] G. Fernández-Anaya, G. Nava-Antonio, J. Jamous-Galante, R. Muñoz-Vega, and E. G. Hernández-Martínez, "Asymptotic stability of distributed order nonlinear dynamical systems Asymptotic stability of distributed order nonlinear dynamical systems," *Communications in Nonlinear Science and Numerical Simulation48541549*, 2017.

[39] Y. Zhang and Y.-P. Tian, "Consentability and protocol design of multi-agent systems with stochastic switching topology," *Automatica*, vol. 45, no. 5, pp. 1195–1201, 2009.

[40] I. Petráš, "Fractional order chaotic systems," 2010, http://www.mathworks.com/matlabcentral/fileexchange/27336-fractional-order-chaotic-systems.

[41] D. Valério, "Variable order derivatives," 2010, https://la.mathworks.com/matlabcentral/fileexchange/24444-variable-order-derivatives.

[42] D. Valério, G. Vinagre, J. Domingues, and J. S. Da Costa, "Variable-order fractional derivatives and their numerical approximations, I—Real orders," *In Fractional Signals and Systems*, 2009.

Research Article

Synchronization Control in Reaction-Diffusion Systems: Application to Lengyel-Epstein System

Adel Ouannas,[1] Mouna Abdelli,[1] Zaid Odibat,[2,3] Xiong Wang ⓘ,[4] Viet-Thanh Pham ⓘ,[5,6] Giuseppe Grassi,[7] and Ahmed Alsaedi[3]

[1]*Department of Mathematics, University of Larbi Tebessi, Tebessa 12002, Algeria*
[2]*Department of Mathematics, Faculty of Science, Al-Balqa Applied University, Salt 19117, Jordan*
[3]*Nonlinear Analysis and Applied Mathematics (NAAM) Research Group, Department of Mathematics, Faculty of Science, King Abdulaziz University, Jeddah 21589, Saudi Arabia*
[4]*Institute for Advanced Study, Shenzhen University, Shenzhen, Guangdong 518060, China*
[5]*Faculty of Electrical and Electronic Engineering, Phenikaa Institute for Advanced Study (PIAS), Phenikaa University, Yen Nghia, Ha Dong district, Hanoi 100000, Vietnam*
[6]*Phenikaa Research and Technology Institute (PRATI), A&A Green Phoenix Group, 167 Hoang Ngan, Hanoi 100000, Vietnam*
[7]*Universita del Salento, Dipartimento Ingegneria Innovazione, 73100 Lecce, Italy*

Correspondence should be addressed to Viet-Thanh Pham; thanh.phamviet@phenikaa-uni.edu.vn

Synchronization and control in high dimensional spatial-temporal systems have received increasing interest in recent years. In this paper, the problem of complete synchronization for reaction-diffusion systems is investigated. Linear and nonlinear synchronization control schemes have been proposed to exhibit synchronization between coupled reaction-diffusion systems. Synchronization behaviors of coupled Lengyel-Epstein systems are obtained to demonstrate the effectiveness and feasibility of the proposed control techniques.

1. Introduction

Synchronization of chaos is a phenomenon that may occur when two, or more, chaotic systems adjust a given property of their motion to a common behavior due to a coupling or to a forcing. This phenomenon has attracted the interest of many researchers from various fields due to its potential applications in physics, biology, chemistry, and engineering sciences since the pioneering work by Pecora and Carroll [1]. Various synchronization types have been presented, such as complete synchronization, phase synchronization, lag synchronization, anticipated synchronization, function projective synchronization, generalized synchronization, and Q-S synchronization.

Most of the research efforts have been devoted to the study of chaos control and chaos synchronization problems in low-dimensional nonlinear dynamical systems [2–10]. Synchronizing high dimensional systems in which state variables depend not only on time but also on the spatial position remains a challenge. These high dimensional systems are generally modelled in spatial-temporal domain by partial differential systems. Recently, the search for synchronization has moved to high dimensional nonlinear dynamical systems. Over the last years, some studies have investigated synchronization of spatially extended systems demonstrating spatiotemporal chaos such as the work presented in [11–32]. Synchronization dynamics of reaction-diffusion systems has been studied in [11, 12] using phase reduction theory. It has been shown that reaction-diffusion systems can exhibit synchronization in a similar way to low-dimensional oscillators. A general approach for synchronizing coupled partial differential equations with spatiotemporally chaotic dynamics by driving the response system only at a finite number of space points has been introduced in [13, 14]. Synchronization and control for spatially extended systems based on local spatially averaged coupling signals have been presented in [17]. The

effect of asymmetric couplings in the synchronization of spatially extended chaotic systems has been investigated in [19]. The effect of time-delay autosynchronization on uniform oscillations in a general model described by the complex Ginzburg-Landau equation has been presented in [20]. Furthermore, generalized synchronization [21], complete-like synchronization [22], the backstepping synchronization approach [26], the graph-theoretic synchronization approach [27], pinning impulsive synchronization [30], and impulsive type synchronization strategy [31] for coupled reaction-diffusion systems have been introduced.

The main aim of the present paper is to study the problem of complete synchronization in coupled reaction-diffusion systems. Linear and nonlinear control schemes have been proposed to realize complete synchronization for partial differential systems. As a special case, we investigate complete synchronization behaviors of coupled Lengyel-Epstein systems.

2. Systems Description and Problem Formulation

Reaction-diffusion systems have shown important roles in modelling various spatiotemporal patterns that arise in chemical and biological systems [33, 34]. Reaction-diffusion systems can describe a wide class of rhythmic spatiotemporal patterns observed in chemical and biological systems, such as circulating pulses on a ring, oscillating spots, target waves, and rotating spirals. The most familiar way to study synchronization is to use a controller to make the output of the slave (response) system copy in some manner the master (drive) system one. In this case, we design the controller in which the difference of states of synchronized systems converges to zero. This phenomenon is called complete synchronization. Consider the master and the slave reaction-diffusion systems as

$$
Master \begin{cases} \dfrac{\partial u_1(x,t)}{\partial t} = \sum_{j=1}^{2} d_{1j}\Delta u_j + \sum_{j=1}^{2} a_{1j}u_j + f_1(u_1,u_2), \\ \dfrac{\partial u_2(x,t)}{\partial t} = \sum_{j=1}^{2} d_{2j}\Delta u_j + \sum_{j=1}^{2} a_{2j}u_j + f_2(u_1,u_2), \end{cases} \tag{1}
$$

and

$$
Slave \begin{cases} \dfrac{\partial v_1(x,t)}{\partial t} = \sum_{j=1}^{2} d_{1j}\Delta v_j + \sum_{j=1}^{2} a_{1j}v_j + f_1(v_1,v_2) + \mathbf{U}_1, \\ \dfrac{\partial v_2(x,t)}{\partial t} = \sum_{j=1}^{2} d_{2j}\Delta v_j + \sum_{j=1}^{2} a_{2j}v_j + f_2(v_1,v_2) + \mathbf{U}_2, \end{cases} \tag{2}
$$

where $(u_1(x,t), u_2(x,t))^T$ and $(v_1(x,t), v_2(x,t))^T$ are the corresponding states, $x \in \Omega$ is a bounded domain in $\mathbb{R}^n$ with smooth boundary $\partial\Omega$, Δ is the Laplacian operator on Ω, $(d_{ij}) \in \mathbb{R}^2$ are the diffusivity constants, $A = (a_{ij}) \in \mathbb{R}^2$, f_1 and f_2 are nonlinear continuous functions, and $\mathbf{U}_1$ and $\mathbf{U}_2$ are controllers to be designed. We impose the homogeneous Neumann boundary conditions

$$
\frac{\partial u_i}{\partial \eta} = \frac{\partial v_i}{\partial \eta} = 0, \quad i = 1, 2, \ for \ all \ x \in \partial\Omega. \tag{3}
$$

where η is the unit outer normal to $\partial\Omega$. The aim of the synchronization process is to force the error between the master and slave systems, defined as

$$
e_i = v_i - u_i, \quad i = 1, 2, \tag{4}
$$

to zero. We assume that the diffusivity constants (d_{ij}) satisfy

$$
\begin{aligned} d_{11}, d_{22} &\geq 0, \\ d_{12} &= -d_{21}, \end{aligned} \tag{5}
$$

and the error system satisfies the homogeneous Neumann boundary condition

$$
\frac{\partial e_1}{\partial \eta} = \frac{\partial e_2}{\partial \eta} = 0, \quad for \ all \ x \in \partial\Omega. \tag{6}
$$

To realize complete synchronization between the master system given in (1) and the slave system given in (2), we discuss the asymptotical stable of zero solution of synchronization error system given in (4). That is, in the following sections, we find the controllers $\mathbf{U}_1$ and $\mathbf{U}_2$, in linear and nonlinear forms, such that the solution of the error system $e_i = v_i - u_i$ go to 0, $i = 1, 2$, as t goes to $+\infty$.

3. Synchronization via Nonlinear Controllers

In this section, we outline the issue of controlling the master-slave reaction-diffusion system given in (1) and (2) via nonlinear controllers. The time partial derivatives of the error system given in (4) can derived as

$$
\begin{aligned} \frac{\partial e_1}{\partial t} &= \sum_{j=1}^{2} d_{1j}\Delta e_j + \sum_{j=1}^{2} a_{1j}e_j + f_1(v_1,v_2) - f_1(u_1,u_2) \\ &\quad + \mathbf{U}_1, \\ \frac{\partial e_2}{\partial t} &= \sum_{j=1}^{2} d_{2j}\Delta e_j + \sum_{j=1}^{2} a_{2j}e_j + f_2(v_1,v_2) - f_2(u_1,u_2) \\ &\quad + \mathbf{U}_2. \end{aligned} \tag{7}
$$

That is,

$$
\begin{aligned} \frac{\partial e_1}{\partial t} &= \sum_{j=1}^{2} d_{1j}\Delta e_j + \sum_{j=1}^{2} \left(a_{1j} - c_{1j}\right)e_j + R_1 + \mathbf{U}_1, \\ \frac{\partial e_2}{\partial t} &= \sum_{j=1}^{2} d_{2j}\Delta e_j + \sum_{j=1}^{2} \left(a_{2j} - c_{2j}\right)e_j + R_2 + \mathbf{U}_2, \end{aligned} \tag{8}
$$

where $C = (c_{ij})_{2\times2}$ is a control matrix to be determined later and

$$
\begin{aligned} R_1 &= \sum_{j=1}^{2} c_{1j}\left(v_j - u_j\right) + f_1(v_1,v_2) - f_1(u_1,u_2), \\ R_2 &= \sum_{j=1}^{2} c_{2j}\left(v_j - u_j\right) + f_2(v_1,v_2) - f_2(u_1,u_2). \end{aligned} \tag{9}
$$

Theorem 1. *If the control matrix C is chosen such that $A - C$ is a negative definite matrix, then the master-slave reaction-diffusion system given in (1) and (2) can be synchronized under the following nonlinear control law*

$$\mathbf{U}_i = -R_i, \quad i = 1, 2. \tag{10}$$

Proof. Substituting the control parameters given in (10) into (8) yields

$$\frac{\partial e_1}{\partial t} = \sum_{j=1}^{2} d_{1j} \Delta e_j + \sum_{j=1}^{2} \left(a_{1j} - c_{1j} \right) e_j,$$

$$\frac{\partial e_2}{\partial t} = \sum_{j=1}^{2} d_{2j} \Delta e_j + \sum_{j=1}^{2} \left(a_{2j} - c_{2j} \right) e_j. \tag{11}$$

We may, now, construct our Lyapunov functional as

$$V = \frac{1}{2} \int_{\Omega} e^T e, \tag{12}$$

where $e = (e_1, e_2)^T$, then

$$\frac{\partial V}{\partial t} = \int_{\Omega} \left(e_1 \frac{\partial e_1}{\partial t} + e_2 \frac{\partial e_2}{\partial t} \right)$$

$$= \int_{\Omega} \left[e_1 \left(\sum_{j=1}^{2} d_{1j} \Delta e_j + \sum_{j=1}^{2} \left(a_{1j} - c_{1j} \right) e_j \right) \right.$$

$$\left. + e_2 \left(\sum_{j=1}^{2} d_{2j} \Delta e_j + \sum_{j=1}^{2} \left(a_{2j} - c_{2j} \right) e_j \right) \right] \tag{13}$$

$$= \sum_{j=1}^{2} \int_{\Omega} d_{jj} e_j \left(\Delta e_j \right) + \int_{\Omega} d_{12} e_1 \Delta e_2 + \int_{\Omega} d_{21} e_2 \Delta e_1$$

$$+ \int_{\Omega} e^T (A - C) e.$$

By using Green formula, we can get

$$\frac{\partial V}{\partial t} = -\sum_{j=1}^{2} \int_{\Omega} d_{jj} \left(\nabla e_j \right)^2$$

$$+ \int_{\partial \Omega} \left(d_{12} \frac{\partial e_2}{\partial \eta} e_1 + d_{21} \frac{\partial e_1}{\partial \eta} e_2 \right) d\sigma \tag{14}$$

$$- \int_{\Omega} (d_{21} + d_{12}) \nabla e_1 \nabla e_2 + \int_{\Omega} e^T (A - C) e,$$

where ∇ is the gradient vector, η is the is the unit outer normal to $\partial \Omega$, and σ is an auxiliary variable for integration. Then, using the assumption given in (6), the condition given in (5), and the fact that $A - C$ is a negative definite matrix, we obtain

$$\frac{\partial V}{\partial t} = -\sum_{j=1}^{2} \int_{\Omega} d_{jj} \left(\nabla e_j \right)^2 - \int_{\Omega} e^T (C - A) e < 0. \tag{15}$$

From Lyapunov stability theory, we can conclude that the zero solution of the error system (11) is globally asymptotically stable and therefore, the master system (1) and the slave system (2) are globally synchronized. $\square$

4. Synchronization via Linear Controllers

In this section, we outline the issue of controlling the master-slave reaction-diffusion system given in (1) and (2) via linear controllers. In this case, we assume that

$$\left| f_1 \left(v_1, v_2 \right) - f_1 \left(u_1, u_2 \right) \right| \le \alpha_1 \left| v_1 - u_1 \right| + \alpha_2 \left| v_2 - u_2 \right|,$$

$$\left| f_2 \left(v_1, v_2 \right) - f_2 \left(u_1, u_2 \right) \right| \le \beta_1 \left| v_1 - u_1 \right| + \beta_2 \left| v_2 - u_2 \right|, \tag{16}$$

where $\alpha_1, \alpha_2, \beta_1, \beta_2$ are positive constants.

Theorem 2. *If there exists a control matrix $L = (l_{ij})_{2 \times 2}$ such that $A - L$ is a definite negative matrix, then the master-slave reaction-diffusion system given in (1) and (2) can be synchronized under the following linear control law*

$$\mathbf{U}_1 = -\sum_{j=1}^{2} l_{1j} e_j - \left(\alpha_1 + \frac{(\beta_1 + \alpha_2)^2}{4} \right) e_1,$$

$$\mathbf{U}_2 = -\sum_{j=1}^{2} l_{2j} e_j - (\beta_2 + 1) e_2. \tag{17}$$

Proof. Substituting (17) into the error system given in (7) yields

$$\frac{\partial e_1}{\partial t} = \sum_{j=1}^{2} d_{1j} \Delta e_j + \sum_{j=1}^{2} \left(a_{1j} - l_{1j} \right) e_j + f_1 \left(v_1, v_2 \right)$$

$$- f_1 \left(u_1, u_2 \right) - \left(\alpha_1 + \frac{(\beta_1 + \alpha_2)^2}{4} \right) e_1,$$

$$\frac{\partial e_2}{\partial t} = \sum_{j=1}^{2} d_{2j} \Delta e_j + \sum_{j=1}^{2} \left(a_{2j} - l_{2j} \right) e_j + f_2 \left(v_1, v_2 \right)$$

$$- f_2 \left(u_1, u_2 \right) - (\beta_2 + 1) e_2. \tag{18}$$

Constructing a Lyapunov function in the form $V = (1/2) \int_{\Omega} e^T e$ gives

$$\frac{\partial V}{\partial t} = \int_{\Omega} \left(e_1 \frac{\partial e_1}{\partial t} + e_2 \frac{\partial e_2}{\partial t} \right) = \sum_{j=1}^{2} \int_{\Omega} d_{1j} e_1 \Delta e_j + \int_{\Omega} e_1$$

$$\cdot \sum_{j=1}^{2} \left(a_{1j} - l_{1j} \right) e_j + \int_{\Omega} e_1 \left[f_1 \left(v_1, v_2 \right) - f_1 \left(u_1, u_2 \right) \right]$$

$$- \int_{\Omega} \left(\alpha_1 + \frac{(\beta_1 + \alpha_2)^2}{4} \right) e_1^2 + \sum_{j=1}^{2} \int_{\Omega} d_{2j} e_2 \Delta e_j$$

$$+ \int_{\Omega} e_2 \sum_{j=1}^{2} \left(a_{2j} - l_{2j} \right) e_j + \int_{\Omega} e_2 \left[f_2 \left(v_1, v_2 \right) \right.$$

$$\left. - f_2 \left(u_1, u_2 \right) \right] - \int_{\Omega} (\beta_2 + 1) e_2^2 = \sum_{j=1}^{2} \int_{\Omega} d_{jj} e_j \Delta e_j$$

$$+ \int_{\Omega} (d_{12} e_1 \Delta e_2 + d_{21} e_2 \Delta e_1)$$

$$+ \int_\Omega \left[e_1 \sum_{j=1}^{2} \left(a_{1j} - l_{1j} \right) e_j + e_2 \sum_{j=1}^{2} \left(a_{2j} - l_{2j} \right) e_j \right]$$

$$+ \int_\Omega \left[e_1 \left(f_1 \left(v_1, v_2 \right) - f_1 \left(u_1, u_2 \right) \right) \right.$$

$$\left. + e_2 \left(f_2 \left(v_1, v_2 \right) - f_2 \left(u_1, u_2 \right) \right) \right] - \int_\Omega \left(\alpha_1 \right.$$

$$\left. + \frac{\left(\beta_1 + \alpha_2 \right)^2}{4} \right) e_1^2 - \int_\Omega \left(\beta_2 + 1 \right) e_2^2$$

$$\leq \sum_{j=1}^{2} \int_\Omega d_{jj} e_j \Delta e_j + \int_\Omega \left(d_{12} e_1 \Delta e_2 + d_{21} e_2 \Delta e_1 \right)$$

$$+ \int_\Omega \left[e_1 \sum_{j=1}^{2} \left(a_{1j} - l_{1j} \right) e_j + e_2 \sum_{j=1}^{2} \left(a_{2j} - l_{2j} \right) e_j \right]$$

$$+ \int_\Omega \left[|e_1| \left| f_1 \left(v_1, v_2 \right) - f_1 \left(u_1, u_2 \right) \right| \right.$$

$$\left. + |e_2| \left| f_2 \left(v_1, v_2 \right) - f_2 \left(u_1, u_2 \right) \right| \right] - \int_\Omega \left(\alpha_1 \right.$$

$$\left. + \frac{\left(\beta_1 + \alpha_2 \right)^2}{4} \right) e_1^2 - \int_\Omega \left(\beta_2 + 1 \right) e_2^2. \tag{19}$$

By using Green formula, we get

$$\frac{\partial V}{\partial t} \leq - \sum_{j=1}^{2} \int_\Omega d_{jj} \left(\nabla e_j \right)^2 - \int_\Omega e^T \left(L - A \right) e$$

$$+ \int_\Omega \left[|e_1| \left| f_1 \left(v_1, v_2 \right) - f_1 \left(u_1, u_2 \right) \right| \right.$$

$$\left. + |e_2| \left| f_2 \left(v_1, v_2 \right) - f_2 \left(u_1, u_2 \right) \right| \right] - \int_\Omega \left(\alpha_1 \right. \tag{20}$$

$$\left. + \frac{\left(\beta_1 + \alpha_2 \right)^2}{4} \right) e_1^2 - \int_\Omega \left(\beta_2 + 1 \right) e_2^2,$$

and by using the conditions given in (16), we obtain

$$\frac{\partial V}{\partial t} \leq - \sum_{j=1}^{2} \int_\Omega d_{jj} \left(\nabla e_j \right)^2 - \int_\Omega e^T \left(L - A \right) e$$

$$+ \int_\Omega \left(\alpha_1 e_1^2 + \left(\alpha_2 + \beta_1 \right) |e_1| |e_2| + \beta_2 e_2^2 \right)$$

$$- \int_\Omega \left(\alpha_1 + \frac{\left(\beta_1 + \alpha_2 \right)^2}{4} \right) e_1^2 - \int_\Omega \left(\beta_2 + 1 \right) e_2^2$$

$$= - \sum_{j=1}^{2} \int_\Omega d_{jj} \left(\nabla e_j \right)^2 - \int_\Omega e^T \left(L - A \right) e$$

$$- \int_\Omega \left[\frac{\left(\beta_1 + \alpha_2 \right)^2}{4} e_1^2 - \left(\beta_1 + \alpha_2 \right) |e_2| |e_1| + e_2^2 \right]$$

$$= - \sum_{j=1}^{2} \int_\Omega d_{jj} \left(\nabla e_j \right)^2 - \int_\Omega e^T \left(L - A \right) e$$

$$- \int_\Omega \left(\frac{\beta_1 + \alpha_2}{2} |e_1| - |e_2| \right)^2 < 0. \tag{21}$$

Therefore, since $\partial V / \partial t < 0$, we can conclude that the master system (1) and the slave system (2) are globally synchronized. □

5. Application and Numerical Simulation

In this section, numerical simulations are given to illustrate and validate the synchronization schemes derived in the previous sections. We take the Lengyel-Epstein system [35] as a special case of reaction-diffusion systems. Consider the following coupled master-slave systems:

$$\frac{\partial u_1 \left(t, x \right)}{\partial t} = \frac{\partial^2 u_1}{\partial x^2} + 5\gamma - u_1 - \frac{4 u_1 u_2}{1 + u_1^2},$$

$$\frac{\partial u_2 \left(t, x \right)}{\partial t} = \delta \left(d \frac{\partial^2 u_2}{\partial x^2} + u_1 - \frac{u_1 u_2}{1 + u_1^2} \right), \tag{22}$$

and

$$\frac{\partial v_1 \left(t, x \right)}{\partial t} = \frac{\partial^2 v_1}{\partial x^2} + 5\gamma - v_1 - \frac{4 v_1 v_2}{1 + u_1^2} + \mathbf{U}_1,$$

$$\frac{\partial v_2 \left(t, x \right)}{\partial t} = \delta \left(d \frac{\partial^2 v_2}{\partial x^2} + v_1 - \frac{v_1 v_2}{1 + v_1^2} \right) + \mathbf{U}_2, \tag{23}$$

where > 0, $x \in (0, \theta)$, $(\delta, \gamma, \theta, d) = (9.7607, 2.7034, 13.03, 1.75)$, and $(\mathbf{U}_1, \mathbf{U}_2)^T$ is the control law to be determined. The reaction-diffusion system given in (22) is called the Lengyel-Epstein system. When the initial conditions associated with system (22) are given by $(u_1(0, x), u_2(0, x)) = (\theta + 0.2 \cos(5\pi x), 1 + \theta^2 + 0.6 \cos(5\pi x))$ then the solutions u_1 and u_2 are shown in Figures 1 and 2. For the uncontrolled system (23) (i.e., $\mathbf{U}_1 = \mathbf{U}_2 = 0$), if the initial conditions are given by $(v_1(0, x), v_2(0, x)) = (\theta + 0.2 \cos(4\pi x), 1 + \theta^2 + 0.6 \cos(4\pi x))$ then the solutions v_1 and v_2 are shown in Figures 3 and 4. The approximation and calculation of the solutions to the Lengyel-Epstein systems given in (22) and (23) are obtained using the Matlab function "pdepe".

Comparing with the master-slave reaction-diffusion systems given (1) and (2), the constants $(d_{ij})_{2 \times 2}$ and $A = (a_{ij})_{2 \times 2}$ can be given as

$$\left(d_{ij} \right)_{2 \times 2} = \begin{pmatrix} 1 & 0 \\ 0 & \delta d \end{pmatrix}, \tag{24}$$

and
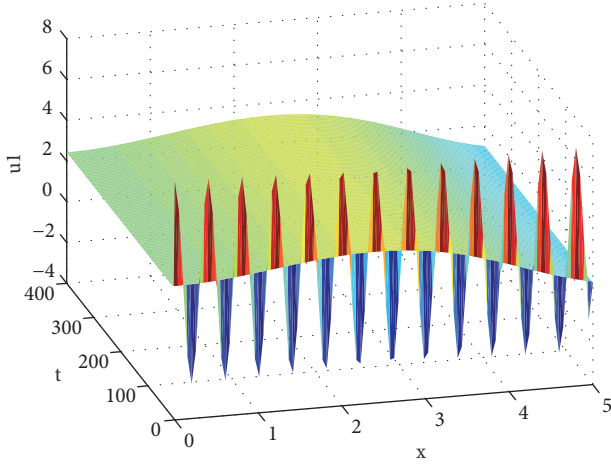
FIGURE 1: Dynamic behavior of solution u_1.
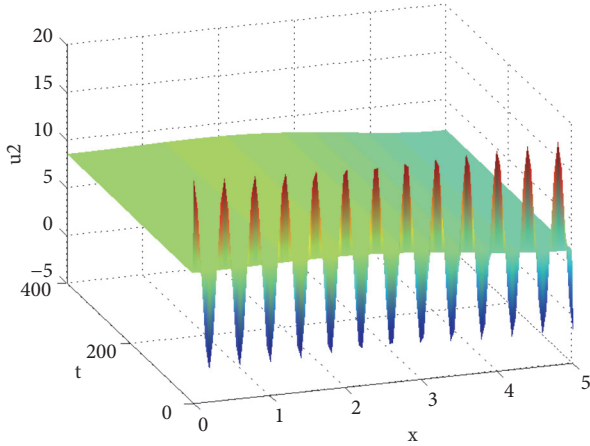
FIGURE 2: Dynamic behavior of solution u_2.

FIGURE 3: Dynamic behavior of solution v_1.
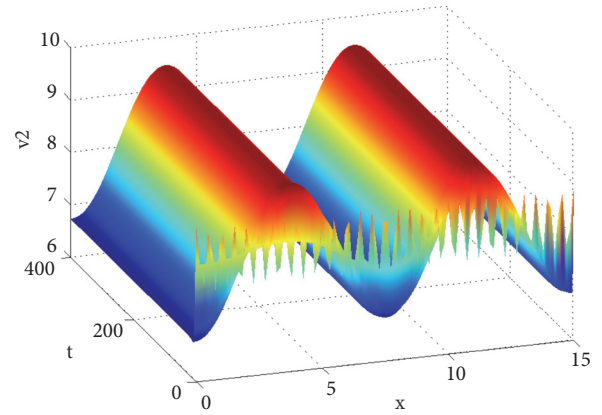
FIGURE 4: Dynamic behavior of solution v_2.

$$A = \left(a_{ij}\right)_{2\times 2} = \begin{pmatrix} -1 & 0 \\ \delta & 0 \end{pmatrix}. \tag{25}$$

It is clear that our assumption (5) is satisfied. Also, the homogeneous Neumann boundary condition for systems (22) and (23) is described as

$$\frac{\partial u_1}{\partial x} = \frac{\partial u_2}{\partial x} = \frac{\partial v_1}{\partial x} = \frac{\partial v_2}{\partial x} = 0, \quad x = 0, \ \theta \ and \ t > 0. \tag{26}$$

5.1. Case 1: Nonlinear Control. According to the control scheme proposed in Section 3, if we choose the control matrix C as

$$C = \begin{pmatrix} 0 & 0 \\ \delta & 2 \end{pmatrix}, \tag{27}$$

then the controllers $\mathbf{U}_1$ and $\mathbf{U}_2$ can be designed as

$$\mathbf{U}_1 = \frac{4v_1v_2}{1 + v_1^2} - \frac{4u_1u_2}{1 + u_1^2},$$

$$\mathbf{U}_2 = -\delta\left(v_1 - u_1\right) - 2\left(v_2 - u_2\right) + \frac{\delta v_1 v_2}{1 + v_1^2} - \frac{\delta u_1 u_2}{1 + u_1^2}, \tag{28}$$

and so, simply, we can show that $A - C$ is a negative definite matrix. Therefore, based on Theorem 1, systems (22) and (23) are globally synchronized. The time evolution of the error system states e_1 and e_2, in this case, is shown in Figures 5 and 6.

5.2. Case 2: Linear Control. First, the assumption given in (16) for controlling the master-slave reaction-diffusion system given in (1) and (2) via linear controllers is satisfied. One can easily verify that

$$\begin{aligned} \left|f_1\left(v_1, v_2\right) - f_1\left(u_1, u_2\right)\right| &\leq \left|v_1 - u_1\right| + 4\left|v_2 - u_2\right|, \\ \left|f_2\left(v_1, v_2\right) - f_2\left(u_1, u_2\right)\right| &\leq \left|v_1 - u_1\right| + \delta\left|v_2 - u_2\right|. \end{aligned} \tag{29}$$

According to the control scheme proposed in Section 4, if we choose the control matrix L as

$$L = \begin{pmatrix} 0 & 0 \\ \delta & 1 \end{pmatrix}, \tag{30}$$
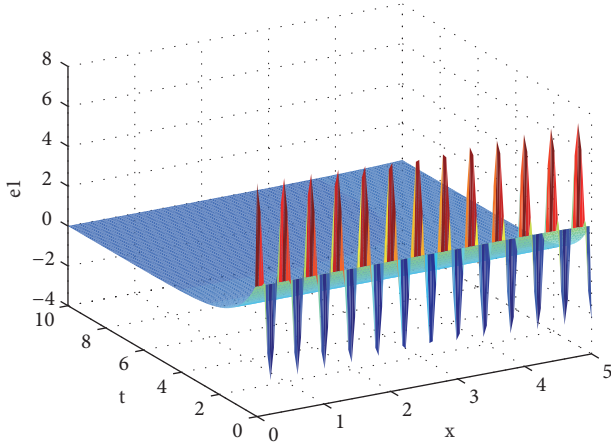
FIGURE 5: Time evolution of the nonlinear synchronization control error e_1.
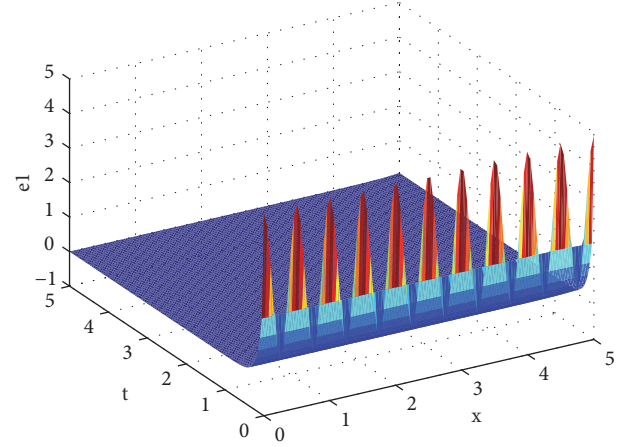
FIGURE 7: Time evolution of the linear synchronization control error e_1.
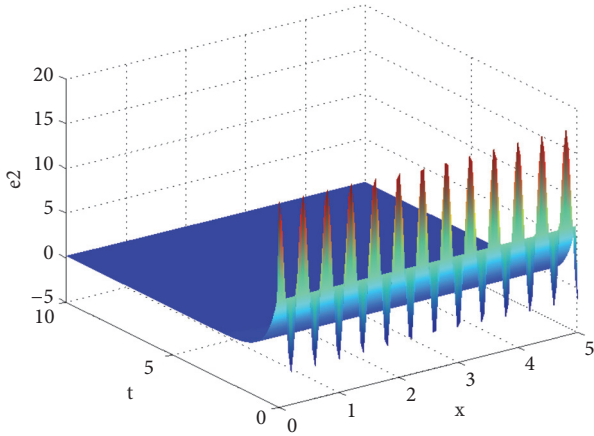
FIGURE 6: Time evolution of the nonlinear synchronization control error e_2.
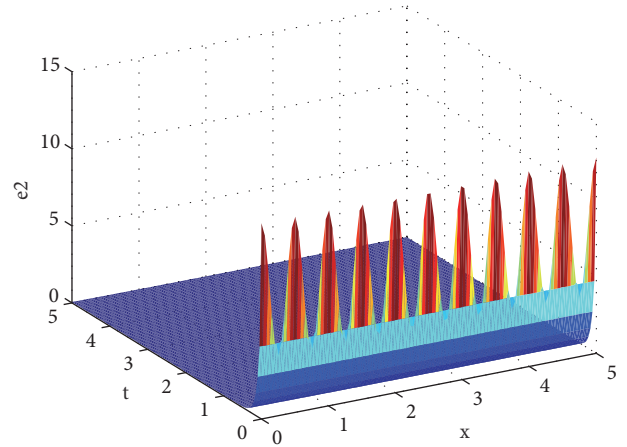
FIGURE 8: Time evolution of the linear synchronization control error e_2.

then the controllers $\mathbf{U}_1$ and $\mathbf{U}_2$ can be designed as

$$\mathbf{U}_1 = -\frac{29}{4}\left(v_1 - u_1\right),$$

$$\mathbf{U}_2 = -\delta\left(v_1 - u_1\right) - \left(\delta + 2\right)\left(v_2 - u_2\right),$$
(31)

and so, simply, we can show that $A - L$ is a negative definite matrix. Therefore, based on Theorem 2, systems (22) and (23) are globally synchronized. The time evolution of the error system states e_1 and e_2, in this case, is shown in Figures 7 and 8.

As a result form the performed numerical simulations, we can observe that the addition of the designed linear and nonlinear controllers to the controlled Lengyel-Epstein system, given in (23), updates the coupled systems, given in (22) and (23), dynamics such that the systems states become synchronized. In both cases, the proposed control schemes stabilize the synchronization error states where the zero solution of the error system becomes globally asymptotically stable.

6. Conclusion

The study investigates the synchronization control for a class of reaction-diffusion systems. First, a spatial-time coupling protocol for the synchronization is suggested, then novel control methods, that include linear and nonlinear controllers, are proposed to realize complete synchronization between coupled reaction-diffusion systems. The synchronization results are derived based on Lyapunov stability theory and using the drive-response concept.

Suitable sufficient conditions for achieving synchronization of coupled Lengyel-Epstein systems via suitable linear and nonlinear controllers applied to the response system are derived. For this purpose, we design the controllers so that the zero solution of the error system becomes globally asymptotically stable. Numerical simulations consisting of displaying synchronization behaviors of coupled Lengyel-Epstein systems are given, using Matlab function "pdepe", to verify the effectiveness of the proposed synchronization schemes. Comparing the numerical simulations shown in Figures 5, 6, 7, and 8, we can easily observe that the

linear control scheme realizes synchronization faster than the nonlinear case. Also, the nonlinear control scheme requires the removal of nonlinear terms from the response system, which may increase the cost of the controllers. So, the cost of the controllers in the nonlinear case is more than the cost in the linear case.

The study confirms that the problem of complete synchronization in coupled high dimensional spatial-temporal systems can be realized using linear and nonlinear controllers. Also, we can easily see that the research results obtained in this paper can be extended to many other types of spatial-temporal systems with reaction-diffusion terms.

Data Availability

The data used to support the findings of this study are included within the article.

Conflicts of Interest

The authors declare that there are no conflicts of interest regarding the publication of this paper.

Acknowledgments

References

[1] L. M. Pecora and T. L. Carroll, "Synchronization in chaotic systems," *Physical Review Letters*, vol. 64, no. 8, pp. 821–824, 1990.

[2] H. Fujisaka and T. Yamada, "Stability theory of synchronized motion in coupled-oscillator systems," *Progress of Theoretical and Experimental Physics*, vol. 69, no. 1, pp. 32–47, 1983.

[3] E. Ott, C. Grebogi, and J. A. Yorke, "Controlling chaos," *Physical Review Letters*, vol. 64, no. 11, pp. 1196–1199, 1990.

[4] C. W. Wu and L. O. Chua, "A unified framework for synchronization and control of dynamical systems," *International Journal of Bifurcation and Chaos*, vol. 4, no. 4, pp. 979–998, 1994.

[5] H. M. Rodrigues, "Abstract methods for synchronization and applications," *Applicable Analysis: An International Journal*, vol. 62, no. 3-4, pp. 263–296, 1996.

[6] A. Acosta and P. García, "Synchronization of non-identical chaotic systems: an exponential dichotomies approach," *Journal of Physics A: Mathematical and General*, vol. 34, no. 43, pp. 9143–9151, 2001.

[7] G. Chen and X. Yu, *Chaos Control: Theory and Applications*, Springer-Verlag, Berlin, Germany, 2003.

[8] A. E. Hramov and A. A. Koronovskii, "An approach to chaotic synchronization," *Chaos: An Interdisciplinary Journal of Nonlinear Science*, vol. 14, no. 3, pp. 603–610, 2004.

[9] M. A. Aziz-Alaoui, "Synchronization of chaos," *Encyclopedia of Mathematical Physics*, pp. 213–226, 2006.

[10] A. Ouannas and Z. Odibat, "Generalized synchronization of different dimensional chaotic dynamical systems in discrete time," *Nonlinear Dynamics*, vol. 81, no. 1-2, pp. 765–771, 2015.

[11] H. Nakao, T. Yanagita, and Y. Kawamura, "Phase-reduction approach to synchronization of spatiotemporal rhythms in reaction-diffusion systems," *Physical Review X*, vol. 4, no. 2, Article ID 021032, 2014.

[12] Y. Kawamura, S. Shirasaka, T. Yanagita, and H. Nakao, "Optimizing mutual synchronization of rhythmic spatiotemporal patterns in reaction-diffusion systems," *Physical Review E: Statistical, Nonlinear, and Soft Matter Physics*, vol. 96, no. 1, Article ID 012224, 2017.

[13] L. Kocarev, Z. Tasev, T. Stojanovski, and U. Parlitz, "Synchronizing spatiotemporal chaos," *Chaos: An Interdisciplinary Journal of Nonlinear Science*, vol. 7, no. 4, pp. 635–643, 1997.

[14] L. Kocarev, Z. Tasev, and U. Parlitz, "Synchronizing spatiotemporal chaos of partial differential equations," *Physical Review Letters*, vol. 79, no. 1, pp. 51–54, 1997.

[15] H. G. Winful and L. Rahman, "Synchronized chaos and spatiotemporal chaos in arrays of coupled lasers," *Physical Review Letters*, vol. 65, no. 13, pp. 1575–1578, 1990.

[16] S. Boccaletti, J. Bragard, F. T. Arecchi, and H. Mancini, "Synchronization in nonidentical extended systems," *Physical Review Letters*, vol. 83, no. 3, pp. 536–539, 1999.

[17] L. Junge and U. Parlitz, "Synchronization and control of coupled Ginzburg-Landau equations using local coupling," *Physical Review E: Statistical, Nonlinear, and Soft Matter Physics*, vol. 61, no. 4, pp. 3736–3742, 2000.

[18] J. Bragard, F. T. Arecchi, and S. Boccaletti, "Characterization of synchronized spatiotemporal states in coupled nonidentical complex Ginzburg-Landau equations," *International Journal of Bifurcation and Chaos*, vol. 10, no. 10, pp. 2381–2389, 2000.

[19] J. Bragard, S. Boccaletti, and H. Mancini, "Asymmetric coupling effects in the synchronization of spatially extended chaotic systems," *Physical Review Letters*, vol. 91, no. 6, Article ID 064103, 2003.

[20] C. Beta and A. S. Mikhailov, "Controlling spatiotemporal chaos in oscillatory reaction-diffusion systems by time-delay autosynchronization," *Physica D: Nonlinear Phenomena*, vol. 199, no. 1-2, pp. 173–184, 2004.

[21] A. E. Hramov, A. A. Koronovskii, and P. V. Popov, "Generalized synchronization in coupled Ginzburg-Landau equations and mechanisms of its arising," *Physical Review E: Statistical, Nonlinear, and Soft Matter Physics*, vol. 72, no. 3, Article ID 037201, 2005.

[22] C. T. Zhou, "Synchronization in nonidentical complex Ginzburg-Landau equations," *Chaos: An Interdisciplinary Journal of Nonlinear Science*, vol. 16, no. 1, Article ID 013124, 2006.

[23] P. García, A. Acosta, and H. Leiva, "Synchronization conditions for master-slave reaction diffusion systems," *EPL (Europhysics Letters)*, vol. 88, no. 6, Article ID 60006, 2009.

[24] B. Ambrosio and M. A. Aziz-Alaoui, "Synchronization and control of coupled reaction-diffusion systems of the FitzHugh-Nagumo type," *Computers & Mathematics with Applications*, vol. 64, no. 5, pp. 934–943, 2012.

[25] L. Wang and H. Zhao, "Synchronized stability in a reaction-diffusion neural network model," *Physics Letters A*, vol. 378, no. 48, pp. 3586–3599, 2014.

[26] K.-N. Wu, T. Tian, and L. Wang, "Synchronization for a class of coupled linear partial differential systems via boundary control," *Journal of The Franklin Institute*, vol. 353, no. 16, pp. 4062–4073, 2016.

[27] T. Chen, R. Wang, and B. Wu, "Synchronization of multi-group coupled systems on networks with reaction-diffusion terms based on the graph-theoretic approach," *Neurocomputing*, vol. 227, pp. 54–63, 2017.

[28] Z. Tu, N. Ding, L. Li, Y. Feng, L. Zou, and W. Zhang, "Adaptive synchronization of memristive neural networks with time-varying delays and reaction-diffusion term," *Applied Mathematics and Computation*, vol. 311, no. 15, pp. 118–128, 2017.

[29] S. Chen, C.-C. Lim, P. Shi, and Z. Lu, "Synchronization control for reaction-diffusion FitzHugh-Nagumo systems with spatial sampled-data," *Automatica*, vol. 93, pp. 352–362, 2018.

[30] H. Chen, P. Shi, and C.-C. Lim, "Pinning impulsive synchronization for stochastic reaction–diffusion dynamical networks with delay," *Neural Networks*, vol. 106, pp. 281–293, 2018.

[31] L. Liu, W.-H. Chen, and X. Lu, "Impulsive H∞ synchronization for reaction–diffusion neural networks with mixed delays," *Neurocomputing*, vol. 272, no. 10, pp. 481–494, 2018.

[32] C. He and J. Li, "Hybrid adaptive synchronization strategy for linearly coupled reaction–diffusion neural networks with time-varying coupling strength," *Neurocomputing*, vol. 275, pp. 1769–1781, 2018.

[33] A. S. Mikhailov and K. Showalter, "Control of waves, patterns and turbulence in chemical systems," *Physics Reports*, vol. 425, no. 2-3, pp. 79–194, 2006.

[34] A. S. Mikhailov and G. Ertl, *Engineering of Chemical Complexity*, World Scientific Publishing Co., Singapore, 2nd edition, 2016.

[35] B. Lisena, "On the global dynamics of the Lengyel-Epstein system," *Applied Mathematics and Computation*, vol. 249, pp. 67–75, 2014.

Research Article

Simulation and Analysis of the Complex Behavior of Supply Chain Inventory System Based on Third-Party Logistics Management Inventory Model with No Accumulating of Unsatisfied Demand

Zusheng Zhang (ID),[1,2] **Xu Wang** (ID),[1,2] **Qianqian Guo,**[1,2] **Zhenrui Li,**[1] **and Yingbo Wu** (ID)[3]

[1]*College of Mechanical Engineering, Chongqing University, Chongqing, China*
[2]*Chongqing Key Laboratory of Logistics, Chongqing University, Chongqing, China*
[3]*School of Software Engineering, Chongqing University, Chongqing, China*

Correspondence should be addressed to Xu Wang; wx921@163.com

Under the third-party logistics management inventory model, the system dynamics method is used to establish a nonlinear supply chain system model with supply capacity limitation and nonpermissible return, which is based on unsatisfied demand nonaccumulation. The theory of singular value and the Jury Test are used to derive the stable interval of the model which is simplified. The Largest Lyapunov Exponent (LLE) of the system is calculated by the Wolf reconstruction method and used to analyze the influence of different parameters of system's stability. Then, the most reasonable and unreasonable combination of decision parameters under different demand environment is found out. Next, this paper compared and analyzed the change of inventory or transportation volume of system members under the combination of rational and irrational decision parameters. All of these provided guidance for decision making, which shows an important practical significance.

1. Introduction

As market competition continues to intensify, competition among enterprises is gradually transformed into competition for interests among supply chains. The competition between supply chains requires that all member companies in the supply chain work together to maximize the overall benefits of the supply chain, thereby increasing the competitiveness of the supply chain. The supply chain is highly competitive, and member companies are highly resistant to risks in the supply chain.

At the same time, maximizing the overall benefits of the supply chain can enable companies to continue to receive significant benefits for longer periods of time. Member companies obtain more benefits, and the company has more funds to carry out research and development innovation and improvement of its own technologies. This, in turn, enhances the competitiveness of the supply chain and enables the supply chain to gain more benefits.

A supply chain network (SCN) is a complex nonlinear system involving multiple entities. The policy of each entity in decision making and the uncertainties of demand and supply (or production) significantly affect the complexity of its behavior [1]. In the traditional SC model, each player is responsible for its inventory control, production, or distribution ordering activities, and each echelon only has their immediate customer information [2]. The lack of visibility of real demand causes a number of problems in traditional SC; many industries were required to improve their SC operations by sharing inventory or demand information for supplier and customer [3]. With the continuous development of information technology, some new supply chain models have gradually emerged. Among them, the application more common is the Vendor-Managed Inventory (VMI) model and

the Third-party Logistics Management Inventory (TMI) model. The traditional individualized inventory management model is prone to the phenomenon that the demand follows the supply chain to scale up from the downstream to the upstream, that is, the bullwhip effect [4]. In the new supply chain model, demand information, inventory information, and production information are fully shared. The problem of gradually increasing demand has been well controlled. Whether it is from the traditional supply chain model to the supplier management inventory model or the supplier management inventory model, they all evolve to the third-party logistics management inventory model; these are in line with the concept of supply chain management specialization, refinement, and information.

2. Literature Review

As for the behavior of supply chain system, many scholars have studied it and obtained rich research results [5, 6]. Mosekilde and Larsen [7] and Thomsen et al. [8] adopted a deterministic supply chain and showed the existence of chaotic behavior in it. For linear systems, García et al. [9] considered one-dimensional time-invariant sampled-data linear systems with constant feedback gain, an arbitrary fixed time delay. The following will be divided into two parts to summarize them.

For the traditional supply chain model, the results are rich. Towill [10] proposed an inventory and order-based production control system (IOBPCS) to study the system's ability to calm down shocks and protect the manufacturing process from random changes in consumption. Lee et al. [11] analyzed four causes of the bullwhip effect and discussed possible actions to mitigate the adverse effects of this distortion. Disney and Towill [12] proposed a discrete control theory model for a general model of replenishment rules and analyzed that extending the validity period of historical data and shortening the production lead time can reduce the bullwhip effect. Nagatani and Helbing [13] studied a variety of production strategies to stabilize the supply chain, analyzed whether the response to the inventory level of other members of the supply chain has a stabilizing effect, proved that the prediction of the future inventory level can stabilize the supply chain, and gave the linear system stable conditions and simulations of different control strategies. Wang et al. [14] studied the stability of a constrained production and inventory system with a Forbidden Returns constraint (that is, a nonnegative order rate) via a piecewise linear model, an eigenvalue analysis, and a simulation investigation. Hwarng and Yuan [15] studied the influence of stochastic demand on the complex dynamic behavior of the supply chain. The research results show the complexity of the interaction between the stochastic demand process and the nonlinear dynamics, and the study considers that there are essential differences between the determination of demand and the impact of stochastic demand on the dynamics of the supply chain. Spiegler et al. [16] use a highly referenced Forrester production distribution model as a reference supply chain system to study nonlinear control structures and apply appropriate

analytical control theory methods. Then, the performance of the linearized model is compared with the numerical solution of the original nonlinear model and other previous studies in the same model. Considering the nonnegative constraints of order quantities, Li et al. [17] studied the performance of inventory systems, including the effects of system stability, service levels, inventory costs, and transportation delay times, to systematically reflect the impact of order policies on inventory system performance. Under the intervention of the government, Dai et al. [18] constructed a continuous two-channel closed-loop supply chain model with time-delay decision and discussed the existence conditions of the local stability of the equilibrium. In addition, the time-delay feedback control method is used to effectively control unstable or chaotic systems.

For the new supply chain models, Disney and Towill [19] used the APIOBPCS ordering strategy to use mathematical models to study the stability of VMI systems, confirmed the instability caused by poor system design through dynamic simulation analysis, and proved that specific production delay can be avoided by setting reasonable parameters. Supply chain instability occurs. Disney and Towill [20] compared the expected performance of the supplier-managed inventory (VMI) supply chain with the traditional "series" supply chain. The analysis found that VMI performed better in response to changes in volatility demand and through simulated VMI and traditional supply. The chain validates the response to a typical retail sales model. Nachiappan and Jawahar [21] discussed the operation of a two-echelon single vendor–multiple buyers supply chain (TSVMBSC) model under the supplier management inventory (VMI) model and presented a mathematical formulation of an integrated inventory model of a two-echelon single vendor–multiple buyers VMI system. Han et al. [22] discussed a decentralized VMI problem in a three-echelon supply chain network in which multiple distributors (third-party logistics companies) are selected to balance the inventory between a vendor (manufacturer) and multiple buyers (manufacturers), and a tri-level decision model to describe the decentralized VMI problem is first proposed.

Most of the existing literature-based models are traditional supply chain models and supplier management inventory models. Few studies are based on third-party logistics management inventory models. Even the model is still in a stage of gradual improvement, and there are few documents which study the situation that the unmet need does not accumulate to the next cycle. At the same time, there are few relevant studies that have considered the fluctuations of the third-party logistics service providers' transportation workload. This paper analyzes the impact of different demand scenarios and the status of stable and unstable third-party logistics service providers on the number of transportation tasks.

Based on the premise of unsatisfied demand no accumulation, this paper constructs a dynamic model of third-party logistics inventory management supply chain system, simplifies the model and uses the Wolf reconstruction method and singular value theory to determine the conditions for simplifying the system stability, and finally uses

Simulink. The system simulation and data analysis verify the correctness and applicability of the model. At the same time, it gives a reasonable decision area for making the supply chain system in a stable state, which provides a reference for practical decision making and has important practical significance.

3. TMI Supply Chain System Dynamic Model

3.1. System Description. The TMI supply chain consists of one supplier, one retailer, and one third-party logistics enterprise. Both suppliers and retailers entrust the third-party logistics with the right of the inventory operation and decision making through the agreement. The third-party logistics enterprise is responsible for inventory management and logistics transportation tasks of the entire supply chain. In order to ensure timely replenishment of retailers, distribution centers are located near retailers. The work of supply chain members is carried out on a periodic basis. The event flow of each supply chain member is as follows: for retailers, at the beginning of the period, they receive replenishment from distribution centers, shipment according to customer demand, inventory, third-party logistics combined with retailer safety stock, suggest that retailers replenish, and retailers issue replenishment notifications to distribution centers; for the distribution center, at the beginning of the period, the distribution center received replenishment from the warehouse, replenished the goods from the retailer, inventoried the inventory, and issued a replenishment notice to the warehouse; for warehouses, at the beginning of the period, they received replenishment from suppliers, replenished them at the distribution center, counted inventory, and sent replenishment notifications to suppliers; For suppliers, production will be carried out at the beginning of the period t, according to the replenishment notice received at end of period $t - 1$.

3.2. Systematic Difference Equations

3.2.1. Demand Forecasting Method. Assume that supply chain members use simple exponential smoothing methods to forecast demand. When suppliers conduct demand forecasting, they do demand forecasting based on the needs of the supply chain's end customer rather than retailer's order. From the perspective of demand forecasting, demand forecasts are more reasonable for the entire supply chain.

$$F(t) = \theta F(t - 1) + (1 - \theta)D(t). \tag{1}$$

3.2.2. Order Policy. This article adopts APVIOBPCS ordering strategy. The basic idea is that ordering has a fixed ordering period, and the order quantity of each period consists of demand forecasting, inventory adjustment, and transit adjustment. The ordering strategy is considered from the perspective of the Warehouse-Distribution Center System. Suppliers, warehouses, and distribution centers are seen as a system when considering warehouse ordering. The system is called the Warehouse-Distribution Center System. The ordering expression of the system is

$$O(t) = \max \left(0, F(t) + \alpha_S\left(I^0(t) - I(t)\right) + \alpha_{SL}\left(Y^0(t) - Y(t)\right)\right). \tag{2}$$

The supplier's work-in-process inventory at time t is given by

$$Y(t) = Y(t - 1) + O(t - 1) - R_w(t). \tag{3}$$

The supplier's expected WIP inventory is given by

$$Y^0(t) = G_w F(t). \tag{4}$$

Using the discrete system Z transform theory, we have drawn the block diagram of the inventory system of warehouse as shown in Figure 1.

3.2.3. For Retailers. The retailer's replenishment point is given by

$$I_r^0(t) = G_r F(t). \tag{5}$$

The retailer's inventory level at time is given by

$$I_r(t) = I_r(t - 1) + R_r(t) - S_r(t). \tag{6}$$

And the retailer replenishment is given by

$$O_r(t) = \max \left(0, I_r^0(t) - I_r(t)\right). \tag{7}$$

The replenishment of the retailer can be quickly obtained, that is, the replenishment notification is issued at the end of the period, and the replenishment can be received at the beginning of the next period:

$$R_r(t) = O_r(t - 1). \tag{8}$$

The retailer's shipments for this period's customer demand is given by

$$S_r(t) = D(t). \tag{9}$$

Using the discrete system Z transform theory, we have drawn the block diagram of the inventory system of the retailer as shown in Figure 2.

3.2.4. For Warehouse-Distribution Center System. The distribution center replenishment point is given by

$$I_d^0(t) = F(t)G_d. \tag{10}$$

The distribution center inventory is given by

$$I_d(t) = I_d(t - 1) + R_d(t) - S_d(t). \tag{11}$$

The distribution center replenishment is given by

$$O_d(t) = \max \left(0, I_d^0(t) - I_d(t)\right). \tag{12}$$

FIGURE 1: The block diagram of the inventory system of warehouse.

FIGURE 2: The block diagram of the inventory system of the retailer.

The distribution center receiving volume is given by

$$R_d(t) = O_d(t - T_P - 1). \tag{13}$$

The distribution center shipments are given by

$$S_d(t) = \begin{cases} I_d(t-1) + R_d(t) & I_d(t-1) + R_d(t) \le O_r(t-1), \\ O_r(t-1) & I_d(t-1) + R_d(t) > O_r(t-1). \end{cases} \tag{14}$$

And the distribution center inventory in transit is given by

$$W_d(t) = W_d(t-1) + O_d(t-1) - R_d(t). \tag{15}$$

The block diagram of the inventory system of distribution center is drawn using the Z transform theory of the discrete system as shown in Figure 3.

The warehouse inventory is given by

$$I_w(t) = I_w(t-1) + R_w(t) - S_w(t). \tag{16}$$

The warehouse receipt is given by

$$R_w(t) = O(t - T_C - 1). \tag{17}$$

The warehouse shipments are given by

$$S_w(t) = \begin{cases} I_w(t-1) + R_w(t) & I_w(t-1) + R_w(t) \le O_d(t-1), \\ O_d(t-1) & I_w(t-1) + R_w(t) > O_d(t-1). \end{cases} \tag{18}$$

The expected inventory of the system is given by

$$I^0(t) = F(t)(T_C + T_P). \tag{19}$$

And the actual inventory of the system is given by

$$I(t) = I(t-1) + R_w(t) - S_d(t). \tag{20}$$

FIGURE 3: The block diagram of the inventory system of distribution center.

4. System Dynamic Behavior Analysis

The model constructed in this paper has nonnegative constraints and piecewise decision conditions, making the system a nonlinear system with switching. It has complex system dynamic behavior. For complex systems, theoretical derivation has some difficulties. Therefore, this paper uses the Wolf reconstruction method to calculate the Largest Lyapunov Exponent (LLE) value and uses LLE index as a quantitative index of the characteristics to analyze the dynamic behavior of complex supply chain systems.

The Lyapunov exponent quantitatively describes the exponential divergence of adjacent orbits in phase space. An orbit near an attractor of a one-dimensional discrete dynamic system can be expressed as

$$d_k = d_0 e^\lambda. \tag{21}$$

Here, d_0 is the initial separation distance of the two orbits, which is the orbital distance after k iterations, and λ is the Lyapunov exponent.

It can be seen that if the Lyapunov exponent is less than zero, the distance between the orbits is gradually reduced, the motion is stable, and the initial value is not felt; if the Lyapunov exponent is equal to zero, it is a critical state, that is, a stable boundary. If the Lyapunov exponent is greater than zero, it means that the adjacent orbits are scattered, and the long-term behavior is very sensitive to the initial value, and the motion is chaotic.

So it can be seen that if the LLE exponent of the system calculated is greater than 0, the system is in a chaotic state.

The model is simplified. It is assumed that there is only a nonnegative constraint on the order quantity of the system in the model. And $S_1 = \{X \mid O \geq 0\}$ and $S_2 = \{X \mid O < 0\}$. If $T_C = 1$, $T_P = 2$, $G_r = 2$, and $G_w = 1$, then the supply chain model in the previous section can be expressed as

$$\begin{cases} O(t) = \max\left(0, F(t) + \alpha_S\left(I^0(t) - I(t)\right) + \alpha_{SL}\left(Y^0(t) - Y(t)\right)\right), \\ I(t) = I_r(t-1) + I(t-1) - 2F(t-1) + O(t-2), \\ I_r(t) = 2F(t-1) - D(t), \\ Y(t) = Y(t-1) + O(t-1) - O(t-2), \\ F(t) = \theta F(t-1) + (1-\theta)D(t). \end{cases} \tag{22}$$

Equation (22) is expressed in the form of a vector equation, which gives the state space description of the system. The following shows

$$X(t) = A_{1f}X(t-1) + A_{2f}X(t-2) + B_f r(t), \begin{cases} X(t-1) \in S_f \\ X(t-2) \in S_f \end{cases} f = 1, 2,$$

$$X(t) = [O(t)\, I(t)\, I_r(t)\, Y(t)\, F(t)]^T, \quad r(t) = D(t). \tag{23}$$

4.1. Subsystem Stability Analysis. Subsystem 1: requirement for replenishment of the warehousing system.

$$\begin{cases} O(t) = -\alpha_{SL}O(t-1) - \alpha_S I(t-1) - \alpha_S I_r(t-1) - \alpha_{SL}Y(t-1) + [\theta(3\alpha_S + \alpha_{SL} + 1) + 2\alpha_S]F(t-1) + (1-\theta)(3\alpha_S + \alpha_{SL} + 1)D(t) + (\alpha_{SL} - \alpha_S)O(t-2), \\ I(t) = I_r(t-1) + I(t-1) - 2F(t-1) + O(t-2), \\ I_r(t) = 2F(t-1) - D(t), \\ Y(t) = Y(t-1) + O(t-1) - O(t-2), \\ F(t) = \theta F(t-1) + (1-\theta)D(t). \end{cases} \tag{24}$$

Equation (24) is expressed in the form of a vector equation, which gives the state space description of the system. The following shows

$$X(t) = A_{11}X(t-1) + A_{21}X(t-2) + B_1 r(t), \quad (25)$$

where

$$A_{11} = \begin{bmatrix} -\alpha_{SL} & -\alpha_S & -\alpha_S & -\alpha_{SL} & \theta(3\alpha_S + 1 + \alpha_{SL}) + 2\alpha_S \\ 0 & 1 & 1 & 0 & -2 \\ 0 & 0 & 0 & 0 & 2 \\ 1 & 0 & 0 & 1 & 0 \\ 0 & 0 & 0 & 0 & \theta \end{bmatrix},$$

$$A_{21} = \begin{bmatrix} (\alpha_{SL} - \alpha_S) & 0 & 0 & 0 & 0 \\ 1 & 0 & 0 & 0 & 0 \\ 0 & 0 & 0 & 0 & 0 \\ -1 & 0 & 0 & 0 & 0 \\ 0 & 0 & 0 & 0 & 0 \end{bmatrix},$$

$$\quad (26)$$

$$B_1 = \begin{bmatrix} (1-\theta)(3\alpha_S + 1 + \alpha_{SL}) \\ 0 \\ -1 \\ 0 \\ (1-\theta) \end{bmatrix}. \quad (27)$$

Subsystem 2: the warehousing system does not need replenishment.

$$\begin{cases} O(t) = 0, \\ I(t) = I_r(t-1) + I(t-1) - 2F(t-1) + O(t-2), \\ I_r(t) = 2F(t-1) - D(t), \\ Y(t) = Y(t-1) + O(t-1) - O(t-2), \\ F(t) = \theta F(t-1) + (1-\theta)D(t). \end{cases} \quad (28)$$

Equation (28) is expressed as the form of a vector equation, which gives the state space description of the system.

The following shows

$$X(t) = A_{12}X(t-1) + A_{22}X(t-2) + B_2 r(t), \quad (29)$$

where

$$A_{12} = \begin{bmatrix} 0 & 0 & 0 & 0 & 0 \\ 0 & 1 & 1 & 0 & -2 \\ 0 & 0 & 0 & 0 & 2 \\ 1 & 0 & 0 & 1 & 0 \\ 0 & 0 & 0 & 0 & \theta \end{bmatrix},$$

$$A_{22} = \begin{bmatrix} 0 & 0 & 0 & 0 & 0 \\ 1 & 0 & 0 & 0 & 0 \\ 0 & 0 & 0 & 0 & 0 \\ -1 & 0 & 0 & 0 & 0 \\ 0 & 0 & 0 & 0 & 0 \end{bmatrix},$$

$$\quad (30)$$

$$B_2 = \begin{bmatrix} 0 \\ 0 \\ -1 \\ 0 \\ (1-\theta) \end{bmatrix}. \quad (31)$$

According to the singular value theory, let $X^* = [O^* \ I^* \ I_r^* \ Y^* \ F^*]^T$ to represent an equilibrium point of (23), then here, the system trajectory near the point can be expressed as

$$X(t) = X^* + \begin{bmatrix} C_1 \\ C_2 \\ C_3 \\ C_4 \\ C_5 \end{bmatrix} \lambda^t, \quad (32)$$

where λ is a complex number, $C1$, $C2$, $C3$, $C4$, and $C5$ are five constants. Substituting (32) into (23), for subsystem 1, we can obtain the nontrivial solution of system 1 with respect to parameters ($C1$, $C2$, $C3$, $C4$, and $C5$) if and only if (33) is satisfied [23].

$$\left| I - A_{11}\lambda^{-1} - A_{21}\lambda^{-2} \right| = \begin{vmatrix} 1 + \alpha_{SL}\lambda^{-1} - (\alpha_{SL} - \alpha_S)\lambda^{-2} & \alpha_S\lambda^{-1} & \alpha_S\lambda^{-1} & \alpha_{SL}\lambda^{-1} & -[\theta(3\alpha_S + 1 + \alpha_{SL}) + 2\alpha_S]\lambda^{-1} \\ -\lambda^{-2} & 1 - \lambda^{-1} & -\lambda^{-1} & 0 & 2\lambda^{-1} \\ 0 & 0 & 1 & 0 & -2\lambda^{-1} \\ -\lambda^{-1} + \lambda^{-2} & 0 & 0 & 1 - \lambda^{-1} & 0 \\ 0 & 0 & 0 & 0 & 1 - \theta\lambda^{-1} \end{vmatrix} = 0. \quad (33)$$

The characteristic equation of (25) determines the stability of the equilibrium solution by (33).

$$\left(1 - \lambda^{-1}\right)\left[1 + (\alpha_{SL} - 1)\lambda^{-1} + (\alpha_S - \alpha_{SL})\lambda^{-2}\right]\left(1 - \theta\lambda^{-1}\right) = 0.$$

$$(34)$$

That is,

$$(\lambda - 1)(\lambda - \theta)\left[\lambda^2 + (\alpha_{SL} - 1)\lambda + \alpha_S - \alpha_{SL}\right] = 0, \qquad (35)$$

where $\lambda \neq 0$. If the root of (35) is within the unit circle, system 1 is stable. From (35), the solution of the equation $\lambda_1 = 1$ and $\lambda_2 = \theta$. According to [24], if the characteristic root of a linear discrete system on the unit circle is the single root of the smallest polynomial of the characteristic polynomial, the system is stable. Because $0 < \theta < 1$, λ_1 and λ_2 are stable. Then, the stability of system 1 is determined by the root of (36).

$$\lambda^2 - (1 - \alpha_{SL})\lambda + \alpha_S - \alpha_{SL} = 0, \qquad (36)$$

when $\alpha_S = \alpha_{SL}$.

The roots of (36) are $\lambda_3 = 1 - \alpha_{SL}$ and $\lambda_4 = 0$. According to the judging criterion Jury Test [25], $0 < \alpha_{SL} < 2$ can guarantee the stability of the system.

Note that α_S represents the magnitude of the deviation of the actual inventory from the expected stock, and α_{SL} represents the magnitude of the deviation of the in-stock inventory from the expected in-process inventory. Then, $\alpha_S = \alpha_{SL}$ means that the same adjustment range is maintained for inventory deviation and work-in-process inventory deviation. Therefore, when $\alpha_S = \alpha_{SL}$ and $0 < \alpha_{SL} < 2$ are set, the system is stable.

When $\alpha_S \neq \alpha_{SL}$,

(1) $\Delta = (1 - \alpha_{SL})^2 - 4(\alpha_S - \alpha_{SL}) < 0$, that is, $\alpha_S > ((1 + \alpha_{SL})^2/4)$

The root of (36) is $\lambda_3 = ((1 - \alpha_{SL}) + i\sqrt{-\Delta})/2$ and $\lambda_4 = ((1 - \alpha_{SL}) - i\sqrt{-\Delta})/2$. According to the law of stability $|\lambda| < 1$, (37) can be obtained.

$$\left(\frac{1 - \alpha_{SL}}{2}\right)^2 + \left(\frac{\sqrt{-\Delta}}{2}\right)^2 < 1. \qquad (37)$$

The solution

$$\begin{cases} \alpha_S - 1 < \alpha_{SL} < \alpha_S, \\ \alpha_S > \dfrac{(1 + \alpha_{SL})^2}{4}, \end{cases} \qquad (38)$$

that is,

$$\begin{cases} \alpha_S - 1 < \alpha_{SL} < 2\sqrt{\alpha_S} - 1, \\ 0 < \alpha_S < 4. \end{cases} \qquad (39)$$

(2) $\Delta = (1 - \alpha_{SL})^2 - 4(\alpha_S - \alpha_{SL}) = 0$, that is, $\alpha_S = (1 + \alpha_{SL})^2/4$

The root of (36) is $\lambda_3 = \lambda_4 = (1 - \alpha_{SL})/2$, according to the law of stability $|\lambda| < 1$. λ_3 and λ_4 should satisfy the following conditions.

$$\begin{cases} -1 < \lambda_3 < 1, \\ -1 < \lambda_4 < 1. \end{cases} \qquad (40)$$

That is,

$$\begin{cases} \alpha_{SL} = 2\sqrt{\alpha_S} - 1, \\ 0 < \alpha_S < 4. \end{cases} \qquad (41)$$

(3) $\Delta = (1 - \alpha_{SL})^2 - 4(\alpha_S - \alpha_{SL}) > 0$, that is, $\alpha_S < (1 + \alpha_{SL})^2/4$

The root of (36) is $\lambda_3 = ((1 - \alpha_{SL}) + \sqrt{\Delta})/2$ and $\lambda_4 = ((1 - \alpha_{SL}) - \sqrt{\Delta})/2$. According to the law of stability $|\lambda| < 1$, λ_3 and λ_4 should satisfy the following conditions.

$$\begin{cases} -1 < \lambda_3 < 1, \\ -1 < \lambda_4 < 1. \end{cases} \qquad (42)$$

That is,

$$\begin{cases} -1 < \dfrac{(1 - \alpha_{SL}) + \sqrt{(1 - \alpha_{SL})^2 - 4(\alpha_S - \alpha_{SL})}}{2} < 1, \\ -1 < \dfrac{(1 - \alpha_{SL}) - \sqrt{(1 - \alpha_{SL})^2 - 4(\alpha_S - \alpha_{SL})}}{2} < 1. \end{cases}$$

$$(43)$$

Combined with (41), the solution is

$$\begin{cases} 2\sqrt{\alpha_S} - 1 < \alpha_{SL} < \dfrac{1}{2}\alpha_S + 1, \\ 0 < \alpha_S < 4. \end{cases} \qquad (44)$$

To sum up, the parameter range for making subsystem 1 stable is [23]

$$\begin{cases} \alpha_S - 1 < \alpha_{SL} < \dfrac{1}{2}\alpha_S + 1, \\ \quad\quad 0 < \alpha_S < 4. \end{cases} \tag{45}$$

For subsystem 2, we can obtain the nontrivial solution of system 2 with respect to parameters ($C1$, $C2$, $C3$, $C4$, and $C5$) if and only if (46) is satisfied [23].

$$\begin{vmatrix} I - A_{12}\lambda^{-1} - A_{22}\lambda^{-2} \end{vmatrix}$$

$$= \begin{vmatrix} 1 & 0 & 0 & 0 & 0 \\ -\lambda^{-2} & 1 - \lambda^{-1} & -\lambda^{-1} & 0 & 2\lambda^{-1} \\ 0 & 0 & 1 & 0 & -2\lambda^{-1} \\ -\lambda^{-1} + \lambda^{-2} & 0 & 0 & 1 - \lambda^{-1} & 0 \\ 0 & 0 & 0 & 0 & 1 - \theta\lambda^{-1} \end{vmatrix} = 0. \tag{46}$$

The characteristic equation of (25) determines the stability of the equilibrium solution by (46). And (47) can be obtained by (46).

$$\left(1 - \lambda^{-1}\right)^2 \left(1 - \theta\lambda^{-1}\right) = 0. \tag{47}$$

That is,

$$(\lambda - 1)^2 (\lambda - \theta) = 0, \tag{48}$$

where $\lambda \neq 0$. If the root of (48) is within the unit circle, system 2 is stable. From (48), the solution of the equation is $\lambda_1 = 1$, $\lambda_2 = 1$, and $\lambda_3 = \theta$. Since the system has 2 characteristic roots on the unit circle, the system is Schur unstable. However, this instability refers to a critical stability. Since the system has no feedback control on the input, its input response is a kind of ramp function, which plays a role in maintaining the initial value. That is, when the inventory system is in this state, inventory keeps declining as demand continues to arrive without replenishment.

4.2. System Switching Model. According to the above analysis, due to the uncertainty of the replenishment volume of the warehouse allocation system, the supply chain system studied in this chapter is not a linear system. It can be regarded as the order control by the warehouse allocation system and the switching between the two subsystems. To switch the system, the two subsystems are determined by (25) and (29), respectively. Since all subsystems are linear systems, the system can be represented as a linear switching system as shown in

$$X(t) = A_{1\sigma(t)}X(t-1) + A_{2\sigma(t)}X(t-2) + B_{\sigma(t)}r(t). \tag{49}$$

The system is an autonomous switching system. The switching rule is a function of the system state. It is

the judgment of the $O(t)$ symbol of the order quantity per cycle:

$$\begin{aligned} \sigma(t) &= \min\left(2, -\text{sign}\left(F(t) + \alpha_S\left(I^0(t) - I(t)\right) + \alpha_{SL}\left(Y^0(t)\right.\right.\right. \\ &\quad\left.\left.\left. - Y(t)\right)\right) + 2\right) = \min\left(2, -\text{sign}\left(F(t) + \alpha_S\left(F(t)\left(T_C\right.\right.\right.\right. \\ &\quad\left.\left.\left.\left. + T_P\right) - I(t)\right) + \alpha_{SL}\left(G_w F(t) - Y(t)\right)\right) + 2\right). \end{aligned} \tag{50}$$

The switching function $\sigma(t)$ is the evaluation of the order quantity of the warehouse allocation system. If $\sigma(t) = 1$, it means that the warehouse allocation system needs replenishment. If $\sigma(t) = 2$, it means that the warehouse allocation system does not need to be in replenishment. The actual stock in the warehouse and the WIP inventories can meet expectations of inventory in the warehouse, expected WIP inventory, and demand forecast.

4.3. Analysis of System Dynamic Characteristics. In the subsystem, the subsystem 1 is stable within a certain parameter range; and the subsystem 2 is not stable due to the existence of a characteristic root located on the unit circle. According to the gist of the average dwell time method, the switching system is stable when the activation time of the stable system is large enough and the ratio of the dwell time of the unstable system to the dwell time of the stable system satisfies a certain condition. From the results of the switching rules (50) and the rules, we can see that when the warehouse allocation system sets a higher expected inventory level $I^0(t)$, that is, when the higher parameters T_C, T_P, and G_w are set, system switching can be avoided to unstable subsystem 2. When α_S and α_{SL} are fixed, setting smaller $I^0(t)$ and $Y^0(t)$ will result in larger $-\text{sign}\left(F(t) + \alpha_S(I^0(t) - I(t)) + \alpha_{SL}(Y^0(t) - Y(t))\right) + 2$ values, so the unstable subsystem 2 has a long activation time and the system tends to be unstable.

5. System Simulation and Data Analysis

5.1. Order Decision Adjustment Parameters. In order to further study the influence of different ordering strategies and inventory management strategies on the nonlinear supply chain system with constraints, this paper designs the simulation experiment to calculate the Largest Lyapunov Exponent of the system and analyzes the effects of the relevant parameters on the stability of the system under different demand types. When LLE is less than or equal to 0, it indicates that the system is in a stable, periodic, or quasiperiodic state. It is an ideal state for ordering decisions. When LLE is greater than 0, the system is in a chaotic or quasi-chaotic state.

From the analysis in the previous section, it can be seen that the inventory adjustment parameter α_S and the adjustment coefficient of work-in-process inventory α_{SL} have important influence on the dynamic characteristics of the system. This paper designs a simulation experiment and calculates LLE values under various order parameter combinations in the decision space $[\alpha_S, \alpha_{SL}]$ under the condition of certain other factors and uses the size of the LLE to examine the dynamic characteristics of the supply chain system. Considering that in the management practice the decision-

makers pay more attention to the inventory adjustment and the adjustment parameters are all less than 1, this paper assumes that the two parameters range from $0 \leq \alpha_{SL} \leq \alpha_S$ to $0.02 \leq \alpha_S \leq 1$. Both α_S and α_{SL} are changed by 0.02 steps. The simulation experiment needs to calculate the LLE value under various parameter combinations.

5.2. Simulation Analysis. Using Matlab to realize simulation experiments, LLE values for different combinations of parameters are calculated and expressed in the form of a contour graph. The simulation runs 1000 times. If the cycle is calculated in days, it will be the data volume in nearly 3 years. Considering that the actual inventory turnover cycle of the company is short, the data volume in 3 years should be sufficient.

In order to take any situation into account in practice, this paper analyzes three kinds of demand scenarios: random demand obeying normal distribution, random demand obeying uniform distribution, and fixed demand. Simulation and mapping LLE diagram of the retailer and warehouse matching system under different demand scenarios are shown.

First, the LLE value under the fixed constant demand scenario is calculated to obtain the LLE contour graph of the retailer and warehouse matching system, as shown in Figure 4.

As can be seen from Figure 4, under the fixed constant requirement, the inventory system is basically in a stable state in the entire decision area. The fixed constant requirement is an ideal scenario, and there are few in practice. Based on the calculation of the LLE for the entire decision area, this paper finds the value of the decision parameter that makes the inventory system in this scenario unstable. When $\alpha_S = 0.92$, $\alpha_{SL} = 0.04$ and $\alpha_S = 0.98$, $\alpha_{SL} = 0.1$, the retailer's LLE is greater than zero. When $\alpha_S = 0.98$ and $\alpha_{SL} = 0.06$, the LLE value of the warehouse allocation system is greater than zero. There is no decision to make when both are more than zero at the same time. Explain that in an ideal demand scenario, unreasonable parameter settings may also lead to system instability. When $\alpha_S = 0.94$ and $\alpha_{SL} = 0.12$, the average LLE values of the retailer and the warehouse match system are the smallest. Few parameters cause the system to be unstable, which also explains the practicability and effectiveness of the system.

Second, we calculate the LLE value under the random demand with normal distribution and obtain the LLE contour graph of the retailer and warehouse allocation system as shown in Figure 5.

Under the random demand subject to normal distribution, in the entire decision area, the average LLE value of the retailer and the warehouse matching system is the smallest when $\alpha_S = 0.1$ and $\alpha_{SL} = 0.1$. The average value of the LLE value is the largest when $\alpha_{SL} = 1$ and $\alpha_S = 0.16$. From Figure 5(a), we can see that for the retailer, although the LLE value in most regions is greater than zero, there are still some regions whose values are less than zero under random demand. It indicates that there are some decision parameters that can make the inventory of the retailer stable under random demand. The periodic or quasiperiodic state provides a more valuable reference for real-world decision making. From Figure 5(b), we can see that under the stochastic

demand, the decision zone with LLE value less than zero in the warehouse allocation system is banded and located above the entire decision zone. As the adjustment coefficient of stock inventory increases, the inventory adjustment coefficient increases. There are some decision-making areas that do not meet this trend and should avoid this part of the decision to prevent the system from entering a chaotic state. That is, when the inventory adjustment coefficient is higher than a certain level, the inventory adjustment coefficient is too high, which may make the system in a chaotic state. Combining the analysis of Figures 5(a) and 5(b), there is a common decision area in which both the retailer's LLE value and the warehouse allocation system's LLE value are less than zero. That is, under random demand, there is a reasonable decision to make each of the TMI supply chain. Member inventory is in a stable, cyclical, or quasiperiodic state, which has important practical significance.

Finally, we calculate the LLE value under the uniform distribution of random demand and obtain the LLE contour graph of the retailer and warehouse allocation system, as shown in Figure 6.

Under the random demand with uniform distribution, in the entire decision region, the average LLE value of the retailer and the warehouse matching system is the smallest when $\alpha_S = 0.08$, $\alpha_{SL} = 0.08$. When $\alpha_S = 0.9$, $\alpha_{SL} = 0.22$, the average LLE value of the retailer and the warehouse matching system is the largest. Figure 6 shows that under the uniform distribution random demand the decision-making area where the inventory of the retailer and the warehouse allocation system is stable is very small because the uniform distribution of demand obeying the 60–100 interval is a very harsh condition for the inventory system. Under actual circumstances, the demand will be subject to periodical laws in a relatively long period of time, and the demand forecast can be more accurate. So it is more likely that the inventory system will be in a stable state. This article draws on existing research and sets safety stock as a multiple of forecasted demand. Safety stocks are inherently more volatile. In order to reduce the volatility of safety stocks, the forecasted demand can be smoothed or smoothed several times, and the volatility of safety stocks can be reduced by reducing the forecasting demand and volatility. In addition, setting the safety stock to a fixed value may also improve the stability of the inventory system. In the existing studies, relevant scholars set the safety stock as a constant and achieved relatively good results. In this regard, this paper does not conduct simulation analysis, leaving it for follow-up studies.

In order to analyze the changes in inventory under different demand scenarios more intuitively, we draw the figure of inventory changes under different demand scenarios. When analyzing the change of inventory in steady state, we select the decision corresponding to the minimum average and the maximum average number of LLEs of retailers and warehouse matching centers under different demand scenarios to simulate them and then map them to steady state and unstable state, respectively. The inventory change chart in steady state and unstable state is shown in Figures 7–12.

In Figures 7 and 8, the retailer can increase the volatility of inventory changes in a steady state or an unstable

(a) Retailer's LLE chart

(b) LLE chart of warehouse allocation system
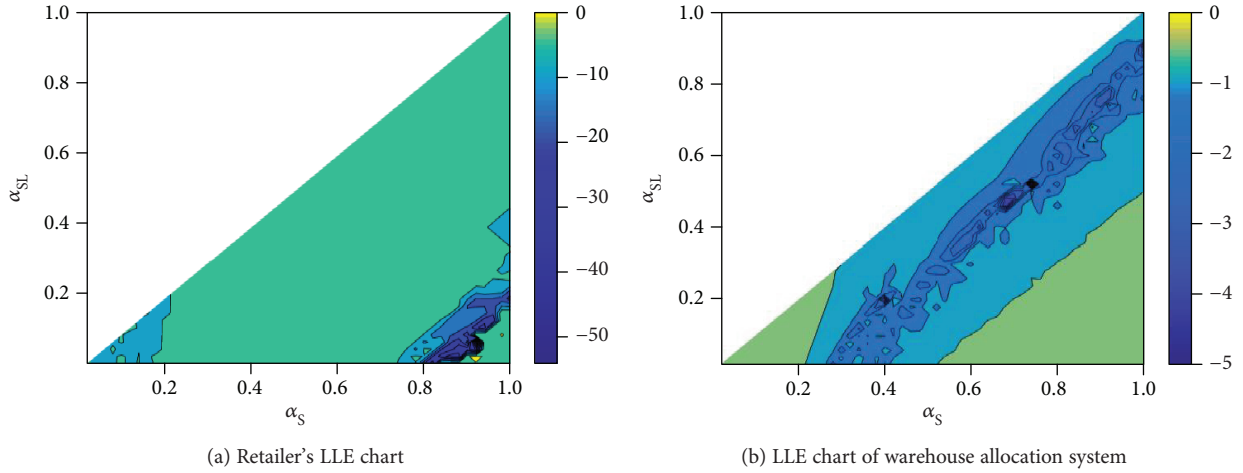
FIGURE 4: LLE diagram of members following fixed constant requirements.

(a) Retailer's LLE chart

(b) LLE chart of warehouse allocation system
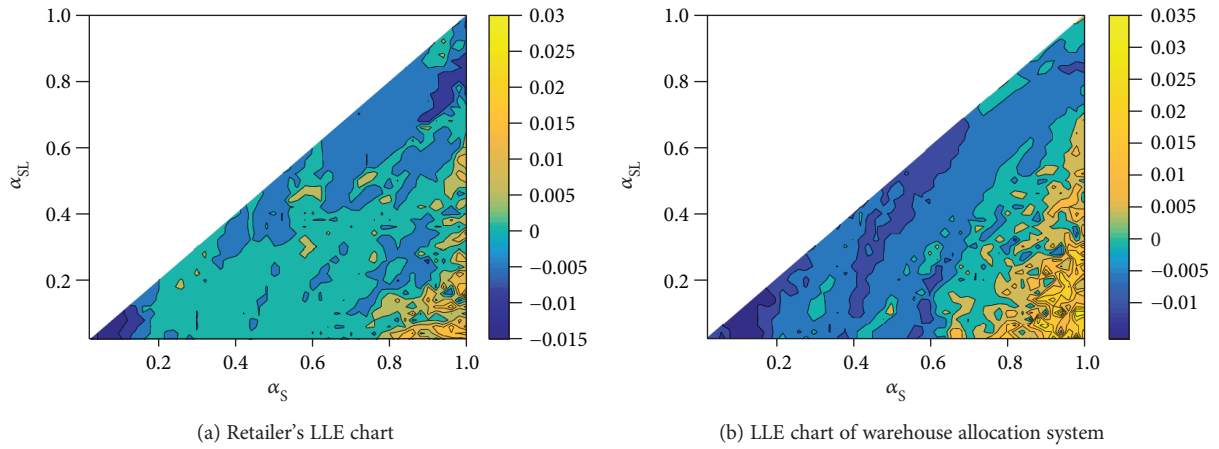
FIGURE 5: LLE diagram of members under the scenario of random demand obeying normal distribution.

(a) Retailer's LLE chart

(b) LLE chart of warehouse allocation system
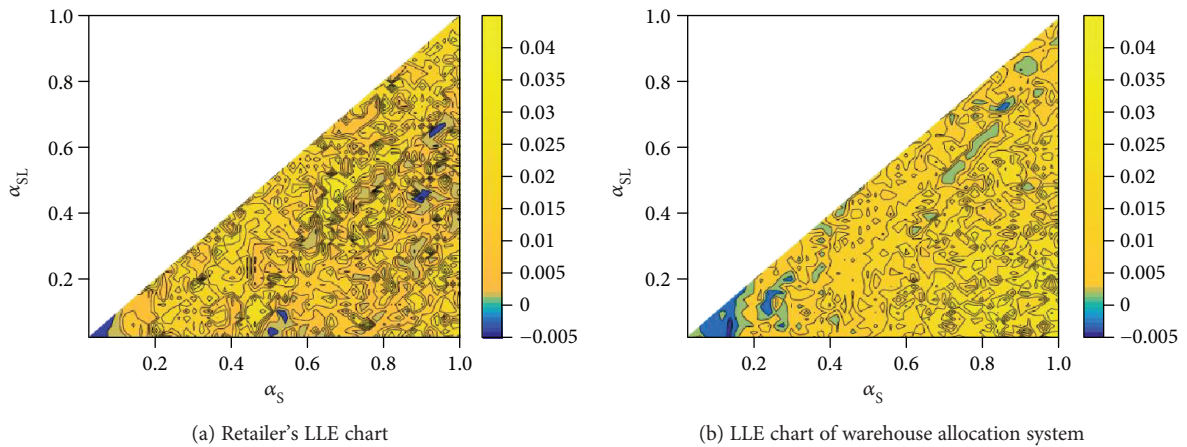
FIGURE 6: LLE diagram of members under the scenario of random demand obeying uniform distribution.

state under a fixed constant demand, a random demand subject to normal distribution, and a random demand subject to uniform distribution. It shows that the demand scenario has a great influence on the stability of the supply chain inventory. The greater the randomness of the demand, the more serious the supply chain instability may be. When the demand is a fixed constant demand, whether the supply chain system is in a stable or unstable
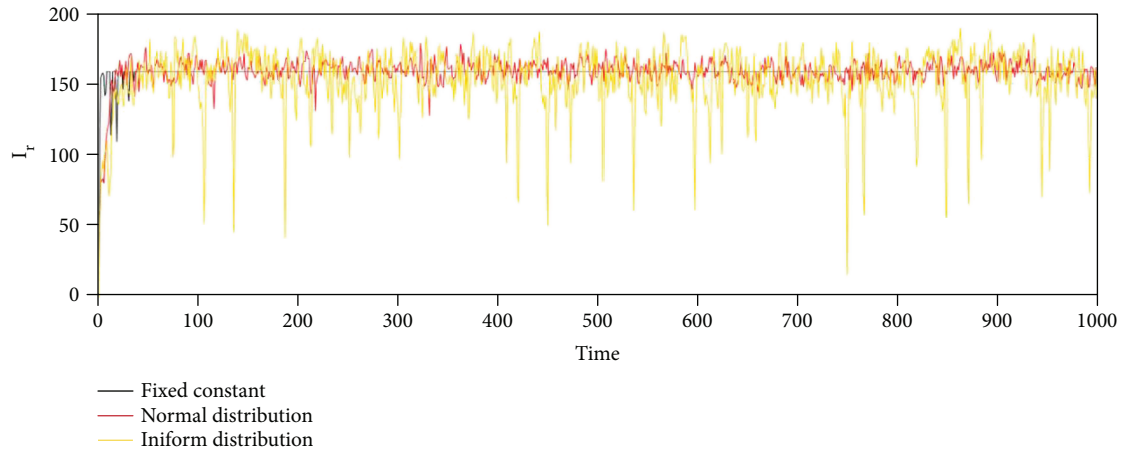
FIGURE 7: Retailers' initial inventory changes in a stable state under three demand scenarios.
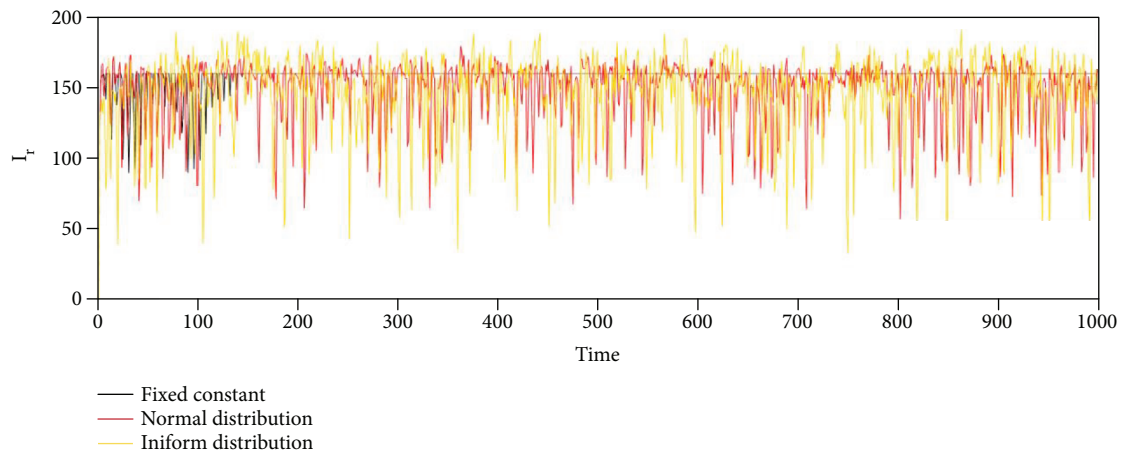
FIGURE 8: Retailers' initial inventory changes in an unstable state under three demand scenarios.
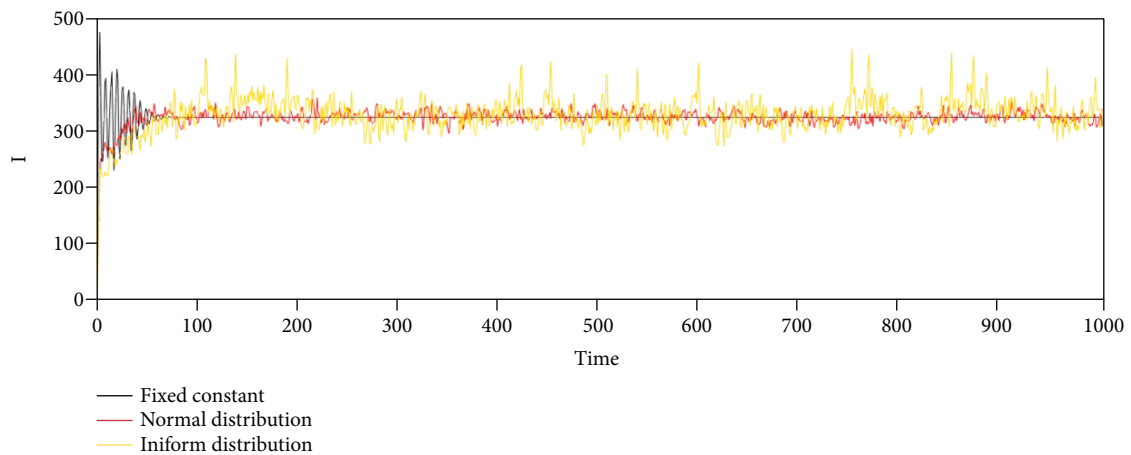
FIGURE 9: Change of initial inventory of warehouse allocation system in a stable state under three demand scenarios.

state, the retailer's inventory will stabilize to a value after a period of time, but the former will use less time than the latter. When the demand is subject to a uniform distribution of random demand, even if the supply chain is in the

most stable state, the volatility of retailer inventory changes is also very large.

From Figure 9, we can see that in the steady state, the initial inventory of the warehouse allocation system under the
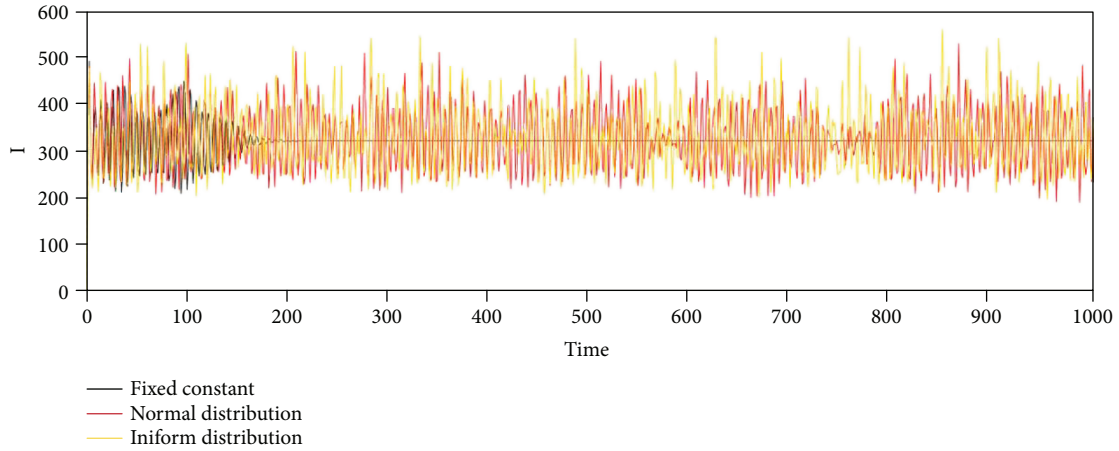
FIGURE 10: Change of initial inventory of warehouse allocation system in an unstable state under three demand scenarios.
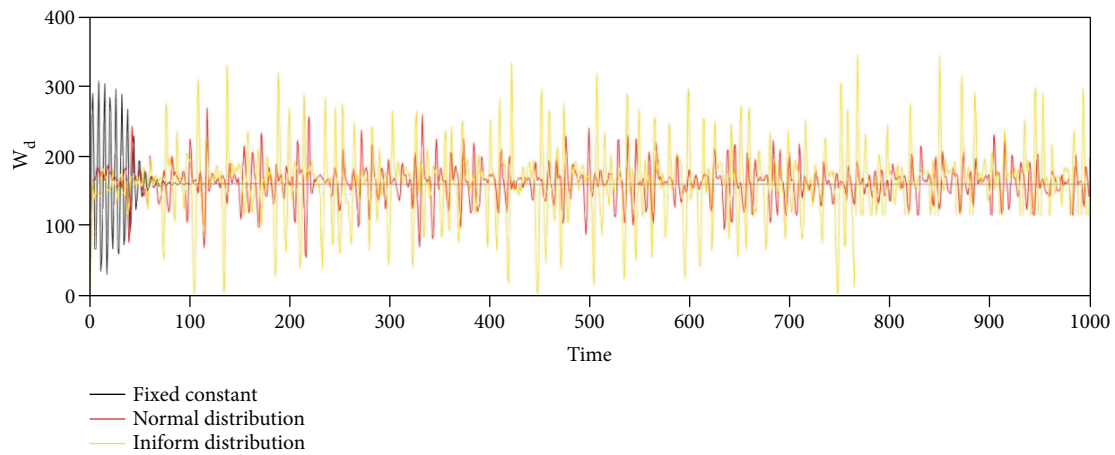
FIGURE 11: Change in traffic volume of third-party logistics service providers in a stable state under three demand scenarios.
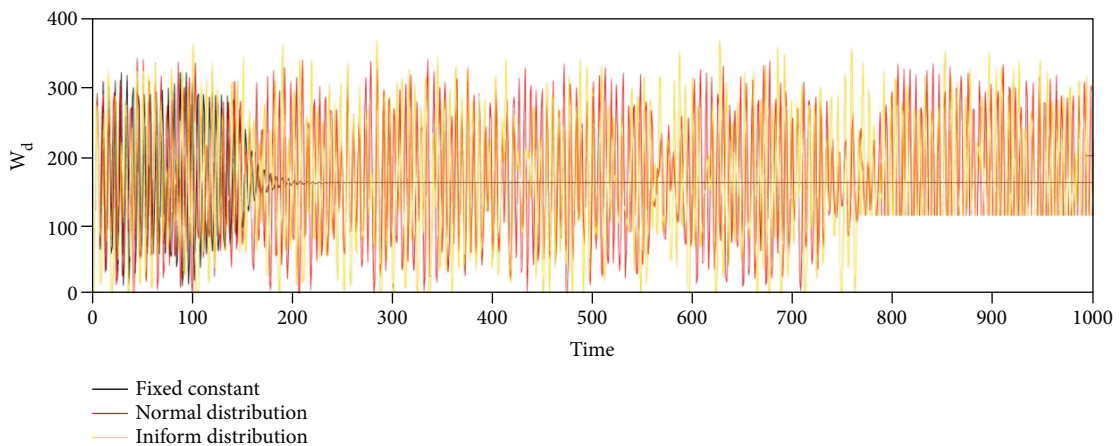
FIGURE 12: Change in traffic volume of third-party logistics service providers in an unstable state under the three demand scenarios.

fixed constant demand shows greater volatility in the initial stage of the three demand scenarios, which the manager should pay attention to. Under the stochastic demand scenario subject to normal distribution, the inventory of the warehouse allocation system fluctuates in a very small range, which is ideal and expected. For the strict random demand scenario with uniform distribution, the supply chain inventory shows satisfactory fluctuations under

reasonable decision parameters. In the unstable state, from Figure 10, we can see that in addition to the fixed constant demand scenario, the inventory change of the warehouse allocation system shows a state of chaos that should be avoided under the three demand scenarios. Under the fixed constant demand scenario, the warehouse inventory system also shows great volatility at the initial stage and then stabilizes.

In the steady state, from Figure 11, we can see that the third-party logistics service provider's traffic under the fixed constant demand scenario has great volatility in the initial stage. For this, logistics service providers are required to make phased planning. Observing that in the steady state, the three-logistics service provider's traffic volume change graph is approximately an axisymmetric pattern under the three demand scenarios. The volatility increases from the fixed constant demand, the stochastic demand with normal distribution to the stochastic demand with uniform distribution. In the unstable state, from Figure 12, we can see that the changes in the traffic volume of the third-party logistics service providers under the three demand scenarios appear chaotic state, and the three curves almost cover the coordinate axis area. However, in the case of fixed constant demand conditions, it eventually stabilized to a certain value after a long period of fluctuation.

In order to analyze the changes of member stocks in stable and unstable conditions under different demand scenarios more clearly, this paper plots the changes in inventory when retailers and warehouse allocation systems are in stable and unstable conditions under different demand scenarios. A comparison chart of changes in traffic volume of third-party logistics service providers in the comparison chart and in different states is shown. Figures 13–15 show the fixed constant demand scenario.

Under the fixed constant demand scenario, it can be seen from Figure 13 that the retailer inventory shows a stable trend after the first fluctuation and a stable state, and the time for the former to reach stability is less than the latter. In Figures 14 and 15, it can be seen that the inventory fluctuations of the warehouse allocation system and the third-party logistics service providers have the same rules as the retailer inventory. In the unstable state, during the simulation period of 0–200 hours, the inventory or transport volume of the three members of the supply chain presented great volatility, which increased the inventory management costs and logistics transportation costs of the entire chain. This is not conducive to the evolution and development of the supply chain.

Under the scenario of evenly distributed stochastic demand, we simulate and draw a comparison chart of changes in inventory when the retailer and warehouse allocation system is in a stable and unstable state. And a comparison chart of changes in the traffic volume of third-party logistics service providers in different states is drawn as shown in Figures 16–18.

Obeying the uniform distribution of stochastic demand is a great challenge for the stability of the supply chain inventory system. In Figures 16 and 17, we can see that the initial inventory of the retailer has a great fluctuation when it is in

the stable state and the unstable state under the condition of the stochastic demand that obeys the uniform distribution. However, the inventory at the beginning of the warehousing system can be stable to a very small interval in the steady state, which verifies the advanced nature and practicality of the supply chain model. As shown in Figure 18, the volatility of the transport volume of the third-party logistics service providers in the unstable state and the stable state is very large, and the volatility is relatively small in the stable state of the two states. Under this demand scenario, the third-party logistics will face arduous transportation tasks and face enormous challenges in the rational allocation of resources. On the other hand, the professionalism of third-party logistics service providers can be reflected to reduce inventory management and logistics transportation costs.

Under the normal distribution stochastic demand scenario, a comparison chart of the changes in inventory when the retailer and the warehouse allocation system is in a stable state and an unstable state and a comparison chart of the changes in the third-party logistics service providers' transportation volumes in different states are shown in Figures 19–21.

From Figure 19, we can see that under the scenario of normal distribution random demand, there is a clear difference between the stable state and the unstable state of the retailer inventory, and the inventory fluctuation in the steady state is much smaller than that in the unstable state. The peaks of retailer inventory fluctuations under both conditions have little difference between the two states, but the trough values in the unstable state are smaller than those in the stable state. So in the unstable state, the utilization rate of the retailer stocks will decrease. From Figure 20, it can be seen that, in the steady state, the inventory matching system can reach a stable interval within a short time and then stay in this interval. In an unstable state, the inventory of the warehouse system fluctuates up and down, showing a nonperiodical change. Inventory fluctuations have an impact on management and costs. Maintaining a stable inventory is desirable; it is easy to manage and can reduce costs. Comparing Figure 19 with Figure 20, it can be seen that in the steady state, inventory fluctuations of the stock allocation system do not amplify retailer inventory fluctuations, which verifies the feasibility of the supply chain inventory system model. In Figure 21, it can be clearly seen that the volatility of the third-party logistics service providers' traffic in the steady state is far greater than the volatility in the unstable state. At the same time, the total transportation volume of the two is equal, and the cost of smooth transportation tasks may be lower. In the unstable state, the third-party logistics may generate higher service costs. Therefore, higher service prices are not conducive to long-term cooperation among the members of the TMI supply chain.

6. Conclusion

Although there are few existing researches on the new supply chain model, it can be found from the study of this paper that the complex behaviors of both the new supply chain and the traditional supply chain have a common part, which is a
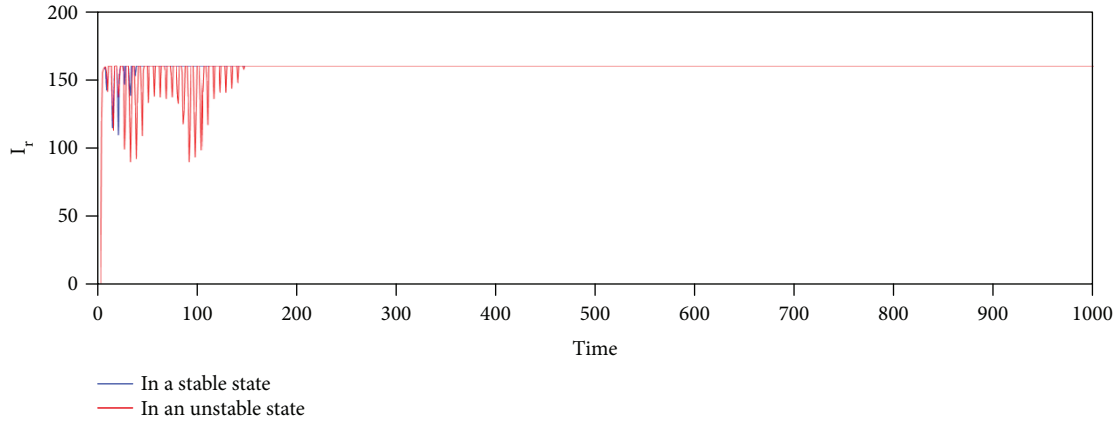
FIGURE 13: Comparison of retailers' opening stock changes in a stable state and unstable state under fixed constant demand.
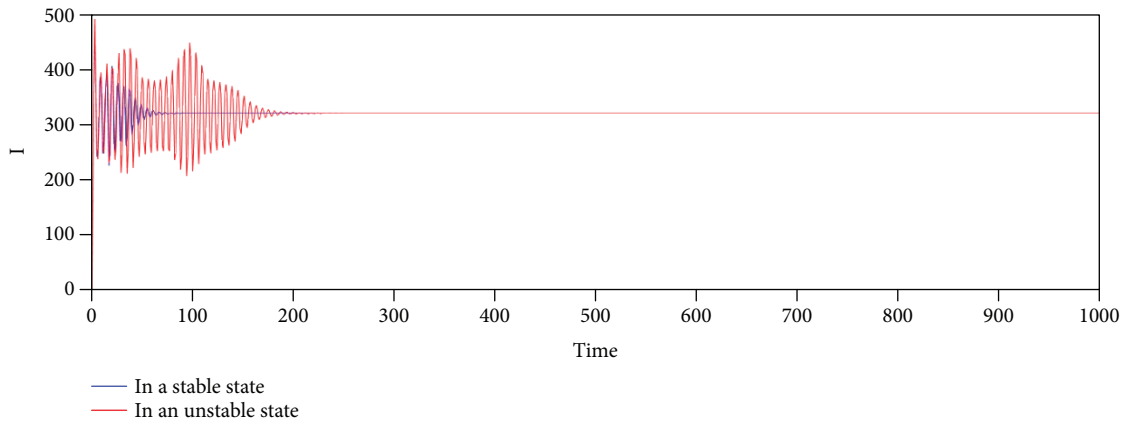
FIGURE 14: Comparison of initial inventory changes of the warehousing system in a stable state and unstable state under fixed constant demand.
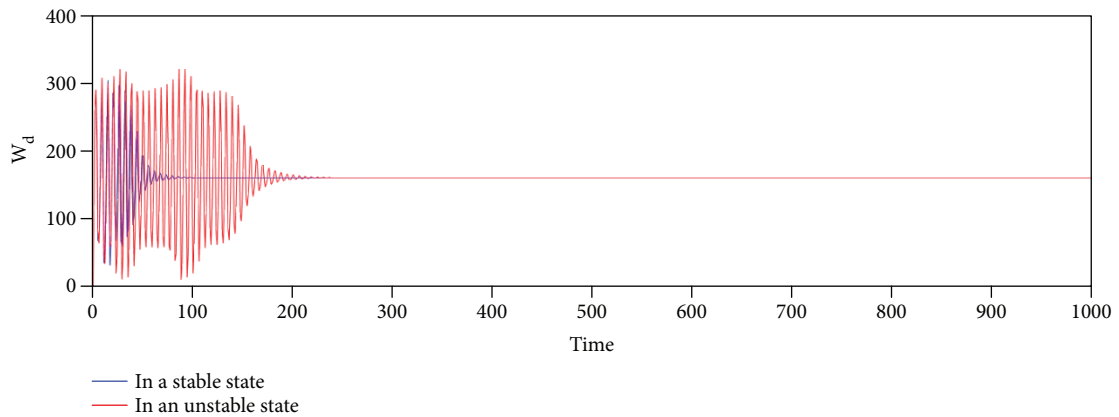
FIGURE 15: Comparison of traffic volume changes by third-party logistics service providers in a stable state and unstable state under fixed constant demand.

reasonable decision parameter that can make the system maintain a stable, periodic, or quasiperiodic state under random demand.

This article supplements and develops existing researches that is based on the premise that the unmet demand does not accumulate to the next cycle. This paper constructs a three-echelon supply chain inventory system model by using the method of system dynamics. The LLE value of the retailer and the warehouse distribution system of 1275 decision parameters under three different demand scenarios is
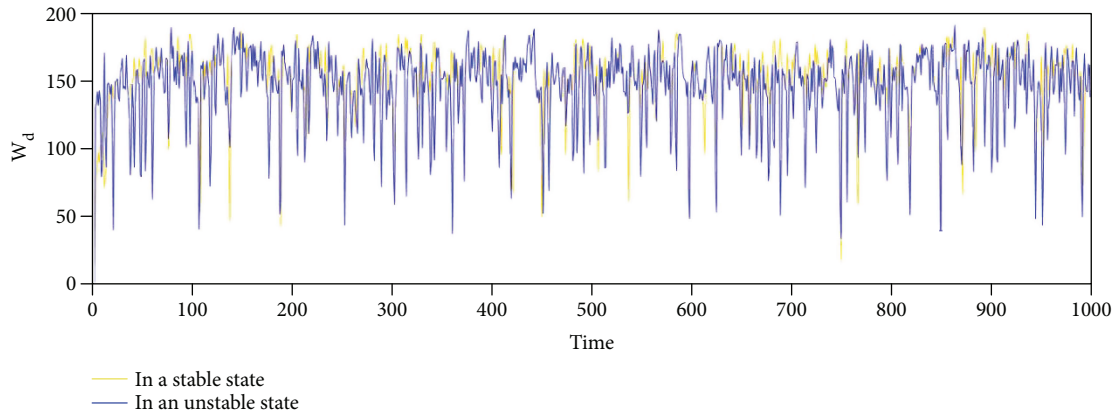
FIGURE 16: Comparison of retailers' initial stock changes in a stable state and unstable state under the scenario of random demand obeying uniform distribution.
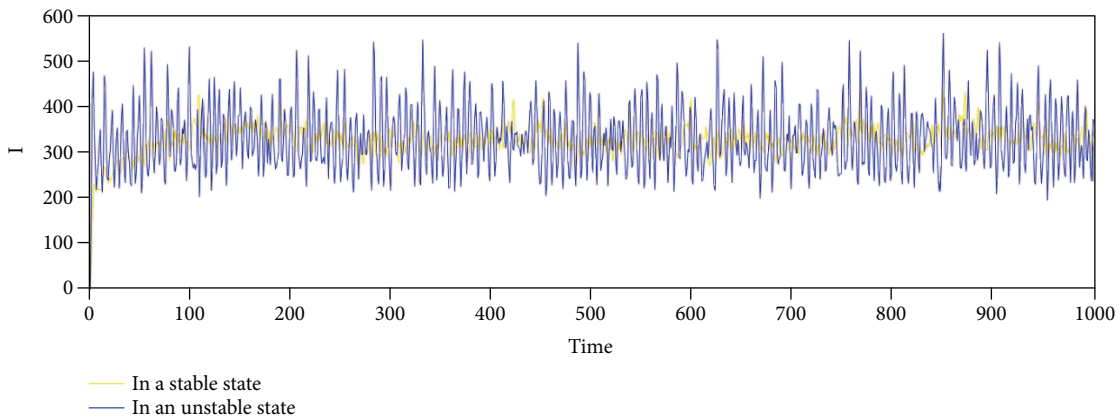
FIGURE 17: Comparison of initial inventory changes of the warehousing system in a stable state and unstable state under the scenario of random demand obeying uniform distribution.
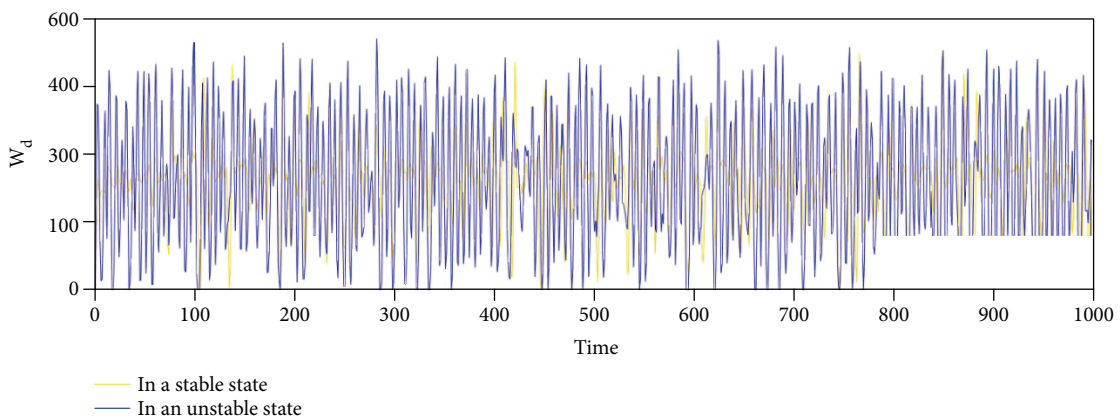
FIGURE 18: Comparison of traffic volume changes of third-party logistics service providers in a stable state and unstable state under the scenario of random demand obeying uniform distribution.

calculated. The whole decision area is covered. Therefore, the reasonable parameters for the stability of the whole supply chain system can be found, which provide a reference for practical decision making and have important practical significance, and the LLE contour diagram of the retailer and the warehouse distribution system under different demand scenarios is drawn, respectively. At the same time, the paper simulated and plotted the inventory changes of the retailer, the warehouse distribution system, and the transport volume change of the third-party logistics service providers in a
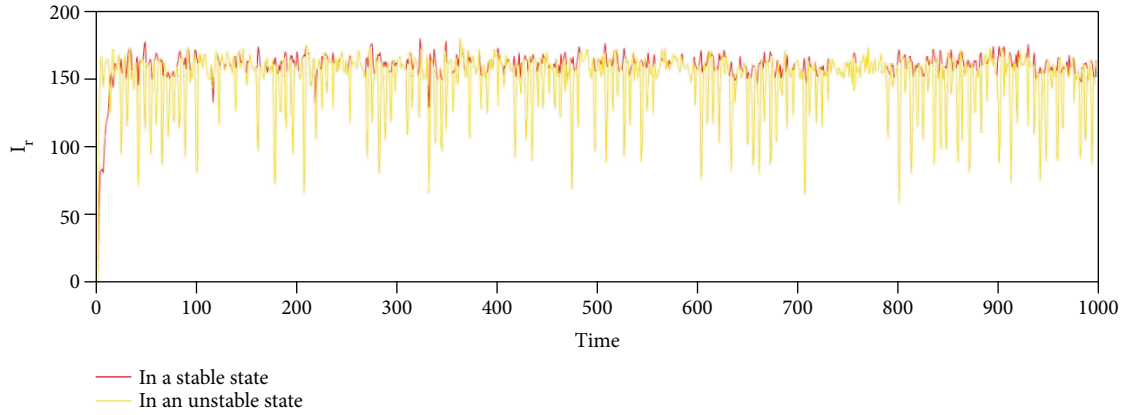
FIGURE 19: Comparison of retailers' initial stock changes in a stable state and unstable state under the scenario of random demand obeying normal distribution.
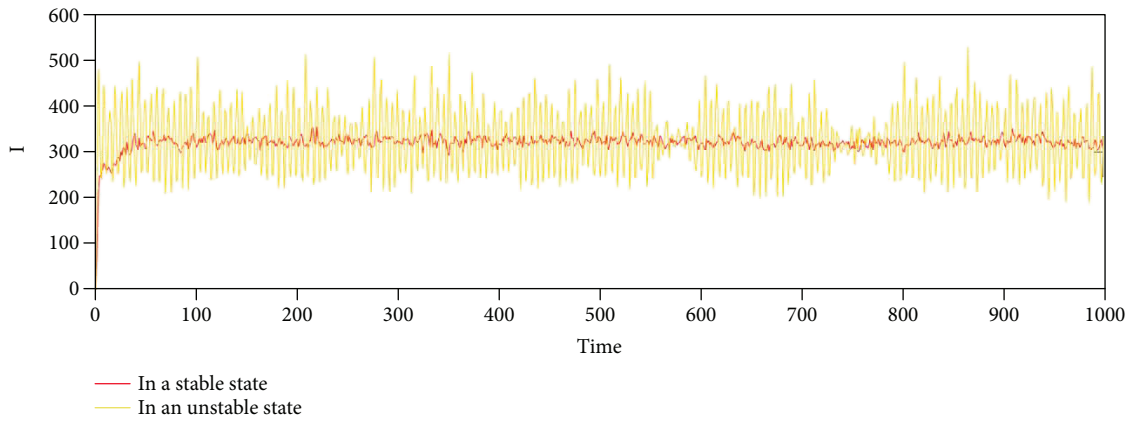
FIGURE 20: Comparison of initial inventory changes of the warehousing system in a stable state and unstable state under the scenario of random demand obeying normal distribution.
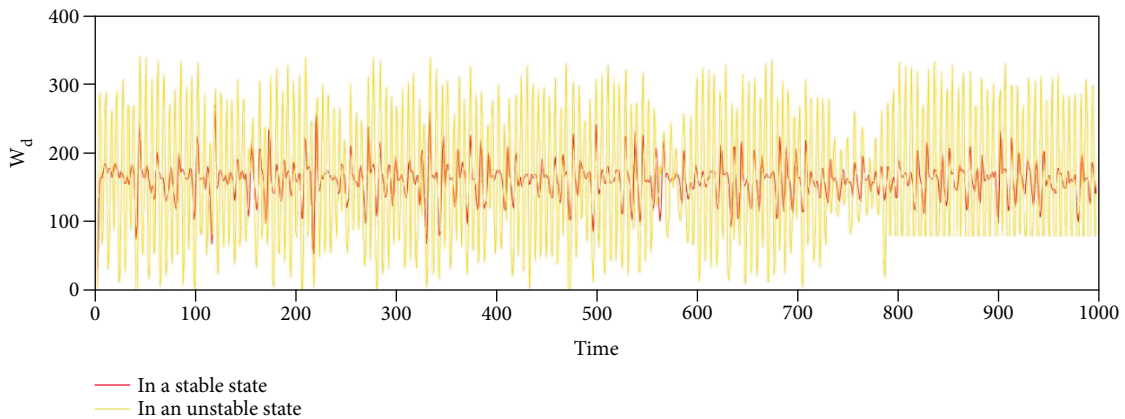
FIGURE 21: Comparison of traffic volume changes of third-party logistics service providers in a stable state and unstable state under the scenario of random demand obeying normal distribution.

stable and unstable state under different demand scenarios. In the steady state, the analysis finds that the initial inventory of the warehouse distribution system and the transport volume of the third-party logistics service providers have more volatility in the initial stage under the scenario of fixed constant demand. However, the volatility of the retailer inventory under the scenario of fixed constant demand is lower than those under the other two scenarios.

Under different demand scenarios, the paper analyzes and compares the changes of the inventory or traffic volume of the members in different states of supply chain, respectively, and concludes the following findings. Under the scenario of fixed constant demand, the inventory or transport volume of the three members of the supply chain has shown great volatility in the steady state during the 0–200 period of simulation, which increases the inventory cost of management and the logistics transportation of the whole chain. It is not conducive to the evolution and development of the supply chain. Under the scenario of random demand, the retailer's initial inventory has a great volatility. But a reasonable decision can make the inventory of the warehouse distribution system stable to a small interval. Under the scenario of random demand obeying normal distribution, there is a distinct difference of the inventory or the transportation task of the members between the stable state and the unstable one. Reasonable decision making can reduce the fluctuation of the stock and transportation volume of the members significantly, thus making the system in a stable state.

Model Parameters and Variables

$D(t)$: The actual demand at time t
$F_r(t)$: The expected demand at time t
$I_r(t)$: Retailer's inventory level at time t
$R_r(t)$: Retailer's receipt amount at time t
$S_r(t)$: Retailer's delivery amount at time t
$O_r(t)$: Retailer's order amount at time t
$S_d(t)$: Distribution center's delivery amount to retailers at time t
$I_d(t)$: Distribution center's inventory level at time t
$R_d(t)$: Distribution center's receipt amount at time t
$W_d(t)$: Distribution center's in-transit inventory at time t
$O_d(t)$: Distribution center's order amount at time t
$I_r^0(t)$: Retailer's expected inventory levels at time t
$I_d^0(t)$: Distribution center's expected inventory levels at time t
$I^0(t)$: Warehouse-distribution center system's expected inventory levels at time t
$S_w(t)$: Warehouse's delivery amount to distribution center at time t
$I_w(t)$: Warehouse's inventory level at time t
$R_w(t)$: Warehouse's receipt amount at time t
$I(t)$: Warehouse-distribution center system's inventory level at time t
$O(t)$: Warehouse-distribution center system's order amount at time t
$Y(t)$: Supplier's work-in-process inventory at time t
$Y^0(t)$: Supplier's expected in-process inventory at time t
α_S: The adjustment coefficient of inventory
α_{SL}: The adjustment coefficient of work-in-process inventory or stock on the way
T_P: Transport lead time
T_C: Production lead time
G_r: Safety inventory coefficient of retailer
G_d: Safety inventory coefficient of distribution center
G_w: Safety inventory coefficient of warehouse.

Data Availability

No data were used to support this study.

Conflicts of Interest

The authors declare that they have no conflicts of interest.

Acknowledgments

References

[1] H. N. Nav, M. R. J. Motlagh, and A. Makui, "Robust H∞ control for chaotic supply chain networks," *Turkish Journal of Electrical Engineering & Computer Sciences*, vol. 25, pp. 3623–3636, 2017.

[2] A. R. Nia, M. H. Far, and S. T. A. Niaki, "A fuzzy vendor managed inventory of multi-item economic order quantity model under shortage: an ant colony optimization algorithm," *International Journal of Production Economics*, vol. 155, pp. 259–271, 2014.

[3] K. P. Lin, P. T. Chang, K. C. Hung, and P. F. Pai, "A simulation of vendor managed inventory dynamics using fuzzy arithmetic operations with genetic algorithms," *Expert Systems with Applications*, vol. 37, no. 3, pp. 2571–2579, 2010.

[4] H. L. Lee, V. Padmanabhan, and S. Whang, "Bullwhip effect in a supply chain," *Sloan Management Review*, vol. 38, pp. 93–102, 1997.

[5] M. Marra, W. Ho, and J. S. Edwards, "Supply chain knowledge management: a literature review," *Expert Systems with Applications*, vol. 39, no. 5, pp. 6103–6110, 2012.

[6] I. Heckmann, T. Comes, and S. Nickel, "A critical review on supply chain risk – definition, measure and modeling," *Omega*, vol. 52, pp. 119–132, 2015.

[7] E. Mosekilde and E. R. Larsen, "Deterministic chaos in the beer production-distribution model," *System Dynamics Review*, vol. 4, no. 1-2, pp. 131–147, 1988.

[8] J. S. Thomsen, E. Mosekilde, and J. D. Sterman, "Hyperchaotic phenomena in dynamic decision making," *Systems Analysis-Modelling-Simulation*, vol. 9, pp. 137–156, 1992.

[9] F. R. García, B. Aguirre, and R. Suárez, "Stabilization of linear sampled-data systems by a time-delay feedback control," *Mathematical Problems in Engineering*, vol. 2008, Article ID 270518, 15 pages, 2008.

[10] D. R. Towill, "Dynamic analysis of an inventory and order based production control system," *International Journal of Production Research*, vol. 20, no. 6, pp. 671–687, 1982.

[11] H. L. Lee, V. Padmanabhan, and S. Whang, "Information distortion in a supply chain: the bullwhip effect," *Management Science*, vol. 43, no. 4, pp. 546–558, 1997.

[12] S. M. Disney and D. R. Towill, "On the bullwhip and inventory variance produced by an ordering policy," *Omega*, vol. 31, no. 3, pp. 157–167, 2003.

[13] T. Nagatani and D. Helbing, "Stability analysis and stabilization strategies for linear supply chains," *Physica A: Statistical Mechanics and its Applications*, vol. 335, no. 3-4, pp. 644–660, 2004.

[14] X. Wang, S. M. Disney, and J. Wang, "Stability analysis of constrained inventory systems with transportation delay," *European Journal of Operational Research*, vol. 223, no. 1, pp. 86–95, 2012.

[15] H. B. Hwarng and X. Yuan, "Interpreting supply chain dynamics: a quasi-chaos perspective," *European Journal of Operational Research*, vol. 233, no. 3, pp. 566–579, 2014.

[16] V. L. M. Spiegler, M. M. Naim, D. R. Towill, and J. Wikner, "A technique to develop simplified and linearised models of complex dynamic supply chain systems," *European Journal of Operational Research*, vol. 251, no. 3, pp. 888–903, 2016.

[17] Z. Li, S. Sun, and Y. Huang, "Exploring inventory order policies impact under the non-negative constraint of order quantity: system stability, service level, and cost," *Chaos, Solitons & Fractals*, vol. 103, pp. 111–122, 2017.

[18] D. Dai, F. Si, and J. Wang, "Stability and complexity analysis of a dual-channel closed-loop supply chain with delayed decision under government intervention," *Entropy*, vol. 19, no. 11, p. 577, 2017.

[19] S. M. Disney and D. R. Towill, "A discrete transfer function model to determine the dynamic stability of a vendor managed inventory supply chain," *International Journal of Production Research*, vol. 40, no. 1, pp. 179–204, 2002.

[20] S. M. Disney and D. R. Towill, "The effect of vendor managed inventory (VMI) dynamics on the bullwhip effect in supply chains," *International Journal of Production Economics*, vol. 85, no. 2, pp. 199–215, 2003.

[21] S. P. Nachiappan and N. Jawahar, "A genetic algorithm for optimal operating parameters of VMI system in a two-echelon supply chain," *European Journal of Operational Research*, vol. 182, no. 3, pp. 1433–1452, 2007.

[22] J. Han, J. Lu, and G. Zhang, "Tri-level decision-making for decentralized vendor-managed inventory," *Information Sciences*, vol. 421, pp. 85–103, 2017.

[23] L. Olien and J. Bélair, "Bifurcations, stability, and monotonicity properties of a delayed neural network model," *Physica D: Nonlinear Phenomena*, vol. 102, no. 3-4, pp. 349–363, 1997.

[24] J. Dorsey, *Continuous and Discrete Control Systems*, McGraw-Hill, 2002.

[25] L. H. Keel and S. P. Bhattacharyya, "A new proof of the jury test," *Automatica*, vol. 35, no. 2, pp. 251–258, 1999.

Research Article

Implementation of a Controller to Eliminate the Limit Cycle in the Inverted Pendulum on a Cart

Mayra Antonio-Cruz [iD],[1,2] **Victor Manuel Hernández-Guzmán** [iD],[3]
Ramón Silva-Ortigoza [iD],[1] **and Gilberto Silva-Ortigoza**[4]

[1]*Instituto Politécnico Nacional, CIDETEC, Área de Mecatrónica y Energía Renovable, 07700 Mexico City, Mexico*
[2]*Instituto Politécnico Nacional, UPIICSA, SEPI, 08400 Mexico City, Mexico*
[3]*Universidad Autónoma de Querétaro, Facultad de Ingeniería, 76010 Querétaro, QRO, Mexico*
[4]*Benemérita Universidad Autónoma de Puebla, Facultad de Ciencias Físico Matemáticas, 72570 Puebla, PUE, Mexico*

Correspondence should be addressed to Victor Manuel Hernández-Guzmán; vmhg@uaq.mx

A frequency response-based linear controller is implemented to regulate the inverted pendulum on a cart at the inverted position. The objective is to improve the performance of the control system by eliminating the limit cycle generated by the dead-zone, induced by static friction, at the actuator of the mechanism. This control strategy has been recently introduced and applied by the authors to eliminate the limit cycle in the Furuta pendulum and the pendubot systems. Hence, the main aim of the present paper is to study the applicability of the control strategy to eliminate the limit cycle in the inverted pendulum on a cart. The successful results that are obtained in experiments corroborate that the approach introduced by the authors to eliminate the limit cycle in the Furuta pendulum and pendubot is also valid for the inverted pendulum on a cart.

1. Introduction

Friction is a phenomenon that can cause nonlinear behavior in mechanical systems involving motion [1]. Such a nonlinear behavior refers, in particular, to a dead-zone [2] which degrades performance of the overall system by generating position error, limit cycle, and even instability [3]. These problems, separately, have been important subjects of study. As a matter of fact, compensation of friction in mechanical systems has been carried out to achieve a better control of position [4–8]. Limit cycles generated by the static and Coulomb friction have been treated in [1, 9–14] and the stability analysis of systems with friction has been introduced in [15–17]. On the other hand, underactuated mechanical systems, and in particular inverted pendulums, have attracted the attention of several researchers because they are an excellent benchmark to study position control, limit cycles, and system stability [18]. Motivated by this scenario and by [19, 20], this paper deals with the elimination of limit cycles generated by a friction-induced dead-zone nonlinearity when regulating the inverted pendulum on a cart.

Different authors have reported important results on limit cycles in the regulation of inverted pendulums which, in general, can be divided into three categories: *(a) generation of stable limit cycles*, *(b) reduction of limit cycles*, and *(c) elimination of limit cycles*.

Regarding *(a)*, Verduzco [21] presented a method for nonlinear systems that have k zero eigenvalues when they are linearized. Such a method contemplates the existence of a curve of Hopf bifurcation points and a change of both coordinates and input control. The pendubot was used to illustrate the method. Also, for the pendubot, Freidovich et al. [22] proposed a feedback control strategy based on motion planning via virtual holonomic constraints. Furthermore, Freidovich et al. [23] developed a control for the Furuta pendulum, which was integrated by a shaping energy control, a passivity-based control, and an auxiliary feedback action.

Andary et al. [24] introduced a control based on partial non-linear feedback linearization and dynamic control. Aguilar et al. [25] used partial feedback linearization with a two-relay controller, which was tuned with the classic tool root locus. The two latter works are for the inertia wheel pendulum.

For *(b)*, Medrano-Cerda [26] considered a scheme based on velocity-sign compensation in the inverted pendulum on a cart. Also, Vasudevan et al. [27] compensated friction via a passivity-based observer for the wheeled inverted pendulum. Eom and Chwa [28] compensated friction, system uncertainties, and an external disturbance through a nonlinear observer for the pendubot.

With regard to *(c)*, Hernández-Guzmán et al. [19] exploited the differential flatness property of the Furuta pendulum to propose a linear state feedback controller which can be designed to regulate the system and to eliminate limit cycles. To achieve this, an educational, experimental, and intuitive procedure based on the time response approach, i.e., root locus, was introduced. As an improvement, Antonio-Cruz et al. [20] presented a modified version of the control in [19]. The design of such a modified control was based on frequency response, instead of time response as in [19], which entailed the obtention of precise formulas that facilitates the limit cycle elimination. A comparison of [19, 20] showed that [20] has better performance when dealing with the limit cycle elimination. On the other hand, some studies that consider the backlash nonlinearity in the Furuta pendulum and cart-pendulum system [29, 30] have been reported. Other papers dealing with performance improvement of inverted pendulums have been reported [31–34]. Finally, papers related to dead-zone compensation for nonlinear systems and suppression of limit cycles in servomechanism are [35–39].

Having undertaken the literature review, it was found that the papers dealing with reduction of friction-induced limit cycles use compensation techniques that have the following disadvantages: (i) most compensation terms are complex and require the numerical values of the frictional parameters [27] and (ii) undercompensation leads to steady-state error and overcompensation may induce limit cycles [9, 40]. Although an important effort has been done in [26] to reduce the limit cycle in the inverted pendulum on a cart, to the authors' knowledge, the elimination of the limit cycle in the inverted pendulum on a cart has not been achieved until now. On the other hand, only two previous papers [19, 20] have achieved limit cycle elimination without using compensation techniques but just by employing a simple linear controller. In both papers the controller was proposed by using a differential flatness representation of the system and the describing function method was employed to study the existence of limit cycles. In [19] the controller was designed via the time response approach (root locus) and in [20] via the frequency response approach (Bode diagrams). Since the root locus is not intrinsically related to the describing function method, the corresponding design procedure presented in [19] is based on intuitive ideas because precise formulas were not obtained. According to [20], this renders the repetition of the result when using a different Furuta pendulum difficult. Hence, [20] presented a simple and precise procedure to eliminate limit
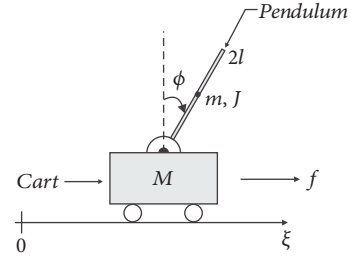
Figure 1: Inverted pendulum on a cart.

cycles caused by the friction-induced dead-zone nonlinearity. In that direction, the controller and the design procedure for limit cycle elimination introduced in [20], for the Furuta pendulum and pendubot systems, are applied to the inverted pendulum on a cart in the present paper with the aim of investigating the possibility to eliminate the limit cycle in this underactuated mechanism.

It is recalled that the advantage of the controller proposed in [20] with regard to compensation techniques is that the model or the characterization of the dead-zone is not required, whereas the advantage with regard to [19] is that the combination of the describing function method and frequency response allows providing precise formulas that render the design of the linear controller and, in consequence, the experimental elimination of limit cycles easier.

The rest of the paper is organized as follows. Section 2 presents the differential flatness model of the linear approximation of the inverted pendulum on a cart, as well as a description of the real prototype used in experiments. Section 3 presents the linear controller to regulate the inverted pendulum on a cart and the procedure to design it. The procedure to eliminate the dead-zone nonlinearity-induced limit cycles in the system is briefly described in Section 4. Lastly, Section 5 gives the conclusions.

2. Inverted Pendulum on a Cart

This section presents the differential flatness model of the inverted pendulum on a cart, as well as the description of the prototype used in the experimental procedure to eliminate limit cycle.

2.1. Flatness Model. The inverted pendulum on a cart shown in Figure 1 consists of a cart that has linear motion on a limited rail, in the horizontal plane, and in one dimension. This motion is due to a force applied by a transmission system actuated by a motor. On the cart, a pendulum is attached which can move angularly in the vertical plane which is parallel to the cart movement. The parameters and variables of this system appear in Figure 1 and are denoted as follows. M and ξ are the mass and the translational position of the cart, respectively, whereas m, $2l$, and ϕ are the mass, length, and angular position of the pendulum, respectively. Lastly, f is the force applied to the cart and g is acceleration of gravity.

The approximate linear model of the inverted pendulum on a cart,

$$\dot{x}_\delta = \mathcal{A} x_\delta + \mathcal{B} u_\delta \tag{1}$$

with

$$x_\delta = \begin{bmatrix} x_{\delta 1} \\ x_{\delta 2} \\ x_{\delta 3} \\ x_{\delta 4} \end{bmatrix} = \begin{bmatrix} \xi - \overline{\xi} \\ \dot{\xi} - \dot{\overline{\xi}} \\ \phi - \overline{\phi} \\ \dot{\phi} - \dot{\overline{\phi}} \end{bmatrix}, \qquad u_\delta = f - \overline{f}, \tag{2}$$

$$\mathcal{A} = \begin{bmatrix} 0 & 1 & 0 & 0 \\ 0 & 0 & -\dfrac{mg}{M} & 0 \\ 0 & 0 & 0 & 1 \\ 0 & 0 & \dfrac{(M+m)\,g}{lM} & 0 \end{bmatrix}, \qquad \mathcal{B} = \begin{bmatrix} 0 \\ \dfrac{1}{M} \\ 0 \\ -\dfrac{1}{lM} \end{bmatrix}, \tag{3}$$

around the operation point

$$\begin{bmatrix} \overline{\xi} & \dot{\overline{\xi}} & \overline{\phi} & \dot{\overline{\phi}} \end{bmatrix}^T = \begin{bmatrix} 0 & 0 & 0 & 0 \end{bmatrix}^T, \tag{4}$$
$$\overline{f} = 0,$$

is controllable [41] and, in consequence, is differentially flat [42], Ch. 2. Therefore, the flat output F, associated with (1), is defined by [42], Ch. 2:

$$F = \lambda \begin{bmatrix} 0 & 0 & 0 & 1 \end{bmatrix} C_0^{-1} x_\delta, \tag{5}$$

where λ is an arbitrary nonzero constant, conveniently chosen as $\lambda = -g/(lM)$, and $C_0 = \begin{bmatrix} \mathcal{B} & \mathcal{A}\mathcal{B} & \mathcal{A}^2\mathcal{B} & \mathcal{A}^3\mathcal{B} \end{bmatrix}$ is the controllability matrix of system (1). After calculations F and its first four time derivatives are obtained:

$$F = x_{\delta 1} + l x_{\delta 3}, \tag{6}$$

$$\dot{F} = x_{\delta 2} + l x_{\delta 4}, \tag{7}$$

$$\ddot{F} = g x_{\delta 3}, \tag{8}$$

$$F^{(3)} = g x_{\delta 4}, \tag{9}$$

$$F^{(4)} = \frac{(M+m)\,g}{lM} \ddot{F} - \frac{g}{lM} u_\delta. \tag{10}$$

This last expression represents the differential flat model that describes the dynamics (1) and since $\overline{f} = 0$, it can be written as

$$f = (M+m)\ddot{F} - \frac{lM}{g} F^{(4)}. \tag{11}$$

2.2. Description of the Prototype. The prototype of the inverted pendulum on a cart used in the experimental procedure to eliminate limit cycle is shown in Figure 2. In general, this prototype has four subsystems: (i) Mechanical structure, (ii) actuator and sensors, (iii) power stage, and (iv) data acquisition and processing, which are described below.
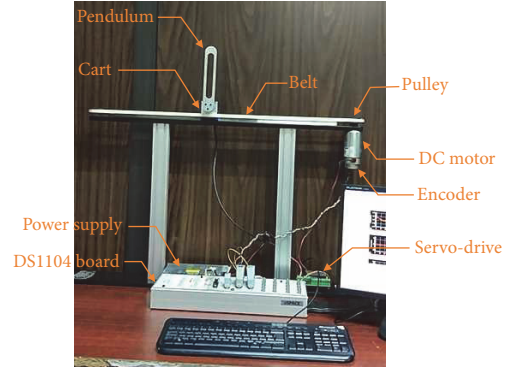
FIGURE 2: Prototype of the inverted pendulum on a cart.

(i) *Mechanical structure* refers to the mechanical elements that compose the mechanism, that is, a cart mounted on a limited rail, the transmission system (toothed belt and two pulleys), and the pendulum.

(ii) *Actuator and sensors* consist in a Pittman 14204S006 DC motor and two incremental encoders used to measure the angular positions of the pulleys and pendulum. Since the DC motor is connected to one pulley, the angular position of this pulley is used to compute the linear position of the cart. The encoder used to measure the angular position of the pulley has 500 PPR and is included in the chassis of the motor. The encoder used to measure the angular position of the pendulum has 1024 PPR and is fabricated by Baumer in the model ITD01B14.

(iii) *Power stage* is integrated by an HF100W-SF-24 switched power supply and an AZ12A8DDC servo-drive manufactured by Advanced Motion Controls. This latter possesses an inner current-loop driven by a PI controller, which ensures that the current of the DC motor, i_m, reaches the current imposed by the control signal, i, that is, $i_m \longrightarrow i$. This means that a desired torque signal can be implemented through the dynamic relation of torque-current: $\tau = k_m i \approx k_m i_m$, where τ and k_m are the torque and torque constant of the DC motor, respectively. Since the input of the inverted pendulum on a cart is the force f, the desired torque is converted to the desired force by using $\tau = fr$, with r being the radius of the pulley connected to the DC motor.

(iv) *Data acquisition and processing* corresponds to a DS1104 board from dSPACE, Matlab-Simulink, and ControlDesk. Through this hardware and software the variables of the system are read, which allows implementation of the controller. It is important to say that, in all experiments, the velocities $\dot{\xi}$ and $\dot{\phi}$ were estimated via a derivative block of Simulink and the sampling period was set to 1 ms.

The mechanical parameters of the inverted pendulum on a cart are presented below, which were found by measuring the length of the pendulum and weighing the cart and pendulum.

$2l = 0.200 \times 10^{-3}$ m,

$m = 0.034$ kg,

$M = 0.385$ kg.

3. Linear Controller

This section presents a linear state feedback controller for position regulation in the inverted pendulum on a cart, which is derived by considering flat model (11). Also, the analysis of the existence of limit cycles is given and the procedure to design the controller is described.

3.1. Controller Proposal. On the one hand, after applying the Laplace transform to (11), the following transfer function is obtained:

$$\frac{F(s)}{f(s)} = \frac{-g/(lM)}{s^2 \left[s^2 - g(M+m)/(lM)\right]}, \tag{12}$$

where $F(s)$ and $f(s)$ stand for Laplace transforms of the flat output and the applied force, respectively.

On the other hand, the dead-zone nonlinearity has the characteristic function shown in Figure 3, whose parameters are described in [19]. An approximate frequency response description of a dead-zone nonlinearity is the following describing function [43], Ch. 5, where it is assumed that the nonlinearity input e is a sinusoidal function of time with amplitude A and frequency ω:

$$N(A) = \frac{2k}{\pi}\left[\frac{\pi}{2} - \arcsin\left(\frac{\delta}{A}\right) - \frac{\delta}{A}\sqrt{1 - \left(\frac{\delta}{A}\right)^2}\right]. \tag{13}$$

This "transfer function," $N(A)$, is real, positive, and frequency independent but dependent on the input amplitude A. Its maximal value is $N(A) = k > 0$, which is reached as $A \longrightarrow \infty$, and its minimal value tends to zero if $A \longrightarrow \delta$.

Since transfer function (12) has similar characteristics to that of the Furuta pendulum obtained in [19, 20], hence, the control scheme proposed in [20] to control the Furuta pendulum and the pendubot, that is,

$$f(s) = k_v F(s) s^3 + \beta F(s) s^2 + k_d F(s) s + k_p F(s), \tag{14}$$

where k_v, β, k_d, and k_p are the control gains, is also used to control (12). The block diagram of the plant (12) in closed loop with controller (14) and considering the dead-zone nonlinearity is shown in Figure 4. There, positive feedback is used due to $-g/(lM) < 0$.

Lastly, when considering the linear state feedback controller

$$u_\delta = f = -k_1 x_{\delta 1} - k_2 x_{\delta 2} - k_3 x_{\delta 3} - k_4 x_{\delta 4}, \tag{15}$$

FIGURE 3: Representation of a dead-zone nonlinearity.

FIGURE 4: Closed-loop system considering a dead-zone nonlinearity.

FIGURE 5: Equivalent representation of block diagram in Figure 4.

where k_1, k_2, k_3, and k_4 are the gains of the controller, u_δ and x_δ stand as defined previously in (2), and using (6)-(10), the following equivalence between (14) and (15) is found:

$$\begin{aligned} k_1 &= -k_p, \\ k_2 &= -k_d, \\ k_3 &= -\left(\beta g + lk_p\right), \\ k_4 &= -\left(k_v g + lk_d\right). \end{aligned} \tag{16}$$

3.2. Analysis of Limit Cycle Existence. The analysis of limit cycle existence in the inverted pendulum on a cart is carried out as in [19, 20] for the Furuta pendulum and pendubot, that is, by using the *describing function method*. This is because the approximation of the dead-zone nonlinearity is based on the describing function.

The describing function method [43], Ch. 5, suggests representing the system in the standard form shown in Figure 5. Also, such a method requires that the linear time invariant system $G(s)$ behaves as a low-pass filter. Thus, the standard form is obtained applying block algebra on Figure 4. In this case, the nonlinearity input is $e = f(s)$ while the linear time invariant system $G(s)$ is

$$G(s) = G_1(s) G_2(s), \tag{17}$$

where

$$G_1(s) = \frac{g/(lM)}{s^2 \left[s^2 - g(M+m)/(lM)\right]}, \tag{18}$$

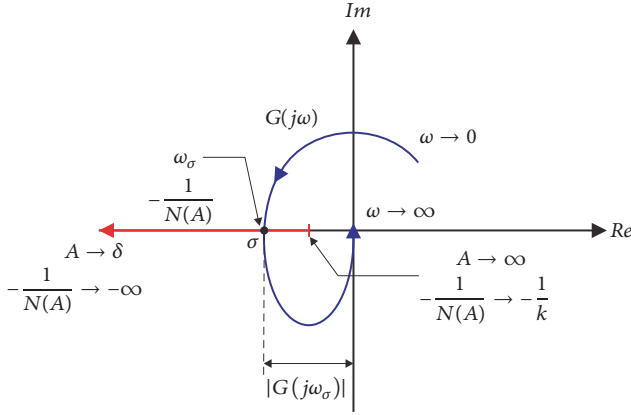$$G_2(s) = k_v s^3 + \beta s^2 + k_d s + k_p \tag{19}$$

FIGURE 6: Polar plot of $G(j\omega)$ and $-1/N(A)$.

are the plant and controller, respectively, and $g/(lM) > 0$. Furthermore, the magnitude of (17) behaves as a low-pass filter, since $G(s)$ has four poles and only three zeros. Then, a limit cycle may exist if [43], Ch. 5,

$$G(j\omega) = -\frac{1}{N(A)}, \qquad (20)$$

which implies that the polar plot of $G(j\omega)$ intersects the negative real axis in the open interval $(-\infty, -1/k)$. This is because $-1/N(A)$ is real and negative. Hence, the oscillation frequency, ω_σ, and the amplitude of the oscillation, A, are found as the values of ω, in $G(j\omega)$, and A, in $-1/N(A)$, at the point σ where their plots intersect [43], Ch. 5. The graphic representation of this is shown in Figure 6.

3.3. Controller Design. The design of the controller gains k_v, β, k_d, and k_p is achieved as described in [20] for the Furuta pendulum case. In this section, particularities of the controller design for the inverted pendulum on a cart case are introduced. Since the following transfer function of the two internal loops is obtained:

$$\frac{-g/(lM)}{s^2 + g/(lM)\,k_v s + \left[g/(lM)\,\beta - g\,(M+m)/(lM)\right]}, \qquad (21)$$

when the dead-zone is omitted from Figure 4, then k_v and β must satisfy the following conditions:

$$k_v > 0 \;\wedge\; \frac{g}{lM}\beta > \frac{(M+m)\,g}{lM} \qquad (22)$$

to ensure that all coefficients of the characteristic polynomial of the transfer function in (21) are positive.

Now, note that when replacing s by $j\omega$ in (18), the phase of $G_1(j\omega)$ is $-360°$ for all $\omega \geq 0$ because $g/(lM) > 0$ and each one of the factors $1/-\omega^2 < 0$ and $1/(-\omega^2 - g(M+m)/(lM)) < 0$ introduces a phase of $-180°$. Hence, with the intention of forcing the polar plot of $G(j\omega)$ to intersect the negative real axis, i.e., to render phase of $G(j\omega)$ equal to $-180°$ at some $\omega > 0$, the frequency analysis performed for the controller $G_2(j\omega)$ in [20] is applied. Such an analysis is described below to facilitate the reference.

The phase of $G_2(j\omega)$ must be as follows:

$$\angle G_2\,(j\omega) = \arctan\left(\frac{k_d\omega - k_v\omega^3}{k_p - \beta\omega^2}\right) = +180°. \qquad (23)$$

This implies that the following conditions have to be satisfied:

$$k_d\omega - k_v\omega^3 = 0. \qquad (24)$$

$$k_p - \beta\omega^2 < 0. \qquad (25)$$

From (24) the following relation to find k_d is obtained:

$$k_d = k_v\omega^2. \qquad (26)$$

Lastly, in order to compute k_p, s is replaced by $j\omega$ in controller (19) to obtain the following:

$$\begin{aligned} G_2\,(j\omega) &= k_v\,(j\omega)^3 + \beta\,(j\omega)^2 + k_d\,(j\omega) + k_p, \\ &= j\left(k_d\omega - k_v\omega^3\right) + \left(k_p - \beta\omega^2\right), \end{aligned} \qquad (27)$$

whose magnitude is determined by

$$\left|G_2\,(j\omega)\right| = \sqrt{\left(k_d\omega - k_v\omega^3\right)^2 + \left(k_p - \beta\omega^2\right)^2}. \qquad (28)$$

Hence, when solving (28) for k_p, the formula below is obtained:

$$k_p = \pm\sqrt{\left|G_2\,(j\omega)\right|^2 - \left(k_d\omega - k_v\omega^3\right)^2} + \beta\omega^2. \qquad (29)$$

Therefore, the sign in this latter expression has to be chosen so that (25) is accomplished.

Finally, to propose the frequency $\omega = \omega_\sigma$ at which it is desired that the polar plot of $G(j\omega)$ intersects the negative real axis it is necessary to compute k_p and k_d. Likewise, the magnitude $|G_2(j\omega_\sigma)|$ that must be introduced by the controller has to be known, for which a desired magnitude of $G(j\omega)$ when $\omega = \omega_\sigma$ has to be proposed. Then, from

$$\left|G\,(j\omega_\sigma)\right| = \left|G_1\,(j\omega_\sigma)\right| \cdot \left|G_2\,(j\omega_\sigma)\right|, \qquad (30)$$

the magnitude $|G_2(j\omega_\sigma)|$ can be computed by

$$\left|G_2\,(j\omega_\sigma)\right| = \frac{\left|G\,(j\omega_\sigma)\right|}{\left|G_1\,(j\omega_\sigma)\right|}. \qquad (31)$$

Since $|G_1(j\omega_\sigma)|$ can be obtained from the Bode diagrams of $G_1(j\omega)$, then Bode diagrams are a suitable tool to design the controller gains k_v, β, k_d, and k_p.

Until here, the procedure and formulas to compute the controller gains have been described. The procedure to choose such gains in order to eliminate limit cycle due to dead-zone nonlinearity is presented in the next section.

4. Experimental Procedure for Limit Cycle Elimination

In this section, the experimental procedure introduced in [20] is applied to eliminate limit cycles in the inverted

pendulum on a cart. In [20], the procedure to eliminate limit cycle was executed departing from knowing the numerical value δ of the dead-zone nonlinearity of the Furuta pendulum and pendubot. Also, in that paper, it was mentioned that the procedure can be applied without requiring the knowledge of such a parameter. Thus, the procedure in [20] is applied here for the inverted pendulum on a cart without requiring the knowledge of δ. Additional steps that help to better address the procedure, which do not modify the generality of the procedure introduced in [20], are indicated. Also, particularities of the application of the procedure in the inverted pendulum on a cart are indicated in each step.

Before starting the application of the procedure for limit cycle elimination in the inverted pendulum on a cart, the conjecture established in [20] is recalled below.

Conjecture. According to the dead-zone nonlinearity characteristic function depicted in Figure 3, if $|e| \leq \delta$ then a zero value appears at the plant input $c = 0$; i.e., the force applied by the motor to the inverted pendulum on a cart is zero and the mechanism might rest at the operation point defined in (4). Since the threshold δ is uncertain because friction is uncertain, it is natural to wonder whether it is possible to render $A < \delta$ in experiments, despite (13) being only valid for $A \geq \delta$. Recall that $A \geq |e|$ because A is the amplitude of e. Then, the mechanism might rest at the operation point if A is chosen to be small enough; i.e., the limit cycle might vanish under these conditions.

It is also recalled that, according to Figure 6, with the purpose of reducing the amplitude of the limit cycle, the polar plot of $G(j\omega)$ must intersect the negative real axis at a point σ located farther to the left of the point $-1/k = -1$. This latter is computed by considering $k = 1$, which is a value usually set for a conventional DC motor. This suggests that $|G(j\omega_\sigma)| \gg 1$ and this must occur at an oscillation frequency $\omega = \omega_\sigma$.

The procedure to eliminate the limit cycle induced by the dead-zone nonlinearity, when regulating position in the inverted pendulum on a cart, was experimentally applied as follows:

(1) Bode diagrams of the plant $G_1(j\omega)$ were plotted as shown in Figure 7. For this, (18) was used.

(2) The frequency $\omega_\sigma = 6$ rad/s and the magnitude $|G(j\omega_\sigma)| = 22$ were initially proposed. The value of ω_σ was proposed since this renders $f_\sigma = \omega_\sigma/(2\pi) \approx 0.9549$ Hz, which is a reasonable frequency in Hertz for the experimental prototype that was built. Using the value of ω_σ and Bode diagrams plotted in Figure 7, the following magnitude in dB was measured:

$$|G_1(j\omega_\sigma)|_{dB} = -26.1 \text{ dB}, \tag{32}$$

which was converted into

$$|G_1(j\omega_\sigma)| = 10^{|G_1(j\omega_\sigma)|_{dB}/20} = 0.0495. \tag{33}$$

The latter numerical value was used in (31) to compute $|G_2(j\omega_\sigma)|$, finding the following:

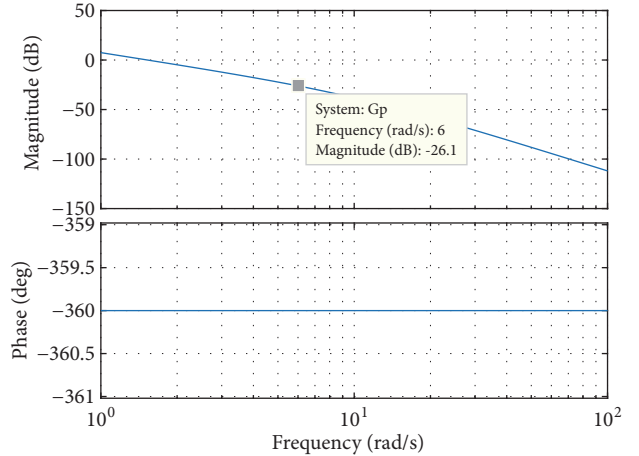$$|G_2(j\omega_\sigma)| = \frac{4}{44.1570} = 444.0406. \tag{34}$$

FIGURE 7: Bode diagrams of $G_1(s)$.

The numerical values of ω_σ and $|G_2(j\omega_\sigma)|$ shall be used to compute k_p.

(3) $k_v = 0.94$ and $\beta = 12.5$ were selected satisfying (22), that is, rendering all coefficients of the characteristic polynomial of (21) positive. Also, the proposed k_v and β achieve that the sign of the square root in (29) is negative, which is implied from (25), and that $k_p > 0$. According to Figure 4, this latter is necessary to ensure closed-loop stability. Note that, in order to avoid negative values for k_p, it is clear from (29) and (25) that larger values of either β or ω_σ are required. From the second degree characteristic polynomial in (21), it is concluded that a larger β is possible if roots of this characteristic polynomial are farther from the origin. This is accomplished since $k_v = 0.94$ and $\beta = 12.5$ assign real poles of (21) at -225.8894 and -13.6275. In the case that the selection of β does not achieve $k_p > 0$ and the designer prefers to increase ω_σ, instead of increasing β, the designer must go back to step (2).

(4) With the numerical values in steps (2) and (3), (29), and (26), k_d and k_p were computed as follows:

$$\begin{aligned} k_d &= 33.84, \\ k_p &= 5.9594. \end{aligned} \tag{35}$$

For (29), a "$-$" sign was chosen because this renders $k_p - \beta\omega_\sigma^2 = -444.0406 < 0$. Notice that this ensures that k_p is real and positive, and hence closed-loop stability is ensured. If this were not the case, the designer would have to go back to step (3).

(5) Through the Bode diagrams of the compensated system $G(s)$ shown in Figure 8, it was corroborated that the open-loop system had the desired phase, $-180°$, at the desired frequency and magnitude, $\omega_\sigma = 6$ rad/s and $|G(j\omega_\sigma)| = 22 \approx 26.9$ dB, respectively. The corresponding polar plot of $G(j\omega)$ is depicted in Figure 9.
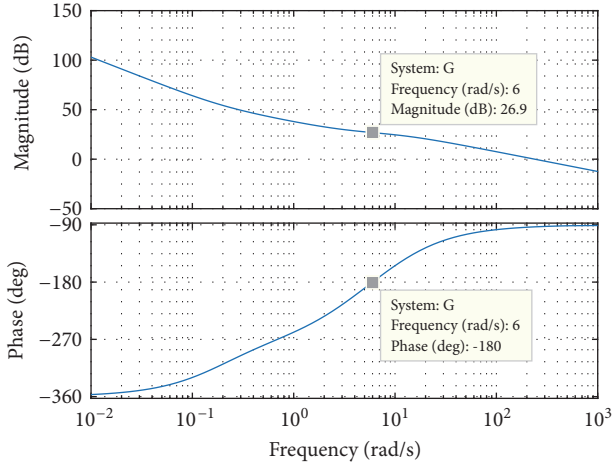
Figure 8: Bode diagrams of $G(s)$.
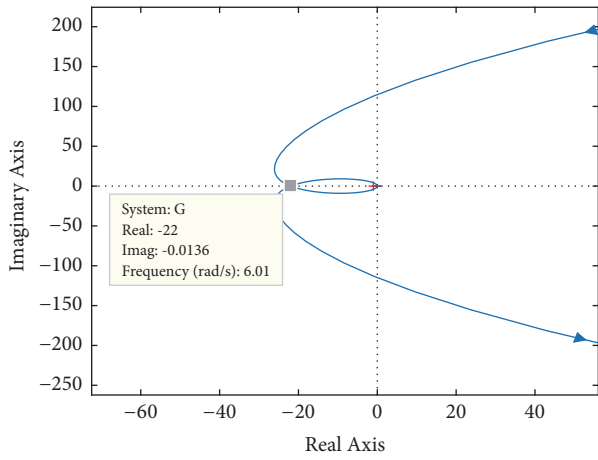
Figure 9: Polar plot of $G(j\omega)$.

(6) Once k_v, β, k_d, and k_p were known, the relations in (16) were used to find the following numerical values for the gains of linear state feedback controller (15):

$$
\begin{aligned}
k_1 &= -5.9594, \\
k_2 &= -33.84, \\
k_3 &= -123.2209, \\
k_4 &= -12.6054.
\end{aligned}
\tag{36}
$$

Using these gains k_1, k_2, k_3, and k_4, linear state feedback controller (15) was experimentally implemented to regulate the prototype of the inverted pendulum on a cart depicted in Figure 2. Since (15) only stabilizes the prototype at $x_\delta = \mathbf{0}$ when operating close to (4), the pendulum was manually taken to near such

an operation point. Hence, the following switching condition was used:

$$
f = \begin{cases} (15) & \text{for } \sqrt{\left(\phi - \overline{\phi}\right)^2 + \dot{\phi}^2} \leq 0.3 \\ 0 & \text{for } \sqrt{\left(\phi - \overline{\phi}\right)^2 + \dot{\phi}^2} > 0.3. \end{cases}
\tag{37}
$$

The experimental results obtained when using (37) with (36) are shown in Figure 10, where a limit cycle is observed. Since there is noise in the control signal f, the amplitude and frequency of the limit cycle are difficult to measure there. But as $e = f(s)$ is linearly related to $F(s)$ through (14), the analysis in Section III about limit cycle is also valid for F. Hence, the amplitude and the frequency of F were measured to observe the behavior of the limit cycle. The measured amplitude of the limit cycle is denoted as A_F and was computed by summing the maximal and the minimum absolute values of F, whereas the measured frequency of the limit cycle is denoted as $\omega_{\sigma F}$ and was computed using the following:

$$
\omega_{\sigma F} = \frac{2\pi n}{t_f - t_i},
\tag{38}
$$

where n is the number of oscillations that occurred in the time interval between t_i and t_f. Thus, $A_F = 0.4323$ m and $\omega_{\sigma F} = 0.2922$ rad/s were obtained.

(7) As a limit cycle appeared in the previous step, $|G(j\omega_\sigma)|$ was increased and we went back to step (3). When $|G(j\omega_\sigma)| = 38$ was reached, $k_v = 1.66$ and $\beta = 21.5$ were selected. Then, $k_d = 59.7600$ and $k_p = 7.0208$ were computed. Thus, the following gains for controller (15) were computed:

$$
\begin{aligned}
k_1 &= -7.0208, \\
k_2 &= -59.7600, \\
k_3 &= -211.6171, \\
k_4 &= -22.2606.
\end{aligned}
\tag{39}
$$

When implementing (37) with (39), the results depicted in Figure 11 were obtained. There, it can be observed that the limit cycle was partially eliminated and that $A_F = 0.1371$ m when it appears.

Since in the previous experiment the limit cycle was partially eliminated, $|G(j\omega_\sigma)|$ was incremented so that $|G(j\omega_\sigma)| = 40$. In this case, $k_v = 1.75$ and $\beta = 22.5$ were chosen, $k_d = 63$ and $k_p = 2.6535$ were computed, and the following gains of (15) were found:

$$
\begin{aligned}
k_1 &= -2.6535, \\
k_2 &= -63, \\
k_3 &= -220.9903, \\
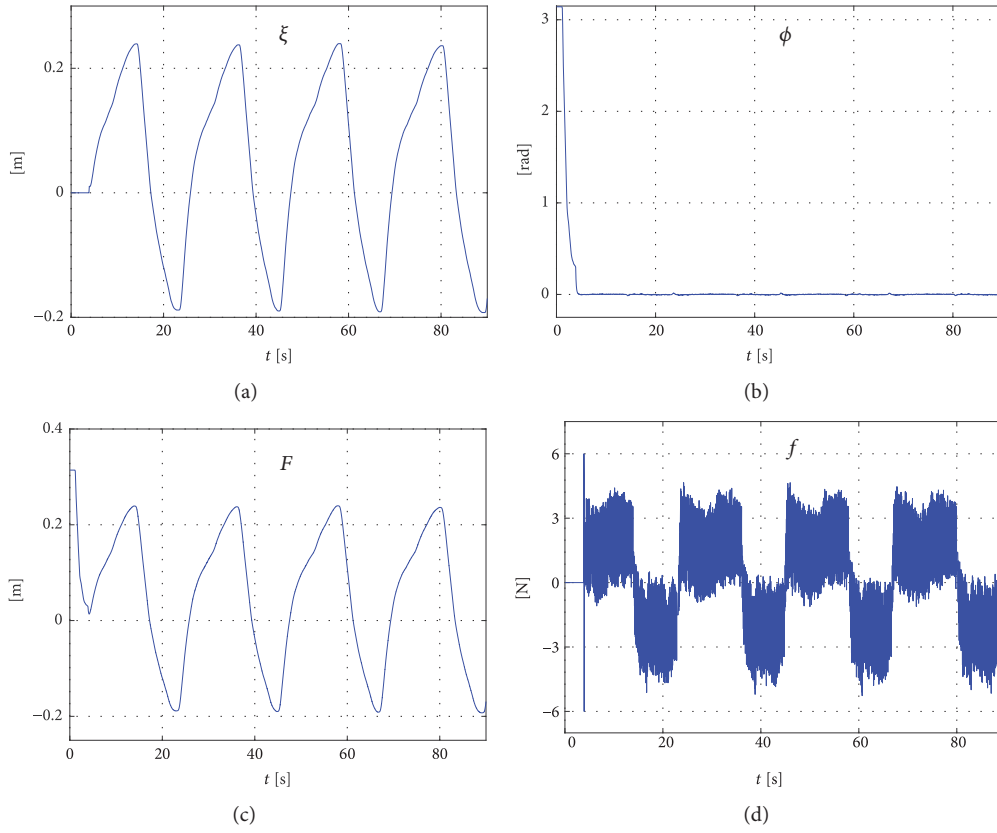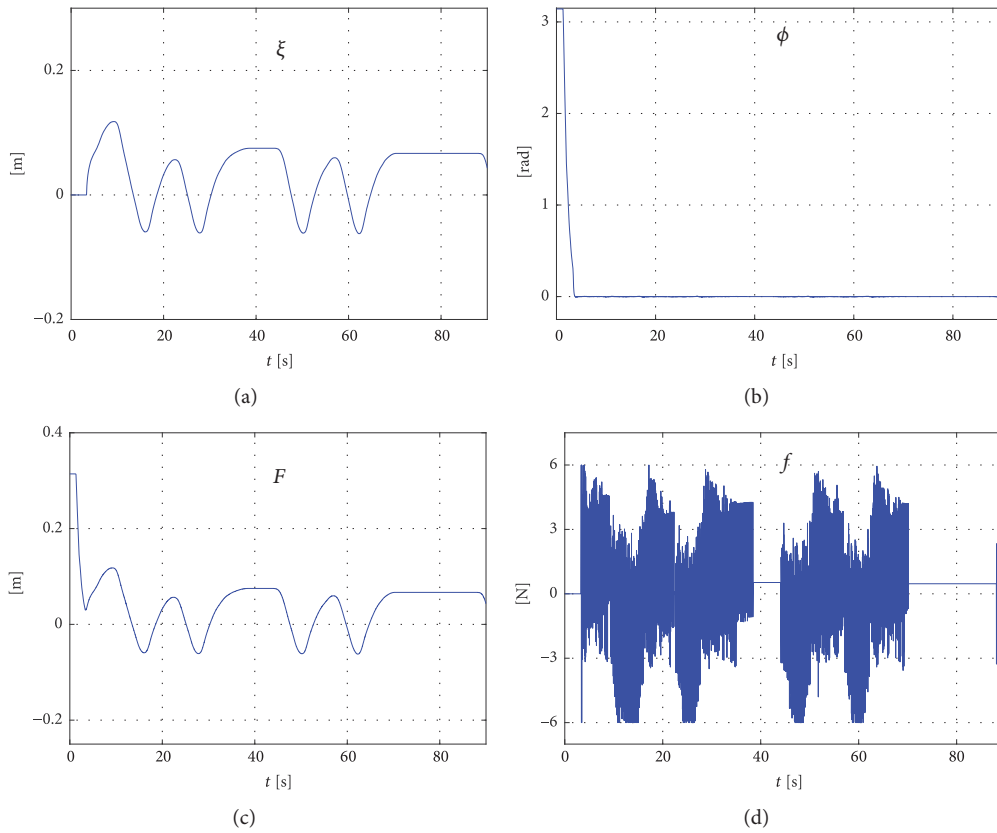k_4 &= -23.4675.
\end{aligned}
\tag{40}
$$

Figure 10: Experimental results when using (36).

Figure 11: Experimental results when $|G(j\omega_\sigma)| = 38$ and $\omega_\sigma = 6$ rad/s.

Although it may be thought that this time the limit cycle would disappear, after executing the experiment of controller (37) with (40), considerable vibration in the prototype was observed and limit cycle reappeared instead of being eliminated. See experimental results in Figure 12, where $A_F = 0.2901$ m and $\omega_{\sigma F} = 0.2365$ rad/s were measured. It is important to highlight that although limit cycle was not eliminated so far, it was actually reduced since $A_F = 0.2901$ m $< A_F = 0.4323$ m. This is in accordance with the conjecture. Also, note that noise in the control signal f is more noticeable because $|G(j\omega_\sigma)|$ was increased (see Figures 10(d), 11(d), and 12(d)).

(8) Since in the previous step limit cycle was not eliminated and considerable vibration was observed in the prototype (see noise in Figure 12(d)), ω_σ was increased to 8 rad/s, $|G(j\omega_\sigma)| = 22$ was set again, and we went back to step (3). As limit cycle still remains, but with a reduced amplitude of oscillation, $|G(j\omega_\sigma)|$ was increased again. As an example of reduction of limit cycle, with regard to the experimental results in Figure 12, the experimental results when $|G(j\omega_\sigma)| = 34$ are depicted in Figure 13. There, it is remarkable that limit cycle was partially eliminated and little oscillations appeared with $A_F = 0.0786$ m, which is less than the amplitude of limit cycle associated with Figures 11 and 12.

To obtain the results in Figure 13, the following gains of controller (15) were used:

$$
\begin{aligned}
k_1 &= -4.8351, \\
k_2 &= -97.28, \\
k_3 &= -226.1135, \\
k_4 &= -24.6392.
\end{aligned}
\tag{41}
$$

Such gains were found departing from selecting $k_v = 1.52$ and $\beta = 23$ and computing $k_d = 97.28$ and $k_p = 4.8351$.

(9) Finally, limit cycle disappeared when $|G(j\omega_\sigma)| = 36$ and $\omega_\sigma = 8$ rad/s. For that, $k_v = 1.61$ and $\beta = 24.5$ were chosen, $k_d = 103.04$ and $k_p = 14.5313$ were computed, and the following gains of controller (15) were found:

$$
\begin{aligned}
k_1 &= -14.5313, \\
k_2 &= -103.04, \\
k_3 &= -241.7981, \\
k_4 &= -26.0981.
\end{aligned}
\tag{42}
$$

The obtained experimental results are shown in Figure 14.

From the experimental results, it was observed that for each ω_σ there is a maximum value of $|G(j\omega_\sigma)|$ allowed by the prototype of the inverted pendulum on a cart to perform experiments. This is because noise in the control signal was increased as $|G(j\omega_\sigma)|$ was increased. The effect of this noise was reflected in the prototype as noticeable vibration when $|G(j\omega_\sigma)|$ reached some high value. Thus, lower frequencies allow larger magnitudes of $G(j\omega)$ and at larger frequencies the magnitude of $G(j\omega)$ must be decreased to avoid noticeable vibration in the closed-loop system and to approach to the limit cycle elimination. Another observation is that the experimental results corroborate the conjecture, i.e., that limit cycle is eliminated as selecting controller gains such that the polar plot of $G(j\omega)$ crosses the negative real axis at a point located farther to the left. Furthermore, an additional observation from the experiments is that limit cycle elimination is accomplished as frequency ω_σ, where the polar plot of $G(j\omega)$ crosses the negative real axis, is chosen larger. Note that these same observations were made for the Furuta pendulum in [20].

On the other hand, some differences were found when comparing frequency $\omega_{\sigma F}$ of the experiments with the desired one. These differences are mainly due to the following:

(i) According to [43], Ch. 5, since the describing function method has an approximate nature, some inaccuracies are found in results: *(a)* the predicted amplitude and frequency might not be accurate, *(b)* a predicted limit cycle might actually not exist, or *(c)* an existing limit cycle is not predicted, the first kind of inaccuracy, i.e., *(a)*, being quite common.

(ii) Dead-zone "transfer function" (13) is an idealization of the nonlinear phenomenon that is actually presented in the practical plant. Hence, not all the dynamics of the dead-zone nonlinearity is concentrated in (13).

Until here it has been shown that the controller and the applied procedure allow elimination of the limit cycle in the inverted pendulum on a cart, but it was previously commented that δ is uncertain because friction is uncertain. This latter implies that knowing the exact value of δ is difficult, which acts as a disturbance. For this reason compensation techniques had to be used to face limit cycle issue online. Thus, it becomes interesting to know the behavior of the linear controller, here implemented for the inverted pendulum on a cart, when the limit cycle in the system changes due to the conditions of operation. Figure 15 presents the results when gains (42) are implemented for the system under study without previously performing an experiment, that is, without "warming up" the actuator. Note that these conditions of operation are different from those when the results of Figure 14 were obtained because then several experiments were consecutively performed before eliminating the limit cycle; that is, the actuator of the system was "warmed up." In Figure 15 it can be observed that in different occasions a limit cycle reappears, which is natural since static friction is greater when there is no previous movement (δ is different). But it is important to remark from Figure 15 is that limit cycle is eliminated after reappearing. Thus, it can be concluded that the simple linear controller here implemented is feasible and robust enough to eliminate limit cycle.

(a)

(b)

(c)

(d)

Figure 12: Experimental results when $|G(j\omega_\sigma)| = 40$ and $\omega_\sigma = 6$ rad/s.
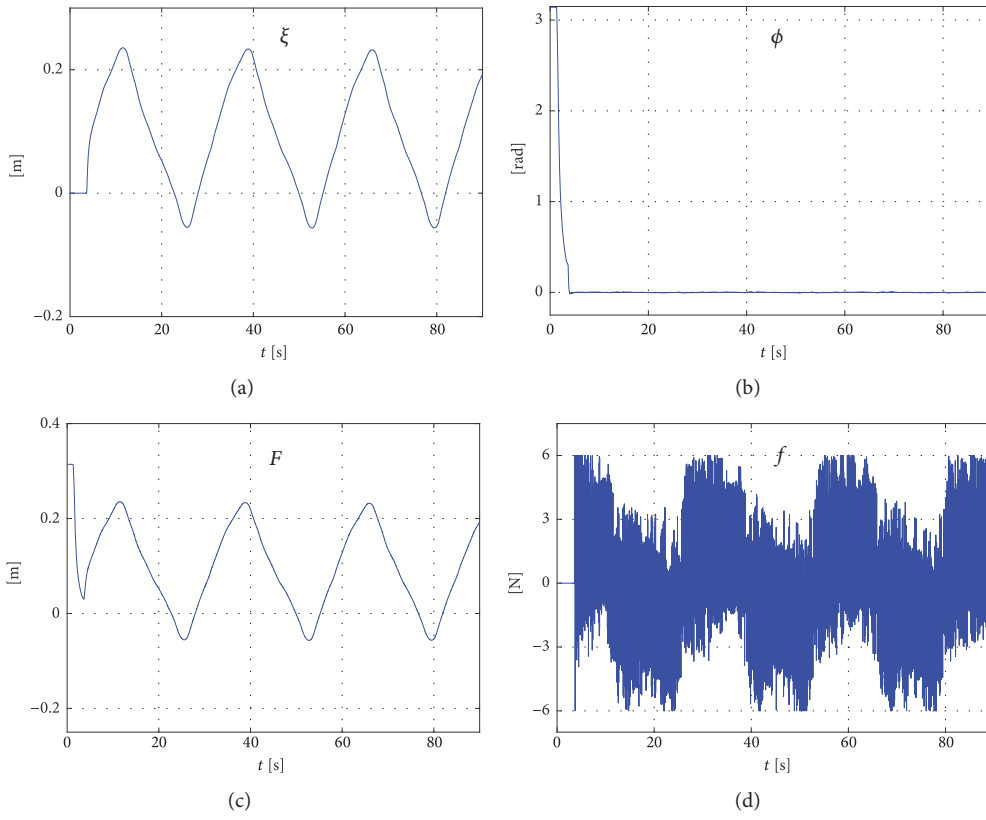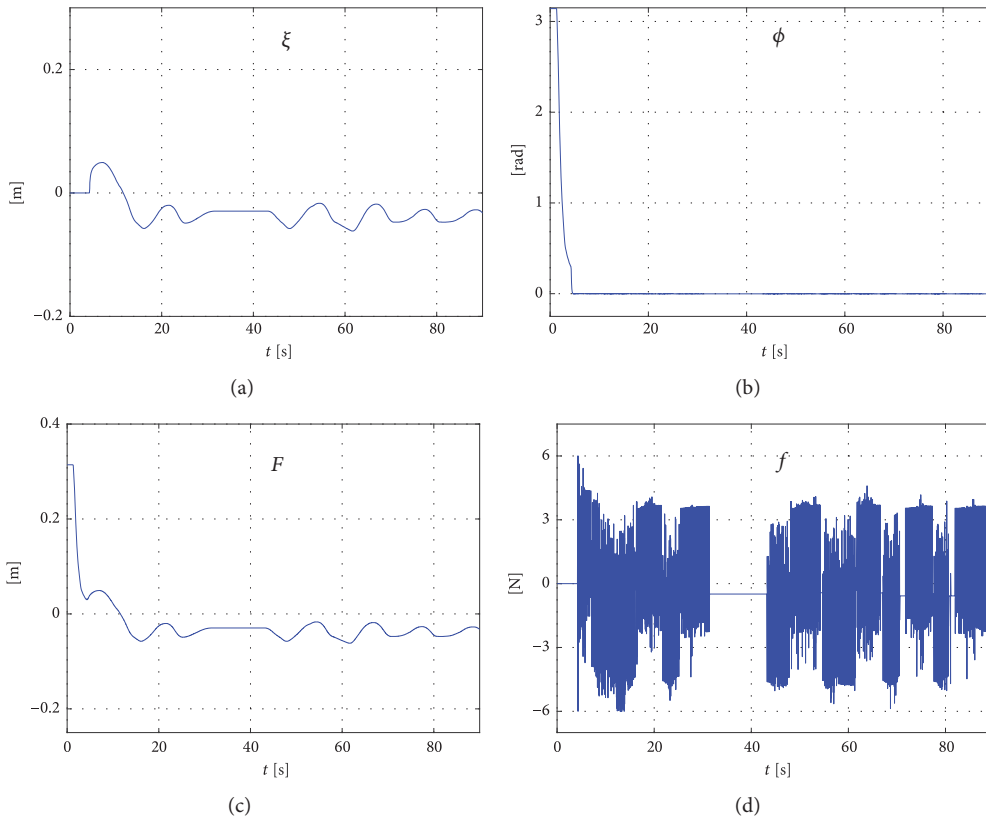

(a)

(b)

(c)

(d)

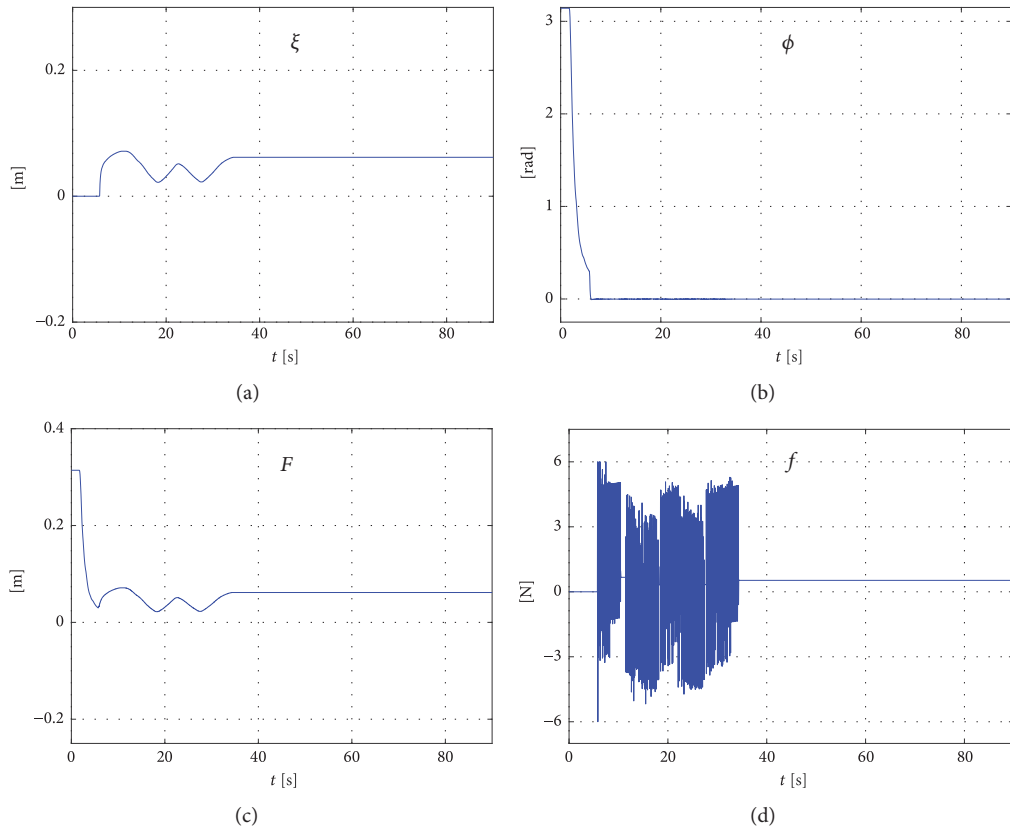Figure 13: Experimental results when $|G(j\omega_\sigma)| = 34$ and $\omega_\sigma = 8$ rad/s.

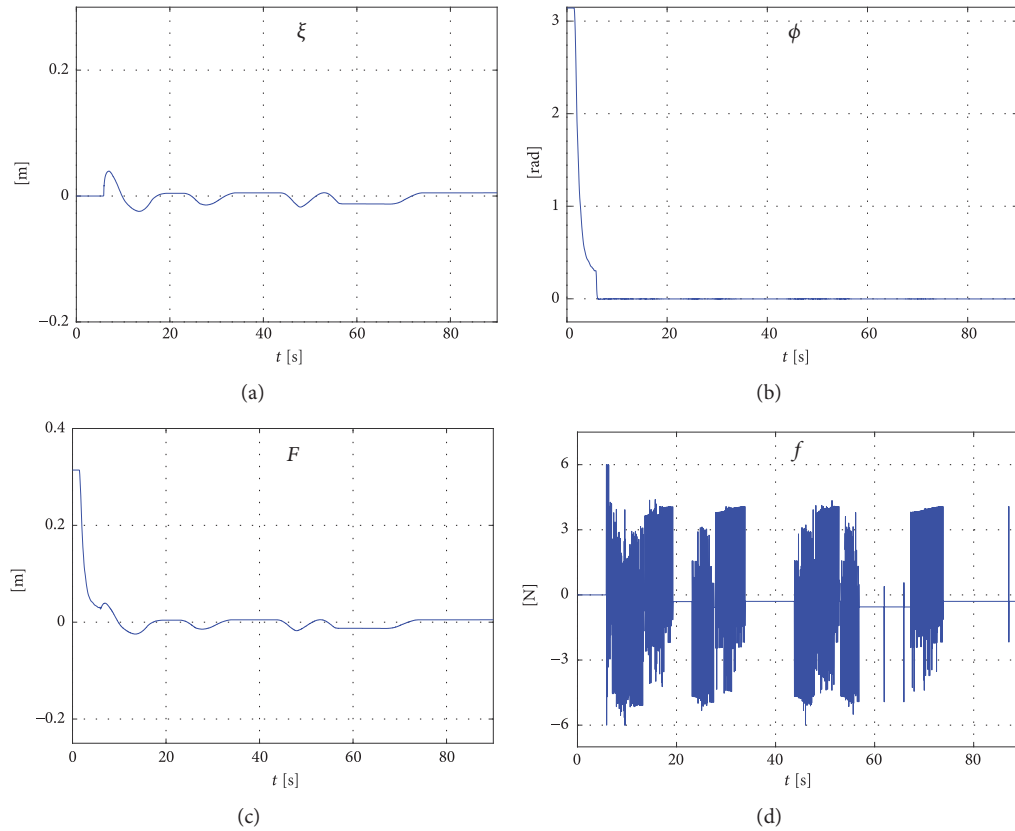Figure 14: Experimental results when $|G(j\omega_\sigma)| = 36$ and $\omega_\sigma = 8$ rad/s.

Figure 15: Experimental results when gains (42) are implemented without previously performing an experiment in the prototype.

5. Conclusion

A linear controller based on the frequency response approach and an experimental procedure, introduced recently by the authors for the Furuta pendulum and the pendubot, has been successfully applied to eliminate the limit cycle in the inverted pendulum on a cart. Therefore, from the experimental results, the following can be concluded. *(i)* The inverted pendulum on a cart has similar behavior to that of the Furuta pendulum under the effect of linear state feedback controller (15), when it is designed through frequency response-based controller (14). *(ii)* The applicability of the approach introduced in [20] to eliminate limit cycle is confirmed for another inverted pendulum, corroborating that the approach can eliminate limit cycles in different inverted pendulums. *(iii)* Robustness of the controller is verified when conditions of operation change.

Data Availability

The data used to support the findings of this study are available from the corresponding author upon request.

Conflicts of Interest

The authors declare that the research was conducted in the absence of any commercial, financial, or personal relationships that could be construed as a potential conflict of interest.

Acknowledgments

References

[1] B. Armstrong-Hélouvry, P. Dupont, and C. C. de Wit, "A survey of models, analysis tools and compensation methods for the control of machines with friction," *Automatica*, vol. 30, no. 7, pp. 1083–1138, 1994.

[2] G. Tao and P. V. Kokotovic, "Adaptive control of plants with unknown dead-zones," *IEEE Transactions on Automatic Control*, vol. 39, no. 1, pp. 59–68, 1994.

[3] G. Tao and F. L. Lewis, *Adaptive Control of Nonsmooth Dynamic Systems*, Springer, New York, NY, USA, 2001.

[4] J. Sandoval, R. Kelly, and V. Santibáñez, "Interconnection and damping assignment passivity-based control of a class of underactuated mechanical systems with dynamic friction," *International Journal of Robust and Nonlinear Control*, vol. 21, no. 7, pp. 738–751, 2011.

[5] A. Nejadfard, M. J. Yazdanpanah, and I. Hassanzadeh, "Friction compensation of double inverted pendulum on a cart using locally linear neuro-fuzzy model," *Neural Computing and Applications*, vol. 22, no. 2, pp. 337–347, 2013.

[6] D. Xia, L. Wang, and T. Chai, "Neural-network-friction compensation-based energy swing-up control of pendubot," *IEEE Transactions on Industrial Electronics*, vol. 61, no. 3, pp. 1411–1423, 2014.

[7] C. Aguilar-Avelar, R. Rodríguez-Calderón, S. Puga-Guzmán, and J. Moreno-Valenzuela, "Effects of nonlinear friction compensation in the inertia wheel pendulum," *Journal of Mechanical Science and Technology*, vol. 31, no. 9, pp. 4425–4433, 2017.

[8] A. Keck, J. Zimmermann, and O. Sawodny, "Friction parameter identification and compensation using the elastoplastic friction model," *Mechatronics*, vol. 47, pp. 168–182, 2017.

[9] H. Olsson and K. J. Åström, "Friction generated limit cycles," *IEEE Transactions on Control Systems Technology*, vol. 9, no. 4, pp. 629–636, 2001.

[10] R. H. Hensen, M. J. van de Molengraft, and M. Steinbuch, "Friction induced hunting limit cycles: a comparison between the LuGre and switch friction model," *Automatica*, vol. 39, no. 12, pp. 2131–2137, 2003.

[11] L. Márton, "On analysis of limit cycles in positioning systems near Striebeck velocities," *Mechatronics*, vol. 18, no. 1, pp. 46–52, 2008.

[12] S.-L. Chen, K. K. Tan, and S. Huang, "Friction modeling and compensation of servomechanical systems with dual-relay feedback approach," *IEEE Transactions on Control Systems Technology*, vol. 17, no. 6, pp. 1295–1305, 2009.

[13] S.-L. Chen, K. K. Tan, and S. Huang, "Limit cycles induced in type-1 linear systems with PID-type of relay feedback," *International Journal of Systems Science*, vol. 40, no. 12, pp. 1229–1239, 2009.

[14] M. M. Z. Shahadat, T. Mizuno, Y. Ishino, and M. Takasaki, "Effect of nonlinearity caused by friction on a negative stiffness control system," *IEEE Transactions on Control Systems Technology*, vol. 22, no. 4, pp. 1385–1395, 2014.

[15] S. Jeon and M. Tomizuka, "Stability of controlled mechanical systems with ideal Coulomb friction," *Journal of Dynamic Systems, Measurement, and Control*, vol. 130, no. 1, pp. 011013-1–011013-9, 2008.

[16] R. Rascón, D. Rosas, and D. Hernandez-Balbuena, "Regulation control of an underactuated mechanical system with discontinuous friction and backlash," *International Journal of Applied Mathematics and Computer Science*, vol. 27, no. 4, pp. 785–797, 2017.

[17] A. Bisoffi, M. Da Lio, A. R. Teel, and L. Zaccarian, "Global asymptotic stability of a PID control system with Coulomb friction," *Institute of Electrical and Electronics Engineers Transactions on Automatic Control*, vol. 63, no. 8, pp. 2654–2661, 2018.

[18] D. J. Block, K. J. Åström, and M. W. Spong, *The Reaction Wheel Pendulum*, M. W. Spong, Ed., Morgan & Claypool, Champaign, IL, USA, 2007.

[19] V. M. Hernandez-Guzman, M. Antonio-Cruz, and R. Silva-Ortigoza, "Linear state feedback regulation of a Furuta pendulum: design based on differential flatness and root locus," *IEEE Access*, vol. 4, pp. 8721–8736, 2016.

[20] M. Antonio-Cruz, V. M. Hernandez-Guzman, and R. Silva-Ortigoza, "Limit cycle elimination in inverted pendulums: Furuta pendulum and pendubot," *IEEE Access*, vol. 6, pp. 30317–30332, 2018.

[21] F. Verduzco, "Control of oscillations from the *k*-zero bifurcation," *Chaos, Solitons & Fractals*, vol. 33, no. 2, pp. 492–504, 2007.

[22] L. Freidovich, A. Robertsson, A. Shiriaev, and R. Johansson, "Periodic motions of the Pendubot via virtual holonomic constraints: theory and experiments," *Automatica*, vol. 44, no. 3, pp. 785–791, 2008.

[23] L. Freidovich, A. Shiriaev, F. Gordillo, F. Gómez-Estern, and J. Aracil, "Partial-energy-shaping control for orbital stabilization of high-frequency oscillations of the Furuta pendulum," *IEEE Transactions on Control Systems Technology*, vol. 17, no. 4, pp. 853–858, 2009.

[24] S. Andary, A. Chemori, and S. Krut, "Control of the underactuated inertia wheel inverted pendulum for stable limit cycle generation," *Advanced Robotics*, vol. 23, no. 15, pp. 1999–2014, 2009.

[25] L. T. Aguilar, I. M. Boiko, L. M. Fridman, and L. B. Freidovich, "Generating oscillations in inertia wheel pendulum via two-relay controller," *International Journal of Robust and Nonlinear Control*, vol. 22, no. 3, pp. 318–330, 2012.

[26] G. A. Medrano-Cerda, "Robust computer control of an inverted pendulum," *IEEE Control Systems Magazine*, vol. 19, no. 3, pp. 58–67, 1999.

[27] H. Vasudevan, A. M. Dollar, and J. B. Morrell, "Design for control of wheeled inverted pendulum platforms," *Journal of Mechanisms and Robotics*, vol. 7, no. 4, pp. 1–12, 2015.

[28] M. Eom and D. Chwa, "Robust swing-up and balancing control using a nonlinear disturbance observer for the pendubot system with dynamic friction," *IEEE Transactions on Robotics*, vol. 31, no. 2, pp. 331–343, 2015.

[29] G. Pujol and L. Acho, "Stabilization of the Furuta pendulum with backlash using H_∞-LMI technique: experimental validation," *Asian Journal of Control*, vol. 12, no. 4, pp. 460–467, 2010.

[30] A. T. Azar and F. E. Serrano, "Stabilization of mechanical systems with backlash by PI loop shaping," *International Journal of System Dynamics Applications*, vol. 5, no. 3, pp. 21–46, 2016.

[31] J. Moreno-Valenzuela, C. Aguilar-Avelar, S. A. Puga-Guzmán, and V. Santibáñez, "Adaptive neural network control for the trajectory tracking of the Furuta pendulum," *IEEE Transactions on Cybernetics*, vol. 46, no. 12, pp. 3439–3452, 2016.

[32] M. Antonio Cruz, R. Silva Ortigoza, C. Márquez Sánchez, V. M. Hernández Guzmán, J. Sandoval Gutierréz, and J. C. Herrera Lozada, "Parallel computing as a tool for tuning the gains of automatic control laws," *IEEE Latin America Transactions*, vol. 15, no. 6, pp. 1189–1196, 2017.

[33] A. Zhang, X. Lai, M. Wu, and J. She, "Nonlinear stabilizing control for a class of underactuated mechanical systems with multi degree of freedoms," *Nonlinear Dynamics*, vol. 89, no. 3, pp. 2241–2253, 2017.

[34] T. Ortega-Montiel, R. Villafuerte-Segura, C. Vázquez-Aguilera, and L. Freidovich, "Proportional retarded controller to stabilize underactuated systems with measurement delays: Furuta pendulum case study," *Mathematical Problems in Engineering*, vol. 2017, Article ID 2505086, 12 pages, 2017.

[35] X.-S. Wang, C.-Y. Su, and H. Hong, "Robust adaptive control of a class of nonlinear systems with unknown dead-zone," *Automatica*, vol. 40, no. 3, pp. 407–413, 2004.

[36] J. Zhou, C. Wen, and Y. Zhang, "Adaptive output control of nonlinear systems with uncertain dead-zone nonlinearity," *IEEE Transactions on Automatic Control*, vol. 51, no. 3, pp. 504–511, 2006.

[37] S. Ibrir, W. F. Xie, and C.-Y. Su, "Adaptive tracking of nonlinear systems with non-symmetric dead-zone input," *Automatica*, vol. 43, no. 3, pp. 522–530, 2007.

[38] C.-H. Liao, F.-C. Chou, P.-C. Tung, and Y.-D. Chen, "Suppression of limit cycles in servo systems using gain limit compensator," *IEICE Transactions on Fundamentals of Electronics, Communications and Computer Sciences*, vol. E91-A, no. 11, pp. 3293–3296, 2008.

[39] S. Jeon, "Integrator leakage for limit cycle suppression in servo mechanisms with stiction," *Journal of Dynamic Systems, Measurement, and Control*, vol. 134, no. 3, pp. 034502-1–034502-8, 2012.

[40] D. Putra, H. Nijmeijer, and N. van de Wouw, "Analysis of undercompensation and overcompensation of friction in 1DOF mechanical systems," *Automatica*, vol. 43, no. 8, pp. 1387–1394, 2007.

[41] I. Fantoni and R. Lozano, *Non-linear Control for Underactuated Mechanichal Systems*, Springer, London, UK, 2002.

[42] H. Sira-Ramírez and S. K. Agrawal, *Differentially flat systems*, Marcel Dekker Inc., New York, NY, USA, 2004.

[43] J. J. Slotine and W. Li, *Applied nonlinear control*, Prentice-Hall, New Jersey, NJ, USA, 1989.

Research Article

Stability of the Evolutionary Game System and Control Strategies of Behavior Instability in Coal Mine Safety Management

Xinhua Wang [iD],[1] **Rongwu Lu** [iD],[2] **Hao Yu** [iD],[1] and **Dan Li** [iD][1]

[1]*College of Economics and Management, Shandong University of Science and Technology, Qingdao 266590, China*
[2]*College of Mathematics and Systems Science, Shandong University of Science and Technology, Qingdao 266590, China*

Correspondence should be addressed to Rongwu Lu; lurong5@sdust.edu.cn

In this paper, we try to find the right control method for the game behavior instability in coal mine safety management. Through the analysis and comparison of the system stability with inflexible and flexible costs and penalties, it can be concluded that the dynamical game system with flexible costs (incentive rewards) and flexible penalty mechanism can significantly reduce the dynamics of unsafe behaviors in coal mine safety supervision. A combined mechanism of incentive rewards and flexible penalty is put forward to improve the stability of the dynamical system and control the instability of behaviors effectively. The results of model simulation show that the combined mechanism has very good property and can optimize and control the instability of behaviors and strategies of the interested parties. Based on the theoretical conclusions, some control strategies and policy advice are proposed for the improvement of the system and measures of safety management for government departments.

1. Introduction

The frequent occurrence of coal mine safety accidents always makes the safety production situation in China become the focus of attention at home and abroad. Management chaos, illegal operations, poor policy implementation, and regulatory dislocation have long become the prominent factors affecting the safety of coal mine production. The traditional safety management is mainly based on experience-oriented administrative regulations and legislations. However, due to the differences of region, staff and technical level, and so on, coal mine safety management has great complexity. The effectiveness of some rules and regulations is temporary and limited in the implementation process.

In order to ensure that the safety legislation is closely integrated with management practice, many scholars have deeply analyzed the influence factors of coal mine safety supervision and studied the relationship between the occurrences of unsafe behaviors and the interest distribution of coal mine safety [1–6].

Through the previous studies on the game of safety supervision, it is found that the dynamical system of safety management game model hardly has the stability and self-control generally, and the game behaviors of the players always have repeated volatility [7, 8]. The volatility of the behaviors may sometimes provide wrong information and cause unrealistic or even error related decisions and measures of coal mine safety management, which will seriously affect the efficiency of safety management.

In the previous studies of evolutionary game model in coal mine safety management, we have obtained the following replicator dynamics [9, 10]:

$$\dot{x_1} = x_1 (1 - x_1) [(x_2 + (1 - x_2) x_3) f_1 - c_1];$$
$$\dot{x_2} = x_2 (1 - x_2) [(1 - x_1) (f_1 + x_3 f_2) - c_2]; \quad (1)$$
$$\dot{x_3} = x_3 (1 - x_3) [(1 - x_1) (1 - x_2) (f_1 + f_2) - c_3]$$

where $c_i (i = 1, 2, 3)$ is the safety cost (input) of coal miners (denoted as player I), safety inspection groups inside the coal
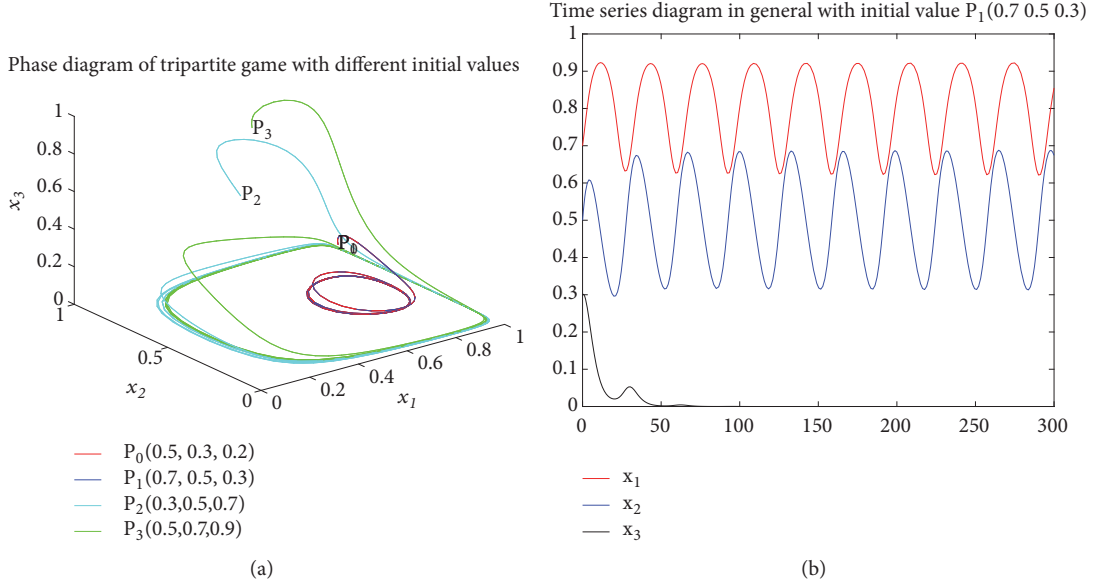
FIGURE 1: Phase graph of dynamical system (1) and time series diagram of players' strategy selection probabilities. Values of model parameters: $(c_1, c_2, c_3, f_1, f_2) = (0.5, 0.2, 0.3, 1, 1.2)$.

mine (player II), and safety regulatory departments of local government (player III). $f_i (i = 1, 2)$ is the penalty index (fine) when player I or player II has made mistakes (unsafe behaviors) and is checked out, respectively.

According to the actual situation of China's coal mine production and coal mine safety regulation, we assume that the parameters described above satisfy the following conditions:

(i) $c_2 \leq c_3 \leq c_1 \leq 1$;

(ii) $f_i \geq 1, i = 1, 2$.

Phase diagram analysis and time series diagram are commonly used methods to study the stability of nonlinear dynamical systems. Phase diagram analysis method has the characteristic of vivid intuition, which represents all possible states of the dynamic system. Phase diagram analysis greatly promotes the wide application of differential dynamical system in many disciplines [11–15]. Time series graph depicts the process of function changing with time variable t, which can simply and clearly describe the evolution process, chaos, and synchronization of differential dynamical systems [16–19]. In addition to the eigenvalue method, a large part of model analysis in this study uses these two methods.

The game model contains too many variables and parameters, it is difficult to obtain the model's analytical solution [10]. In this paper, we mainly use numerical simulation method to analyze the evolutionary process. So, it is very important to properly set the initial values of parameters and variables. Coal mine safety management involves various types of coal production enterprises with different technological development levels in different regions, and the coal production process and safety management status of these enterprises themselves have great differences. The corresponding parameters and initial values of variables will

not be the same and changeless. Supposing that the relevant method is applied in a specific coal production enterprise or a specific mining area, the model parameters and initial values of variables should be deduced and estimated according to the actual situation of coal production. In this way, the model analysis will be more pertinent and the corresponding conclusions will be more accurate. In this paper, we merely set the values of model parameters and the initial value of the variables theoretically reasonably but do not make detailed and specific statistical reasoning.

In order to reflect the dependence of the stability of dynamic system on the initial value, we choose several different initial values of variables (each player's strategy selection probabilities of x_1, x_2, and x_3) in the system. For example, we set the value of $(x_1(0), x_2(0), x_3(0))$ to $P_0(0.5, 0.3, 0.2)$, $P_1(0.7, 0.5, 0.3)$, $P_2(0.3, 0.5, 0.7)$, $P_3(0.5, 0.7)$, and $P_3(0.5, 0.7, 0.9)$, respectively, in Figure 1(a).

Through the stability analysis of the dynamical system (1) (see Figure 1, where Figure 1(a) is phase graph of dynamical system and Figure 1(b) demonstrates the time series of players' strategy selection probabilities), we can find that there are repeated fluctuations in the game process of multiparty safety management. It agrees with the actual situation of safety management to a certain extent. If the coal miners do not adopt a safety production strategy (or the proportion of unsafe strategies in the production worker group is larger) at the beginning, the regulators will increase the level of safety supervision. With the increase of supervision intensity, coal miners will take safe production behaviors (or increase the proportion of safety behavior choice) or even completely do not choose unsafe behavior. Then coal production safety conditions will improve, and then regulators will reduce supervision, and then the unsafe behaviors will be more likely to happen. Over time, coal mine safety will always be in the process of cyclical fluctuations. This phenomenon appears

not only in coal mine safety management but also in other processes of production safety management [20–23].

The game model of safety regulation does not have global stability under general conditions [10]. Most of the existing studies proposed the system and measures for safety management from the points of view of the policy makers, according to the specific situation (such as types of accidents or illegal behaviors) [24–28]. In this way, even if the relevant policies and measures have played a certain role in a short period, in a short period, the long-term effectiveness can not be guaranteed because of the lack of control (inhibition or avoidance) of behavior volatility of the interested groups. The repeated fluctuations and volatility (instability) often provide the decision-makers with wrong information, which will lead to unrealistic or even error decisions and measures of coal mine safety management, and seriously affect the efficiency of coal mine safety management.

In order to definitely improve the efficiency of safety management, some control methods are needed for restraining the instability of players's dynamical behavior and strategies in the process of coal mine safety supervision. So, in this paper, we proceed from the relationship between the model parameters (or variables) and explore the functionary mechanism of those model parameters (or variables) on the stability of game behaviors. As the design mechanism of model parameters and variables (i.e., the formulation of incentive and penalty measures in the process of safety supervision) is found out, then we could put forward the control methods and control strategies for the behavior instability. First, the stability of the dynamical system of the game model is studied in the cases of the generally inflexible cost subsidies and penalties index. Second, the stability of the dynamical system is considered under the flexible cost functions and flexible penalty functions. We believe that the relevant dynamic control methods and strategies will provide a theoretical basis for the regulation and control of coal mine safety management system and measures.

The rest of this paper is organized as follows. In Section 2, we analyze and compare the system stability of evolutionary game models in four cases: inflexible cost subsidies, flexible costs (incentive rewards), inflexible penalties, and flexible penalties. In Section 3, we carry out further theoretical analysis under the combined mechanism of incentive rewards and flexible penalties. Then, in Section 4, we put forward some control strategies to suppress the behavior instability in safety management system. Our paper is finally concluded in Section 5.

2. Analysis on Stability of the Dynamical Game System

2.1. Stability of the Dynamical Game System with Inflexible Cost Subsidies. The inflexible cost subsidy mentioned in this article refers to those policy oriented fixed subsidies for the workers which are undifferentiated and averagely shared, such as the underground allowances and the post allowances, etc. The increase of inflexible subsidies is equivalent to when the reduction of the safety production costs of coal miners,

or the safety inspection cost of safety inspection team, or the safety supervision cost of the government department ($c_i, i = 1, 2, 3$) becomes smaller. Therefore, based on the general situation as shown in Figure 1, we decrease the values of c_1, c_2, and c_3, respectively, or synchronously to comparatively analyze the stability of dynamical system of the game model.

Here, Figures 2(a), 2(b), and 2(c) are time series graphs of strategy selection probabilities (x_1, x_2, x_3) when c_1 decreases gradually. Similarly, we get Figures 2(d), 2(e), and 2(f) when c_2 decreases gradually and Figures 2(g), 2(g), and 2(i) when c_3 decreases gradually. Figures 3(a), 3(b), and 3(c) show the time series of strategy selection probabilities when c_1, c_2, and c_3 decreases synchronously.

As can be seen from Figures 2 and 3, the volatility of the game system has been reduced when the value of c_1, c_2, or c_3 becomes smaller. However, the stability of the game system has not changed substantially. Under normal circumstances (see Figures 2(a), 2(d), and 2(g)), x_1 still has no asymptotic stability (controllability). Only under some extreme conditions such as $c_1 = 0, c_2 < 0$, or $c_3 < 0$ which are difficult to reach in practice, will x_1 (probability of coal miners selecting safe production behaviors) quickly and steadily approach 1 (see Figures 2(c), 2(f), 2(i), and 3(c)).

So, on the premise of guaranteeing the economic benefits of coal enterprises, it is necessary to suitably raise the policy subsidies and the welfare level of the employees, which will relevantly reduce the safety input cost of the interested groups and promote them to increase investment in production. Then the production safety of coal enterprises and safety management work can be run at a higher level.

2.2. Stability of the Dynamical Game System with Flexible Cost (Incentive Rewards). In Section 2.1, we found that general cost reductions do not completely bring down the volatility of the dynamical system of game models. Salary is the sum of various forms of remuneration or return obtained by the employees of the enterprise for providing labor or labor to their work units, including job salary, performance salary, bonus (month award, quarterly award, annual award, etc.), allowance, labor bonus, welfare, and so on. Salary management is the key to reflect the vital interests and social values of employees, and also it is the internal power of enterprise operation [29, 30], so that the incentive salary system must adhere to the principle of pay according to performance. The implementation of performance compensation should be based on a scientific performance evaluation system. Otherwise, the fairness of performance compensation will not reach the purpose of motivating employees. In recent years, various enterprises (including various types of enterprises in the coal industry) pay more and more the wages of employees, quarterly awards, year-end awards, and other variable income to the total income of workers. The discretionary variable part (performance salary, bonus, etc.) plays a very important role in stimulating the working enthusiasm in coal enterprises and improving safety efficiency.

Therefore, performance salary and bonus and some other incentive rewards should be taken into account of the players' costs of safety production. Those who perform better will get more rewards, and their safety cost inputs will be reduced

(a) $c_1 = 0.2$

(b) $c_1 = 0.05$

(c) $c_1 = 0$

(d) $c_2 = 0.1$

(e) $c_2 = 0$

(f) $c_2 = -0.1$

(g) $c_3 = 0.1$

(h) $c_3 = 0$

(i) $c_3 = -0.1$
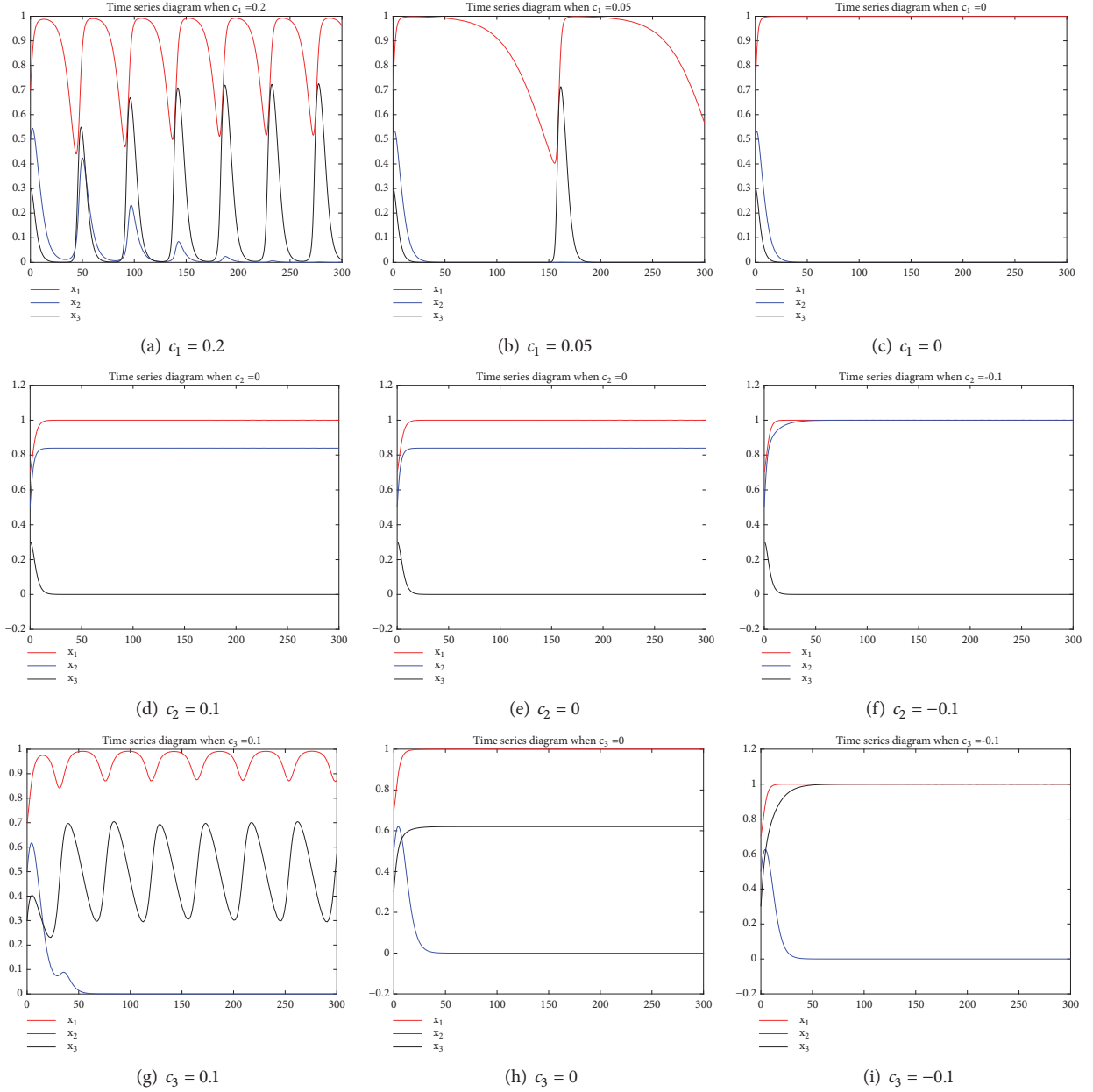
FIGURE 2: Time series graph of players' strategy selection probabilities when c_1, c_2, c_3 have smaller values separately. Initial values of variables: $(x_1, x_2, x_3)|_{t=0} = P_1(0.7, 0.5, 0.3)$.

accordingly. So we construct some flexible cost functions, such as $c_i(x_i) = c_i(1-x_i), c_i(x_i) = c_i(1-x_i^2), c_i(x_i) = c_i(1-\sqrt{x_i})$, to analyze the stability of dynamical system with incentive rewards.

If $c_i(x_i) = c_i(1-x_i), i = 1, 2, 3$, are taken, income functions of the three players in the game model are

$$\pi_1 = -x_1(1-x_1)c_1 - (1-x_1)(x_2 + x_3 - x_2 x_3) f_1;$$

$$\pi_2 = -x_2(1-x_2)c_2$$
$$\quad + (1-x_1)[x_2 f_1 - (1-x_2) x_3 f_2];$$

$$\pi_3 = -x_3(1-x_3)c_3 + (1-x_1)(1-x_2) x_3 (f_1 + f_2).$$
$$\tag{2}$$

The replicator dynamics corresponding to the game model are as follows:

$$\dot{x}_1 = x_1(1-x_1)[x_1 c_1 + (x_2 + (1-x_2) x_3) f_1];$$

$$\dot{x}_2 = x_2(1-x_2)[x_2 c_2 + (1-x_1)(f_1 + x_3 f_2)];$$
$$\tag{3}$$

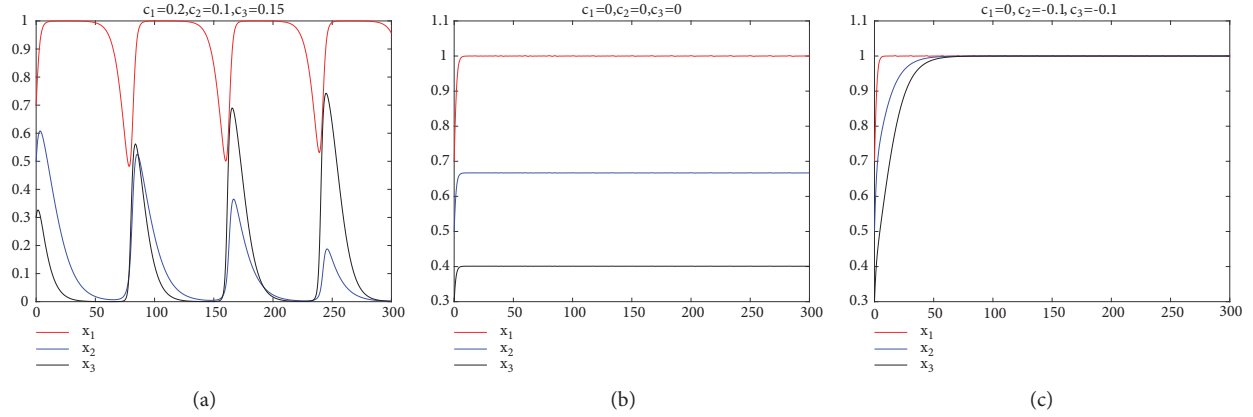$$\dot{x}_3 = x_3(1-x_3)[x_3 c_3 + (1-x_1)(1-x_2)(f_1 + f_2)].$$

FIGURE 3: Time series graph of players' strategy selection probability when c_1, c_2, c_3 become smaller simultaneously. $(x_1, x_2, x_3)|_{t=0} = P_1(0.7, 0.5, 0.3)$.

The Jacobian matrix of the dynamical system (3) is

$$J = \frac{\partial(\dot{x}_1, \dot{x}_2, \dot{x}_3)}{\partial(x_1, x_2, x_3)} = \begin{pmatrix} l_1 & x_1(1-x_1)(1-x_3)f_1 & x_1(1-x_1)(1-x_2)f_1 \\ x_2(1-x_2)(f_1+f_2x_3) & l_2 & x_2(1-x_1)(1-x_2)f_2 \\ -x_3(1-x_3)(1-x_2)(f_1+f_2) & -x_3(1-x_3)(1-x_1)(f_1+f_2) & l_3 \end{pmatrix} \quad (4)$$

where

$$l_1 = (1-2x_1)(x_2+x_3-x_2x_3)f_1 + (2x_1-3x_1^2)c_1;$$

$$l_2 = (1-2x_2)(1-x_1)(f_1+x_3f_2) + (2x_2-3x_2^2)c_2;$$

$$l_3 = (1-2x_3)(1-x_1)(1-x_2)(f_1+f_2)$$
$$+ (2x_3-3x_3^2)c_3. \tag{5}$$

Let $\dot{x}_1 = \dot{x}_2 = \dot{x}_3 = 0$, and we get eight pure strategy equilibrium points of system (3), $X_i (i = 0, 1, \ldots, 8)$:

$$(0,0,0),(1,0,0),(0,1,0),(0,0,1),(1,1,0),(1,0,1),$$
$$(0,1,1),(1,1,1). \tag{6}$$

According to Formula (4), all of the Jacobian matrices at the equilibrium points are diagonal matrices (see Table 1). And all of the eigenvalues are not larger than zero at the four points with $x_1 = 1$ (i.e., coal miners will choose safety production behaviors), and the first eigenvalues of them are negative.

According to the eigenvalue judgment method of evolutionary game strategy (ESS) [31, 32], the ESS of coal miners is $x_1 = 1$, which means they will surely choose the safety production strategy in the case of this function form of flexible costs.

As can be shown in Figures 4 and 5, dynamical system (3) goes into evolutionary stable state despite different initial values. Especially for some reasonable initial state values, the evolutionary process of the game system is very anticipated and preferable (see Figures 4(a) and 4(b)).

Therefore, if the incentive salary system is established in coal enterprise, the proportion of unsafe behaviors will greatly be reduced and coal mine safety will be maintained in a stable and controllable state. An incentive salary system means that the salary should be linked to the performance of coal workers with the efficiency of safety production and the frequency of unsafe behavior, and the variable part of coal enterprise workers' performance wages, bonuses, welfare, and so on should be increased in their personal incomes.

2.3. Stability of the Dynamical Game System with Inflexible Penalties.

As can be seen in Figure 6, the volatility of the dynamical system would be reduced when value of f_1 or f_2 increases. In contrast to Figures 6(a), 6(b), and 6(c), we find that x_1 approaches 1 and x_2 increases with smaller amplitudes when f_1 becomes larger. That is, the increase in the intensity of player I's penalty can make coal workers increase the willingness to choose the behaviors of safe production, and the enterprise safety inspection department is also willing to increase the intensity of safety inspection.

By contrasting Figure 6(d) with Figure 6(e), we also find that x_1 approaches 1 with smaller amplitudes when f_2 becomes larger. However, the volatilities of x_2 and x_3 have no significant reduction when f_1 or f_2 becomes larger (even when f_1 and f_2 become large synchronously; see Figure 6(f)), while the values of x_2 and x_3 have the trends of increasing. In addition, the increase in the intensity of player II's penalty may increase the workload and tension in safety regulation.

So the conclusion is that although the behavior instability will decrease with the increase of the values of f_1 and

$c_i(x_i) = c_i(1-x_i)$, i=1,2,3; initial value= P_1(0.7,0.5,0.3)

(a)

$c_i(x_i) = c_i(1-x_i)$, i=1,2,3; initial value= P_0 (0.5,0.3,0.2)

(b)

$c_i(x_i) = c_i(1-x_i)$, i=1,2,3; initial value= P_2(0.3,0.5,0.7)

(c)

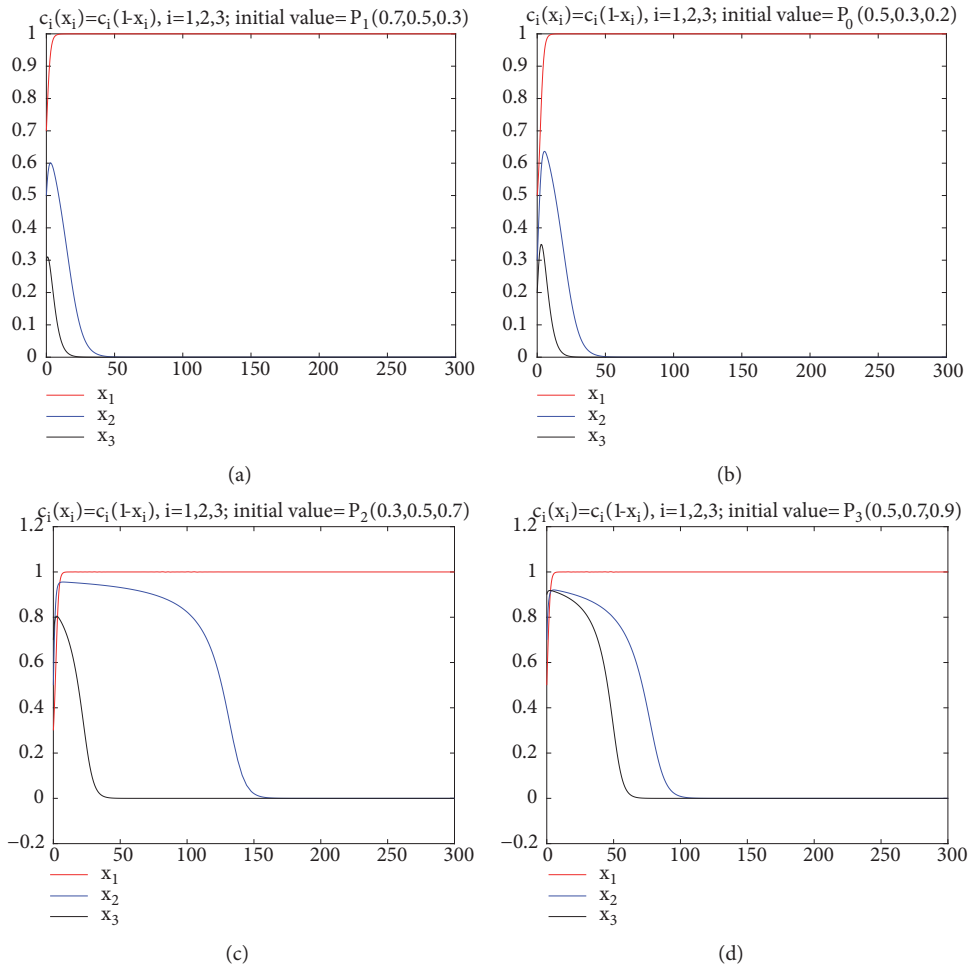$c_i(x_i) = c_i(1-x_i)$, i=1,2,3; initial value= P_3(0.5,0.7,0.9)

(d)

Figure 4: Time series graph of players' strategy selection probability when costs become flexible. $c_i(x_i) = c_i(1 - x_i), i = 1, 2, 3$.

Flexible costs: $c_i(x_i) = c_i(1-x_i)$, i=1,2,3.

P_0(0.5, 0.3, 0.2)
P_1(0.7, 0.5, 0.3)
P_2(0.3,0.5,0.7)
P_3(0.5,0.7,0.9)
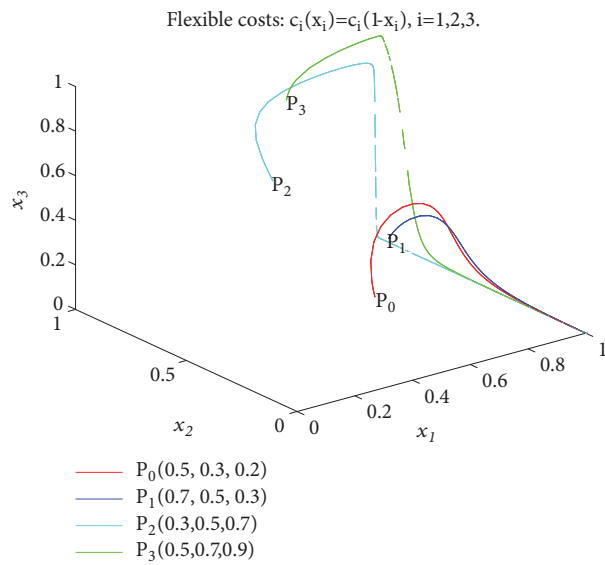
Figure 5: Phase diagram of the tripartite game system with incentive rewards.

TABLE 1: Jacobian Matrix of Equilibrium Points with Dynamical costs.

Equilibrium points	$(0,0,0)$	$(0,1,0)$	$(0,0,1)$	$(0,1,1)$
J	$\text{diag}(0, f_1, f_1 + f_2)$	$\text{diag}(f_1, -c_2 - f_1, 0)$	$\text{diag}(f_1, f_1 + f_2, -c_3 - f_1 - f_2)$	$\text{diag}(f_1, -c_2 - f_1 - f_2, -c_3)$
Equilibrium points	$(1,0,0)$	$(1,1,0)$	$(1,0,1)$	$(1,1,1)$
J	$\text{diag}(-c_1, 0, 0)$	$\text{diag}(-c_1, -c_2, 0)$	$\text{diag}(-c_1, 0, -c_3)$	$\text{diag}(-c_1 - f_1, -c_2, -c_3)$

(a) $f_1 = 2, f_2 = 1.2$

(b) $f_1 = 4, f_2 = 1.2$

(c) $f_1 = 8, f_2 = 1.2$

(d) $f_1 = 1, f_2 = 4$

(e) $f_1 = 1, f_2 = 8$

(f) Both f_1 and f_2 are large
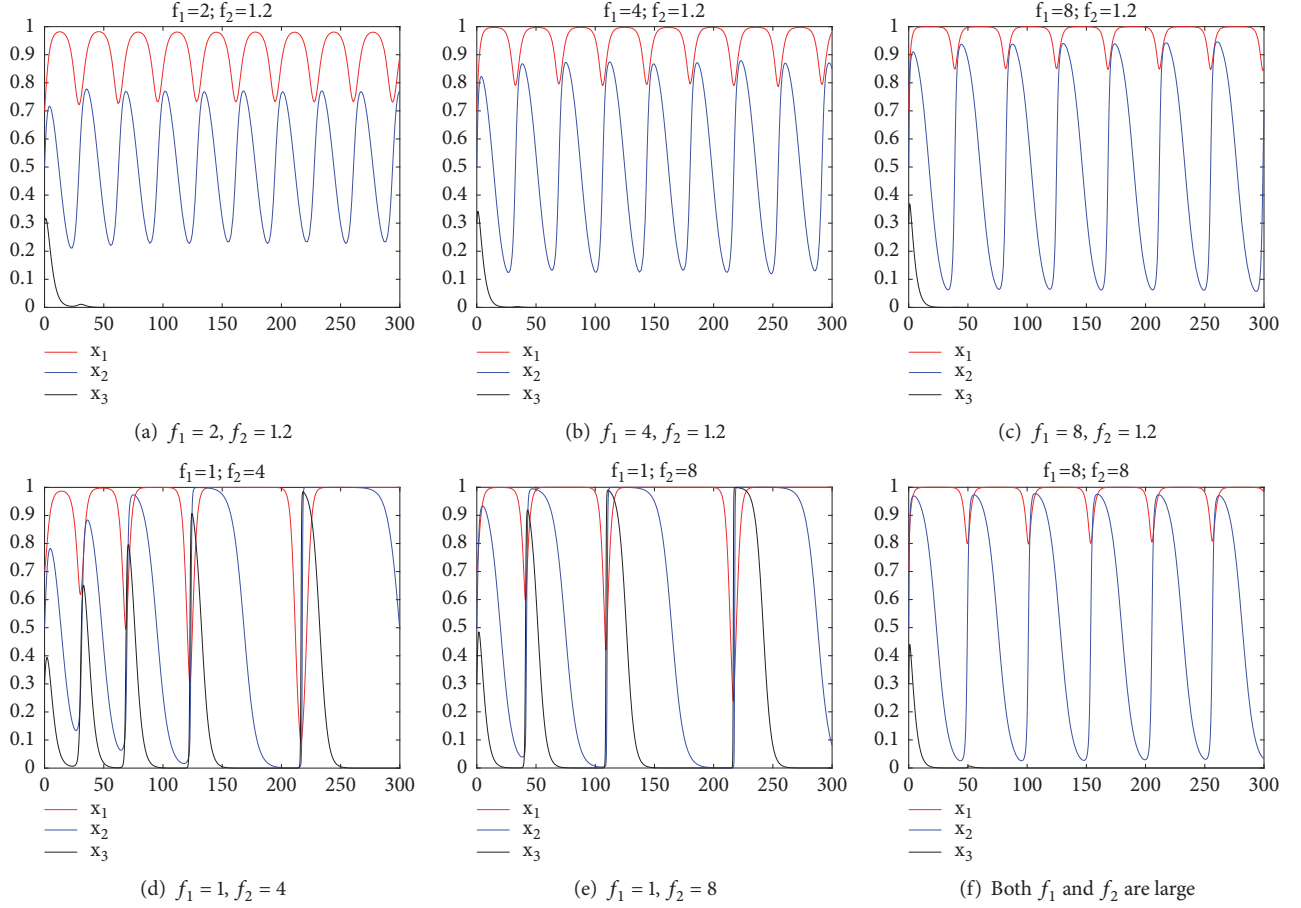
FIGURE 6: Time series graph of players' strategy selection probability when f_1 or f_2 has larger values. Initial value of variables $(x_1, x_2, x_3)|_{t=0} = P_1(0.7, 0.5, 0.3)$.

f_2, there is no essential change of the volatility of the dynamical system. That is, the ordinary increase of penalty index can not completely eliminate the behavior instability of game models. So, on the one hand, it is necessary to make proper punishment for unsafe behaviors strictly in the coal mine safety management. On the other hand, too, excessively severe penalty measures may lead to the instability of the working state of the supervised objects, which may bring negative effects on the efficiency of coal mine safety supervision.

2.4. Stability of the Dynamical Game System with Flexible Penalties.
According to the conclusion of Section 2.3, the stability of players' selections has not been completely controlled as the values of f_1, f_2 become larger simply. Therefore, we consider some flexible penalty functions $f_i(x_i)$ to substitute

for general penalty index f_i and analyze the influence of flexible penalty mechanism on system stability.

The design of the flexible penalty function in this part is based on the following considerations: for the players who do not often make mistakes, the penalty for accidental mistakes is relatively light; for the players who often make mistakes (repeatedly taught not to change), the more frequent the mistakes are, the larger the corresponding penalty will be. Therefore, the flexible penalty functions $f_i(x_i)$ mainly discuss three functional forms to analyze and be compared with each other: $M_i(1 - x_i), M_i(x_i^{-1} - 1), M_i(x_i^{-2} - 1), i = 1, 2$. Set the values of function parameters $M_1 = 1$ and $M_2 = 1.2$ (separately equivalent to the preceding parameter values of f_1 and f_2), and numerical simulation results indicate that flexible penalty mechanism can significantly improve the stability of dynamical systems of evolutionary game models

Flexible penalties: $f_i(x_i)=f_i(1/x_i-1)$, $i=1,2$.

Flexible penalties: $f_i(x_i)=f_i(1/x_i^2-1)$, $i=1,2$.

P₀(0.5, 0.3, 0.2)
P₁(0.7, 0.5, 0.3)
P₂(0.3,0.5,0.7)
P₃(0.5,0.7,0.9)

(a) $f_i(x_i) = f_i(x_i^{-1} - 1)$, $i = 1, 2$

P₀(0.5, 0.3, 0.2)
P₁(0.7, 0.5, 0.3)
P₂(0.3,0.5,0.7)
P₃(0.5,0.7,0.9)
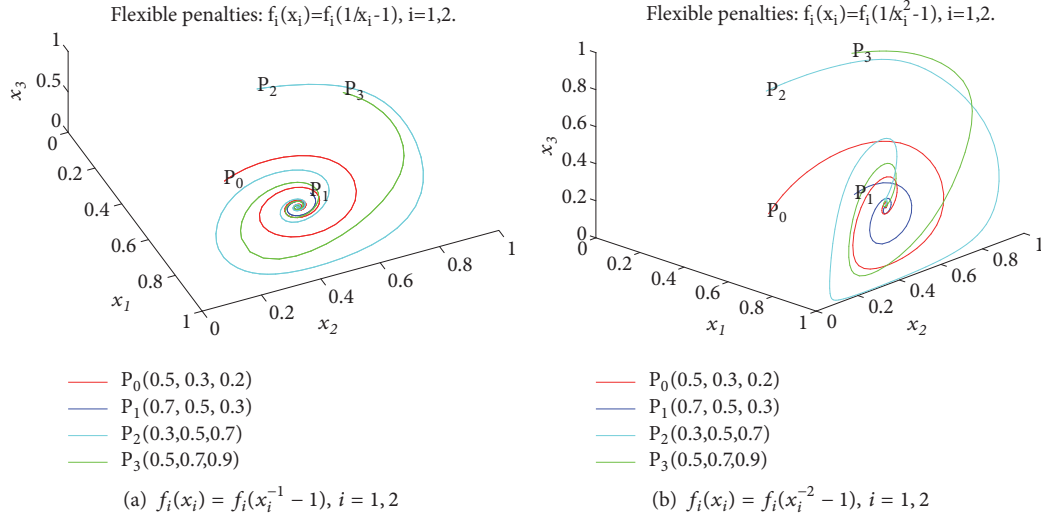
(b) $f_i(x_i) = f_i(x_i^{-2} - 1)$, $i = 1, 2$

Figure 7: Phase diagram of dynamical system of tripartite game with flexible penalty strategy.

(see Figures 7, 8, and 9). In particular the latter two types of flexible penalty function can effectively control the evolutionary stability of game model, which can make the probability of players' strategy selection x_1, x_2, and x_3 stabilize quickly. In addition, the latter two types can theoretically avoid the unwanted situations like any equilibrium point x_i equals zero (where x_i appears on the denominator).

The comparison between Figures 7(a) and 7(b) demonstrates that the last function form $M_i(x_i^{-2} - 1)$ is even better one because x_1 can quickly and steadily tends to 1. Suppose that $f_i(x_i) = f_i(x_i^{-2} - 1), i = 1, 2$, and then we get the income function of the three players in the game model as follows:

$$\pi_1 = -x_1 c_1 - (1 - x_1)(x_2 + x_3 - x_2 x_3) f_1 (x_1^{-2} - 1);$$

$$\pi_2 = -x_2 c_2 + (1 - x_1)$$
$$\cdot [x_2 f_1 (x_1^{-2} - 1) - (1 - x_2) x_3 f_2 (x_2^{-2} - 1)];$$ (7)

$$\pi_3 = -x_3 c_3 + (1 - x_1)(1 - x_2)$$
$$\cdot x_3 (f_1 (x_1^{-2} - 1) + f_2 (x_2^{-2} - 1)).$$

Replicator dynamic equations corresponding to game models are

$$\dot{x}_1 = x_1 (1 - x_1) [-c_1 + (x_2 + x_3 - x_2 x_3) f_1 (x_1^{-2} - 1)];$$

$$\dot{x}_2 = x_2 (1 - x_2) [-c_2$$
$$+ (1 - x_1)(f_1 (x_1^{-2} - 1) + x_3 f_2 (x_2^{-2} - 1))];$$ (8)

$$\dot{x}_3 = x_3 (1 - x_3) [-c_3$$
$$+ (1 - x_1)(1 - x_2)(f_1 (x_1^{-2} - 1) + f_2 (x_2^{-2} - 1))].$$

The Jacobian matrix of the dynamical system of the game model is

$$J = \frac{\partial (\dot{x}_1, \dot{x}_2, \dot{x}_3)}{\partial (x_1, x_2, x_3)} = (j_{ij})_{3 \times 3}$$ (9)

where

$$j_{11} = (1 - 2x_1)[(x_2 + x_3 - x_2 x_3) f_1 (x_1^{-2} - 1) - c_1]$$
$$- \frac{2(1 - x_1)(x_2 + x_3 - x_2 x_3) f_1}{x_1^2};$$

$$j_{12} = x_1 (1 - x_1)(1 - x_3) f_1 (x_1^{-2} - 1);$$

$$j_{13} = x_1 (1 - x_1)(1 - x_2) f_1 (x_1^{-2} - 1);$$

$$j_{21} = x_2 (1 - x_2)\left(-f_1 (x_1^{-2} - 1) - \frac{2(1 - x_1) f_1}{x_1^3}\right.$$
$$\left. + f_2 (x_2^{-2} - 1) x_3\right);$$

$$j_{22} = (1 - 2x_2)$$
$$\cdot [(1 - x_1)(f_1 (x_1^{-2} - 1) + x_3 f_2 (x_2^{-2} - 1)) - c_2]$$
$$- \frac{2(1 - x_1)(1 - x_2) x_2 x_3 f_2}{x_2^3};$$ (10)

$$j_{23} = x_2 (1 - x_1)(1 - x_2) f_2 (x_2^{-2} - 1);$$

$$j_{31} = -x_3 (1 - x_3)(1 - x_2)\left[-f_1 (x_1^{-2} - 1)\right.$$
$$\left. - \frac{2(1 - x_1) f_1}{x_1^3} + f_2 (x_2^{-2} - 1)\right];$$

$$j_{32} = -x_3 (1 - x_3)(1 - x_1)\left[-f_2 (x_2^{-2} - 1)\right.$$
$$\left. - \frac{2(1 - x_2) f_2}{x_2^3} + f_1 (x_1^{-2} - 1)\right];$$

$$j_{33} = (1 - 2x_3)$$
$$\cdot [(1 - x_1)(1 - x_2)(f_1 (x_1^{-2} - 1) + f_2 (x_2^{-2} - 1))$$
$$- c_3].$$

(a) $f_i(x_i) = f_i(1 - x_i), i = 1, 2$

(b) $f_i(x_i) = f_i(x_i^{-1} - 1), i = 1, 2$

(c) $f_i(x_i) = f_i(x_i^{-2} - 1), i = 1, 2$

FIGURE 8: Time series graph of dynamical system under flexible penalty mechanism. Initial value is $P_0(0.5, 0.3, 0.2)$.

Let $\dot{x}_1 = \dot{x}_2 = \dot{x}_3 = 0$, it is found that there are only two pure policy equilibrium points in the system, $X_0 = (1, 1, 0)$; $X_1 = (1, 1, 1)$, and there may be a mixed policy equilibrium point X_2 satisfying the following conditions:

$$(x_2 + x_3 - x_2 x_3) f_1 \left(x_1^{-2} - 1 \right) = c_1;$$

$$(1 - x_1) \left[f_1 \left(x_1^{-2} - 1 \right) + x_3 f_2 \left(x_2^{-2} - 1 \right) \right] = c_2; \quad (11)$$

$$(1 - x_1)(1 - x_2) \left[f_1 \left(x_1^{-2} - 1 \right) + f_2 \left(x_2^{-2} - 1 \right) \right] = c_3.$$

Through calculating, we get $J(X_0) = \text{diag}(c_1, c_2, -c_3)$; $J(X_1) = \text{diag}(c_1, c_2, c_3)$. The dynamical systems do not have evolutionary stability in the two equilibrium fields because both Jacobian matrices at the two pure strategy equilibrium points have positive eigenvalues. In addition, Formula (11) shows that the solution of x_1 must be less than 1 even if the equilibrium point of mixed strategy X_2 exists.

So it can be concluded from the numerical simulations that flexible penalty mechanism can significantly reduce the dynamics of unsafe behaviors in coal mine safety supervision. Once the penalties can be closely correlated with the frequency of their mistakes, the players would like to consistently choose the safe behaviors (or improve the efficiency of safety supervision) with great probability. Then the controllability of safety supervision system and the performance efficiency of safety management measures can be guaranteed. However, a shortcoming of flexible penalties is that although x_1 is an ESS, it does not regularly converge to 1 (see Figure 9(c)).

3. Stability of the Dynamical Game System under Combined Mechanism of Incentive Rewards and Flexible Penalties

Through the previous analysis in Sections 2.2 and 2.4, we find that incentive rewards (flexible costs) can raise players' selection probabilities of safe behaviors and flexible penalties can bring system stability. Considering the actual situation of coal production, we certainly prefer to have an ESS of $x_1 = 1$ in the dynamical safety management system. So we propose a combined mechanism of incentive rewards and flexible penalties and then analyze the stability of the evolutionary dynamical system on this basis.

(a) $f_i(x_i) = f_i(1 - x_i), i = 1, 2$

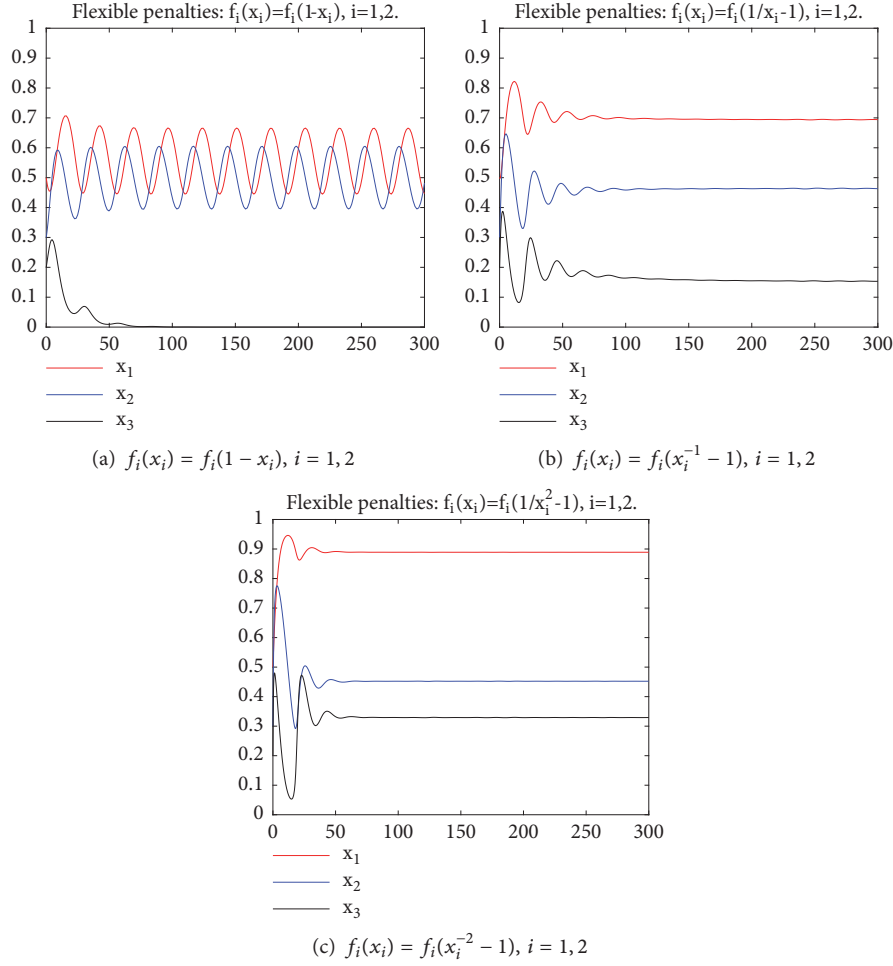(b) $f_i(x_i) = f_i(x_i^{-1} - 1), i = 1, 2$
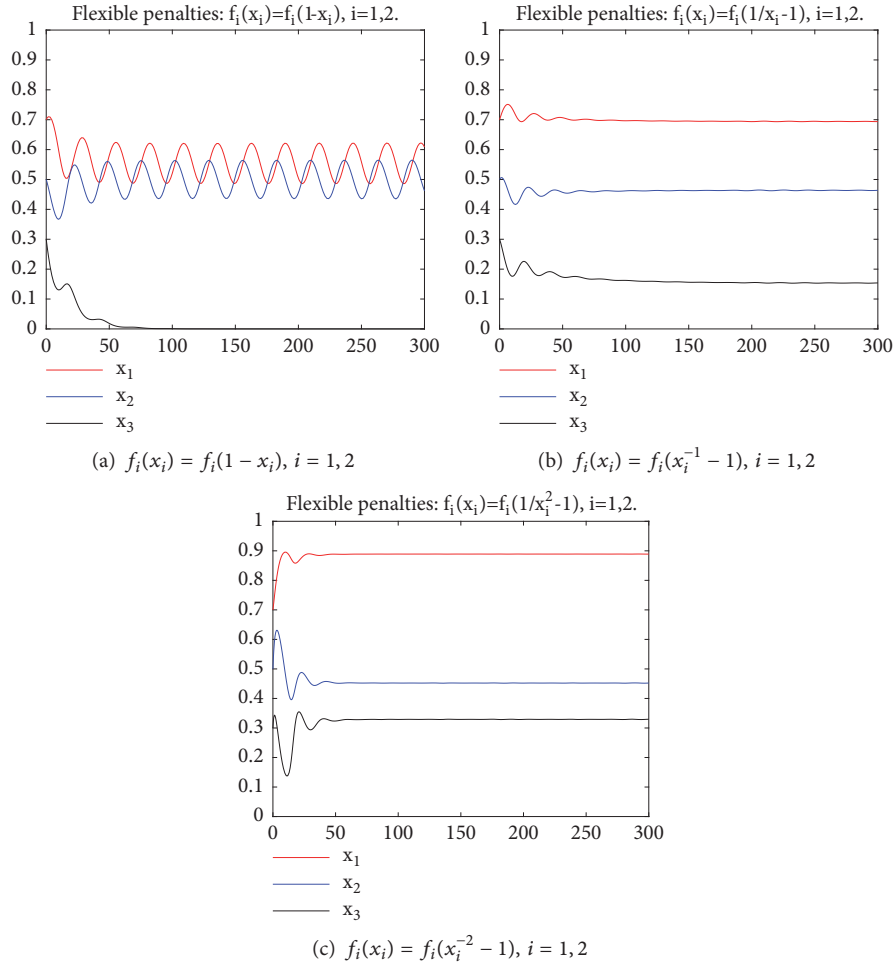
(c) $f_i(x_i) = f_i(x_i^{-2} - 1), i = 1, 2$

FIGURE 9: Time series graph of dynamical system under flexible penalty mechanism. Initial value is $P_1(0.7, 0.5, 0.3)$.

Two cases are chosen as an example to be analyzed and compared in this part. One case is all players unified incentive rewards and flexible penalties; i.e., $c_i(x_i) = c_i(1 - x_i), i = 1, 2$, and $f_i(x_i) = f_i(x_i^{-2} - 1), i = 1, 2, 3$. The other case is that player I (coal miners) is subjected to incentive reward mechanism, and player II is subjected to flexible penalty mechanism, and player III is not given any incentive reward and flexible penalty (i.e., $c_1(x_1) = c_1(1 - x_1)$, $f_2(x_2) = f_2(x_2^{-2} - 1)$, and the rest of the parameters remain unchanged). As shown in the phase diagrams (see Figure 10), both results of the two cases of combined mechanisms are very satisfying ($x_1 = 1$ is ESS).

The evolutionary processes of more cases of combined mechanisms are demonstrated by the time series graphs (see Figure 11). Through mutual comparison among them, we can find that some of them bring more satisfying results (see Figures 11(a) and 11(b)). Although starting from different initial values, the dynamical system always tends to be ideally stable in very short time (player I chooses safe production strategy with $x_1 = 1$ and the values of x_2 and x_3 are also stable in some reasonable values). Therefore, we can conclude that this combined mechanism of incentive reward and flexible penalties can optimize and control the instability of the behavior strategy selection in the safety supervision

model. This conclusion is undoubtedly a highlight of this study. These combined mechanisms may be the key measure to solve the behavior fluctuations in the safety management system.

4. Control Strategies for the Improvement of the System and Measures of Safety Management

At present, the formulation of safety management policies and measures is mostly based on the temporary measures taken according to the occurrence of accidents [1, 33]. The policies are adjusted with the occurrence of accidents. The relevant supervision measures are often characterized by accident types and lack of comprehensive analysis of safety system, which is one of the important reasons for frequent accidents. There are many factors that affect the game behavior and game strategy of each interested group. The study of the regulatory mechanism of influencing factors is an important guarantee for the rationality of the formulation of management rules. Only when the management rules can regulate the bad game behavior of the players and the game rules can the management rules be effective.

Flexible costs and penalties: $c_i(x_i)=c_i(1-x_i), i=1,2,3; f_i(x_i)=f_i(1/x_i^2-1), i=1,2.$ Flexible c_1 and f_2: $c_1(x_1)=c_1(1-x_1); f_2(x_2)=f_2(1/x_2^2-1)$

—— $P_0(0.5, 0.3, 0.2)$	—— $P_0(0.5, 0.3, 0.2)$
—— $P_1(0.7, 0.5, 0.3)$	—— $P_1(0.7, 0.5, 0.3)$
—— $P_2(0.3, 0.5, 0.7)$	—— $P_2(0.3, 0.5, 0.7)$
—— $P_3(0.5, 0.7, 0.9)$	—— $P_3(0.5, 0.7, 0.9)$

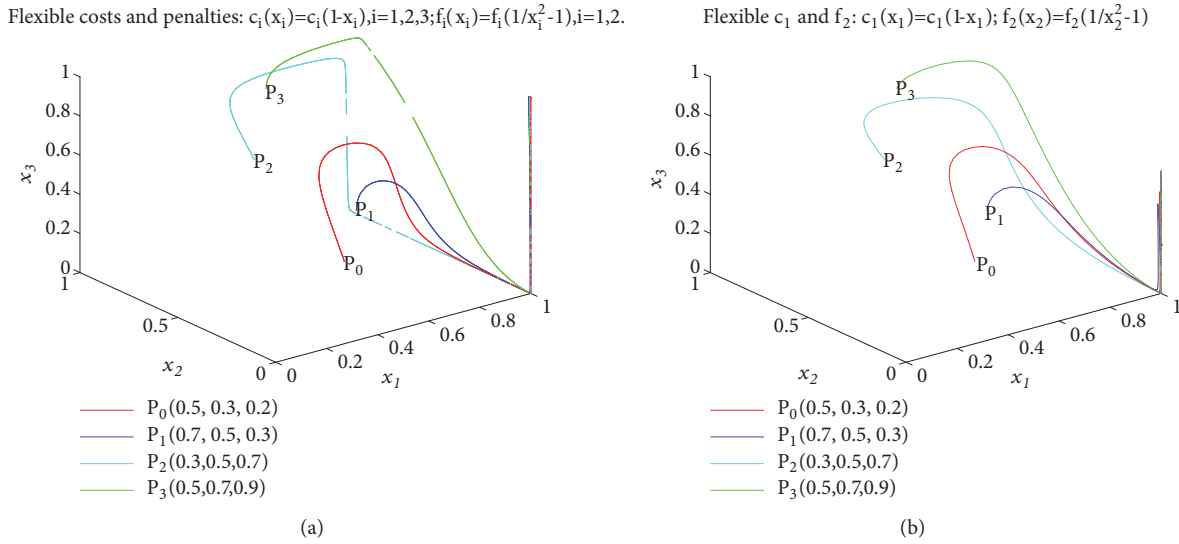(a)   (b)

FIGURE 10: Phase diagrams of dynamical system of tripartite game under combined mechanisms of incentive reward and flexible penalty.

According to the researches of the coal mine safety supervision model in Sections 2 and 3, we finally put forward the following regulation and control strategies of coal mine safety management system and supervision measures.

(1) Restraint Measures in Safety Supervision System of Coal Mine Safety Management. In Section 2.1, it is concluded that raising policy subsidies and the welfare level of the employees would relevantly reduce the safety input cost and make the production safety of coal enterprises and safety management work run at a higher level. So the governmental supervision department should formulate some policy-based or industry-specific constraints for safety supervision behaviors, including mandatory provisions on the supervision strategies of internal and external safety supervision and inspection departments. In order to better improve the overall production safety level and safety management level, the majority of front-line production workers in coal enterprises can be called upon to exercise self-restraint on their own safety production activities spontaneously (strictly disciplined and supervised by each other). It is more important especially in large and medium-sized state-owned coal enterprises, where the quality of coal mine workers is very good and the technology of safety production is more advanced.

It should be noted that the so-called subsidies and employee benefits are not necessarily limited to the economic level. For ordinary employees, especially the coal miners working in the production line, enterprises should increase investment in regular safety knowledge training and safety skills drills to improve the safety quality and safety awareness of employees and inhibit the occurrence of unsafe behavior. For enterprise safety managers and government personnel in charge of safety supervision departments, it is necessary to carry out regular or irregular study of safety skills and safety management knowledge in coal mine safety, so as to improve the safety knowledge and safety management level of safety management personnel and ensure the implementation of safety supervision policies and measures.

(2) Energetically Promoting the Incentive Salary System in the Coal Industry. In Section 2.2, we found that incentive salary system can greatly reduce the proportion of unsafe behaviors and impels coal mine safety to be stable and controllable. Incentive reward system will reform the traditional unreasonable wage and salary distribution in coal enterprises and significantly increase wage distribution ratio of safety-related posts and production links, such as high technical requirements, high production safety intensity, and heavy management responsibility. Then the staff and workers of coal enterprises can be guided to spontaneously strengthen the improvement of safety production technology and the exertion of safety production capacity.

There are still some backward phenomena in the salary distribution system of nowadays' coal enterprises in China, such as the serious tendency of internal income distribution equalitarianism and unreasonable internal income distribution relationship, which seriously affect the efficiency of safety supervision in coal enterprises and the level of safety management [34]. Safety production is the most important task in the coal enterprises. So we should vigorously promote the incentive salary system in the coal industry, especially in large and medium-sized state-owned coal enterprises. Post-performance pay system, year-end accident-free incentives, and other ways should be adopted properly to improve the correlation between the income of workers and their safety production efficiency and safety behavior.

(3) Establishing the Flexible Penalty Mechanism of Unsafe Behavior in Coal Mine Safety System. It can be seen from the research results in Sections 2.4 and 3 that the flexible penalty mechanism based on the frequency of unsafe behavior can better reflect the management mode of tight integration in safety management. More closely related to the occurrence of coal mine safety behaviors, the flexible penalty mechanism can better guarantee the stability of coal mine safety management.
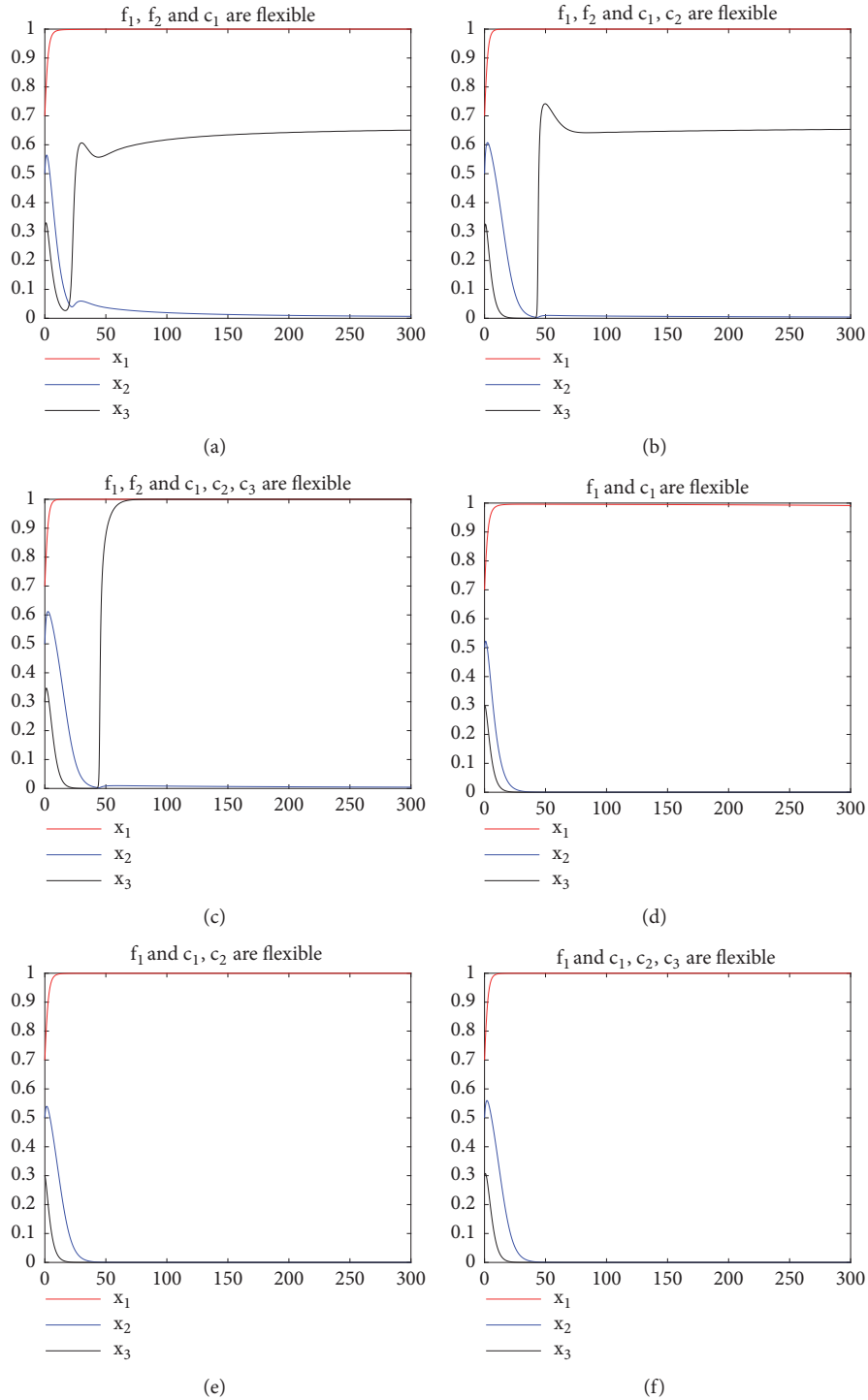
FIGURE 11: Time series graphs of dynamical system under combined mechanisms of incentive reward and flexible penalty. Initial value is $P_1(0.7, 0.5, 0.3)$.

In coal mine safety management, the penalty measures against unsafe behaviors of coal miners are very important. The difficulty and inadequacy of flexible cost mechanism are to have certain requirements for the operation profitability of coal mine enterprises. Actually, for many slow-growing small and medium-sized coal mine enterprises, they may prefer to motivate employees through punitive measures.

5. Conclusions

To control players' behavior instability in coal mine safety management, this study starts from the stability analysis of the dynamical game system under the four cases of inflexible costs (static subsidies), flexible costs (incentive rewards), inflexible penalties, and flexible penalties. Then, we

discuss the stability of the dynamical system under combined mechanism of cost and penalty and find out which method is more effective to control the instability of dynamical system. Through the comparative analysis of inflexible and flexible rewards and penalties mechanism, it can be found that if the salary and penalty mechanism of coal enterprises can be closely related to their safety production behaviors (or safety supervision behaviors), the stability of the game dynamical system of coal enterprises' safety supervision can be enhanced. We propose a combined mechanism of incentive reward and flexible penalties for the improvement of the safety management system to restrain the emergence and spread of unsafe behaviors in the coal mine safety system. Some results of this research provide a theoretical basis for more reasonable and more effective policies of coal mine safety management.

It is worth noting that it is necessary to carry out the modern financial management of coal enterprises. The coal industry should vigorously improve the performance wages, quarterly awards, year-end bonuses, welfare, and other variable income in the proportion of employees'salaries and strive to build and improve the incentive salary system for coal enterprise employees. And, more importantly, more close connection should be established between the system of staff safety performance evaluation and the system of rewards and punishment.

In the future, the corresponding tuning mechanism for the parameters will be investigated in different safety management systems. In order to improve the accuracy of model parameters, we should investigate and analyze the actual situation of coal mine safety management by means of questionnaire survey and field visit, so as to improve the practicability of the model method in this paper. Besides, some optimal techniques should also be considered for improving control performance of the dynamical system, such as extremum seeking control (ESC) method [35, 36]. We will continue our efforts to study the optimization of the dynamical system stability.

Data Availability

The data used to support the findings of this study are included within the article.

Conflicts of Interest

The authors declare that there are no conflicts of interest regarding the publication of this paper.

Acknowledgments

References

[1] W. Yin, G. Fu, C. Yang, Z. Jiang, K. Zhu, and Y. Gao, "Fatal gas explosion accidents on Chinese coal mines and the characteristics of unsafe behaviors: 2000–2014," *Safety Science*, vol. 92, pp. 173–179, 2017.

[2] G. Lan, Y. Chen, H. E. Gang, and Y. Zhu, "Research of the influences of mine environment on coal miners unsafe behaviors," *Industrial Safety & Environmental Protection*, vol. 43, no. 10, pp. 51–54, 2017.

[3] H. Jia, Q. Cao, S. Wang, and S. Zhang, "Analysis of big data in coal mine and pre-control of workers' unsafe behaviors," *Journal of Shandong University of Science & Technology*, vol. 34, no. 2, pp. 14–18, 2015.

[4] R. Yu, "Study on coal mine personnel unsafe behaviors mechanism," *Coal & Chemical Industry*, vol. 37, no. 11, pp. 130–133, 2014.

[5] S. Li, H. Liu, and Y. Yang, "Model of coal safety prediction and evaluation based on miners unsafe behavior," *Safety in Coal Mines*, vol. 48, no. 8, pp. 242–245, 2017.

[6] L. Li, S. Tian, and Y. Chen, "Influential factors index system of coal miners' unsafe behaviors based on sem-anp," *Journal of Xian University of Science & Technology*, vol. 37, no. 04, pp. 529–536, 2017.

[7] D. Liu, X. Xiao, H. Li, and W. Wang, "Historical evolution and benefit–cost explanation of periodical fluctuation in coal mine safety supervision: An evolutionary game analysis framework," *European Journal of Operational Research*, vol. 243, no. 3, pp. 974–984, 2015.

[8] Q. Liu, X. Li, and M. Hassall, "Evolutionary game analysis and stability control scenarios of coal mine safety inspection system in China based on system dynamics," *Safety Science*, vol. 80, pp. 13–22, 2015.

[9] R. Lu, X. Wang, and D. Li, "A fractional supervision game model of multiple stakeholders and numerical simulation," *Mathematical Problems in Engineering*, vol. 2017, Article ID 9123624, 9 pages, 2017.

[10] R. Lu, X. Wang, H. Yu, and D. Li, "Multiparty evolutionary game model in coal mine safety management and its application," *Complexity*, vol. 2018, Article ID 9620142, 10 pages, 2018.

[11] F. Tramontana, A. A. Elsadany, B. Xin, and H. N. Agiza, "Local stability of the Cournot solution with increasing heterogeneous competitors," *Nonlinear Analysis: Real World Applications*, vol. 26, pp. 150–160, 2015.

[12] M. Chi and W. Zhao, "Dynamical analysis of multi-nutrient and single microorganism chemostat model in a polluted environment," *Advances in Difference Equations*, vol. 2018, no. 1, p. 120, 2018.

[13] T. Zhang, X. Meng, and T. Zhang, "Global analysis for a delayed SIV model with direct and environmental transmissions," *Journal of Applied Analysis and Computation*, vol. 6, no. 2, pp. 479–491, 2016.

[14] Z. Bai, S. Zhang, S. Sun, and C. Yin, "Monotone iterative method for fractional differential equations," *Electronic Journal of Differential Equations*, vol. 2016, no. 6, pp. 1–8, 2016.

[15] Y. Li, W. Zhang, and X. Liu, "Stability of nonlinear stochastic discrete-time systems," *Journal of Applied Mathematics*, vol. 2013, Article ID 356746, 8 pages, 2013.

[16] B. Xin and Y. Li, "0-1 test for chaos in a fractional order financial system with investment incentive," *Abstract and Applied Analysis*, vol. 2013, Article ID 876298, 10 pages, 2013.

[17] H. Qi, L. Liu, and X. Meng, "Dynamics of a nonautonomous stochastic SIS epidemic model with double epidemic hypothesis," *Complexity*, vol. 2017, Article ID 4861391, 14 pages, 2017.

[18] Y. Cui, "Uniqueness of solution for boundary value problems for fractional differential equations," *Applied Mathematics Letters*, vol. 51, pp. 48–54, 2016.

[19] X. Z. Meng, S. N. Zhao, T. Feng, and T. H. Zhang, "Dynamics of a novel nonlinear stochastic SIS epidemic model with double epidemic hypothesis," *Journal of Mathematical Analysis and Applications*, vol. 433, no. 1, pp. 227–242, 2016.

[20] S. Kalantari, M. J. Jafari, M. Gharari, L. Omidi, M. Ghaffari, and G. R. A. Fardi, "The influence of safety training on improvement in safety climate in construction sites of a firm," *Circulation*, vol. 2, no. 6, pp. 257–264, 2015.

[21] L. Mooren, R. Grzebieta, A. Williamson, J. Olivier, and R. Friswell, "Safety management for heavy vehicle transport: A review of the literature," *Safety Science*, vol. 62, no. 2, pp. 79–89, 2014.

[22] T. Kontogiannis, M. C. Leva, and N. Balfe, "Total Safety Management: Principles, processes and methods," *Safety Science*, vol. 100, pp. 128–142, 2017.

[23] F. W. Guldenmund and Y. Li, "Safety management systems: A broad overview of the literature," *Safety Science*, vol. 103, pp. 94–123, 2018.

[24] Q. Liu, X. Meng, M. Hassall, and X. Li, "Accident-causing mechanism in coal mines based on hazards and polarized management," *Safety Science*, vol. 85, no. 6191, pp. 276–281, 2016.

[25] H. Chen, Q. Feng, D. Zhu, S. Han, and R. Long, "Impact of rent-seeking on productivity in Chinese coal mine safety supervision: a simulation study," *Energy Policy*, vol. 93, pp. 315–329, 2016.

[26] Q. Sun, H. Ji, and Y. Cui, "Positive solutions for boundary value problems of fractional differential equation with integral boundary conditions," *Journal of Function Spaces*, vol. 2018, Article ID 6461930, 6 pages, 2018.

[27] X.-X. Xu and Y.-P. Sun, "Two symmetry constraints for a generalized Dirac integrable hierarchy," *Journal of Mathematical Analysis and Applications*, vol. 458, no. 2, pp. 1073–1090, 2018.

[28] J. Wang, J. Zhang, K. Zhu, and L. Zhou, "Anatomy of explosives spontaneous combustion accidents in the Chinese underground coal mine: Causes and prevention," *Process Safety Progress*, vol. 35, no. 3, pp. 221–227, 2016.

[29] H. Risher, *Emerging Model for Salary Management*, Public Management, 1997.

[30] S. Zhang, "Analysis of salary management in state-owned enterprises," *Management & Technology of Sme*, 2017.

[31] K. Ritzberger and J. W. Weibull, "Evolutionary selection in normal-form games," *Econometrica*, vol. 63, no. 6, pp. 1371–1399, 1995.

[32] N. B. Khalifa, R. El-Azouzi, Y. Hayel, and I. Mabrouki, "Evolutionary games in interacting communities," *Dynamic Games and Applications*, vol. 7, no. 2, pp. 1–26, 2016.

[33] K. Lee, H.-M. Kwon, S. Cho, J. Kim, and I. Moon, "Improvements of safety management system in Korean chemical industry after a large chemical accident," *Journal of Loss Prevention in the Process Industries*, vol. 42, no. 8, pp. 6–13, 2016.

[34] S. Kortmann, C. Gelhard, C. Zimmermann, and F. T. Piller, "Linking strategic flexibility and operational efficiency: The mediating role of ambidextrous operational capabilities," *Journal of Operations Management*, vol. 32, no. 7-8, pp. 475–490, 2014.

[35] C. Yin, S. Dadras, X. Huang, J. Mei, H. Malek, and Y. Cheng, "Energy-saving control strategy for lighting system based on multivariate extremum seeking with Newton algorithm," *Energy Conversion and Management*, vol. 142, pp. 504–522, 2017.

[36] C. Yin, X. Huang, S. Dadras et al., "Design of optimal lighting control strategy based on multi-variable fractional-order extremum seeking method," *Information Sciences*, vol. 465, pp. 38–60, 2018.

Research Article

Dynamics Induced by Delay in a Nutrient-Phytoplankton Model with Multiple Delays

Chuanjun Dai,[1,2] **Hengguo Yu** (iD)**,**[3] **Qing Guo,**[4] **He Liu,**[4] **Qi Wang,**[1,2] **Zengling Ma,**[1,2] **and Min Zhao** (iD)[1,2]

[1]*Zhejiang Provincial Key Laboratory for Water Environment and Marine Biological Resources Protection, Wenzhou University, Wenzhou, Zhejiang, 325035, China*

[2]*College of Life and Environmental Science, Wenzhou University, Wenzhou, Zhejiang, 325035, China*

[3]*College of Mathematics, Physics and Electronic Information Engineering, Wenzhou University, Wenzhou, Zhejiang, 325035, China*

[4]*Environmental Engineering Program, University of Northern British Columbia, Prince George, British Columbia, V2N 4Z9, Canada*

Correspondence should be addressed to Min Zhao; zmcn@tom.com

A nutrient-phytoplankton model with multiple delays is studied analytically and numerically. The aim of this paper is to study how the delay factors influence dynamics of interaction between nutrient and phytoplankton. The analytical analysis indicates that the positive equilibrium is always globally asymptotically stable when the delay does not exist. On the contrary, the positive equilibrium loses its stability via Hopf instability induced by delay and then the corresponding periodic solutions emerge. Especially, the stability switches for positive equilibrium occur as the delay is increased. Furthermore, the numerical simulations show that periodic-2 and periodic-3 solutions can appear due to the existence of delays. Numerical results are consistent with the analytical results. Our results demonstrate that the delay has a great impact on the nutrient-phytoplankton dynamics.

1. Introduction

Some phytoplankton, for example, Cyanobacteria, can form dense and sometimes toxic blooms in freshwater and marine environments, which threaten ecological balance, drinking water, fisheries, and even human health [1]. However, the mechanism, by which phytoplankton blooms occur, is currently not very clear, which contribute to the difficulty to prevent or mitigate the proliferation of phytoplankton blooms. These have stimulated lots of researches aiming to understand the growth mechanisms of phytoplankton.

In recent years, dynamics in phytoplankton growth have drawn increasing attention from experimental ecologists, as well as mathematical ecologists. Some results from experiments and field observations imply that many factors affecting the dynamics of phytoplankton growth are bound to exist, such as nutrient [2], light [3], temperature [4], iron supply [5], zooplankton [6]. Especially, due to the effects of limiting factors including temperature, light, and day length, it has been indicated by Rhee and Gotham [7] that the population dynamics of phytoplankton in aquatic environments can change with season, latitude, and depth. Among factors affecting phytoplankton growth, nutrient has been an essential element [8–10], mainly including nitrogen and phosphate. Results reported by Ryther [11] indicated that phytoplankton indeed consumes lots of nitrogen and phosphate in their growth process, but reducing the nitrogen content in aquatic cannot slow the eutrophication. Using data from 17 lakes, Smith [8] analysed the influence of ratio of total nitrogen to phosphorus on the growth of blue-green algae (Cyanophya) and showed that controlling the ratio can help us improve the quality of aquatic environment very well. Obviously, the production process of phytoplankton is more complex.

However, due to the complexity and nonlinearity of aquatic ecosystem, there are some difficulties in understanding nutrient-phytoplankton dynamics only depending on experiment or field observation, which makes it necessary

to use models to provide quantitative insights into dynamic mechanism of phytoplankton growth. For different aquatic environments, we can use various modifications of the classical prey-predator models by introducing functional responses to model nutrient-phytoplankton dynamics [12–14]. For example, Huppert et al. [15] describe the dynamics of nutrient-driven phytoplankton blooms by a simple model and identify, using the model analysis, an important threshold effect that a bloom will only be triggered when nutrients exceed a certain defined level. Additionally, most nutrient-phytoplankton models reveal that phytoplankton population and nutrient population can coexist at equilibrium globally under some conditions [16, 17]. However, Sherratt and Smith [18] have reported that a constant population density may not exist in reality because of the existence of some factors, such as noise and physical factors. Actually, experiments and field observations show that the changes of phytoplankton population density usually possess oscillatory behaviour [19, 20].

For the single cell phytoplankton species, in most studies of nutrient-phytoplankton models, it is usually assumed that the processes, such as conversion process of nutrient, in the dynamics of phytoplankton growth are instantaneous [14–17, 19–23]. It may be doubtful whether there exists the delay in the growth of phytoplankton over the large area or not. Yet, J. Caperon [24] studied time lag in population growth response of *Isochrysis galbana*, a phytoplankton species, to a variable nitrate environment by both experiments and model, and demonstrated the existence of delay in the growth of *Isochrysis galbana*. Hence, the delay may indeed exist in the phytoplankton growth, which means that it is necessary to consider delay in nutrient-phytoplankton models. An approach that has been attempted by researchers to model the dynamics of phytoplankton is the role of delay since delay appears as an important component in biosystems and ecosystems [25–30].

Actually, growing evidence shows that there exists time lag in some conversion processes from one state to another in some systems, and delay is an important factor because it can affect the dynamics of these systems. Volterra [31] considered time delay in a prey-predator model first and found oscillatory behaviour for the spatial distribution. For a long time, it has been recognized that delays can give rise to destabilizing effect of the dynamics of systems, where periodic solutions, as well as chaos, may emerge [32–35]. Models incorporating delays in diverse biological and ecological models are extensively studied [36–42]. Especially, the characteristic equation with respect to the linearized system of delay differential equations plays a key role in dynamic analysis, by which we can obtain some information on the stability of equilibrium. In addition, using the normal form theory, one can carry out the bifurcation analysis, such as the direction and stability of periodic solutions arising through Hopf bifurcation [43, 44].

The main purpose of this paper is to consider the effects of multiple delays on the nutrient-phytoplankton dynamics. In [15], Huppert et al. presented a simple model to investigate effect of nutrient on phytoplankton blooms, and much better results are obtained. Here, this model is extended into a "two

preys-one predator" type to describe nitrogen- phosphorus-phytoplankton dynamics, as follows:

$$\frac{dN}{dt} = I_1 - q_1 N - \alpha_1 N A$$

$$\frac{dP}{dt} = I_2 - q_2 P - \alpha_2 P A \qquad (1)$$

$$\frac{dA}{dt} = \beta_1 \alpha_1 N (t - \tau_1) A + \beta_2 \alpha_2 P (t - \tau_2) A - mA$$

where N, P, and A represent nitrogen, phosphorus, and phytoplankton population density at time t, respectively; I_1 is the nitrogen nutrients input flowing into the system and I_2 is the phosphorus nutrients input flowing into the system; q_1 is the loss rate of the nitrogen nutrients, and q_2 is the loss rate of the phosphorus nutrients; α_1 is nitrogen nutrient uptake rate of phytoplankton, and α_2 is phosphorus nutrient uptake rate of phytoplankton; β_1 and β_2 denote the efficiency of nutrient utilization; τ_1 and τ_2 are time delay parameters; m is the mortality rate of phytoplankton. Although the function, which describes nutrient uptake dynamics, is not a Michaelis-Menten function, but Lotka-Volterra type, Huppert et al. [15] have indicated that the Lotka-Volterra term is a good first approximation to the Michaelis-Menten type. From biological viewpoint, all parameters are nonnegative. $N(t)$, $P(t)$, and $A(t) \geq 0$ are continuous on $-\tau \leq t < 0$, where $\tau = \max(\tau_1, \tau_2)$ and $N(0)$, $P(0)$, and $A(0) > 0$.

The paper is organized as follows. In Section 2, we analyze the existence and stability of positive equilibrium in model (1) without delays. In Section 3, we discuss stability of positive equilibrium and Hopf bifurcation under five different cases for delay effect. Subsequently, the direction of bifurcation and the stability of periodic solutions arising through Hopf bifurcation are given in Section 4. In order to analyze further how delay effects influence nutrient-phytoplankton dynamics, a series of numerical simulations are carried out in Section 5. Finally, the paper ends with conclusion in Section 6.

2. Existence and Stability of Positive Equilibrium in Model (1) without Delays

In this section, it is presented first that the first octant is positive invariant in model (1) without delays and the following lemma holds.

Lemma 1. *All the solutions of model (1) with initial conditions that initiate in $\{R_+^3\}$ are positive invariant in the absence of delays.*

Proof. From the first equation of model (1), we have

$$\frac{dN}{dt} = I_1 - q_1 N - \alpha_1 N A \geq -(q_1 + \alpha_1 A) N. \qquad (2)$$

Hence, $N(t) \geq N(0) \exp[-\int_0^t (q_1 + \alpha_1 A) ds] > 0$ under $N(0) > 0$.

Likewise, from the second equation of model (1), we have $P(t) \geq P(0) \exp[-\int_0^t (q_2 + \alpha_2 A) ds] > 0$ under $P(0) > 0$.

In the absence of delays in model (1), from the third equation of model (1), if $A(0) > 0$, it can be obtained that

$$A(t) = A(0) \exp\left[\int_0^t (\beta_1 \alpha_1 N + \beta_2 \alpha_2 P - m)\, ds\right] > 0 \quad (3)$$

Obviously, all the solutions of model (1) without delays are positive invariant if the initial conditions initiate in $\{R_+^3\}$.

Then, we complete the proof. $\qquad\square$

For model (1), it is obvious that the extinction equilibrium, $(I_1/q_1, I_2/q_2, 0)$, exists. Moreover, in order to discuss the existence of positive equilibrium, the following function is defined:

$$f(x) = \alpha_1 \alpha_2 m x^2$$
$$+ \left[(mq_1 - \alpha_1 \beta_1 I_1)\alpha_2 + (mq_2 - \alpha_2 \beta_2 I_2)\alpha_1\right] x \quad (4)$$
$$+ (mq_1 q_2 - \beta_1 \alpha_1 I_1 q_2 - \beta_2 \alpha_2 I_2 q_1),$$

and then we can obtain

$$N^* = \frac{I_1}{q_1 + \alpha_1 A^*},$$
$$\quad (5)$$
$$P^* = \frac{I_2}{q_2 + \alpha_2 A^*},$$

where A^* is the positive root of (4).

For the function $f(x)$, we have $f(0) = 0$ when the condition, $m = (\beta_1 \alpha_1 I_1/q_1) + (\beta_2 \alpha_2 I_2/q_2)$, holds, and then there is no positive equilibrium in model (1). Obviously, $f(0) < 0$ holds if $m < (\beta_1 \alpha_1 I_1/q_1) + (\beta_2 \alpha_2 I_2/q_2)$, and then there exists a unique positive root with respect to $f(x) = 0$, which means that there exists a unique positive equilibrium in model (1) under this condition. However, when $m > (\beta_1 \alpha_1 I_1/q_1) + (\beta_2 \alpha_2 I_2/q_2)$, it can be verified directly that $f(0) > 0$ and $(mq_1 - \alpha_1 \beta_1 I_1)\alpha_2 + (mq_2 - \alpha_2 \beta_2 I_2)\alpha_1 > 0$, which implies that there is no positive equilibrium in model (1). Thus, summarizing these results, the following theorem can be obtained.

Theorem 2. *If $0 < m < (\beta_1 \alpha_1 I_1/q_1) + (\beta_2 \alpha_2 I_2/q_2)$ holds, then there exists a unique positive equilibrium in model (1); otherwise, there is no positive equilibrium in model (1) if $m \geq (\beta_1 \alpha_1 I_1/q_1) + (\beta_2 \alpha_2 I_2/q_2)$ holds.*

Letting the unique positive equilibrium be $E_* = (N^*, P^*, A^*)$, then the following theorem holds for model (1) without delays.

Theorem 3. *If the unique positive equilibrium exists in model (1) without delays, then it is globally asymptotically stable.*

Proof. We construct a Lyapunov function, as follows:

$$V = \beta_1 \int_{N^*}^{N} \frac{s - N^*}{s}\, ds + \beta_2 \int_{P^*}^{P} \frac{s - P^*}{s}\, ds$$
$$+ \int_{A^*}^{A} \frac{s - A^*}{s}\, ds \quad (6)$$

In the model (1) without delays,

$$\frac{dV}{dt} = \beta_1 \frac{N - N^*}{N}\frac{dN}{dt} + \beta_2 \frac{P - P^*}{P}\frac{dP}{dt} + \frac{A - A^*}{A}\frac{dA}{dt}$$
$$= \beta_1 \frac{N - N^*}{N}(I_1 - q_1 N - \alpha_1 NA) + \beta_2 \frac{P - P^*}{P}(I_2$$
$$- q_2 P - \alpha_2 PA) + \frac{A - A^*}{A}(\beta_1 \alpha_1 NA + \beta_2 \alpha_2 PA$$
$$- mA) = \beta_1 \frac{N - N^*}{N}((q_1 N^* + \alpha_1 N^* A^*)$$
$$\quad (7)$$
$$- (q_1 N + \alpha_1 NA)) + \beta_2 \frac{P - P^*}{P}((q_2 P^* + \alpha_2 P^* A^*)$$
$$- (q_2 P + \alpha_2 PA)) + \frac{A - A^*}{A}(\beta_1 \alpha_1 NA + \beta_2 \alpha_2 PA$$
$$- (\beta_1 \alpha_1 N^* + \beta_2 \alpha_2 P^*)A) = -\beta_1 (q_1 + \alpha_1 A^*)$$
$$\cdot \frac{(N - N^*)^2}{N} - \beta_2 (q_2 + \alpha_2 A^*)\frac{(P - P^*)^2}{P}$$

Obviously, $dV/dt \leq 0$ holds under existence of positive equilibrium and $dV/dt = 0$ holds if and only if $N = N^*$ and $P = P^*$. The largest invariant subset of the set of the point where $dV/dt = 0$ is $E_* = (N^*, P^*, A^*)$. Therefore, according to LaSalle's theorem, $E_* = (N^*, P^*, A^*)$ is globally asymptotically stable.

Then, we complete the proof. $\qquad\square$

Letting the extinction equilibrium be $E_0 = (N_0, P_0, 0) = (I_1/q_1, I_2/q_2, 0)$, then we can obtain the following theorem in model (1) in the absence of delay.

Theorem 4. *In the absence of delays, let $m^* = (\beta_1 \alpha_1 I_1/q_1) + (\beta_2 \alpha_2 I_2/q_2)$, so that*

(i) *if $m > m^*$, then the extinction equilibrium E_0 is locally asymptotically stable;*

(ii) *if $m < m^*$, then the extinction equilibrium E_0 is unstable;*

(iii) *if $m = m^*$, then the model (1) undergoes transcritical bifurcation at the extinction equilibrium E_0.*

Proof. For simplicity, let

$$f_w(X, m) = \begin{pmatrix} I_1 - q_1 N - \alpha_1 NA \\ I_2 - q_2 P - \alpha_2 PA \\ \beta_1 \alpha_1 NA + \beta_2 \alpha_2 PA - mA \end{pmatrix} \quad (8)$$

and $X = [N, P, A]^T$.

The Jacobian matrix at E_0 is

$$J(E_0) = \begin{pmatrix} -q_1 & 0 & -\dfrac{\alpha_1 I_1}{q_1} \\ 0 & -q_2 & -\dfrac{\alpha_2 I_2}{q_2} \\ 0 & 0 & -(m - m^*) \end{pmatrix}. \quad (9)$$

The eigenvalues are $-q_1, -q_2, -(m - m^*)$.

Obviously, if $m > m^*$, then the extinction equilibrium E_0 is locally asymptotically stable.

If $m < m^*$, then the extinction equilibrium E_0 is unstable. When $m = m^*$, the Jacobian matrix at E_0 is

$$J(E_0) = \begin{pmatrix} -q_1 & 0 & -\dfrac{\alpha_1 I_1}{q_1} \\ 0 & -q_2 & -\dfrac{\alpha_2 I_2}{q_2} \\ 0 & 0 & 0 \end{pmatrix}. \tag{10}$$

Then $J(E_0)$ has a geometrically simple zero eigenvalue with right eigenvector $\Phi = (\alpha_1 I_1 q_2^2, \alpha_2 I_2 q_1^2, -q_1^2 q_2^2)^T$ and left eigenvector $\Psi = (0, 0, 1)$.

Now

$$D_m f_w = \begin{pmatrix} 0 \\ 0 \\ -A \end{pmatrix} \tag{11}$$

and

$$\left(\Psi \left(D_X D_m f_w \right) \Phi \right)_{E_0} = q_1^2 q_2^2 \neq 0,$$

$$\Psi \left(\left(D_{XX} f_w \right) (\Phi, \Phi) \right)$$

$$= \left(\Psi \sum_{i=1}^{3} \left(e_i \Phi^T D_X \left(D_X f_i \right)^T \Phi \right) \right)_{E_0} \tag{12}$$

$$= -2 q_1^2 q_2^2 \left(\beta_1 I_1 \alpha_1^2 q_2^2 + \beta_2 I_2 \alpha_2^2 q_1^2 \right) \neq 0$$

According to [45], the model (1) undergoes transcritical bifurcation at the extinction equilibrium E_0 in the absence of delays.

Then, we complete the proof.   □

Actually, when $m > m^*$ holds, the positive equilibrium does not exist, and the extinction equilibrium E_0 is globally asymptotically stable. Then, the following theorem holds.

Theorem 5. *If* $m > (\beta_1 \alpha_1 I_1 / q_1) + (\beta_2 \alpha_2 I_2 / q_2)$ *holds, then the extinction equilibrium* $E_0 = (N_0, P_0, 0) = (I_1/q_1, I_2/q_2, 0)$ *is globally asymptotically stable.*

Proof. We construct a Lyapunov function, as follows:

$$V = \beta_1 \int_{N_0}^{N} \frac{s - N_0}{s} ds + \beta_2 \int_{P_0}^{P} \frac{s - P_0}{s} ds + A \tag{13}$$

In the model (1) without delays,

$$\frac{dV}{dt} = \beta_1 \frac{N - N_0}{N} \frac{dN}{dt} + \beta_2 \frac{P - P_0}{P} \frac{dP}{dt} + \frac{dA}{dt}$$

$$= \beta_1 \frac{N - N_0}{N} \left(I_1 - q_1 N - \alpha_1 N A \right)$$

$$+ \beta_2 \frac{P - P_0}{P} \left(I_2 - q_2 P - \alpha_2 PA \right)$$

$$+ \left(\beta_1 \alpha_1 NA + \beta_2 \alpha_2 PA - mA \right)$$

$$= \beta_1 \frac{N - N_0}{N} \left(q_1 N_0 - q_1 N - \alpha_1 NA \right)$$

$$+ \beta_2 \frac{P - P_0}{P} \left(q_2 P_0 - q_2 P - \alpha_2 PA \right)$$

$$+ \left(\beta_1 \alpha_1 NA + \beta_2 \alpha_2 PA - mA \right)$$

$$= -\beta_1 q_1 \frac{(N - N_0)^2}{N} - \beta_2 q_2 \frac{(P - P_0)^2}{P}$$

$$+ \left(\beta_1 \alpha_1 N_0 + \beta_2 \alpha_2 P_0 - m \right) A$$

$$= -\beta_1 q_1 \frac{(N - N_0)^2}{N} - \beta_2 q_2 \frac{(P - P_0)^2}{P}$$

$$+ \left(\frac{\beta_1 \alpha_1 I_1}{q_1} + \frac{\beta_2 \alpha_2 I_2}{q_2} - m \right) A \tag{14}$$

Obviously, $dV/dt < 0$ holds if $m > (\beta_1 \alpha_1 I_1 / q_1) + (\beta_2 \alpha_2 I_2 / q_2)$. Therefore, the extinction equilibrium $E_0 = (N_0, P_0, 0) = (I_1/q_1, I_2/q_2, 0)$ is globally asymptotically stable when $m > (\beta_1 \alpha_1 I_1 / q_1) + (\beta_2 \alpha_2 I_2 / q_2)$.

Then, we complete the proof.   □

3. Local Stability Analysis and the Hopf Bifurcation

In this section, we first state the following positive invariant theorem.

Lemma 6. *All the solutions of model (1) with initial conditions that initiate in* $\{R_+^3\}$ *are positive invariant.*

Proof. We consider (N, P, A) a noncontinuable solution of model (1); see [46], defined on $[-\tau, B)$, where $B \in (0, +\infty]$. Then we can use the method from [47] to prove that, for all $t \in [0, B)$, $N(t) > 0$, $P(t) > 0$, and $A(t) > 0$. Suppose that is not true. Then, there exists $0 < T < B$ such that, for all $t \in [0, T)$, $N(t) > 0$, $P(t) > 0$, and $A(t) > 0$ and either $N(T) = 0$, $P(T) = 0$, or $A(T) = 0$. According to Lemma 1, for all $t \in [0, T)$, we have

$$N(t) > N(0) \exp \left[-\int_0^t (q_1 + \alpha_1 A) ds \right],$$

$$P(t) > P(0) \exp \left[-\int_0^t (q_2 + \alpha_2 A) ds \right], \tag{15}$$

and

$$A(t) = A(0)$$

$$\cdot \exp \left[\int_0^t (\beta_1 \alpha_1 N(s - \tau_1) + \beta_2 \alpha_2 P(s - \tau_2) - m) ds \right]. \tag{16}$$

As (N, P, A) is defined and continuous on $[-\tau, T]$, there is a $M \geq 0$ such that, for all $t \in [-\tau, T)$,

$$N(t) > N(0) \exp\left[-\int_0^t (q_1 + \alpha_1 A)\, ds\right]$$

$$\geq N(0) \exp(-TM),$$

$$P(t) > P(0) \exp\left[-\int_0^t (q_2 + \alpha_2 A)\, ds\right] \tag{17}$$

$$\geq P(0) \exp(-TM)$$

and

$$A(t) = A(0)$$

$$\cdot \exp\left[\int_0^t (\beta_1 \alpha_1 N(s - \tau_1) + \beta_2 \alpha_2 P(s - \tau_2) - m)\, ds\right] \tag{18}$$

$$\geq A(0) \exp(-TM).$$

Taking the limit, as $t \longrightarrow T$, we can get

$$N(T) \geq N(0) \exp(-TM) > 0,$$

$$P(T) \geq P(0) \exp(-TM) > 0 \tag{19}$$

and

$$A(T) \geq A(0) \exp(-TM) > 0, \tag{20}$$

which contradicts the fact that either $N(T) = 0$, $P(T) = 0$, or $A(T) = 0$. Thus, for all $t \in [0, B)$, $N(t) > 0$, $P(t) > 0$, and $A(t) > 0$.

Therefore, all the solutions of model (1) are positive invariant if the initial conditions initiate in $\{R_+^3\}$.

Then, we complete the proof. □

Next, we will discuss the stability of the unique positive equilibrium and existence of Hopf bifurcation in model (1) for five different cases: $\tau_1 > 0, \tau_2 = 0$; $\tau_1 = 0, \tau_2 > 0$; $\tau_1 = \tau_2 = \tau$; $\tau_1 \in (0, \tau_{10}), \tau_2 > 0$; $\tau_1 > 0, \tau_2 \in (0, \tau_{20})$.

According to Theorem 2, let $u_1 = N(t) - N^*$, $u_2 = P(t) - P^*$, $u_3 = A(t) - A^*$; the linearized form of model (1) can be obtained as follows:

$$\dot{u}_1 = a_{11} u_1(t) + a_{13} u_3(t)$$

$$\dot{u}_2 = a_{22} u_2(t) + a_{23} u_3(t) \tag{21}$$

$$\dot{u}_3 = a_{31} u_1(t - \tau_1) + a_{32} u_2(t - \tau_2)$$

where

$$a_{11} = -q_1 - \alpha_1 A^*;$$

$$a_{13} = -\alpha_1 N^*;$$

$$a_{22} = -q_2 - \alpha_2 A^*;$$

$$a_{23} = -\alpha_2 P^*; \tag{22}$$

$$a_{31} = \beta_1 \alpha_1 A^*;$$

$$a_{32} = \beta_2 \alpha_2 A^*.$$

Then, we obtain the associated characteristic equation of model (21) as follows:

$$\lambda^3 + B\lambda^2 + C\lambda + D\lambda e^{-\lambda\tau_1} + E e^{-\lambda\tau_1} + F\lambda e^{-\lambda\tau_2}$$

$$+ G e^{-\lambda\tau_2} = 0, \tag{23}$$

where

$$B = -(a_{11} + a_{22});$$

$$C = a_{11} a_{22};$$

$$D = -a_{13} a_{31};$$

$$E = a_{13} a_{31} a_{22}; \tag{24}$$

$$F = -a_{23} a_{32};$$

$$G = a_{11} a_{23} a_{32}.$$

Case 1. $\tau_1 > 0, \tau_2 = 0$.

Due to $\tau_1 > 0, \tau_2 = 0$, (23) becomes

$$\lambda^3 + B\lambda^2 + (C + F)\lambda + (D\lambda + E)e^{-\lambda\tau_1} + G = 0. \tag{25}$$

Assuming $\lambda = i\omega_1(\omega_1 > 0)$ is the pure imaginary root of (25), then the following can be obtained:

$$-\omega_1^3 + (C + F)\omega_1 = E\sin(\omega_1\tau_1) - D\omega_1\cos(\omega_1\tau_1),$$

$$-B\omega_1^2 + G = -E\cos(\omega_1\tau_1) - D\omega_1\sin(\omega_1\tau_1), \tag{26}$$

Then

$$\omega_1^6 + \left(B^2 - 2(C + F)\right)\omega_1^4$$

$$+ \left((C + F)^2 - 2BG - D^2\right)\omega_1^2 + G^2 - E^2 = 0. \tag{27}$$

Now, we define a function as follows:

$$f_1(v_1) = v_1^3 + \left(B^2 - 2(C + F)\right)v_1^2$$

$$+ \left((C + F)^2 - 2BG - D^2\right)v_1 + G^2 - E^2. \tag{28}$$

(i) If $(H_{21}): G^2 - E^2 < 0$ holds, then, (28) has at least one positive root. Without loss of generality, we denote v_{11}, v_{12}, and v_{13} as the roots of (28); hence $\omega_{1k} = \sqrt{v_{1k}}$, $k = 1, 2, 3$, if $v_{1k} > 0$.

(ii) If $(H_{22}): G^2 - E^2 > 0$ holds, let $M_1 = B^2 - 2(C + F)$ and $M_2 = (C + F)^2 - 2BG - D^2$. When $\Delta = M_1^2 - 3M_2 \leq 0$, then (28) has no positive roots. However, when $\Delta > 0$, $f_1'(v_1) = 0$ has two real roots, denoted as

$$x_1^* = \frac{-M_1 + \sqrt{\Delta}}{3},$$

$$x_2^* = \frac{-M_1 - \sqrt{\Delta}}{3}. \tag{29}$$

Obviously, $\lim_{x \to +\infty} f_1(x) = +\infty$. If (H_{22}) and $\Delta = M_1^2 - 3M_2 > 0$ holds, then (28) has two positive real roots if and only if $x_1^* > 0$ and $f_1(x_1^*) < 0$. In addition, we denote two positive roots of (28) as χ_1 and χ_2; then, (27) has two positive roots, namely, $\omega_{1a} = \sqrt{\chi_1}$ and $\omega_{1b} = \sqrt{\chi_2}$. Furthermore, we can have the following results.

Proposition 7.

(i) *If* (H_{21}) *holds, then* (28) *has at least one positive root.*

(ii) *If* (H_{22}) *and* $\Delta = M_1^2 - 3M_2 \leq 0$ *holds, then,* (28) *has no positive root.*

(iii) *If* (H_{22}) *and* $\Delta = M_1^2 - 3M_2 > 0$ *holds, then,* (28) *has two positive roots if and only if* $x_1^* > 0$, *and* $f_1(x_1^*) < 0$.

Then, according to (26), *the critical delay can be obtained as follows:*

$$\tau_{1p}^j = \frac{1}{\omega_{1p}} \left(\arccos \frac{D\omega_{1p}^4 + (BE - (CD + DF))\omega_{1p}^2 - EG}{D^2\omega_{1p}^2 + E^2} \right.$$
$$\left. + 2j\pi \right), \quad j = 0, 1, 2, \ldots, \ p = 1, 2, 3, a, b \tag{30}$$

Letting $\tau_{10} = \min_{p=1,2,3,a,b} \tau_{1p}^0$, *from* [37] *we know that* $\mathrm{Re}(d\lambda/d\tau_1) \neq 0$ *also needs to be proved. Differentiating left side of* (26) *with respect to* τ_1, *we have*

$$\left(\frac{d\lambda}{d\tau_1} \right)^{-1} = \frac{3\lambda^2 + 2B\lambda + (C + F) + De^{-\lambda\tau_1}}{\lambda(D\lambda + E)e^{-\lambda\tau_1}} - \frac{\tau_1}{\lambda}, \tag{31}$$

so that the following can be obtained:

$$\mathrm{Re}\left(\frac{d\lambda}{d\tau_1} \right)^{-1}_{\lambda = i\omega_{10}} = \frac{\omega_{10}^2}{\Delta} f_1'\left(\omega_{10}^2\right), \tag{32}$$

where

$$\Delta = \left(-D\omega_{10}^2 \cos(\omega_{10}\tau_1) + E\omega_{10}\sin(\omega_{10}\tau_1)\right)^2$$
$$+ \left(E\omega_{10}\cos(\omega_{10}\tau_1) + D\omega_{10}^2\sin(\omega_{10}\tau_1)\right)^2. \tag{33}$$

If (i) in Proposition 7 and (H_{23}): $f_1'(\omega_{10}^2) \neq 0$ hold, then we have $\mathrm{Re}(d\lambda/d\tau_1)^{-1}_{\lambda = i\omega_{10}} \neq 0$. However, if (iii) in Proposition 7 holds, assuming $\tau_{1a}^j < \tau_{1b}^j$, then we obtain $f_1'(\chi_1) > 0$ and $f_1'(\chi_2) < 0$. Hence, we have $(d\,\mathrm{Re}\,\lambda(\tau)/d\tau)|_{\tau=\tau_{1a}^j} > 0$, $(d\,\mathrm{Re}\,\lambda(\tau)/d\tau)|_{\tau=\tau_{1b}^j} < 0$, and $j = 0, 1, 2, \ldots$. Therefore, we have the following results.

Theorem 8. *For model* (1) *with* $\tau_1 > 0$, $\tau_2 = 0$,

(i) *If* (H_{21}) *and* (H_{23}) *both hold, then the positive equilibrium* E_* *is locally asymptotically stable for* $\tau_1 \in (0, \tau_{10})$ *and Hopf bifurcation occurs at* $\tau_1 = \tau_{10}$.

(ii) *If* (ii) *in Proposition 7 holds, then the positive equilibrium* E_* *is locally asymptotically stable for all* $\tau_1 \geq 0$.

(iii) *If* (iii) *in Proposition 7 holds, there exists a nonnegative integer n, such that the positive equilibrium* E_* *is locally asymptotically stable whenever* $\tau_1 \in [0, \tau_{1a}^0) \cup (\tau_{1b}^0, \tau_{1a}^1) \cup \cdots \cup (\tau_{1b}^{n-1}, \tau_{1a}^n)$ *and is unstable whenever* $\tau_1 \in [\tau_{1a}^0, \tau_{1b}^0) \cup (\tau_{1a}^1, \tau_{1b}^1) \cup \cdots \cup (\tau_{1a}^{n-1}, \tau_{1b}^{n-1}) \cup (\tau_{1a}^n, +\infty)$. *Then, model* (1) *undergoes Hopf bifurcation around* E_* *at every* $\tau_1 = \tau_{1a}^j$ *and* τ_{1b}^j, $j = 0, 1, 2, \ldots$.

Case 2. $\tau_1 = 0, \tau_2 > 0$.

Since $\tau_1 = 0, \tau_2 > 0$, (23) becomes

$$\lambda^3 + B\lambda^2 + (C + D)\lambda + (F\lambda + G)e^{-\lambda\tau_2} + E = 0. \tag{34}$$

Similar to Case 1, let $\lambda = i\omega_2 (\omega_2 > 0)$ be the pure imaginary root of (34); then we obtain

$$-\omega_2^3 + (C + D)\omega_2 = G\sin(\omega_2\tau_2) - F\omega_2\cos(\omega_2\tau_2),$$
$$-B\omega_2^2 + E = G\cos(\omega_2\tau_2) - F\omega_2\sin(\omega_2\tau_2). \tag{35}$$

That is,

$$\omega_2^6 + \left(B^2 - 2(C + D)\right)\omega_2^4$$
$$+ \left((C + D)^2 - 2BE - F^2\right)\omega_2^2 + E^2 - G^2 = 0. \tag{36}$$

Letting $v_2 = \omega_2^2$, we define the following function:

$$f_2(v_2) = v_2^3 + \left(B^2 - 2(C + D)\right)v_2^2$$
$$+ \left((C + D)^2 - 2BE - F^2\right)v_2 + E^2 - G^2. \tag{37}$$

(i) If (H_{31}): $E^2 - G^2 < 0$ holds, then (37) has at least one positive root. Without loss of generality, we denote v_{21}, v_{22}, v_{23} as the roots of (37); then $\omega_{2k} = \sqrt{v_{2k}}$, $k = 1, 2, 3$, if $v_{2k} > 0$.

(ii) If (H_{32}): $E^2 - G^2 > 0$ holds, let $M_1 = B^2 - 2(C + D)$ and $M_2 = (C + D)^2 - 2BE - F^2$. When $\Delta = M_1^2 - 3M_2 \leq 0$, then (37) has no positive roots. However, when $\Delta > 0$, $f_2'(v_2) = 0$ has two real roots, denoted as

$$x_1^{**} = \frac{-M_1 + \sqrt{\Delta}}{3},$$
$$x_2^{**} = \frac{-M_1 - \sqrt{\Delta}}{3}. \tag{38}$$

Obviously, $\lim_{x \to +\infty} f_2(x) = +\infty$. If (H_{32}) and $\Delta = M_1^2 - 3M_2 > 0$ holds, then (37) has two positive real roots if and only if $x_1^{**} > 0$ and $f_2(x_1^{**}) < 0$. In addition, we denote two positive roots of (37) as χ_1^* and χ_2^*; then (36) has two positive roots, namely, $\omega_{2a} = \sqrt{\chi_1^*}$ and $\omega_{2b} = \sqrt{\chi_2^*}$. Furthermore, we can obtain the following results.

Proposition 9.

(i) *If* (H_{31}) *holds, then* (36) *has at least one positive root.*

(ii) *If* (H_{32}) *and* $\Delta = M_1^2 - 3M_2 \leq 0$ *holds, then,* (36) *has no positive root.*

(iii) If (H_{32}) and $\Delta = M_1{}^2 - 3M_2 > 0$ holds, then, (36) has two positive roots if and only if $x_1^{**} > 0$ and $f_2(x_1^{**}) < 0$.

Then the critical delay can be derived by (35):

$$\tau_{2p}^j = \frac{1}{\omega_{2p}} \left(\arccos \frac{D\omega_{2p}^4 + (BE - (CD + DF))\omega_{2p}^2 - EG}{D^2\omega_{2p}^2 + E^2} + 2j\pi \right), \quad j = 0, 1, 2, \ldots, \quad p = 1, 2, 3, a, b \tag{39}$$

Let $\tau_{20} = \min_{p=1,2,3,a,b} \tau_{2p}^0$. Differentiating left side of (34) with respect to τ_2, we obtain

$$\left(\frac{d\lambda}{d\tau_2} \right)^{-1} = \frac{3\lambda^2 + 2B\lambda + (C + D) + Fe^{-\lambda\tau_2}}{\lambda(F\lambda + G)e^{-\lambda\tau_2}} - \frac{\tau_2}{\lambda}, \tag{40}$$

Hence, we obtain the following:

$$\operatorname{Re} \left(\frac{d\lambda}{d\tau_2} \right)^{-1}_{\lambda = i\omega_{20}} = \frac{\omega_{20}^2}{\Delta} f_2{}'\left(\omega_{20}^2 \right), \tag{41}$$

where

$$\Delta = \left(-F\omega_{20}^2 \cos(\omega_{20}\tau_2) + G\omega_{20} \sin(\omega_{20}\tau_2) \right)^2 + \left(G\omega_{20} \cos(\omega_{20}\tau_2) + F\omega_{20}^2 \sin(\omega_{20}\tau_2) \right)^2. \tag{42}$$

If (i) in Proposition 9 and $(H_{33}): f_2{}'(\omega_{20}^2) \neq 0$ both hold, then $\operatorname{Re}(d\lambda/d\tau_2)^{-1}_{\lambda=i\omega_{20}} \neq 0$ is obtained. However, if (iii) in Proposition 9 holds, assuming $\tau_{2a}^j < \tau_{2b}^j$, we obtain $f_2{}'(\chi_1^*) > 0$ and $f_2{}'(\chi_2^*) < 0$. Then, we have $(d\operatorname{Re}\lambda(\tau)/d\tau)|_{\tau=\tau_{2a}^j} > 0$, $(d\operatorname{Re}\lambda(\tau)/d\tau)|_{\tau=\tau_{2b}^j} < 0$, and $j = 0, 1, 2, \ldots$. Therefore, we have the following theorem.

Theorem 10. *For model (1) with $\tau_1 = 0$, $\tau_2 > 0$,*

(i) *If H_{31} and H_{33} hold, then, the positive equilibrium E_* is locally asymptotically stable for $\tau_2 \in (0, \tau_{20})$ and Hopf bifurcation occur at $\tau_2 = \tau_{20}$.*

(ii) *If (ii) in Proposition 9 holds, then the positive equilibrium E_* is locally asymptotically stable for all $\tau_2 \geq 0$.*

(iii) *If (iii) in Proposition 9 holds, then there exists a nonnegative integer n, such that the positive equilibrium E_* is locally asymptotically stable whenever $\tau_2 \in [0, \tau_{2a}^0) \cup (\tau_{2b}^0, \tau_{2a}^1) \cup \cdots \cup (\tau_{2b}^{n-1}, \tau_{2a}^n)$ and is unstable whenever $\tau_2 \in [\tau_{2a}^0, \tau_{2b}^0) \cup (\tau_{2a}^1, \tau_{2b}^1) \cup \cdots \cup (\tau_{2a}^n, \tau_{2b}^{n-1}) \cup (\tau_{2a}^n, +\infty)$. Then, model (1) undergoes Hopf bifurcation around E_* for every $\tau_2 = \tau_{2a}^j$ and τ_{2b}^j, $j = 0, 1, 2, \ldots$.*

Case 3. $\tau_1 = \tau_2 = \tau$.
When $\tau_1 = \tau_2 = \tau$, (23) becomes

$$\lambda^3 + B\lambda^2 + C\lambda + (D + F)\lambda e^{-\lambda\tau} + (E + G)e^{-\lambda\tau} = 0. \tag{43}$$

Leting $\lambda = i\omega_3 (\omega_3 > 0)$ be the pure imaginary root of (43), then

$$-\omega_3^3 + C\omega_3 = (E + G)\sin(\omega_3\tau)$$
$$- (D + F)\omega_3 \cos(\omega_3\tau),$$
$$-B\omega_3^2 = -(E + G)\cos(\omega_3\tau)$$
$$- (D + F)\omega_3 \sin(\omega_3\tau), \tag{44}$$

that is,

$$\omega_3^6 + \left(B^2 - 2C \right)\omega_3^4 + \left[C^2 - (D + F)^2 \right]\omega_3^2 - (E + G)^2 = 0. \tag{45}$$

Let $v_3 = \omega_3^2$ and define the following function:

$$f_3(v_3) = v_3^3 + \left(B^2 - 2C \right)v_3^2 + \left[C^2 - (D + F)^2 \right]v_3 - (E + G)^2, \tag{46}$$

From (46), we can clearly see that $f_3(0) = -(E + G)^2 < 0$; hence (46) has at least one positive root. Without loss of generality, we denote v_{31}, v_{32}, and v_{33} as the roots of (46); then we have $\omega_{3k} = \sqrt{v_{3k}}$, $k = 1, 2, 3$, if $v_{3k} > 0$ holds. Hence, the critical delay can be derived by (44):

$$\tau_{3k}^j = \frac{1}{\omega_{3k}} \left(\arccos \frac{(D + F)\omega_{3k}^4 + B(E + G)\omega_{3k}^2 - C(D + F)\omega_{3k}^2}{(D + F)^2 \omega_{3k}^2 + (E + G)^2} + 2\pi j \right), \quad (j = 0, 1, 2 \ldots, \ k = 1, 2, 3). \tag{47}$$

Let $\tau_{30} = \min_{k=1,2,3} \tau_{3k}^0$. Differentiating left side of (43) with respect to τ, we obtain

$$\left(\frac{d\lambda}{d\tau} \right)^{-1} = \frac{3\lambda^2 + 2B\lambda + C + (D + F)e^{-\lambda\tau}}{\lambda[(D + F)\lambda + (E + G)]e^{-\lambda\tau}} - \frac{\tau}{\lambda}. \tag{48}$$

Hence, we obtain the following:

$$\operatorname{Re} \left(\frac{d\lambda}{d\tau} \right)^{-1}_{\lambda = i\omega_{30}} = \frac{\omega_{30}^2}{\Delta} f_3{}'\left(\omega_{30}^2 \right), \tag{49}$$

where

$$\Delta = \left(-(D + F)\omega_{30}^2 \cos(\omega_{30}\tau) + (E + G)\omega_{30} \sin(\omega_{30}\tau) \right)^2 + \left((E + G)\omega_{30} \cos(\omega_{30}\tau) + (D + F) \cdot \omega_{30}^2 \sin(\omega_{30}\tau) \right)^2. \tag{50}$$

If (H_{41}): $f_3'(\omega_{30}^2) \neq 0$ holds, then $\mathrm{Re}(d\lambda/d\tau)_{\lambda=i\omega_{30}}^{-1} \neq 0$ is obtained; hence, we have the following result.

Theorem 11. *For model (1), when $\tau_1 = \tau_2 = \tau$, if (H_{41}) holds, then the positive equilibrium E_* is locally asymptotically stable for $\tau \in (0, \tau_{30})$ and Hopf bifurcation occurs at $\tau = \tau_{30}$.*

Case 4. $\tau_1 \in (0, \tau_{10})$, $\tau_2 > 0$.

Under this case, τ_2 is considered as a parameter. The same as Case 1, let $\lambda = i\omega_2^*$ be the root of (23); then we have the following:

$$R_{51} \cos(\omega_2^* \tau_2) - R_{52} \sin(\omega_2^* \tau_2) = R_{53},$$
$$R_{51} \sin(\omega_2^* \tau_2) + R_{52} \cos(\omega_2^* \tau_2) = R_{54}, \tag{51}$$

where

$$R_{51} = F\omega_2^*;$$
$$R_{53} = \omega_2^{*3} - C\omega_2^* - D\omega_2^* \cos(\omega_2^* \tau_1) + E \sin(\omega_2^* \tau_1);$$
$$R_{52} = G; \tag{52}$$
$$R_{54} = B\omega_2^{*2} - D\omega_2^* \sin(\omega_2^* \tau_1) - E \cos(\omega_2^* \tau_1).$$

According to (51), the following holds:

$$F_1(\omega_2^*) + F_2(\omega_2^*) \sin(\omega_2^* \tau_1) + F_3(\omega_2^*) \cos(\omega_2^* \tau_1)$$
$$= 0, \tag{53}$$

where

$$F_1(\omega_2^*) = \omega_2^{*6} + (B^2 - 2C)\omega_2^{*4}$$
$$+ (C^2 + D^2 - F^2)\omega_2^{*2} + (E^2 - G^2), \tag{54}$$
$$F_2(\omega_2^*) = 2(E - BD)\omega_2^{*3} - 2CE\omega_2^*,$$
$$F_3(\omega_2^*) = -2D\omega_2^{*4} + 2(CD - BE)\omega_2^{*2}.$$

Assuming (H_{51}): (53) has finite positive root and denoting as ω_{2k}^*, $(k = 1, 2, \ldots, l_1)$, then the critical value can be represented as follows:

$$\tau_{2k}^{*\,(j)}$$
$$= \frac{1}{\omega_{2k}^*} \left(\arccos\left(\frac{R_{51} \cdot R_{53} + R_{52} \cdot R_{54}}{R_{51}^2 + R_{52}^2} \right) + 2\pi j \right), \tag{55}$$
$$(j = 0, 1, 2 \ldots; \ k = 1, 2, \ldots l_1).$$

Let $\tau_{20}^* = \min \tau_{2k}^{*\,(0)}$, $(k = 1, 2, \ldots l_1)$. Differentiating left side of (23) with respect to τ_2, the following is obtained:

$$\left(\frac{d\lambda}{d\tau_2} \right)^{-1}$$
$$= \frac{3\lambda^2 + 2B\lambda + C + (D - D\lambda\tau_1 - \tau_1 E)e^{-\lambda\tau_1} + Fe^{-\lambda\tau_2}}{\lambda(F\lambda + G)e^{-\lambda\tau_2}} \tag{56}$$
$$- \frac{\tau_2}{\lambda},$$

and then, we have

$$\mathrm{Re}\left(\frac{d\lambda}{d\tau_2} \right)_{\lambda=i\omega_{20}^*}^{-1} = \frac{F_{51}F_{53} + F_{54}F_{52}}{F_{51}^2 + F_{52}^2}, \tag{57}$$

where

$$F_{51} = -F\omega_{20}^{*2} \cos(\omega_{20}^* \tau_{20}) + G\omega_{20}^* \sin(\omega_{20}^* \tau_{20}),$$
$$F_{52} = G\omega_{20}^* \cos(\omega_{20}^* \tau_{20}) + F\omega_{20}^{*2} \sin(\omega_{20}^* \tau_{20}),$$
$$F_{53} = -3\omega_{20}^{*2} + C + D \cos(\omega_{20}^* \tau_1) - \tau_1 E \cos(\omega_{20}^* \tau_1)$$
$$- \tau_1 D\omega_{20}^* \sin(\omega_{20}^* \tau_1) + F \cos(\omega_{20}^* \tau_{20}), \tag{58}$$
$$F_{54} = 2B\omega_{20}^* - D \sin(\omega_{20}^* \tau_1) + \tau_1 E \sin(\omega_{20}^* \tau_1)$$
$$- \tau_1 D\omega_{20}^* \cos(\omega_{20}^* \tau_1) - F \sin(\omega_{20}^* \tau_{20}).$$

Supposing (H_{52}): $F_{51}F_{53} + F_{54}F_{52} \neq 0$, then we have the following.

Theorem 12. *For model (1), when $\tau_1 \in (0, \tau_{10})$ and $\tau_2 > 0$, if both H_{51} and H_{52} hold, then the positive equilibrium E_* is locally asymptotically stable for $\tau_2 \in (0, \tau_{20}^*)$ and Hopf bifurcation occurs at $\tau_2 = \tau_{20}^*$.*

Case 5. $\tau_1 > 0$, $\tau_2 \in (0, \tau_{20})$.

Since $\tau_1 > 0$, $\tau_2 \in (0, \tau_{20})$, we consider τ_1 as a parameter. The same as Case 4, letting $\lambda = i\omega_1^*$ be the root of (23), we obtain:

$$R_{61} \cos(\omega_1^* \tau_1) - R_{62} \sin(\omega_1^* \tau_1) = R_{63},$$
$$R_{61} \sin(\omega_1^* \tau_1) + R_{62} \cos(\omega_1^* \tau_1) = R_{64}, \tag{59}$$

where

$$R_{61} = D\omega_1^*;$$
$$R_{63} = \omega_1^{*3} - C\omega_1^* - F\omega_1^* \cos(\omega_1^* \tau_2) + G \sin(\omega_1^* \tau_2);$$
$$R_{62} = E; \tag{60}$$
$$R_{64} = B\omega_1^{*2} - F\omega_1^* \sin(\omega_1^* \tau_2) - G \cos(\omega_1^* \tau_2).$$

According to (59), the following holds:

$$G_1(\omega_1^*) + G_2(\omega_1^*) \sin(\omega_1^* \tau_2) + G_3(\omega_1^*) \cos(\omega_1^* \tau_2)$$
$$= 0, \tag{61}$$

where

$$G_1(\omega_1^*) = \omega_1^{*6} + (B^2 - 2C)\omega_1^{*4}$$
$$+ (C^2 + F^2 - D^2)\omega_1^{*2} + (G^2 - E^2), \tag{62}$$
$$G_2(\omega_1^*) = 2(G - BF)\omega_1^{*3} - 2CG\omega_1^*,$$
$$G_3(\omega_1^*) = -2F\omega_1^{*4} + 2(CF - BG)\omega_2^{*2}.$$

Supposing (H_{61}): (61) has finite positive root ω_{2k}^*, $(k = 1, 2, \ldots, l_2)$, then we obtain

$$\tau_{1k}^{*\ (j)}$$

$$= \frac{1}{\omega_{1k}^*}\left(\arccos\left(\frac{R_{61}\cdot R_{63} + R_{62}\cdot R_{64}}{R_{61}^2 + R_{62}^2}\right) + 2\pi j\right), \quad (63)$$

$$(j = 0, 1, 2\ldots;\ k = 1, 2, \ldots l_2).$$

Assuming $\tau_{10}^* = \min \tau_{1k}^{*\ (0)}$, $(k = 1, 2, \ldots l_2)$ and differentiating left side of (23) with respect to τ_1, therefore, the following is obtained:

$$\left(\frac{d\lambda}{d\tau_1}\right)^{-1}$$

$$= \frac{3\lambda^2 + 2B\lambda + C + (F - F\lambda\tau_2 - \tau_2 G)\,e^{-\lambda\tau_2} + D e^{-\lambda\tau_1}}{\lambda\,(F\lambda + G)\,e^{-\lambda\tau_2}} \quad (64)$$

$$- \frac{\tau_1}{\lambda},$$

Hence, we have

$$\mathrm{Re}\left(\frac{d\lambda}{d\tau_1}\right)^{-1}_{\lambda = i\omega_{10}^*} = \frac{F_{61}F_{63} + F_{64}F_{62}}{F_{61}^2 + F_{62}^2}, \quad (65)$$

where

$$F_{61} = -D\omega_{10}^{*\ 2}\cos\left(\omega_{10}^*\tau_{10}^*\right) + E\omega_{10}^*\sin\left(\omega_{10}^*\tau_{10}^*\right),$$

$$F_{62} = E\omega_{10}^*\cos\left(\omega_{10}^*\tau_{10}^*\right) + D\omega_{10}^{*\ 2}\sin\left(\omega_{10}^*\tau_{10}^*\right),$$

$$F_{63} = -3\omega_{10}^{*\ 2} + C + D\cos\left(\omega_{10}^*\tau_{10}^*\right) - \tau_2 G\cos\left(\omega_{10}^*\tau_2\right)$$

$$\quad - \tau_2 F\omega_{10}^*\sin\left(\omega_{10}^*\tau_2\right) + F\cos\left(\omega_{10}^*\tau_2\right),$$

$$F_{64} = 2B\omega_{10}^* - D\sin\left(\omega_{10}^*\tau_{10}^*\right) + \tau_2 G\sin\left(\omega_{10}^*\tau_2\right)$$

$$\quad - \tau_2 F\omega_{10}^*\cos\left(\omega_{10}^*\tau_2\right) - F\sin\left(\omega_{10}^*\tau_2\right),$$

$$(66)$$

Supposing (H_{62}): $F_{61}F_{63} + F_{64}F_{62} \neq 0$ holds, then we obtain the following theorem.

Theorem 13. *For model (1), when $\tau_1 > 0$ and $\tau_2 \in (0, \tau_{20})$, if both H_{61} and H_{62} hold, then the positive equilibrium E_* is locally asymptotically stable for $\tau_1 \in (0, \tau_{10}^*)$ and Hopf bifurcation occurs at $\tau_1 = \tau_{10}^*$.*

4. Properties of Periodic Solution

In this section, we will discuss the direction of Hopf bifurcation and the stability of the bifurcating periodic solutions under Case 4 by using normal form method and center manifold theorem [43], and methods of other four cases are similar to Case 4. Assuming $\tau_1 \in (0, \tau_{10})$, $\tau_{20}^* > \tau_1$, and Hopf bifurcation occurs at (N^*, P^*, A^*) in model (1) when $\tau = \tau_{20}^*$.

Let $\tau_2 = \tau_{20}^* + \mu$, $t = s\tau_2$, $x(s\tau_2) = \hat{x}(s)$, $y(s\tau_2) = \hat{y}(s)$, and $z = (s\tau_2) = \hat{z}(s)$, and we also denote $\hat{x}(s)$, $\hat{y}(s)$, and $\hat{z}(s)$

as $x(s)$, $y(s)$, and $z(s)$. Then, model (1) could be rewritten as follows in $C = C([-1, 0], R^3)$:

$$\dot{u}(t) = L_\mu(u_t) + f(\mu, u_t), \quad (67)$$

where $u(t) = (x(t), y(t), z(t))^T \in R^3$. $L_\mu(\phi) : C \longrightarrow R^3$ and $f(\mu, u(t))$ are given as follows:

$$L_\mu(\phi)$$

$$= (\tau_{20}^* + \mu)\left(A\phi(0) + B\phi\left(-\frac{\tau_1}{\tau_{20}^*}\right) + C\phi(-1)\right), \quad (68)$$

$$f(\mu, \phi) = (\tau_{20}^* + \mu)\,(f_1\ \ f_2\ \ f_3)^T,$$

where

$$A = \begin{pmatrix} a_{11} & 0 & a_{13} \\ 0 & a_{22} & a_{23} \\ 0 & 0 & 0 \end{pmatrix},$$

$$B = \begin{pmatrix} 0 & 0 & 0 \\ 0 & 0 & 0 \\ a_{31} & 0 & 0 \end{pmatrix},$$

$$C = \begin{pmatrix} 0 & 0 & 0 \\ 0 & 0 & 0 \\ 0 & a_{32} & 0 \end{pmatrix}, \quad (69)$$

$$f_1 = -\alpha_1\phi_1(0)\,\phi_3(0),$$

$$f_2 = -\alpha_2\phi_2(0)\,\phi_3(0),$$

$$f_3 = \beta_1\alpha_1\phi_1\left(-\frac{\tau_1}{\tau_{20}^*}\right)\phi_3(0) + \beta_2\alpha_2\phi_2(-1)\,\phi_3(0).$$

According to the Riesz representation theorem, we know that there exists a function $\eta(\theta, \mu)$ of bounded variation for $\theta \in [-1, 0]$ such that $L_\mu\phi = \int_{-1}^{0} d\eta(\theta, \mu)\phi(\theta)$, for all $\phi \in C([-1, 0], R^3)$. Choosing

$$\eta(\theta, \mu)$$

$$= \begin{cases} (\tau_{20}^* + \mu)\,(A + B + C), & \theta = 0 \\[2mm] (\tau_{20}^* + \mu)\,(B + C), & \theta \in \left[-\dfrac{\tau_1}{\tau_{20}^*}, 0\right) \\[2mm] (\tau_{20}^* + \mu)\,C, & \theta \in \left(-1, -\dfrac{\tau_1}{\tau_{20}^*}\right) \\[2mm] 0, & \theta = -1 \end{cases} \quad (70)$$

For $\phi \in C^1([-1, 0], R^3)$, we define

$$A(\mu)\phi = \begin{cases} \dfrac{d\phi(\theta)}{d\theta}, & \theta \in [-1, 0) \\ \displaystyle\int_{-1}^{0} d\eta(\mu, s) \cdot \phi(s), & \theta = 0 \end{cases} \tag{71}$$

$$R(\mu)\phi = \begin{cases} 0, & \theta \in [-1, 0) \\ f(\mu, \phi), & \theta = 0 \end{cases}$$

Then, model (1) can be rewritten as

$$\dot{u}(t) = A(\mu)u_t + R(\mu)u_t. \tag{72}$$

For $\psi \in C^1([0, 1], (R^3)^*)$, the adjoint operator A^* of A is defined as follows:

$$A^*\psi(s) = \begin{cases} -\dfrac{d\psi(s)}{ds}, & s \in (0, 1], \\ \displaystyle\int_{-1}^{0} d\eta^T(t, 0)\psi(-t), & s = 0. \end{cases} \tag{73}$$

Associated with a bilinear inner product

$$\langle \psi(s), \phi(\theta) \rangle = \overline{\psi}(0)\phi(0) \\ - \int_{-1}^{0} \int_{\xi=0}^{\theta} \overline{\psi}(\xi - \theta) d\eta(\theta)\phi(\xi) d\xi, \tag{74}$$

where $\eta(\theta) = \eta(\theta, 0)$ and we know that $\pm i\omega_{20}^* \tau_{20}^*$ are the eigenvalues of $A(0)$ and $A^*(0)$.

Choose $q(\theta) = (1, q_2, q_3)^T e^{i\omega_{20}^* \tau_{20}^* \theta}$ to be the eigenvector of $A(0)$ corresponding to the eigenvalue $i\omega_{20}^* \tau_{20}^*$ and $q^*(s) = D(1, q_2^*, q_3^*)e^{i\omega_{20}^* \tau_{20}^* s}$ to be the eigenvector of $A^*(0)$ corresponding to the eigenvalue $-i\omega_{20}^* \tau_{20}^*$. By computation, we obtain

$$q_2 = \frac{a_{23}(i\omega_{20}^* - a_{11})}{a_{13}(i\omega_{20}^* - a_{22})};$$

$$q_3 = \frac{i\omega_{20}^* - a_{11}}{a_{13}};$$

$$q_2^* = \frac{a_{32}e^{i\omega_{20}^* \tau_1}(a_{11} + i\omega_2^*)}{a_{31}e^{i\omega_{20}^* \tau_1}(a_{22} + i\omega_2^*)};$$

$$q_3^* = \frac{-(a_{11} + i\omega_2^*)}{a_{31}e^{i\omega_{20}^* \tau_1}}. \tag{75}$$

Besides, from (74) we have

$$\overline{D}$$

$$= \frac{1}{1 + q_2\overline{q}_2^* + q_3\overline{q}_3^* + \overline{q}_3^* a_{31}\tau_1 e^{-i\omega_{20}^* \tau_1} + q_2\overline{q}_3^* a_{32}\tau_{20}^* e^{-i\omega_{20}^* \tau_{20}^*}}, \tag{76}$$

such that $\langle q^*(s), q(\theta) \rangle = 1$ and $\langle q^*(s), \overline{q}(\theta) \rangle = 0$.

Then, according to [44], we obtain the following relevant parameter, which helps to determine the direction and stability of Hopf bifurcation:

$$g_{20} = 2\overline{D}\tau_{20}^* \left(-\alpha_1 q_3 - \alpha_2 \overline{q}_2^* q_2 q_3 + \beta_1 \alpha_1 q_3 \overline{q}_3^* e^{-i\omega_{20}^* \tau_1} \\ + \beta_2 \alpha_2 q_2 q_3 \overline{q}_3^* e^{-i\omega_{20}^* \tau_{20}^*} \right),$$

$$g_{11} = \overline{D}\tau_{20}^* \left[-\alpha_1(q_3 + \overline{q}_3) - \alpha_2 \overline{q}_2^*(q_2\overline{q}_3 + \overline{q}_2 q_3) \\ + \beta_1 \alpha_1 \overline{q}_3^* \left(\overline{q}_3 e^{-i\omega_{20}^* \tau_1} + q_3 e^{i\omega_{20}^* \tau_1} \right) \\ + \beta_2 \alpha_2 \overline{q}_3^* \left(q_2 \overline{q}_3 e^{-i\omega_{20}^* \tau_{20}^*} + q_3 \overline{q}_2 e^{i\omega_{20}^* \tau_{20}^*} \right) \right],$$

$$g_{02} = 2\overline{D}\tau_{20}^* \left(-\alpha_1 \overline{q}_3 - \alpha_2 \overline{q}_2^* \overline{q}_2 \overline{q}_3 + \beta_1 \alpha_1 \overline{q}_3 \overline{q}_3^* e^{i\omega_{20}^* \tau_1} \\ + \beta_2 \alpha_2 \overline{q}_2 \overline{q}_3 \overline{q}_3^* e^{i\omega_{20}^* \tau_{20}^*} \right),$$

$$g_{21} = 2\overline{D}\tau_{20}^* \left\{ -\alpha_1 \left[W_{11}^{(3)}(0) + \frac{1}{2}W_{20}^{(3)}(0) \right. \right. \tag{77}$$

$$+ \frac{1}{2}\overline{q}_3 W_{20}^{(1)}(0) + q_3 W_{11}^{(1)}(0) \right] - \alpha_2 \overline{q}_2^* \left[q_2 W_{11}^{(3)}(0) \right.$$

$$\left. + \overline{q}_2 \frac{1}{2}W_{20}^{(3)}(0) + \frac{1}{2}\overline{q}_3 W_{20}^{(2)}(0) + q_3 W_{11}^{(2)}(0) \right]$$

$$+ \overline{q}_3^* \beta_1 \alpha_1 \left[q_3 W_{11}^{(1)}\left(-\frac{\tau_1}{\tau_{20}^*}\right) + \overline{q}_3 \frac{1}{2}W_{20}^{(1)}\left(-\frac{\tau_1}{\tau_{20}^*}\right) \right.$$

$$\left. + \frac{1}{2}W_{20}^{(3)}(0)e^{i\omega_{20}^* \tau_1} + W_{11}^{(3)}(0)e^{-i\omega_{20}^* \tau_1} \right]$$

$$+ \overline{q}_3^* \beta_2 \alpha_2 \left[q_3 W_{11}^{(2)}(-1) + \overline{q}_3 \frac{1}{2}W_{20}^{(2)}(-1) \right.$$

$$\left. \left. + \overline{q}_2 \frac{1}{2}W_{20}^{(3)}(0)e^{i\omega_{20}^* \tau_{20}^*} + q_2 W_{11}^{(3)}(0)e^{-i\omega_{20}^* \tau_{20}^*} \right] \right\},$$

and

$$W_{20}(\theta) = \frac{ig_{20}q(0)}{\omega_{20}^* \tau_{20}^*}e^{i\theta\omega_{20}^* \tau_{20}^*} + \frac{\overline{g}_{02}i}{3\omega_{20}^* \tau_{20}^*}\overline{q}(0)e^{-i\theta\omega_{20}^* \tau_{20}^*} \\ + E_1 e^{2i\theta\omega_{20}^* \tau_{20}^*},$$

$$W_{11}(\theta) = \frac{-ig_{11}q(0)}{\omega_{20}^* \tau_{20}^*}e^{i\theta\omega_{20}^* \tau_{20}^*} + \frac{\overline{g}_{11}i}{\omega_{20}^* \tau_{20}^*}\overline{q}(0)e^{-i\theta\omega_{20}^* \tau_{20}^*} \\ + E_2, \tag{78}$$

where E_1 and E_2 can be determined by the following, respectively:

$$\begin{pmatrix} 2i\omega_{20}^* - a_{11} & 0 & -a_{13} \\ 0 & 2i\omega_{20}^* - a_{22} & -a_{23} \\ -a_{31}e^{-2i\omega_{20}^* \tau_1} & -a_{32}e^{-2i\omega_{20}^* \tau_{20}^*} & 2i\omega_{20}^* \end{pmatrix} \cdot E_1$$

$$= 2 \begin{pmatrix} K_{11} \\ K_{21} \\ K_{31} \end{pmatrix},$$

$$\begin{pmatrix} a_{11} & 0 & a_{13} \\ 0 & a_{22} & a_{23} \\ a_{31} & a_{32} & 0 \end{pmatrix} \cdot E_2 = - \begin{pmatrix} K_{12} \\ K_{22} \\ K_{32} \end{pmatrix},$$

(79)

where

$$K_{11} = -\alpha_1 q_3;$$

$$K_{21} = -\alpha_2 q_2 q_3;$$

$$K_{31} = \beta_1 \alpha_1 q_3 e^{-i\omega_{20}^* \tau_1} + \beta_2 \alpha_2 q_2 q_3 e^{-i\omega_{20}^* \tau_{20}^*};$$

$$K_{12} = -\alpha_1 (q_3 + \overline{q}_3);$$

$$K_{22} = -\alpha_2 (q_2 \overline{q}_3 + \overline{q}_2 q_3);$$

$$K_{32} = \beta_1 \alpha_1 \left(q_3 e^{i\omega_{20}^* \tau_1} + \overline{q}_3 e^{-i\omega_{20}^* \tau_1} \right)$$
$$\quad + \beta_2 \alpha_2 \left(\overline{q}_2 q_3 e^{i\omega_{20}^* \tau_{20}^*} + q_2 \overline{q}_3 e^{-i\omega_{20}^* \tau_{20}^*} \right).$$

(80)

Then, we can compute the following values:

$$c_1(0) = \frac{i}{2\omega_{20}^* \tau_{20}^*} \left(g_{20} g_{11} - 2 |g_{11}|^2 - \frac{|g_{02}|^2}{3} \right) + \frac{g_{21}}{2},$$

$$\mu = -\frac{\operatorname{Re}(c_1(0))}{\operatorname{Re} \lambda'(\tau_{20}^*)},$$

(81)

$$\beta = 2 \operatorname{Re}(c_1(0)),$$

$$T = -\frac{\operatorname{Im}\{c_1(0)\} + \mu_2 \operatorname{Im}\{\lambda'(\tau_{20}^*)\}}{\omega_{20}^* \tau_{20}^*}.$$

This determine the properties of bifurcating periodic solutions and the Hopf bifurcation at $\tau = \tau_{20}^*$. That is,

(i) μ determines the direction of the Hopf bifurcation. Specifically, when $\mu > 0 (< 0)$, the Hopf bifurcation is supercritical (subcritical).

(ii) β determines the stability of the bifurcating periodic solutions; when $\beta < 0 (> 0)$, the bifurcating periodic solution is stable (unstable).

(iii) T determines the period of the bifurcating periodic solutions; when $T > 0 (< 0)$, the period of bifurcating periodic solution increases (decrease).

5. Numerical Simulations

Due to the complexity of model (1), we perform some numerical simulations in this section to investigate further how the delay influences dynamics in model (1). The following parameter values are used $I_1 = I_2 = 0.5$, $q_1 = q_2 = 0.001$, $\alpha_1 = \alpha_2 = 0.08$, $\beta_1 = 0.3$, and $m = 0.8$. Other parameters are chosen as control parameters.

According to the standard linear analysis, when τ_2 is equal to zero, the analysis reveals that the $\beta_2 - \tau_1$ parameter plane is divided into four parts (see Figure 1(a)). In Figure 1(a), before β_2 reaching black dashed line, there exists τ_{10} in model (1) such that the unique positive equilibrium loses its stability when the condition, $\tau_1 > \tau_{10}$, holds. When the locus of β_2 is between black dashed line and green dashed line, the stability switches for positive equilibrium do not exist although (28) has two positive roots, which means that there exists τ_{10} in model (1) such that the unique positive equilibrium loses its stability when the condition, $\tau_1 > \tau_{10}$, holds. However, the stability switches for positive equilibrium emerge when β_2 is beyond green dashed line but it does not reach blue zone. When the locus of β_2 is in blue zone, the unique positive equilibrium is always stable, which suggests that τ_1 cannot influence the stability of the positive equilibrium. When τ_1 equals zero, the similar results for $\beta_2 - \tau_2$ parameter plane are shown in Figure 1(b), but the sequence is reversed. Additionally, according to results in Section 4, we calculate the values of μ, β, and T at $\tau_1 = \tau_{10}$ with $\beta_2 \in (0, 0.3)$, and the corresponding results are shown in Figure 1(c), where we can find that the Hopf bifurcation is supercritical and the bifurcating periodic solutions are stable; especially, the period of the bifurcating periodic solutions increases as β_2 increases. For other cases of τ_1 and τ_2, the same procedures with respect to calculations of μ, β, and T can be performed like Figure 1(c).

As examples corresponding to stability of the positive equilibrium with $\beta_2 = 0.2$, taken $\tau_1 = 1$ and $\tau_1 = 3$ in Figure 1(a), respectively, the corresponding numerical solutions are shown in Figure 2. Obviously, the positive equilibrium is stable because $\tau_1 = 1$ is below τ_{10} (see Figure 2(a)). In contrast, due to $3 = \tau_1$ beyond τ_{10}, a periodic solution exists (see Figure 2(b)). Furthermore, set $\beta_2 = 0.7$, then we have $\tau_{1a}^0 \approx 4.9050 < \tau_{1b}^0 \approx 19.0615 < \tau_{1a}^1 \approx 38.6683$. Taken $\tau_1 = 4$, $\tau_1 = 18$ and $\tau_1 = 21$ in Figure 1(a), respectively, the corresponding numerical solutions are shown in Figure 3. Obviously, the positive equilibrium is stable when $\tau_1 = 4$ and $\tau_1 = 21$ (see Figures 3(a) and 3(c)), but the positive equilibrium is unstable when $\tau_1 = 18$ (see Figure 3(b)), which means that the positive equilibrium can gain its stability again for $\tau_1 > \tau_{10}$. In Figure 3, the same initial values are applied, and other parameter values except for τ_1 are also identical. Clearly, the delay is the principal factor giving rise to the difference among (a), (b), and (c).

Numerical solutions in Figure 3 suggest that the stability switches induced by delay may exist. Hence, the bifurcation diagram in $\tau_1 - \tau_2$ parameter plane is given (see Figure 4(a)). For case $\tau_2 = 0$, there exists a τ_1^* such that the positive equilibrium with respect to $\tau_1 \in (0, \tau_1^*)$ is stable. For case $\tau_1 = 0$, there exists a τ_2^* such that the positive equilibrium with respect to $\tau_2 \in (0, \tau_2^*)$ is stable. Additionally, when $\tau_2 \in (0, \tau_2^*)$, Figure 4(a) shows that τ_{10} exists such that the positive equilibrium with respect to $\tau_1 \in (0, \tau_{10})$ is stable. Likewise, when $\tau_1 \in (0, \tau_1^*)$, Figure 4(a) also display that τ_{20} exists such that the positive equilibrium with respect to $\tau_2 \in$

(a)

(b)

(c)
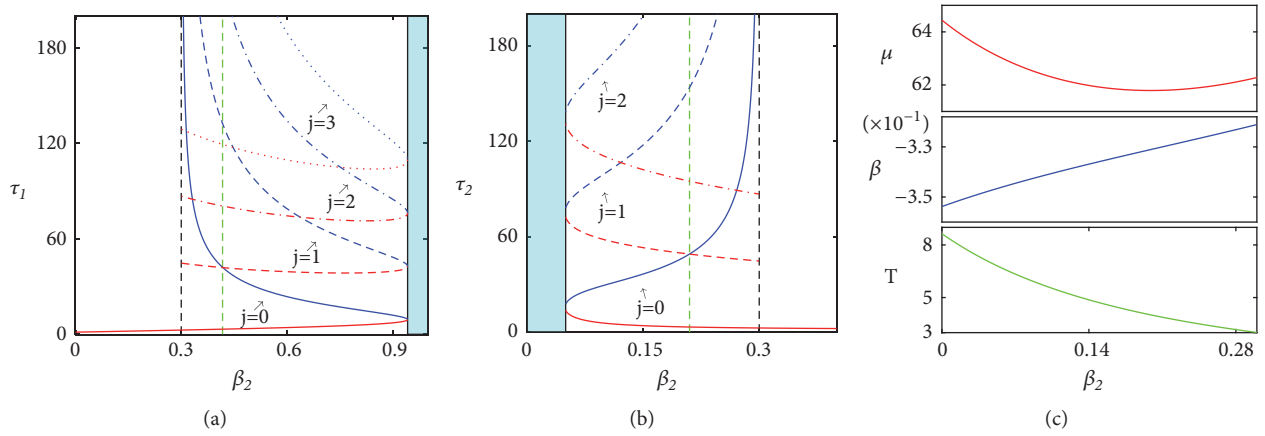
FIGURE 1: (a) Bifurcation diagram with $\tau_2 = 0$ corresponding to τ_1 V.S. β_2, where solid, dashed, dash-dot, and dotted curves represent the critical values of τ_1 in (30) for $j = 0, 1, 2, 3$, respectively, and the green dashed line denotes $\beta_2 = 0.417238$. (b) Bifurcation diagram with $\tau_1 = 0$ corresponding to τ_2 V.S. β_2, where solid, dashed, dash-dot, and dotted curves represent the critical values of τ_2 in (39) for $j = 0, 1, 2, 3$, respectively, and the green dashed line denotes $\beta_2 = 0.21$. (c) Examples for μ, β, and T at $\tau_1 = \tau_{10}$ with respect to β_2, where $\tau_2 = 0$.

(a)

(b)
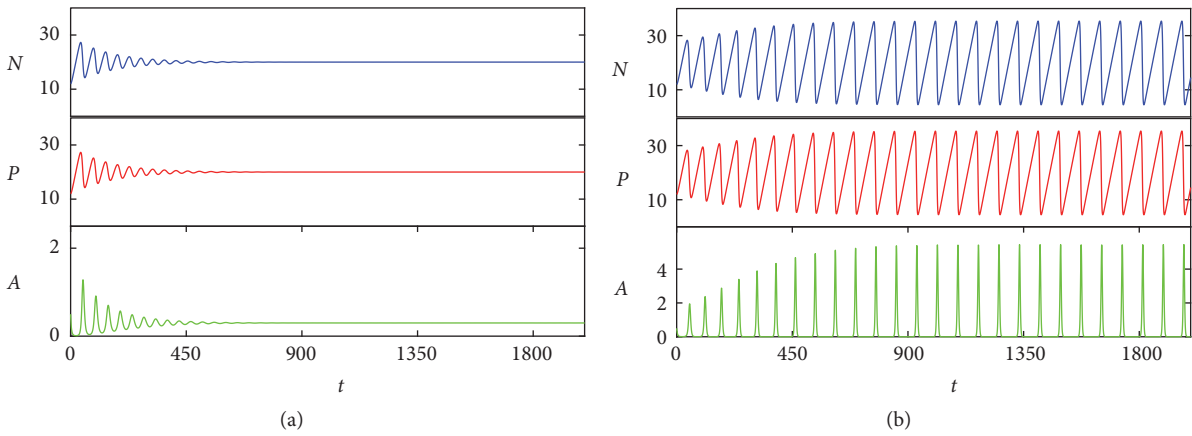
FIGURE 2: Numerical solutions of model (1) with $\tau_2 = 0$ and $\beta_2 = 0.2$, (a) $\tau_1 = 1$; (b) $\tau_1 = 3$.

(a)

(b)

(c)

FIGURE 3: Numerical solutions of model (1) with $\tau_2 = 0$ and $\beta_2 = 0.7$, (a) $\tau_1 = 4$; (b) $\tau_1 = 18$ (c) $\tau_1 = 21$.

FIGURE 4: (a) Bifurcation diagram with $\beta_2 = 0.7$ for τ_1 V.S. τ_2, where the symbol "S" denotes stable and the symbol "US" denotes unstable; (b) bifurcation diagram with $\beta_2 = 0.7$ for the effect of τ_2 on nutrient-phytoplankton dynamics, where dashed line denotes unstable; solid line denotes stable; the green solid square is Hopf bifurcation point, dot-dashed line corresponding to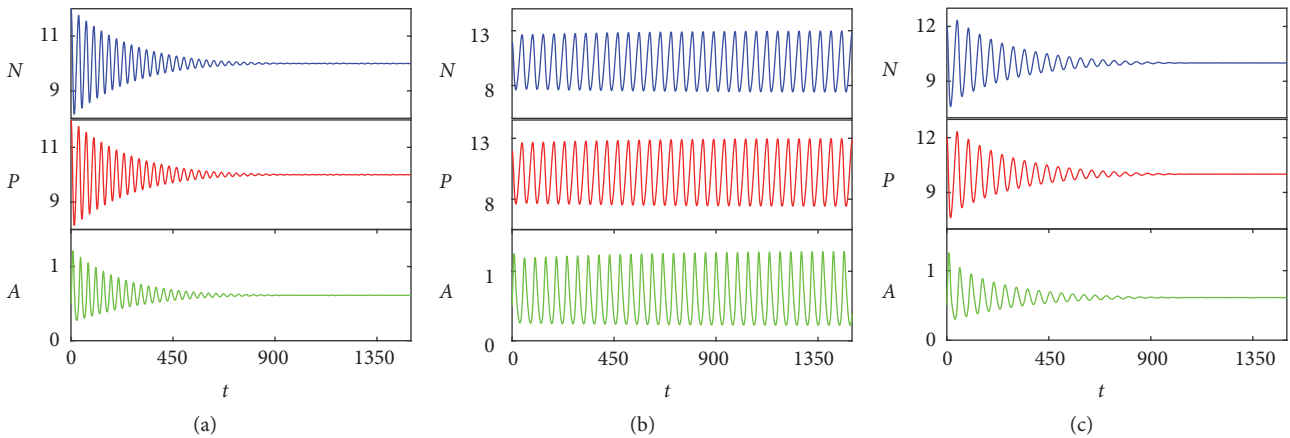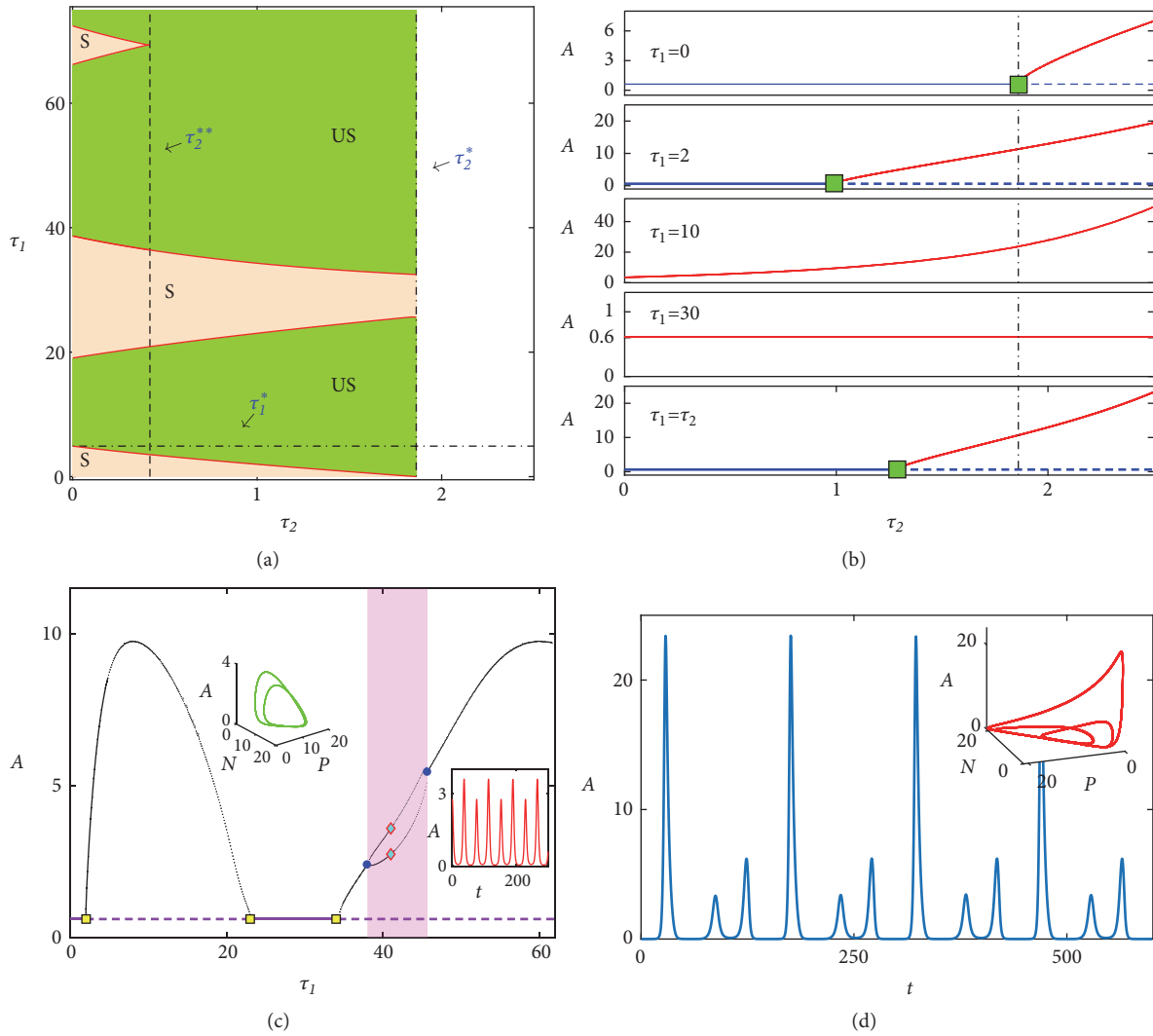 τ_2^* in (a), blue line represents equilibrium, and red line represents amplitude of periodic solutions. (c) Bifurcation diagram with $\beta_2 = 0.7$ and $\tau_2 = 1$, where the yellow solid square is Hopf bifurcation point, the blue solid circle is bifurcation point for periodic-2 solution, the magenta zone indicates the existence of periodic-2 solutions, and the cyan solid diamond denotes the value of τ_1 for a phase and a time-series in the inner of (c). (d) A periodic-3 solution for phytoplankton population, where $\beta_2 = 0.7$, $\tau_1 = 100$, and $\tau_2 = 2$.

$(0, \tau_{20})$ is stable. Significantly, Figure 4(a) demonstrates that the stability switches for positive equilibrium with respect to τ_1 emerge when τ_2 below τ_2^* is fixed.

Figure 4(b) depicts the dependence of stability of positive equilibrium on delay τ_2 in the fully nonlinear regime for τ_1 in sequence $[0, 2, 10, 30]$ and $\tau_1 = \tau_2$, which is consistent with results in Figure 4(a). However, when τ_2 is fixed, Figure 4(c) shows that the stability switches emerge with τ_1 increases. Especially, periodic-2 solutions exist for some values of τ_2 (see magenta zone in Figure 4(c)). As an example of periodic-2 solution existence, taking $\tau_1 = 41$, a phase and a time-series are given in the inner of Figure 4(c). Moreover, Figure 4(d) shows that there exist periodic-3 solutions in model (1). According to results in Section 2, the positive equilibrium is

globally asymptotically stable in the model (1) without delay if it exists. Obviously, the results shown in Figure 4 are induced by delay.

In Figure 4(a), we can find that the number of intervals corresponding to stability of positive equilibrium for small values of τ_2 equals 3. However, when τ_2 is beyond dashed line (τ_2^{**}), the number of intervals is 2. So the number of intervals for stability switches may be different for diverse τ_2. Accordingly, we calculate the number of intervals with respect to parameter β_2, as shown in Figure 5(a). Figure 5(b) shows that there exist 3 stable intervals when $\beta_2 = 0.7$ and $\tau_2 = 0$, which is an example of Figure 5(a). Evidently, parameter β_2 can remarkably influence the number of intervals for stability of positive equilibrium.
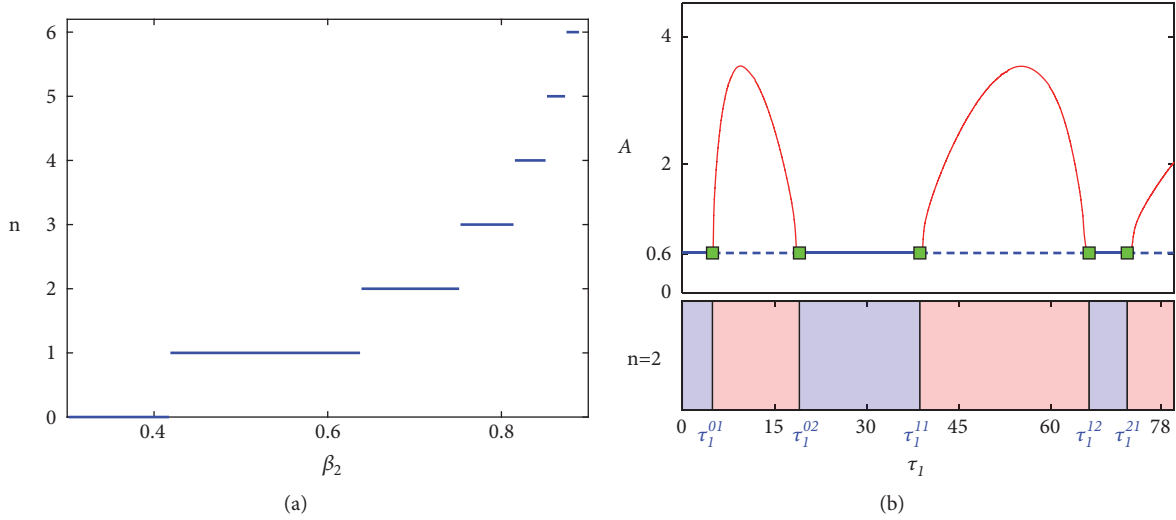
(a)

(b)

FIGURE 5: (a) The number of intervals for stability switches of positive equilibrium with respect to β_2, where $\tau_2 = 0$; (b) based on (a), an example for comparison between results predicted by linear analysis and numerical results in the fully nonlinear regime with (β_2, τ_2) at $(0, 0.7)$, where top panel represents numerical results for model (1) in the fully nonlinear regime; bottom panel depicts the results predicted by linear analysis, and blue and red area denote stable and unstable, respectively.

6. Conclusions

In this paper we proposed a nitrogen-phosphorus-phytoplankton model with multiple delays. The analysis focused on the effect of delay on nutrient-phytoplankton dynamics. In the absence of delay, theoretical analysis indicated that the unique positive equilibrium is globally asymptotically stable in model (1) if it exists. Deng et al. [48] also studied a nitrogen-phosphorus-phytoplankton model without delay, where Holling II function was employed to describe the nutrient uptake dynamics of phytoplankton. Although the function modelling the nutrient uptake dynamics of phytoplankton is different, they get the same results. These results mean that the nutrient-phytoplankton ecosystem will approach the stable equilibrium. However, it has been reported [18] that a constant population density may not exist because of the existence of some factors including noise, interval factors, and physical factors. And ecological studies [49, 50] also criticized this idea of "the balance of nature." Actually, the existence of nutrient-plankton oscillations has been detected by laboratory experiments and field observation [19, 20]. Additionally, Benincà et al. [49] present the first experimental demonstration of chaos in a long-term experiment with a complex food web, where the food web was consisted of bacteria, several phytoplankton species, herbivorous and predatory zooplankton species, and detritivores. And they also find that the community moved back and forth between stabilizing and chaotic dynamics during the cyclic succession, and their findings provide a field demonstration of nonequilibrium coexistence of competing species through a cyclic succession at the edge of chaos [50]. These reports support that the nonequilibrium dynamics, such as oscillations and chaos, can exist in reality.

In the present paper, we find that the unique positive equilibrium may lose its stability via Hopf bifurcation when delay

appears, and then a periodic solution emerges, which means that nutrient-phytoplankton oscillation occurs. Obviously, the factor giving rise to nutrient-phytoplankton oscillation is delay in our studies. And the period and the stability of the bifurcating periodic solutions with respect to delay are discussed by using center manifold argument and normal form theory. In fact, instability induced by delay in nutrient-plankton model has been studied widely, and many studies indicate that the equilibrium is always unstable when delay is beyond a critical value [25, 29, 51, 52]. Yet, it should be emphasized in the present paper that the stability switches induced by delay can occur under some conditions.

Moreover, numerical simulations showed how the delay influences nutrient-phytoplankton dynamics. Numerical results for model (1) in the fully nonlinear regime are consistent with the linear analysis. In numerical simulations, we found that delay indeed gives rise to the emergence of stability switches for the positive equilibrium. Yet, the numerical results show that the parameter intervals for stability switches may depend on other parameters as well, e.g., β_2. Additionally, numerical results also indicated that periodic-2 solutions and periodic-3 solutions can emerge under some conditions for delay, which means that complex dynamics induced by delay exist in model (1). From biological viewpoint, the existence of periodic solutions implies that the fluctuations exist in density of phytoplankton population; that is, nutrient-phytoplankton oscillation emerges. Especially, by Li and York's theory, periodic-3 solution implies chaos, which means that chaotic density fluctuations can display a variety of different periodicities and the long-term prediction of phytoplankton density can be fundamentally impossible. The chaotic density fluctuations do not contribute to the control of phytoplankton bloom. Consequently, the importance of the present paper is not the precision with which it predicts specific events for

phytoplankton blooms but its contribution to the studies on how the delay influences nutrient-phytoplankton dynamics.

Data Availability

The data used to support the findings of this study are included within the article.

Conflicts of Interest

The author declares that there are no conflicts of interest.

Acknowledgments

References

[1] J. Huisman, G. A. Codd, H. W. Paerl, B. W. Ibelings, J. M. Verspagen, and P. M. Visser, "Cyanobacterial blooms," *Nature Reviews Microbiology*, vol. 16, no. 8, pp. 471–483, 2018.

[2] A. Burson, M. Stomp, E. Greenwell, J. Grosse, and J. Huisman, "Competition for nutrients and light: Testing advances in resource competition with a natural phytoplankton community," *Ecology*, vol. 99, no. 5, pp. 1108–1118, 2018.

[3] M. Stomp, J. Huisman, F. De Jongh, A. J. Veraart, D. Gerla, M. Rijkeboer et al., "Adaptive divergence in pigment composition promotes phytoplankton biodiversity," *Nature*, vol. 432, no. 7013, pp. 104–107, 2004.

[4] Z. Ma, T. Fang, R. W. Thring et al., "Toxic and non-toxic strains of Microcystis aeruginosa induce temperature dependent allelopathy toward growth and photosynthesis of Chlorella vulgaris," *Harmful Algae*, vol. 48, pp. 21–29, 2015.

[5] P. W. Boyd, A. J. Watson, C. S. Law et al., "A mesoscale phytoplankton bloom in the polar Southern Ocean stimulated by iron fertilization," *Nature*, vol. 407, no. 6805, pp. 695–702, 2000.

[6] Z. Ma, H. Yu, R. Thring, C. Dai, A. Shen, and M. Zhao, "Interaction between simulated dense Scenedesmus dimorphus (Chlorophyta) bloom and freshwater meta-zooplankton community," *Journal of Limnology*, vol. 77, no. 2, pp. 255–263, 2018.

[7] G. Rhee and I. J. Gotham, "The effect of environmental factors on phytoplankton growth: Temperature and the interactions of temperature with nutrient limitation," *Limnology and Oceanography*, vol. 26, no. 4, pp. 635–648, 1981.

[8] V. H. Smith, "Low nitrogen to phosphorus ratios favor dominance by blue-green algae in lake phytoplankton," *Science*, vol. 221, no. 4611, pp. 669–671, 1983.

[9] J. A. Downing and E. McCauley, "The nitrogen: Phosphorus relationship in lakes," *Limnology and Oceanography*, vol. 37, no. 5, pp. 936–945, 1992.

[10] H. Xu, H. W. Paerl, B. Qin, G. Zhu, and G. Gao, "Nitrogen and phosphorus inputs control phytoplankton growth in eutrophic Lake Taihu, China," *Limnology and Oceanography*, vol. 55, no. 1, pp. 420–432, 2010.

[11] J. H. Ryther and W. M. Dunstan, "Nitrogen, phosphorus, and eutrophication in the coastal marine environment," *Science*, vol. 171, no. 3975, pp. 1008–1013, 1971.

[12] J. E. Truscott and J. Brindley, "Ocean plankton populations as excitable media," *Bulletin of Mathematical Biology*, vol. 56, no. 5, pp. 981–998, 1994.

[13] J. A. Freund, S. Mieruch, B. Scholze, K. Wiltshire, and U. Feudel, "Bloom dynamics in a seasonally forced phytoplankton-zooplankton model: Trigger mechanisms and timing effects," *Ecological Complexity*, vol. 3, no. 2, pp. 129–139, 2006.

[14] T. Zhang and W. Wang, "Hopf bifurcation and bistability of a nutrient-phytoplankton-zooplankton model," *Applied Mathematical Modelling*, vol. 36, no. 12, pp. 6225–6235, 2012.

[15] A. Huppert, B. Blasius, and L. Stone, "A model of phytoplankton blooms," *The American Naturalist*, vol. 159, no. 2, pp. 156–171, 2002.

[16] H. Ishii and I. Takagi, "Global stability of stationary solutions to a nonlinear diffusion equation in phytoplankton dynamics," *Journal of Mathematical Biology*, vol. 16, no. 1, pp. 1–24, 1982.

[17] A. Fan, P. Han, and K. Wang, "Global dynamics of a nutrient-plankton system in the water ecosystem," *Applied Mathematics and Computation*, vol. 219, no. 15, pp. 8269–8276, 2013.

[18] J. A. Sherratt and M. J. Smith, "Periodic travelling waves in cyclic populations: Field studies and reaction-diffusion models," *Journal of the Royal Society Interface*, vol. 5, no. 22, pp. 483–505, 2008.

[19] G. F. Fussmann, S. P. Ellner, K. W. Shertzer, and N. G. Hairston Jr., "Crossing the hopf bifurcation in a live predator-prey system," *Science*, vol. 290, no. 5495, pp. 1358–1360, 2000.

[20] J. Huisman, N. N. Pham Thi, D. M. Karl, and B. Sommeijer, "Reduced mixing generates oscillations and chaos in the oceanic deep chlorophyll maximum," *Nature*, vol. 439, no. 7074, pp. 322–325, 2006.

[21] Y. Li, Y. Liu, L. Zhao, A. Hastings, and H. Guo, "Exploring change of internal nutrients cycling in a shallow lake: A dynamic nutrient driven phytoplankton model," *Ecological Modelling*, vol. 313, pp. 137–148, 2015.

[22] B. Liu, H. E. de Swart, and V. N. de Jonge, "Phytoplankton bloom dynamics in turbid, well-mixed estuaries: A model study," *Estuarine, Coastal and Shelf Science*, vol. 211, pp. 137–151, 2018.

[23] S. G. Ruan, "Persistence and coexistence in zooplankton-phytoplankton-nutrient models with instantaneous nutrient recycling," *Journal of Mathematical Biology*, vol. 31, no. 6, pp. 633–654, 1993.

[24] J. Caperon, "Time lag in population growth response of isochrysis galbana to a variable nitrate environment," *Ecology*, vol. 50, no. 2, pp. 188–192, 1969.

[25] J. Zhao and J. Wei, "Dynamics in a diffusive plankton system with delay and toxic substances effect," *Nonlinear Analysis: Real World Applications*, vol. 22, pp. 66–83, 2015.

[26] S. Ruan and X.-Q. Zhao, "Persistence and extinction in two species reaction-diffusion systems with delays," *Journal of Differential Equations*, vol. 156, no. 1, pp. 71–92, 1999.

[27] Y. Wang, W. Jiang, and H. Wang, "Stability and global Hopf bifurcation in toxic phytoplankton-zooplankton model with delay and selective harvesting," *Nonlinear Dynamics*, vol. 73, no. 1-2, pp. 881–896, 2013.

[28] C. Dai, M. Zhao, H. Yu, and Y. Wang, "Delay-induced instability in a nutrient-phytoplankton system with flow," *Physical Review E: Statistical, Nonlinear, and Soft Matter Physics*, vol. 91, no. 3, p. 032929, 2015.

[29] C. Dai, M. Zhao, and H. Yu, "Dynamics induced by delay in a nutrient-phytoplankton model with diffusion," *Ecological Complexity*, vol. 26, pp. 29–36, 2016.

[30] K. Chakraborty, K. Das, and T. K. Kar, "Modeling and analysis of a marine plankton system with nutrient recycling and diffusion," *Complexity*, vol. 21, no. 1, pp. 229–241, 2015.

[31] V. Volterra, *Lecons Sur La Théorie Mathématique De La Lutte Par La Vie*, Gauthier-Villars, Paris, 1931.

[32] J. K. Hale and L. Verduyn, *Theory of Functional Differential Equations*, Springer, New York, NY, USA, 1993.

[33] Y. Kuang, *Delay differential equations with applications in population dynamics*, Academic Press, Boston, Mass, USA, 1993.

[34] J. Wu, *Theory and Applications of Partial Functional Differential Equations*, Springer, New York, NY, USA, 1996.

[35] S. Gakkhar and A. Singh, "Complex dynamics in a prey predator system with multiple delays," *Communications in Nonlinear Science and Numerical Simulation*, vol. 17, no. 2, pp. 914–929, 2012.

[36] N. MacDonald, "Time delay in prey-predator models," *Mathematical Biosciences*, vol. 28, no. 3-4, pp. 321–330, 1976.

[37] S. Ruan and J. Wei, "On the zeros of transcendental function with applications to stability of delay differential equations with two zeros," *Dynamics of Continuous, Discrete and Impulsive Systems Series A: Mathematical Analysis*, vol. 10, pp. 863–874, 2003.

[38] C. Xu, "Delay-induced oscillations in a competitor-competitor-mutualist lotka-volterra model," *Complexity*, vol. 2017, Article ID 2578043, 12 pages, 2017.

[39] S. S. Chen and J. J. Wei, "Stability and bifurcation in a diffusive logistic population model with multiple delays," *International Journal of Bifurcation & Chaos*, vol. 25, no. 8, p. 1550107, 2015.

[40] K. Wang, W. Wang, H. Pang, and X. Liu, "Complex dynamic behavior in a viral model with delayed immune response," *Physica D: Nonlinear Phenomena*, vol. 226, no. 2, pp. 197–208, 2007.

[41] Y. Song, J. Wei, and Y. Yuan, "Stability switches and Hopf bifurcations in a pair of delay-coupled oscillators," *Journal of Nonlinear Science*, vol. 17, no. 2, pp. 145–166, 2007.

[42] S. Chen, Y. Lou, and J. Wei, "Hopf bifurcation in a delayed reaction- diffusion-advection population model," *Journal of Differential Equations*, vol. 264, no. 8, pp. 5333–5359, 2018.

[43] B. D. Hassard, N. D. Kazarinoff, and Y.-H. Wan, *Theory and Applications of Hopf Bifurcation*, Cambridge University Press, Cambridge, UK, 1981.

[44] Y. Song and J. Wei, "Bifurcation analysis for Chen's system with delayed feedback and its application to control of chaos," *Chaos, Solitons & Fractals*, vol. 22, no. 1, pp. 75–91, 2004.

[45] J. Guckenheimer and P. Holmes, *Nonlinear Oscillations, Dynamical Systems, and Bifurcation of Vector Fields*, Springer-Verlag, New York, NY, USA, 1983.

[46] Y. Kuang, *Delay Differential Equations with Applications in Population Dynamics*, Academic Press, New York, NY, USA, 1993.

[47] A. F. Nindjin, M. A. Aziz-Alaoui, and M. Cadivel, "Analysis of a predator-prey model with modified Leslie-Gower and Holling-type II schemes with time delay," *Nonlinear Analysis: Real World Applications*, vol. 7, no. 5, pp. 1104–1118, 2006.

[48] Y. Deng, M. Zhao, H. Yu, and Y. Wang, "Dynamical analysis of a nitrogen-phosphorus-phytoplankton model," *Discrete Dynamics in Nature and Society*, vol. 2015, Article ID 823026, 8 pages, 2015.

[49] E. Benincá, J. Huisman, R. Heerkloss et al., "Chaos in a long-term experiment with a plankton community," *Nature*, vol. 451, no. 7180, pp. 822–825, 2008.

[50] E. Benincà, B. Ballantine, S. P. Ellner, and J. Huisman, "Species fluctuations sustained by a cyclic succession at the edge of chaos," *Proceedings of the National Acadamy of Sciences of the United States of America*, vol. 112, no. 20, pp. 6389–6394, 2015.

[51] K. Das and S. Ray, "Effect of delay on nutrient cycling in phytoplankton-zooplankton interactions in estuarine system," *Ecological Modelling*, vol. 215, no. 1-3, pp. 69–76, 2008.

[52] H. Zhao, X. Huang, and X. Zhang, "Hopf bifurcation and harvesting control of a bioeconomic plankton model with delay and diffusion terms," *Physica A: Statistical Mechanics and its Applications*, vol. 421, pp. 300–315, 2015.

Research Article

Stability of Traveling Waves to the Lotka-Volterra Competition Model

Ahmad Alhasanat [1,2] and Chunhua Ou [1]

[1]*Department of Mathematics and Statistics, Memorial University of Newfoundland, St. John's, Newfoundland, Canada A1C 5S7*
[2]*Department of Mathematics and Statistics, Al-Hussein Bin Talal University, Ma'an, Jordan*

Correspondence should be addressed to Chunhua Ou; ou@mun.ca

In this paper, the stability of traveling wave solutions to the Lotka-Volterra diffusive model is investigated. First, we convert the model into a cooperative system by a special transformation. The local and the global stability of the traveling wavefronts are studied in a weighted functional space. For the global stability, comparison principle together with the squeezing technique is applied to derive the main results.

1. Introduction

We are concerned here with the diffusive Lotka-Volterra competition model

$$
\begin{aligned}
\phi_t &= d_1 \phi_{xx} + r_1 \phi \left(1 - b_1 \phi - a_1 \psi\right), \\
\psi_t &= d_2 \psi_{xx} + r_2 \psi \left(1 - a_2 \phi - b_2 \psi\right),
\end{aligned}
\tag{1}
$$

with the initial data

$$
\begin{aligned}
\phi(x, 0) &= \phi_0(x) \geq 0, \\
\psi(x, 0) &= \psi_0(x) \geq 0, \\
&\forall x \in \mathbb{R}.
\end{aligned}
\tag{2}
$$

Here $\phi(x, t)$ and $\psi(x, t)$ are the population densities at time t and location x; d_1 and d_2 are the diffusive coefficients; r_1 and r_2 are the net birth rates; a_1 and a_2 are the competition coefficients; $1/b_1$ and $1/b_2$ are the carrying capacities for each species. For derivation and biological interpretation of this model, we refer readers to [1, 2].

Using the transformations

$$
\sqrt{\frac{r_1}{d_1}} x \longrightarrow x,
$$

$$
r_1 t \longrightarrow t,
$$

$$
\begin{aligned}
b_1 \phi(x, t) &= \widetilde{\phi}(x, t), \\
b_2 \psi(x, t) &= \widetilde{\psi}(x, t), \\
d &= \frac{d_2}{d_1}, \\
r &= \frac{r_2}{r_1}, \\
\frac{a_1}{b_2} &\longrightarrow a_1, \\
\frac{a_2}{b_1} &\longrightarrow a_2,
\end{aligned}
\tag{3}
$$

the nondimensional form of the system becomes

$$
\begin{aligned}
\widetilde{\phi}_t &= \widetilde{\phi}_{xx} + \widetilde{\phi} \left(1 - \widetilde{\phi} - a_1 \widetilde{\psi}\right), \\
\widetilde{\psi}_t &= d \widetilde{\psi}_{xx} + r \widetilde{\psi} \left(1 - a_2 \widetilde{\phi} - \widetilde{\psi}\right).
\end{aligned}
\tag{4}
$$

By letting $u = \widetilde{\phi}$, $v = 1 - \widetilde{\psi}$, this model can be further written as a cooperative system

$$
\begin{aligned}
u_t &= u_{xx} + u \left(1 - a_1 - u + a_1 v\right), \\
v_t &= d v_{xx} + r (1 - v)(a_2 u - v),
\end{aligned}
\tag{5}
$$

with

$$u(x, 0) = u_0(x) = \widetilde{\phi}(x, 0),$$

$$v(x, 0) = v_0(x) = 1 - \widetilde{\psi}(x, 0), \tag{6}$$

$$\forall x \in \mathbb{R}.$$

For our study, we will assume that $u_0(x)$ and $v_0(x)$ are nonnegative. The existence and uniqueness of the solution of the above problem can be easily verified by a classical argument of Picard's iteration. Throughout this paper, we assume that the condition

$$0 < a_1 < 1 < a_2 \tag{C1}$$

is satisfied. Under this condition, equilibria to system (5) in the region $\{(u, v) \mid 0 \le u \le 1, 0 \le v \le 1\}$ are only $(0, 0), (0, 1)$, and $(1, 1)$. In the absence of diffusion in the system (5), it can be shown that $(0, 0)$ is unstable and $(1, 1)$ is stable. For the system, we are particularly interested in the traveling wave solution, connecting $(1, 1)$ and $(0, 0)$, in the form

$$(u, v)(x, t) = (\overline{U}, \overline{V})(z), \tag{7}$$

where $z = x - ct$ is the wave variable, $c \ge 0$ is the wave speed, and $(\overline{U}, \overline{V})$ is called the wavefront and satisfies

$$0 = \overline{U}_{zz} + c\overline{U}_z + \overline{U}\left(1 - a_1 - \overline{U} + a_1\overline{V}\right),$$
$$0 = d\overline{V}_{zz} + c\overline{V}_z + r\left(1 - \overline{V}\right)\left(a_2\overline{U} - \overline{V}\right), \tag{8}$$

subject to

$$(\overline{U}, \overline{V})(-\infty) = (1, 1),$$
$$(\overline{U}, \overline{V})(\infty) = (0, 0). \tag{9}$$

This is equivalent to studying traveling waves for the original competition system (4) that connect the boundary equilibria $(0, 1)$ and $(1, 0)$.

The existence of traveling waves to the above problem is well-studied in literature. It is known that there exists $c^* \ge 0$ so that problem (8)-(9) has a monotone solution $(\overline{U}, \overline{V})(z)$ for $c \ge c^*$ and no wavefront exists for $c < c^*$; see [3–6]. c^* is called the minimal wave speed for this system and satisfies $c^* \ge 2\sqrt{1 - a_1}$. When $c^* = 2\sqrt{1 - a_1}$, we say that the minimal wave speed is *linearly determined*; see the details in [4].

We know that $(\overline{U}, \overline{V})(x - ct)$ is a special pattern that only satisfies the first two equations in (5). For the stability of this pattern, we want to know if the solution of (5) tends to $(\overline{U}, \overline{V})(x - ct)$ for given initial data $u_0(x)$ and $v_0(x)$. To this end, we use the (z, t)-coordinate and

$$(u, v)(x, t) = (U, V)(z, t), \tag{10}$$

to transform the uv-model (5) into the partial differential model

$$U_t = U_{zz} + cU_z + U\left(1 - a_1 - U + a_1V\right),$$
$$V_t = dV_{zz} + cV_z + r\left(1 - V\right)\left(a_2U - V\right), \tag{11}$$

subject to

$$U(z, 0) = u_0(z),$$
$$V(z, 0) = v_0(z), \tag{12}$$

$$\forall z \in \mathbb{R}.$$

It is easy to see that $(\overline{U}, \overline{V})(z)$ is the steady-state to the above new system.

We should mention that dynamics for (4) is very rich. There are always three nonnegative equilibria $(0, 0), (1, 0)$, and $(0, 1)$. In the case when $a_1 < 1, a_2 < 1$, or the case when $a_1 > 1, a_2 > 1$, there exists a unique positive coexistence equilibrium

$$(\widetilde{\phi}^*, \widetilde{\psi}^*) = \left(\frac{1 - a_1}{1 - a_1a_2}, \frac{1 - a_2}{1 - a_1a_2}\right). \tag{13}$$

Based on the phase plane analysis to the ordinary differential system of (4) without diffusion terms, the nonlinearity of the model (4) when $a_1 < 1$ and $a_2 < 1$ is called the persistence case (or coexistence). Likewise, the nonlinearity is called the monostable case when $a_1 < 1$ and $a_2 > 1$ are satisfied, or the bistable case when $a_1 > 1$ and $a_2 > 1$. Traveling waves to (4) have been investigated considerably. For the bistable case, please see [7, 8] for the existence of traveling waves connecting $(1, 0)$ and $(0, 1)$, and [9] for the uniqueness and parameter dependence of wave speeds. For the monostable case, we refer to [3, 10] for the existence of traveling waves, and [11, 12] for the selection of the minimal speed. For the persistence (coexistence), the existence of traveling wave connecting $(0, 0)$ and $(\widetilde{\phi}^*, \widetilde{\psi}^*)$ has been studied in [13, 14]. When time delays are incorporated into (4) in the persistence case, Li et al. [15] and Gourley and Ruan [16] have proved the existence of traveling waves.

The stability of traveling waves to a scalar partial differential equation has been well-studied, e.g., [17–27], the monograph [6, 28] and the survey paper [29]. Indeed, the extension of this study to a general system is not trivial. As we know, when time delays are directly incorporated in the competition terms in (4), the system becomes nonmonotone and the comparison principle cannot work. Alternatively, in [30, 31], the authors studied the stability of traveling waves for the so-called cooperative delayed reaction diffusion system by changing the signs of a_1 and a_2. To be exact, with putting delay = 0, they studied the cooperative system

$$\phi_t = d_1\phi_{xx} + r_1\phi\left(1 - \widehat{b}_1\phi + \widehat{a}_1\psi\right),$$
$$\psi_t = d_2\psi_{xx} + r_2\psi\left(1 + \widehat{a}_2\phi - \widehat{b}_2\psi\right), \tag{14}$$

where $d_i, r_i, \widehat{a}_i$, and $\widehat{b}_i$ are all positive. This corresponds to the persistence case in our model (4). Under the condition $\widehat{b}_1\widehat{b}_2 - \widehat{a}_1\widehat{a}_2 > 0$, a positive equilibrium

$$(\phi_+, \psi_+) = \left(\frac{\widehat{a}_1 + \widehat{b}_2}{\widehat{b}_1\widehat{b}_2 - \widehat{a}_1\widehat{a}_2}, \frac{\widehat{b}_1 + \widehat{a}_2}{\widehat{b}_1\widehat{b}_2 - \widehat{a}_1\widehat{a}_2}\right) \tag{15}$$

exists. They proved that the traveling wave fronts, connecting $(0, 0)$ and (ϕ_+, ψ_+), are exponentially stable in some weighted

L^∞ spaces, and obtained the decay rates by the weighted energy estimate.

Despite the success in the study of the stability of traveling waves to the classical model (4) in the bistable and persistence cases, the stability of traveling wave in the monostable remains still unsolved. The purpose of this paper is to systematically study the local and the global stability of the steady-state $(\overline{U}, \overline{V})(z)$. Using the method of spectrum analysis in [32], we give the local stability. For the global stability, we construct an upper and a lower solutions to the system (11), and prove their convergence to the traveling wave $(\overline{U}, \overline{V})(z)$. In view of comparison together with the squeezing technique, we arrive at new results on the global stability of the traveling waves. We remark that our method is different from that in [30, 31] where weighted energy method was applied.

The rest of the paper is organized as follows. Local analysis of the wave profile near the unstable point is studied in Section 2. In Section 3, we study the local stability of the steady-state by applying the standard linearization. The resulting spectrum problem is studied by the method in [32]. A suitable weighted functional space is chosen to proceed the analysis. In Section 4, besides the weighted functional space, the upper-lower solution method together with the squeezing technique is applied to derive the global stability results. Conclusions are presented in Section 5.

2. The Local Analysis of the Wave Profile Near the Equilibrium $(0, 0)$

In this section, we study the behavior of the traveling wave $(\overline{U}, \overline{V})(z)$ locally near the equilibrium $(0, 0)$. Assume that the solution has exponential decay as $z \longrightarrow \infty$. Indeed this claim can be easily verified by the maximum principal coupled with a comparison near the neighborhood of infinity. Therefore, we set

$$\left(\overline{U}, \overline{V}\right)(z) \sim \left(\zeta_1 e^{-\mu z}, \zeta_2 e^{-\mu z}\right) \quad \text{as } z \longrightarrow \infty, \qquad (16)$$

for positive constants ζ_1, ζ_2, and μ. By substituting this into (8) and linearizing the equations we have

$$A(\mu) \begin{pmatrix} \zeta_1 \\ \zeta_2 \end{pmatrix} = \begin{pmatrix} 0 \\ 0 \end{pmatrix}, \qquad (17)$$

where $A(\mu)$ is given by

$$A(\mu) = \begin{pmatrix} \mu^2 - c\mu + 1 - a_1 & 0 \\ ra_2 & d\mu^2 - c\mu - r \end{pmatrix}. \qquad (18)$$

The system of algebraic equations (17) has a nontrivial solution if and only if $\det(A) = 0$. This implies $\mu = \mu_{1,2,3} > 0$, where

$$\mu_1(c) = \frac{c - \sqrt{c^2 - 4(1 - a_1)}}{2},$$
$$\qquad (19)$$
$$\mu_2(c) = \frac{c + \sqrt{c^2 - 4(1 - a_1)}}{2},$$

and

$$\mu_3(c) = \frac{c + \sqrt{c^2 + 4dr}}{2d}. \qquad (20)$$

Indeed, a condition so that μ_1 and μ_2 are reals is

$$c \geq 2\sqrt{1 - a_1} := c_0. \qquad (21)$$

For $c > c_0$, obviously $\mu_1 < \mu_2$. When $0 \leq d < 1$, we have also $\mu_2 < \mu_3$ for all $c > c_0$, i.e., $e^{-\mu_1 z}$ dominates both of $e^{-\mu_2 z}$ and $e^{-\mu_3 z}$. In this case, the eigenvector of $A(\mu)$ corresponding to μ_i, for $i = 1, 2$, is the strongly positive vector $(\zeta_1(\mu_i) \ \zeta_2(\mu_i))^T$, where

$$\zeta_1(\mu_i) = -\left(d\mu_i^2 - c\mu_i - r\right)$$
$$\qquad (22)$$
$$\text{and } \zeta_2(\mu_i) = ra_2.$$

It follows that

$$\begin{pmatrix} \overline{U}(z) \\ \overline{V}(z) \end{pmatrix} = C_1 \begin{pmatrix} \zeta_1(\mu_1) \\ \zeta_2(\mu_1) \end{pmatrix} e^{-\mu_1 z} + C_2 \begin{pmatrix} \zeta_1(\mu_2) \\ \zeta_2(\mu_2) \end{pmatrix} e^{-\mu_2 z},$$
$$\qquad (23)$$
$$\text{as } z \longrightarrow \infty,$$

for $C_1 > 0$ or $C_1 = 0, C_2 > 0$. For the case when

$$1 < d < 2 + \frac{r}{1 - a_1} := \widehat{d}, \qquad (24)$$

the same behavior in (23) is still true if $c^* < c \leq \widehat{c}$, where

$$\widehat{c} = \sqrt{\frac{r + 1 - a_1}{d - 1}} + (1 - a_1)\sqrt{\frac{d - 1}{r + 1 - a_1}}. \qquad (25)$$

If $c > \widehat{c}$, then $\mu_1 < \mu_3 < \mu_2$ and we have

$$\begin{pmatrix} \overline{U}(z) \\ \overline{V}(z) \end{pmatrix} = C_1 \begin{pmatrix} \zeta_1(\mu_1) \\ \zeta_2(\mu_1) \end{pmatrix} e^{-\mu_1 z}$$
$$+ C_2 \begin{pmatrix} -\zeta_1(\mu_2) \\ -\zeta_2(\mu_2) \end{pmatrix} e^{-\mu_2 z} + C_3 \begin{pmatrix} 0 \\ 1 \end{pmatrix} e^{-\mu_3 z},$$
$$\qquad (26)$$
$$\text{as } z \longrightarrow \infty,$$

for $C_1 > 0$ or $C_1 = 0, C_{2,3} > 0$. Here, $(0 \ 1)^T$ is the eigenvector of $A(\mu)$ corresponding to μ_3, and note that $\zeta_1(\mu_2) < 0$ in this case. On the other hand, when

$$d > \widehat{d}, \qquad (27)$$

$(\overline{U}, \overline{V})(z)$ behaves like (26) if $c > \widehat{c}$. For the case when $c^* < c < \widehat{c}$, we have $\mu_3 < \mu_1 < \mu_2$. Hence,

$$\begin{pmatrix} \overline{U}(z) \\ \overline{V}(z) \end{pmatrix} = C_1 \begin{pmatrix} -\zeta_1(\mu_1) \\ -\zeta_2(\mu_1) \end{pmatrix} e^{-\mu_1 z}$$
$$+ C_2 \begin{pmatrix} -\zeta_1(\mu_2) \\ -\zeta_2(\mu_2) \end{pmatrix} e^{-\mu_2 z} + C_3 \begin{pmatrix} 0 \\ 1 \end{pmatrix} e^{-\mu_3 z},$$
$$\qquad (28)$$
$$\text{as } z \longrightarrow \infty,$$

for $C_{1,3} > 0$, or $C_1 = 0, C_{2,3} > 0$. We summarize the above behaviors in Table 1.

TABLE 1: The asymptotic behavior of the wave profile $(\overline{U}, \overline{V})$ near infinity.

Condition on d	Condition on c	The asymptotic behavior
$0 \leq d < 1$	$c > c^*$	(23)
$1 < d < \widehat{d}$	$c^* < c < \widehat{c}$	(23)
$1 < d$	$c > \widehat{c}$	(26)
$d > \widehat{d}$	$c^* < c < \widehat{c}$	(28)

Kan-on in [3] derived the asymptotic behaviors of $(\overline{U}, \overline{V})(z)$ near infinity when $c \geq c^*$. After deriving the behavior of $\overline{U}(z)$, he used it into the V-equation to find the behavior of $\overline{V}(z)$ when $\mu_1 \leq \mu_2 \leq \mu_3$ and when $\mu_3 \leq \mu_1 \leq \mu_2$. Our result here agrees with that in [3] when $c > c^*$. We further study the case when $\mu_1 < \mu_3 < \mu_2$.

Finally, we have the asymptotic behavior for the solution $\overline{U}(z)$ when the wave speed is greater than the minimal speed c^*.

Theorem 1. *For $c > c^*$, the wavefront $\overline{U}$ has the following behavior:*

$$\overline{U}(z) \sim C_1 e^{-\mu_1 z}, \quad as\ z \longrightarrow \infty \qquad (29)$$

for some $C_1 > 0$.

Proof. On the contrary, assume that for some $c_1 > c^*$, the wavefront $\overline{U}$ has the following behavior:

$$\overline{U}(z) \sim C_2 e^{-\mu_2 z}, \quad as\ z \longrightarrow \infty \qquad (30)$$

for some $C_2 > 0$. By this assumption, it follows that $(\overline{U}, \overline{V})(x - c_1 t)$ is a solution to the following partial differential equation:

$$u_t = u_{xx} + u(1 - a_1 - u + a_1 v),$$
$$v_t = dv_{xx} + r(1 - v)(a_2 u - v), \qquad (31)$$

with the initial conditions

$$u(x, 0) = \overline{U}(x)$$
$$and\ v(x, 0) = \overline{V}(x). \qquad (32)$$

We know that there exists a monotonic traveling wavefront to the system (31) for any $c \geq c^*$. In particular, assume $(U, V)(x - ct)$ is a solution for some $c \in (c^*, c_1)$ with the initial condition

$$u(x, 0) = U(x)$$
$$and\ v(x, 0) = V(x). \qquad (33)$$

By a simple computation of the asymptotic behavior of this solution to (8)-(9) near $\pm \infty$, we can always obtain (by shifting if necessary) $\overline{U}(x) \leq U(x)$ for all $x \in (-\infty, \infty)$. From the second equation of (8), we have $\overline{V}(x) \leq V(x)$ for all $x \in (-\infty, \infty)$. From (31), by comparison, we get

$$\overline{U}(x - c_1 t) \leq U(x - ct),$$
$$\overline{V}(x - c_1 t) \leq V(x - ct), \qquad (34)$$

for all $(x, t) \in (\mathbb{R}, \mathbb{R}^+)$. On the other hand, fix $\xi = x - c_1 t$. Then $\overline{U}(\xi) > 0$ is fixed, and we have

$$U(x - ct) = U(\xi + (c_1 - c)t) \sim U(+\infty) = 0 \qquad (35)$$
$$as\ t \longrightarrow \infty.$$

By (34), this implies that $\overline{U}(\xi) \leq 0$, which is a contradiction. The proof is complete. $\square$

3. The Local Stability

To study the local stability, as usual, we add a small perturbation to the traveling wave and study the behavior of this perturbation for large time period. If this perturbation decays, then we say that the traveling wave is locally stable. For $\delta \ll 1$ and a parameter λ, let

$$U(z, t) = \overline{U}(z) + \delta \phi_1(z) e^{\lambda t},$$
$$V(z, t) = \overline{V}(z) + \delta \phi_2(z) e^{\lambda t}, \qquad (36)$$

where ϕ_1 and ϕ_2 are two real functions. Substitute these formulas into (11) and linearize the system about $(\overline{U}, \overline{V})$ to get the following spectrum problem:

$$\lambda \Phi = \mathscr{L} \Phi := D \Phi'' + c \Phi' + J(z) \Phi, \qquad (37)$$

where $\Phi = (\phi_1 \ \phi_2)^T$, D and $J(z)$ are 2×2 matrices given by

$$D = \begin{pmatrix} 1 & 0 \\ 0 & d \end{pmatrix}$$

and $J(z)$ $\qquad\qquad (38)$

$$= \begin{pmatrix} 1 - a_1 - 2\overline{U} + a_1\overline{V} & a_1\overline{U} \\ ra_2(1 - \overline{V}) & r(-1 - a_2\overline{U} + 2\overline{V}) \end{pmatrix}.$$

For Φ in a suitable space, we shall find sign of the maximal real part to the spectrum (λ) of the operator $\mathscr{L}$ to determine the local stability of the traveling wave solution. To proceed, we introduce a weighted functional space L_w^p,

$$L_w^p = \{f(z) : w(z) f(z) \in L^p(\mathbb{R}),\ p \geq 1\} \qquad (39)$$

with the norm

$$\|f(z)\|_{L_w^p} = \left(\int_{-\infty}^{\infty} w(z) |f(z)|^p dz \right)^{1/p}, \qquad (40)$$

where

$$w(z) = \left(\frac{1}{w_1(z)},\ \frac{1}{w_2(z)} \right) \qquad (41)$$

is the weight function with

$$w_1(z) = \begin{cases} e^{-\alpha(z - z_0)}, & z > z_0 \\ 1, & z \leq z_0, \end{cases}$$
$$\qquad\qquad (42)$$
$$w_2(z) = \begin{cases} e^{-\beta(z - z_0)}, & z > z_0 \\ 1, & z \leq z_0, \end{cases}$$

for some positive constants α, β, and z_0 to be chosen. Here, $L^p(\mathbb{R})$, for $p \geq 1$, is the well-known Lebesgue space of integrable functions defined on $\mathbb{R}$. Then we consider the operator $\mathscr{L}$ on this new space and find its spectrum. To do this, we write $\Phi(z)$ in the form

$$\Phi = \begin{pmatrix} \phi_1 \\ \phi_2 \end{pmatrix} = \begin{pmatrix} w_1 \psi_1 \\ w_2 \psi_2 \end{pmatrix}, \tag{43}$$

for L^p-functions ψ_1 and ψ_2. Substituting (43) into (37) gives a new spectrum problem in the weighted space L^p_w,

$$\lambda \Psi = \mathscr{L}_w \Psi := D\Psi'' + M(z)\Psi' + N(z)\Psi, \tag{44}$$

where $\Psi = (\psi_1 \ \psi_2)^T$, $M(z)$ and $N(z)$ are 2×2 matrices defined by

$$M(z) = \begin{pmatrix} c + 2\dfrac{w_1'}{w_1} & 0 \\ 0 & c + 2d\dfrac{w_2'}{w_2} \end{pmatrix} \tag{45}$$

and

$$N(z) = \begin{pmatrix} \dfrac{w_1''}{w_1} + c\dfrac{w_1'}{w_1} & 0 \\ 0 & d\dfrac{w_2''}{w_2} + c\dfrac{w_2'}{w_2} \end{pmatrix} + Y(z), \tag{46}$$

with the ik-element of the matrix $Y(z)$, y_{ik}, being given in terms of the ik-element of the matrix $J(z)$ as $y_{ik} = (w_k/w_i)j_{ik}$; that is,

$$N(z) = \begin{pmatrix} \dfrac{w_1''}{w_1} + c\dfrac{w_1'}{w_1} + 1 - a_1 - 2\overline{U} + a_1\overline{V} & a_1\overline{U}\dfrac{w_2}{w_1} \\ ra_2\left(1 - \overline{V}\right)\dfrac{w_1}{w_2} & d\dfrac{w_2''}{w_2} + c\dfrac{w_2'}{w_2} + r\left(-1 - a_2\overline{U} + 2\overline{V}\right) \end{pmatrix}. \tag{47}$$

The details to find the essential spectrum of the operator $\mathscr{L}_w$ can be finalized by using Theorem A.2 in [32] and are given below. After we choose the weight function so that the essential spectrum is on the left-half complex plane, we can determine the sign of the maximal real part of the point spectrum in the weighted space as well.

First of all, to apply the method in [32], we need to choose α and β so that the matrix functions $M(z)$ and $N(z)$ are bounded; i.e., the limits

$$\lim_{z \to \infty} \overline{U}(z)\frac{w_2(z)}{w_1(z)} = A_1$$

$$\text{and } \lim_{z \to \infty} \left(1 - \overline{V}(z)\right)\frac{w_1(z)}{w_2(z)} = A_2, \tag{48}$$

for some constants A_1 and A_2, are satisfied. We choose

$$\alpha - \mu_1 < \beta \leq \alpha, \tag{49}$$

where μ_1 is defined in (19). This makes, by using Theorem 1, $A_1 = 0$ and

$$A_2 = \begin{cases} 0 & \text{when } \beta < \alpha, \\ 1 & \text{when } \beta = \alpha. \end{cases} \tag{50}$$

Now, we define

$$S_\pm := \left\{\lambda \mid \det\left(-\tau^2 D + i\tau M_\pm + N_\pm - \lambda I\right) = 0, \ -\infty < \tau < \infty\right\}, \tag{51}$$

where $M_\pm$ and $N_\pm$ are the limits of $M(z)$ and $N(z)$ as $z \to \pm\infty$, respectively. Then the essential spectrum of the operator

$\mathscr{L}_w$ is contained in the union of regions inside or on the curves S_+ and S_-; see [32, pp. 140]. By letting $z \to +\infty$, M_+, and N_+ are given as (taking condition (49) into account)

$$M_+ = \begin{pmatrix} c - 2\alpha & 0 \\ 0 & c - 2d\beta \end{pmatrix}$$

$$\text{and } N_+ = \begin{pmatrix} \alpha^2 - c\alpha + 1 - a_1 & 0 \\ A_2 & d\beta^2 - c\beta - r \end{pmatrix}. \tag{52}$$

The equation $\det(-\tau^2 D + i\tau M_+ + N_+ - \lambda I) = 0$ has two solutions $\lambda = \lambda_{1,2}$, where

$$\lambda_1 = -\tau^2 + i\tau(c - 2\alpha) + \alpha^2 - c\alpha + 1 - a_1,$$
$$\lambda_2 = -\tau^2 d + i\tau(c - 2d\beta) + d\beta^2 - c\beta - r. \tag{53}$$

This means that S_+ is the union of two parabolas in the complex plane which are symmetric about the real axis; namely,

$$S_{+,1} = \{\lambda_1 \mid -\infty < \tau < \infty\} \text{ and}$$
$$S_{+,2} = \{\lambda_2 \mid -\infty < \tau < \infty\}. \tag{54}$$

The most right points of these curves are $\alpha^2 - c\alpha + 1 - a_1$ and $d\beta^2 - c\beta - r$, respectively, which are negative if

$$\alpha \in (\mu_1, \mu_2) \text{ and}$$
$$\beta \in (0, \mu_3), \tag{55}$$

where μ_1, μ_2, and μ_3 are defined in (19)-(20). Hence, when the above condition satisfies, $S_+ = S_{+,1} \cup S_{+,2}$ is on the left-half complex plane.

Similarly, we find S_- by solving the equation $\det(-\tau^2 D + i\tau M_- + N_- - \lambda I) = 0$, with

$$M_- = \begin{pmatrix} c & 0 \\ 0 & c \end{pmatrix} \text{ and}$$

$$N_- = \begin{pmatrix} -1 & a_1 \\ 0 & r(1-a_2) \end{pmatrix}. \tag{56}$$

This gives two solutions $\lambda = \lambda_{3,4}$, where

$$\lambda_3 = -\tau^2 + i\tau c - 1,$$

$$\lambda_4 = -\tau^2 d + i\tau c + r(1-a_2). \tag{57}$$

From (**C1**), $S_- = \{\lambda_3 \mid -\infty < \tau < \infty\} \cup \{\lambda_4 \mid -\infty < \tau < \infty\}$ is on the left-half complex plane.

The above analysis shows that the essential spectrum of $\mathcal{L}_w$ is on the left-half complex plane as long as conditions (49) and (55) are satisfied. In fact, there are many choices of α and β satisfying these conditions depending on μ_1, μ_2, and μ_3. We choose them by the following algorithm.

Algorithm 2. Two mechanisms are valid to choose α and β so that all conditions in (49) and (55) hold:

(1) If $\mu_1 < \mu_3$, then we choose $\beta = \alpha$ for any $\alpha \in (\mu_1, \min\{\mu_2, \mu_3\})$.

(2) If $\mu_1 \geq \mu_3$, then we choose $\epsilon < \beta < \mu_3$ and $\alpha = \mu_1 + \epsilon$ for small $\epsilon > 0$. In particular, we can choose $\beta = 2\epsilon$ and $\alpha = \mu_1 + \epsilon$, for $\epsilon < \min\{\mu_2 - \mu_1, \mu_3/2\}$.

Finally, in order to get a local stability result, we need to check the sign of the principal eigenvalue in the point spectrum for (37)-(38). Consider the associated linear partial differential system

$$u_t = Du_{zz} + cu_z + J(z)u, \tag{58}$$

where $u(z,t) = (u_1(z,t), u_2(z,t))$. The eigenpair (λ, Φ) of (37) implies a solution $e^{\lambda t}\Phi$ to the above system. Let $Q_t = u(t, z, \phi)$ denote the solution semiflow of (58) for any given initial data ϕ in L^p. It is easy to see Q_t is compact and strongly positive. By the well-known Krein-Rutman theorem (see, e.g., [33]), Q_t has a simple principal eigenvalue $\lambda_{\max}$ with a strongly positive eigenvector, and all other eigenvalues $e^{\lambda t}$ must satisfy

$$\left|e^{\lambda t}\right| < e^{\lambda_{\max} t}. \tag{59}$$

For any $c > c^*$, we have from Theorem 1 that $\overline{U}(z) \sim C_1 e^{-\mu_1 z}$, $C_1 > 0$, as $z \longrightarrow \infty$. $\lambda = 0$ is an eigenvalue to the operator $\mathcal{L}$ defined in (37) with the one-sign (strongly positive) eigenvector $(-\overline{U}', -\overline{V}')(z)$. By the choice of the weighted functional space L_w^p, the one-sign eigenvector $(\overline{U}', \overline{V}')(z)$ is not inside. Hence, the real parts of point spectrum of the operator $\mathcal{L}_w$ in L_w^p are all negative. We can also explain this in a simple analysis. Assume to the contrary that (λ, Φ) is an eigenpair of the eigenvalue problem (37)-(38) with $\lambda > 0$ and $\Phi \in L_w^p$. Obviously, the one-sign function $\overline{\Phi} = (-\overline{U}', -\overline{V}')(z)$

satisfies (58). For Φ in the L_w^p-space, we have essentially (or except for a set of zero measure) $\overline{\Phi}(z) > \Phi(z)$ as $z \longrightarrow \infty$. On the other hand, when $z \longrightarrow -\infty$, we can apply the method of asymptotic analysis and assume that the eigenfunction of (37) behaves like $ke^{\mu z}$ for some positive values k and μ. By substituting it into the eigenvalue problem and using the behavior of $J(z)$, we obtain that μ is increasing with respect to λ. This implies that $\overline{\Phi}(z) > \Phi(z)$ as $z \longrightarrow -\infty$. Hence, by choosing $\overline{k}$ sufficient large, we can have $\overline{k}\,\overline{\Phi} \geq |\Phi|$. By comparison, from the partial differential system (58), we obtain $\overline{k}\,\overline{\Phi}(z) \geq |\Phi|e^{\lambda t}$, which contradicts $\lambda > 0$. This implies that for $\Phi \in L_w^p$, the real parts of all eigenvalues λ of (37) should be nonpositive.

Now we are in a position to state the local stability result.

Theorem 3. *For any $c > c^*$, the wavefront $(\overline{U}, \overline{V})(z)$ is locally stable in the weighted functional space L_w^p with the weight function $w(z)$ defined in (41)-(42), where α and β in the formula of $w(z)$ are chosen by Algorithm 2.*

4. The Global Stability

We study here the global stability of the steady-state $(\overline{U}, \overline{V})(z)$ in a special choice of the weighted functional space $L_w^p(\mathbb{R})$. Let $p = \infty$ and define the norm $\|f\|_{L_w^\infty} = \text{ess sup}_{z \in \mathbb{R}} |w(z)f(z)|$, for some weight function $w(z)$. Assume $\mu_1 < \mu_3$. By Algorithm 2, we choose $\alpha = \beta \in (\mu_1, \min\{\mu_2, \mu_3\})$. Specifically, let $\alpha = \beta = \mu_1 + \epsilon$, for small positive number ϵ. Also, we assume that the functions $\overline{U}(z)$ and $\overline{V}(z)$ satisfy the condition

$$\frac{\overline{V}(z)}{\overline{U}(z)} \leq \min\left\{a_2, \frac{1}{a_1}\right\}, \quad \forall z \in (-\infty, +\infty). \tag{C2}$$

Theorem 4. *Suppose $c > c^*$, $\mu_1 < \mu_3$, and conditions (**C1**) - (**C2**) hold true. Assume that the initial data $U(z,0) = U_0(z)$ and $V(z,0) = V_0(z)$ satisfy*

$$(0,0) \leq (U_0, V_0)(z) \leq (1,1),$$

$$\forall z \in \mathbb{R}, \tag{60}$$

$$\lim_{z \to -\infty} \inf(U_0, V_0)(z) > (0,0),$$

and

$$\left|U_0(z) - \overline{U}(z)\right| \in L_w^\infty(\mathbb{R}),$$

$$\left|V_0(z) - \overline{V}(z)\right| \in L_w^\infty(\mathbb{R}). \tag{61}$$

Then the solution $(U,V)(z,t)$ to (11) exists globally with

$$(0,0) \leq (U,V)(z,t) \leq (1,1), \quad \forall(z,t) \in \mathbb{R} \times \mathbb{R}^+, \tag{62}$$

and converges to the steady-state $(\overline{U}, \overline{V})(z)$ exponentially in the sense of

$$\sup_{z \in \mathbb{R}} \left|U(z,t) - \overline{U}(z)\right| \leq ke^{-\eta t}, \quad t > 0,$$

$$\sup_{z \in \mathbb{R}} \left|V(z,t) - \overline{V}(z)\right| \leq ke^{-\eta t}, \quad t > 0, \tag{63}$$

for positive constants k and η.

To prove Theorem 4, we will find an upper and a lower solution to the partial differential equations system (11). For $z \in \mathbb{R}$, define

$$U_0^+(z) = \max\left\{U_0(z), \overline{U}(z)\right\},$$

$$V_0^+(z) = \max\left\{V_0(z), \overline{V}(z)\right\},$$

$$U_0^-(z) = \min\left\{U_0(z), \overline{U}(z)\right\},$$

$$V_0^-(z) = \min\left\{V_0(z), \overline{V}(z)\right\}. \tag{64}$$

It is easy to see that the following inequalities are true:

$$(0,0) \le \left(U_0^-, V_0^-\right)(z) \le (U_0, V_0)(z) \le \left(U_0^+, V_0^+\right)(z)$$

$$\le (1,1),$$

$$(0,0) \le \left(U_0^-, V_0^-\right)(z) \le \left(\overline{U}, \overline{V}\right)(z) \le \left(U_0^+, V_0^+\right)(z) \tag{65}$$

$$\le (1,1).$$

Denote $(U^+, V^+)(z,t)$ and $(U^-, V^-)(z,t)$ as the solutions to the system (11) with the initial data $(U_0^+, V_0^+)(z)$ and $(U_0^-, V_0^-)(z)$, respectively; that is,

$$U_t^\pm = U_{zz}^\pm + cU_z^\pm$$

$$+ U^\pm\left(1 - a_1 - U^\pm + a_1 V^\pm\right),$$

$$V_t^\pm = dV_{zz}^\pm + cV_z^\pm \tag{66}$$

$$+ r\left(1 - V^\pm\right)\left(a_2 U^\pm - V^\pm\right),$$

$$\left(U^\pm, V^\pm\right)(z,0) = \left(U_0^\pm, V_0^\pm\right)(z).$$

By the comparison principle, one gets

$$(0,0) \le \left(U^-, V^-\right)(z,t) \le (U, V)(z,t)$$

$$\le \left(U^+, V^+\right)(z,t) \le (1,1), \quad \forall (z,t) \in \mathbb{R} \times \mathbb{R}^+,$$

$$(0,0) \le \left(U^-, V^-\right)(z,t) \le \left(\overline{U}, \overline{V}\right)(z) \le \left(U^+, V^+\right)(z,t) \tag{67}$$

$$\le (1,1), \quad \forall (z,t) \in \mathbb{R} \times \mathbb{R}^+.$$

In the following lemmas we shall prove the convergence of $(U^+, V^+)(z,t)$ and $(U^-, V^-)(z,t)$ to the wavefront $(\overline{U}, \overline{V})(z)$. Then we apply the squeezing theorem to obtain the result in Theorem 4.

Lemma 5. *Under the conditions in Theorem 4, $(U^+, V^+)(z,t)$ converges to $(\overline{U}, \overline{V})(z)$.*

Proof. For $(z,t) \in \mathbb{R} \times \mathbb{R}^+$, define

$$P(z,t) = U^+(z,t) - \overline{U}(z)$$

$$\text{and } Q(z,t) = V^+(z,t) - \overline{V}(z). \tag{68}$$

These functions, P and Q, satisfy the initial value conditions

$$P(z,0) = U_0^+(z) - \overline{U}(z)$$

$$\text{and } Q(z,0) = V_0^+(z) - \overline{V}(z). \tag{69}$$

By (65) and (67), for all $z \in \mathbb{R}$ and $t \ge 0$, we have

$$(0,0) \le (P,Q)(z,t) \le (1,1). \tag{70}$$

By (8) and (66) and using condition (**C2**), we can verify that P and Q satisfy

$$P_t \le P_{zz} + cP_z + (1 - a_1)P + \left(P + \overline{U}\right)\left(-P + a_1 Q\right),$$

$$Q_t \le Q_{zz} + cQ_z + r\left(a_2 P - Q\right) \tag{71}$$

$$+ r\left(Q + \overline{V}\right)\left(-a_2 P + Q\right).$$

To study the stability in the weighted functional space L_w^∞, with $w(z)$ defined in (41), we first let

$$\binom{P}{Q}(z,t) = e^{-\alpha(z-z_0)}\binom{\overline{P}}{\overline{Q}}(z,t),$$

$$\text{for all } (z,t) \in \mathbb{R} \times \mathbb{R}^+, \tag{72}$$

where $\overline{P}$ and $\overline{Q}$ are functions in $L^\infty(\mathbb{R})$ and z_0 is the same number used in the weight function $w(z)$. This gives

$$\binom{\overline{P}}{\overline{Q}}_t \le D\binom{\overline{P}}{\overline{Q}}_{zz} + M\binom{\overline{P}}{\overline{Q}}_z + A(\alpha)\binom{\overline{P}}{\overline{Q}}$$

$$+ \left(\begin{array}{c} \left(\overline{U} + e^{-\alpha(z-z_0)}\overline{P}\right)\left(-\overline{P} + a_1\overline{Q}\right) \\ r\left(\overline{V} + e^{-\alpha(z-z_0)}\overline{Q}\right)\left(-a_2\overline{P} + \overline{Q}\right) \end{array}\right) \tag{73}$$

$$:= \binom{\mathscr{L}_1\left(\overline{P}, \overline{Q}\right)}{\mathscr{L}_2\left(\overline{P}, \overline{Q}\right)},$$

where $A(\alpha)$ is the same matrix defined in (18) and $M = \text{diag}(c - 2\alpha, c - 2d\alpha)$.

Define $\overline{P}_1(z,t)$ and $\overline{Q}_1(z,t)$ as

$$\overline{P}_1(z,t) = k_1\zeta_1 e^{-\eta_1 t}$$

$$\text{and } \overline{Q}_1(z,t) = k_1\zeta_2 e^{-\eta_1 t}, \tag{74}$$

$$\forall (z,t) \in \mathbb{R} \times \mathbb{R}^+,$$

for some constants $k_1, \eta_1 > 0$ to be chosen and $(\zeta_1, \zeta_2) = (\zeta_1(\alpha), \zeta_2(\alpha))$ is the eigenvector of the matrix $A(\alpha)$ associated with the eigenvalue $\alpha^2 - c\alpha + 1 - a_1$. Simple computations give

$$\zeta_1(\alpha) = \left(\alpha^2 - c\alpha + 1 - a_1\right) - \left(d\alpha^2 - c\alpha - r\right)$$

$$= \left(\mu_1^2 + \epsilon\right)(1 - d) + 1 - a_1 + r, \tag{75}$$

$$\zeta_2(\alpha) = ra_2,$$

which are positive for small ϵ and $\mu_1 < \mu_3$. Since the initial values $\overline{P}(z,0)$ and $\overline{Q}(z,0)$ are in the space L_w^∞, we can choose $k_1 \ge \max_{z \in \mathbb{R}}\{\overline{P}(z,0)/\zeta_1, \overline{Q}(z,0)/\zeta_2\}$. Direct computations and using condition (**C2**) show that both of $\mathscr{L}_1(\overline{P}_1, \overline{Q}_1)$ and

(a) $a_1 = 0.5$ and $a_2 = 2.4$. We choose $\delta = 1$

(b) $a_1 = 0.5$ and $a_2 = 1.4$. The maximal possible value of δ is in $(0.3984, 1)$

(c) $a_1 = 0.3$ and $a_2 = 1.4$. The maximal possible value of δ becomes close to 0.3984
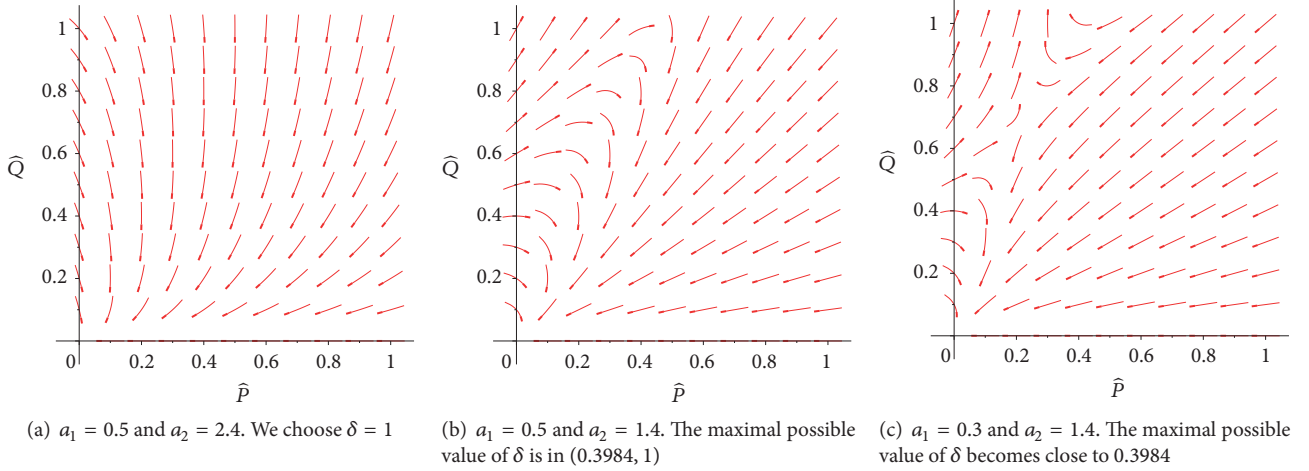
Figure 1: The phase portrait of system (80) when $\epsilon_1 = 0.003$ and $r = 1.875$.

$\mathscr{L}_2(\overline{P}_1, \overline{Q}_1)$ are negative. This allows choosing a positive value to η_1 so that the inequality

$$\begin{pmatrix} \overline{P}_1 \\ \overline{Q}_1 \end{pmatrix}_t = -\eta_1 k_1 \begin{pmatrix} \zeta_1 \\ \zeta_2 \end{pmatrix} e^{-\eta_1 t} \geq \begin{pmatrix} \mathscr{L}_1(\overline{P}_1, \overline{Q}_1) \\ \mathscr{L}_2(\overline{P}_1, \overline{Q}_1) \end{pmatrix} \tag{76}$$

holds. Hence, since $(\overline{P}_1, \overline{Q}_1)(0, z) \geq (\overline{P}, \overline{Q})(0, z)$ and by comparison on unbounded domain, see, e.g., [34, Proposition 2.1],

$$(P, Q)(z, t) = (\overline{P}, \overline{Q}) e^{-\alpha(z - z_0)}$$
$$\leq k_1 (\zeta_1, \zeta_2) e^{-\alpha(z - z_0) - \eta_1 t}, \tag{77}$$

$$\forall (z, t) \in \mathbb{R} \times \mathbb{R}^+.$$

In particular, this is true when $z \in [z_0, \infty)$, for any fixed z_0.

Now, we introduce the weight function $w(z)$ defined in (41)-(42) with $\alpha = \beta = \mu_1 + \epsilon$. By the above analysis, we need to prove the convergence of $(P, Q)(z, t)$ to $(0, 0)$ for $z \in (-\infty, z_0]$. Note that the full system of $(P, Q)(z, t)$ can be expressed as

$$\begin{pmatrix} P \\ Q \end{pmatrix}_t = D \begin{pmatrix} P \\ Q \end{pmatrix}_{zz} + c \begin{pmatrix} P \\ Q \end{pmatrix}_z + J(z) \begin{pmatrix} P \\ Q \end{pmatrix}$$
$$+ \begin{pmatrix} (-P + a_1 Q) P \\ r(-a_2 P + Q) Q \end{pmatrix}. \tag{78}$$

Here, $J(z)$ is the same 2×2 matrix defined in (38). Let z_0 be chosen so that

$$J(z) \leq \begin{pmatrix} -1 + \epsilon_1 & a_1 + \epsilon_1 \\ \epsilon_1 & r(1 - a_2) + \epsilon_1 \end{pmatrix} := J_{\epsilon_1}, \tag{79}$$

for some given small $\epsilon_1 > 0$, when $z \leq z_0$. This is equivalent to require that $(\overline{U}, \overline{V})(z)$ is close to $(1, 1)$ for all $z \leq z_0$. Define $(\widehat{P}, \widehat{Q})(t)$ as the solution of the autonomous system

$$\begin{pmatrix} \widehat{P} \\ \widehat{Q} \end{pmatrix}_t = J_{\epsilon_1} \begin{pmatrix} \widehat{P} \\ \widehat{Q} \end{pmatrix} + \begin{pmatrix} (-\widehat{P} + a_1 \widehat{Q}) \widehat{P} \\ r(-a_2 \widehat{P} + \widehat{Q}) \widehat{Q} \end{pmatrix}, \tag{80}$$

with the initial data

$$\widehat{P}(0) \geq \overline{P}(z, 0),$$
$$\widehat{Q}(0) \geq \overline{Q}(z, t), \tag{81}$$
$$\forall z \in \mathbb{R}.$$

Then $(\widehat{P}, \widehat{Q})$ is an upper solution to system (78).

Now we need to prove the convergence of $(\widehat{P}, \widehat{Q})(t)$ to $(0, 0)$ as $t \longrightarrow \infty$. The Jacobian matrix $J(0, 0) = J_{\epsilon_1}$ of system (80) at the fixed point $(0, 0)$ has two eigenvalues, $\widehat{\lambda}_2 < \widehat{\lambda}_1 < 0$. By the phase plane analysis, there exists $0 < \delta \leq 1$ so that the flow in the $\widehat{P}\widehat{Q}$–space converges to origin for any initial data $(\widehat{P}, \widehat{Q})(0)$ in the box $[0, 1] \times [0, \delta]$. Hence, we conclude that

$$(\widehat{P}, \widehat{Q}) = \widehat{k}_1 (\widehat{C}_1, \widehat{C}_2) e^{\widehat{\lambda}_1 t} \quad \text{as } t \longrightarrow \infty, \tag{82}$$

for positive constant $\widehat{k}_1$ and $(\widehat{C}_1 \ \widehat{C}_2)^T$ is the eigenvector of J_{ϵ_1} corresponding to $\widehat{\lambda}_1$. For the maximal possible choice of the constant δ so that we have the convergence result inside the box $[0, 1] \times [0, \delta]$; see Remark 6.

We can choose $\widehat{k}_1$ large and $\overline{\lambda}_1 = \min\{\eta_1, -\widehat{\lambda}_1\}$ so that, at the boundary $z = z_0$, we have

$$(P, Q)(z_0, t) \leq k_1 (\zeta_1, \zeta_2) e^{-\eta_1 t} \leq \widehat{k}_1 (\zeta_1, \zeta_2) e^{-\overline{\lambda}_1 t}. \tag{83}$$

Hence, by comparison on the domain $(-\infty, z_0] \times [0, \infty)$, see, e.g., [35, Lemma 3.2],

$$(P, Q)(z, t) \leq \widehat{k}_1 (\zeta_1, \zeta_2) e^{-\overline{\lambda}_1 t}, \tag{84}$$
$$\forall (z, t) \in (-\infty, z_0] \times \mathbb{R}^+.$$

This completes the proof. □

Remark 6. The maximal possible value of the constant δ, which could be 1, depends on the location of the fourth fixed point to the system (80) near or inside the box $[0, 1] \times [0, 1]$. See Figure 1 for all possible different cases. In Figure 1(a), the

positive fixed point is far away from the box $[0, 1] \times [0, 1]$ and does not affect the flow. This happens when $a_2 > 2$. Hence we set $\delta = 1$. Figure 1(b) shows the effect of the positive fixed point on the flow, which still outside the box. The maximal choice of δ for this case exists in the interval $(a_2 - 1 - \epsilon_1/r, 1)$. The number $a_2 - 1 - \epsilon_1/r$ is the positive $\widehat{Q}$-intercept of the nullcline $\widehat{Q}_t = 0$. A fixed point exists inside the box $[0, 1] \times [0, 1]$ in Figure 1(c), where δ becomes close to the value $a_2 - 1 - \epsilon_1/r$.

Lemma 7. *Under the conditions in Theorem 4, $(U^-, V^-)(z, t)$ converges to $(\overline{U}, \overline{V})(z)$.*

Proof. For $(z, t) \in \mathbb{R} \times \mathbb{R}^+$, define

$$R(z, t) = \overline{U}(z) - U^-(z, t)$$
$$\text{and } S(z, t) = \overline{V}(z) - V^-(z, t). \tag{85}$$

These functions, R and S, satisfy the initial value conditions

$$R(z, 0) = \overline{U}(z) - U_0^-(z)$$
$$\text{and } S(z, 0) = \overline{V}(z) - V_0^-(z). \tag{86}$$

From (65) and (67), for all $z \in \mathbb{R}$ and $t \geq 0$, we have

$$(0, 0) \leq (R, S)(z, t) \leq (1, 1). \tag{87}$$

From (8) and (66), R and S satisfy the system

$$\begin{pmatrix} R \\ S \end{pmatrix}_t = D \begin{pmatrix} R \\ S \end{pmatrix}_{zz} + c \begin{pmatrix} R \\ S \end{pmatrix}_z + J(z) \begin{pmatrix} R \\ S \end{pmatrix} \\ - \begin{pmatrix} (-R + a_1 S) R \\ r(-a_2 R + S) S \end{pmatrix}, \tag{88}$$

with $J(z)$ defined in (38). By condition (**C2**), we have

$$R_t \leq R_{zz} + cR_z + (1 - a_1) R + (R - \overline{U})(R - a_1 S),$$
$$S_t \leq dS_{zz} + cS_z + r(a_2 R - S) + r(S - \overline{V})(a_2 R - S). \tag{89}$$

Similar to the previous analysis in the proof of Lemma 5, and making a use of the facts $R < \overline{U}$ and $S < \overline{V}$, we can prove that there exist $\eta_2 > 0$ and

$$k_2 \geq e^{\alpha(z - z_0)} \max_{z \in \mathbb{R}} \left\{ \frac{R(z, 0)}{\zeta_1}, \frac{S(z, 0)}{\zeta_2} \right\} \tag{90}$$

so that

$$(R, S)(z, t) \leq k_2 (\zeta_1, \zeta_2) e^{-\eta_2 t}, \quad \forall (z, t) \in \mathbb{R} \times \mathbb{R}^+. \tag{91}$$

For the choice of z_0 in proof of Lemma 5, we study the stability in the weighted space L_w^∞. To this end, define $(\widehat{R}, \widehat{S})(t)$ as the solution of the system

$$\begin{pmatrix} \widehat{R} \\ \widehat{S} \end{pmatrix}_t = J_{\epsilon_1} \begin{pmatrix} \widehat{R} \\ \widehat{S} \end{pmatrix} - w_1 \begin{pmatrix} (-\widehat{R} + a_1 \widehat{S}) \widehat{R} \\ r(-a_2 \widehat{R} + \widehat{S}) \widehat{S} \end{pmatrix}, \tag{92}$$

with the initial data

$$\widehat{R}(0) \geq R(z, 0),$$
$$\widehat{S}(0) \geq S(z, 0), \tag{93}$$
$$\forall z \in \mathbb{R}.$$

It is easy to see that $(\widehat{R}, \widehat{S})$ is an upper solution to the system (88). The phase plane analysis shows that $(\widehat{R}, \widehat{S})(t)$ converges to origin for any initial data in the region $[0, 1] \times [0, 1]$ except the point $(1, 1)$. Similar to the previous lemma,

$$(R, S)(z, t) \leq \widehat{k}_2 (\zeta_1, \zeta_2) e^{-\overline{\lambda}_2 t}, \tag{94}$$
$$\forall (z, t) \in (-\infty, z_0] \times \mathbb{R}^+.$$

for some positive constants $\widehat{k}_2$ and $\overline{\lambda}_2$. This completes the proof. □

Now, we are ready to give the proof of Theorem 4.

Proof of Theorem 4. From (67), for all $(z, t) \in \mathbb{R} \times \mathbb{R}^+$, we have

$$|R(z, t)| \leq |U(z, t) - \overline{U}(z)| \leq |P(z, t)|,$$
$$|S(z, t)| \leq |V(z, t) - \overline{V}(z)| \leq |Q(z, t)|. \tag{95}$$

By Lemmas 5 and 7 and the squeezing theorem, it follows that there exist $k > 0$ and $\eta > 0$ so that

$$|U(z, t) - \overline{U}(z)| \leq ke^{-\eta t},$$
$$|V(z, t) - \overline{V}(z)| \leq ke^{-\eta t}, \tag{96}$$

for all $(z, t) \in \mathbb{R} \times \mathbb{R}^+$. This proves the desired result. □

Condition (**C2**) is used in the previous analysis to construct the upper solutions in the proof of Lemmas 5 and 7. It implies that, at $c = c_0$ and $z \longrightarrow +\infty$,

$$\frac{\zeta_2(\mu_1)}{\zeta_1(\mu_1)} \leq \min \left\{ a_2, \frac{1}{a_1} \right\}, \tag{97}$$

and it can be guaranteed by

$$d \leq 2,$$
$$(a_1 a_2 - 1) r \leq (2 - d)(1 - a_1). \tag{98}$$

This condition arose in the linear speed selection studies; see [36]. To see that the condition (**C2**) can be realized for all $z \in \mathbb{R}$, we prove the following claim.

Claim 8. $d = 0$ and $a_1 a_2 \leq 1$ imply (**C2**).

Proof. In the case when $d = 0$, the $\overline{V}$−equation can be written in the form

$$\overline{V}' = \frac{r}{c}(1 - \overline{V})(\overline{V} - a_2 \overline{U}),$$
$$\overline{V}(-\infty) = 1, \tag{99}$$
$$\overline{V}(+\infty) = 0.$$

Since $a_1 a_2 \leq 1$, we need to prove $\overline{V}(z) \leq a_2 \overline{U}(z)$ for all $z \in \mathbb{R}$. Assume, for contrary, this is not true for some $\overline{z} \in \mathbb{R}$. By (99), $\overline{V}$ is increasing at the neighborhood of $\overline{z}$. Since $\overline{U}(z)$ is a decreasing function, we have $\overline{V}(\overline{z} + \delta) > \overline{V}(\overline{z}) > a_2 \overline{U}(\overline{z}) > a_2 \overline{U}(\overline{z} + \delta)$, for some $\delta > 0$. Similarly, we can show that $\overline{V}(z)$ is increasing for all $z \geq \overline{z}$, which contradicts the fact $\overline{V}(+\infty) = 0$. This implies that condition (**C2**) holds true. $\square$

5. Conclusions

The local and the global stability of traveling waves to the two-species Lotka-Volterra competition model (5) under the condition (**C1**) are investigated. Using the linearization and the essential spectrum analysis in [32], we find that the traveling wavefront is stable in some weighted functional space; see Theorem 3. Many choices of the exponential weight functions are valid; see Algorithm 2.

Under some further condition (**C2**), we apply the upper-lower solution method to obtain a global stability result. Indeed, we prove that both the upper and the lower solutions tend to the wavefront. Our main results are presented in Theorem 4.

Data Availability

We have used Maple codes to do the figure in the paper. They are available from the corresponding author upon request. No other data were used in this study.

Conflicts of Interest

The authors declare that there are no conflicts of interest regarding the publication of this paper.

Acknowledgments

References

[1] A. Okubo, P. K. Maini, M. H. Williamson, and J. D. Murray, "On the spatial spread of the grey squirrel in Britain," *Proceedings - Royal Society of London, B*, vol. 238, no. 1291, pp. 113–125, 1989.

[2] J. D. Murray, *Journal of Mathematical Biology*, vol. 19, Springer, Berlin, Germany, 1989.

[3] Y. Kan-on, "Fisher wave fronts for the Lotka-Volterra competition model with diffusion," *Nonlinear Analysis. Theory, Methods & Applications. An International Multidisciplinary Journal*, vol. 28, no. 1, pp. 145–164, 1997.

[4] B. Li, H. F. Weinberger, and M. A. Lewis, "Spreading speeds as slowest wave speeds for cooperative systems," *Mathematical Biosciences*, vol. 196, no. 1, pp. 82–98, 2005.

[5] X. Liang and X.-Q. Zhao, "Asymptotic speeds of spread and traveling waves for monotone semiflows with applications," *Communications on Pure and Applied Mathematics*, vol. 60, no. 1, pp. 1–40, 2007.

[6] A. I. Volpert, V. A. Volpert, and V. Volpert, *Traveling Wave Solutions of Parabolic Systems*, vol. 140 of *Translations of Mathematical Monographs*, American Mathematical Society, Providence, RI, USA, 1994.

[7] C. Conley and R. Gardner, "An application of the generalized Morse index to travelling wave solutions of a competitive reaction-diffusion model," *Indiana University Mathematics Journal*, vol. 33, no. 3, pp. 319–343, 1984.

[8] R. A. Gardner, "Existence and stability of travelling wave solutions of competition models: a degree theoretic approach," *Journal of Differential Equations*, vol. 44, no. 3, pp. 343–364, 1982.

[9] Y. Kan-on, "Parameter dependence of propagation speed of travelling waves for competition-diffusion equations," *SIAM Journal on Mathematical Analysis*, vol. 26, no. 2, pp. 340–363, 1995.

[10] Y. Hosono, "The minimal speed of traveling fronts for a diffusive Lotka-Volterra competition model," *Bulletin of Mathematical Biology*, vol. 60, no. 3, pp. 435–448, 1998.

[11] A. Alhasanat and C. Ou, "On a Conjecture Raised by Yuzo Hosono," *Journal of Dynamics and Differential Equations*.

[12] W. Huang, "Problem on minimum wave speed for a Lotka-Volterra reaction-diffusion competition model," *Journal of Dynamics and Differential Equations*, vol. 22, no. 2, pp. 285–297, 2010.

[13] M. M. Tang and P. C. Fife, "Propagating fronts for competing species equations with diffusion," *Archive for Rational Mechanics and Analysis*, vol. 73, no. 1, pp. 69–77, 1980.

[14] J. H. van Vuuren, "The existence of travelling plane waves in a general class of competition-diffusion systems," *IMA Journal of Applied Mathematics*, vol. 55, no. 2, pp. 135–148, 1995.

[15] W.-T. Li, G. Lin, and S. Ruan, "Existence of travelling wave solutions in delayed reaction-diffusion systems with applications to diffusion-competition systems," *Nonlinearity*, vol. 19, no. 6, pp. 1253–1273, 2006.

[16] S. A. Gourley and S. Ruan, "Convergence and travelling fronts in functional differential equations with nonlocal terms: a competition model," *SIAM Journal on Mathematical Analysis*, vol. 35, no. 3, pp. 806–822, 2003.

[17] P. C. Fife and J. B. McLeod, "A phase plane discussion of convergence to travelling fronts for nonlinear diffusion," *Archive for Rational Mechanics and Analysis*, vol. 75, no. 4, pp. 281–314, 1981.

[18] T. Gallay, "Local stability of critical fronts in nonlinear parabolic partial differential equations," *Nonlinearity*, vol. 7, no. 3, pp. 741–764, 1994.

[19] X. Hou and Y. Li, "Local stability of traveling-wave solutions of nonlinear reaction-diffusion equations," *Discrete and Continuous Dynamical Systems - Series A*, vol. 15, no. 2, pp. 681–701, 2006.

[20] K. Kirchgässner, "On the nonlinear dynamics of travelling fronts," *Journal of Differential Equations*, vol. 96, no. 2, pp. 256–278, 1992.

[21] S. Ma and X.-Q. Zhao, "Global asymptotic stability of minimal fronts in monostable lattice equations," *Discrete and Continuous Dynamical Systems - Series A*, vol. 21, no. 1, pp. 259–275, 2008.

[22] H. J. K. Moet, "A note on the asymptotic behavior of solutions of the KPP equation," *SIAM Journal on Mathematical Analysis*, vol. 10, no. 4, pp. 728–732, 1979.

[23] D. H. Sattinger, "On the stability of waves of nonlinear parabolic systems," *Advances in Mathematics*, vol. 22, no. 3, pp. 312–355, 1976.

[24] W. Shen, "Travelling waves in time almost periodic structures governed by bistable nonlinearities. I. Stability and uniqueness," *Journal of Differential Equations*, vol. 159, no. 1, pp. 1–54, 1999.

[25] J.-C. Tsai and J. Sneyd, "Existence and stability of traveling waves in buffered systems," *SIAM Journal on Applied Mathematics*, vol. 66, no. 1, pp. 237–265, 2005.

[26] Y. Wu and X. Xing, "Stability of traveling waves with critical speeds for p-degree Fisher-type equations," *Discrete and Continuous Dynamical Systems - Series A*, vol. 20, no. 4, pp. 1123–1139, 2008.

[27] G. Lv and M. Wang, "Nonlinear stability of travelling wave fronts for delayed reaction diffusion equations," *Nonlinearity*, vol. 23, no. 4, pp. 845–873, 2010.

[28] M. Bramson, "Convergence of solutions of the Kolmogorov equation to travelling waves," *Memoirs of the American Mathematical Society*, vol. 44, no. 285, iv+190 pages, 1983.

[29] J. Xin, "Front propagation in heterogeneous media," *SIAM Review*, vol. 42, no. 2, pp. 161–230, 2000.

[30] G. Lv and M. Wang, "Nonlinear stability of traveling wave fronts for delayed reaction diffusion systems," *Nonlinear Analysis: Real World Applications*, vol. 13, no. 4, pp. 1854–1865, 2012.

[31] Y. Meng, W. Zhang, and Z. Yu, "Existence and asymptotic of traveling wave fronts for the delayed Volterra-type cooperative system with spatial diffusion," *Advances in Difference Equations*, Paper No. 203, 19 pages, 2018.

[32] D. Henry, *Geometric Theory of Semilinear Parabolic Equations*, vol. 840 of *Lecture Notes in Mathematics*, Springer, New York, NY, USA, 1993.

[33] P. Hess, *Periodic-Parabolic Boundary Value Problems and Positivity*, vol. 247 of *Pitman Research Notes in Mathematics Series*, Longman Scientific & Technical, Harlow, UK, 1991.

[34] D. G. Aronson and H. F. Weinberger, "Multidimensional nonlinear diffusion arising in population genetics," *Advances in Mathematics*, vol. 30, no. 1, pp. 33–76, 1978.

[35] H. R. Thieme, "Asymptotic estimates of the solutions of nonlinear integral equations and asymptotic speeds for the spread of populations," *Journal für die reine und angewandte Mathematik*, vol. 306, pp. 94–121, 1979.

[36] M. A. Lewis, B. Li, and H. F. Weinberger, "Spreading speed and linear determinacy for two-species competition models," *Journal of Mathematical Biology*, vol. 45, no. 3, pp. 219–233, 2002.

Research Article

Parameter Identification and Adaptive Control of Uncertain Goodwin Oscillator Networks with Disturbances

Jianbao Zhang [iD],[1,2,3] Wenyin Zhang,[1,2] Chengdong Yang [iD],[1,2,3] Haifeng Wang,[1,2] Jianlong Qiu,[2,4,5] and Fawaz Alsaadi[5]

[1]*School of Information Science and Engineering, Linyi University, Linyi 276005, China*
[2]*Key Laboratory of Complex Systems and Intelligent Computing in Universities of Shandong (Linyi University), Linyi 276005, China*
[3]*Department of Mathematics, Southeast University, Nanjing 210096, China*
[4]*School of Automation and Electrical Engineering, Linyi University, Linyi 276005, China*
[5]*Department of Information Technology, King Abdulaziz University, Jeddah 21589, Saudi Arabia*

Correspondence should be addressed to Jianbao Zhang; jianbaozhang@163.com

This paper investigates the dynamic properties of a differential equation model of mammals' circadian rhythms, including parameter identification, adaptive control, and outer synchronization. The circadian oscillator network is described by a Goodwin oscillator network, the couplings of which are from vasoactive intestinal polypeptides described by modified Van der Pol oscillators. We build up a drive-response system consisting of two networks with unknown parameters and disturbances. Then, we propose effective parameter updating laws to identify the unknown parameters and design adaptive control strategies to achieve outer synchronization in the drive-response system. As special cases, two succinct corollaries are presented for different instances. All the theoretical results are proved through strict mathematical deduction based on Lyapunov stability theory, and a numerical example is also carried out to illustrate the effectiveness.

1. Introduction

In the past decades, there has been tremendous interest in studying circadian rhythms of mammals at the cellular level [1–8]. Based on experimental findings of system biology and network biology, several gene regulatory network models have been established to describe the circadian rhythm system [3, 4]. Experimental evidence has shown that the circadian rhythms are controlled by a pacemaker located in the suprachiasmatic nucleus (SCN) of the hypothalamus [5] and the circadian oscillator is usually described by a Goodwin oscillator model, which describes a protein which represses the transcription of its own gene via an inhibitor [6]. Now, the Goodwin oscillator model and its variants have been widely adopted as one of the classic hypothetical genetic oscillators [7, 8]. The SCN consists of a dorsomedial shell and a ventrolateral core, and the ventrolateral core can be defined by cells containing vasoactive intestinal polypeptide

(VIP) [9]. The circadian oscillators are coupled with each other via the rhythmic influence from VIP, and the VIP is required to maintain circadian synchrony of the SCN [10]. However, we know nothing about the dynamics of the VIP except its fundamental observational properties. Based on these observational properties, the Van der Pol oscillator was usually employed to describe the dynamics of the VIP [11]. In this paper, we will carry out a modified circadian rhythm network model with unknown parameters and investigate its several dynamical properties from the viewpoint of complex network dynamics with the help of nonlinear dynamics theory.

Recent years have seen significant advances in the study of complex network dynamics [12, 13], and its related studies will lead to more potential applications in the future. Synchronization is a kind of typical collective behaviors and basic motions in nature, which is one of the main research focuses in complex network science. From the viewpoint of

mathematics, the core of synchronization is the stability of the zero solution of network error systems [14–16]. In previous studies, two effective methods are usually employed: the first one is to study synchronization induced by the mutual couplings between nodes [17, 18], and the second one is to design reasonable control laws [19–21]. A great number of researches on the first method have indicated that synchronization without external control needs certain requirement in both network structures and node dynamics. Therefore, a variety of external control approaches have been developed such as pinning control [22, 23], sliding mode control [24, 25], and feedback control [26, 27].

However, there are still lots of urgent and challenging problems in practical application. For instance, we often know very little about the exact values of system parameters, or there are some time-varying parameters. Under the effects of these uncertainties, the achieved synchronization might be destroyed and broken. Therefore, it is necessary to design an adaptive control law that adapts itself to these uncertainties, which is a popular control technique used for complex network models with unknown parameters [28–30]. The theoretical basis of adaptive control is parameter identification. As far as complex networks are concerned, three dynamic properties of uncertain networks need to be discussed, i.e., parameter identification, adaptive control, and outer synchronization [31]. In order to achieve each one of the three research goals above, Lyapunov stability is usually employed, which will show the convergence of the error systems and the parameter identification laws at the same time. Due to the convenience and effectiveness of adaptive control, it has been widely applied to many fields of science and technology, including secure communication, chaos generator design, biological systems, and information science.

As far as the circadian rhythm model is concerned, it is more difficult to get the exact values of the system parameters, and this becomes one of the interesting and significant questions remaining open for discussion. In order to estimate or evaluate the unknown parameters existing in the circadian rhythm model, lots of researches have been carried out. Based on the time series data of a certain group of individuals in a circadian rhythm model, Tong [32] obtained the estimations of the group level, group amplitude, and group phase. Later, the estimations of the true values of unknown parameters were investigated for different circadian rhythm models [33–35]. Now, it has become an interesting and significant research direction in the fields of system biology. To the best of our knowledge, most of the previous results were based on the statistical method or experimental data, and few theoretical researches have been carried out. Motivated by the discussions mentioned above, this paper aims at providing theoretical estimations of unknown parameters existing in such a network. It may help us build more accurate mathematical models and better understand the circadian rhythms of mammals. Therefore, the subject of this paper has a certain degree of innovation, and it may also have some latent applications. By proposing appropriate parameter updating laws and adaptive control strategies, we identify the unknown parameters successfully and the network realizes outer synchronization. Based on Lyapunov stability theory and matrix theory, we give theoretical proof for adaptive outer synchronization of the Goodwin oscillator network with unknown parameters. As special cases, we present two succinct corollaries for different instances.

The organization of the remaining sections is as follows. In Section 2, some preliminaries are introduced, including the model descriptions of the Goodwin oscillator network with unknown parameters. In Section 3, adaptive controllers and parameter updating laws are designed, and their effectiveness is also proved theoretically. In Section 4, a simple example is provided to verify the validity of the theoretical results. In the last section, conclusions are provided to summarize the contributions of this paper and to highlight some interesting issues as a further work.

1.1. Model Descriptions. The Goodwin model describes a circadian oscillator consisting of three variables, which is illustrated in Figure 1. A clock gene mRNA (a) produces a clock protein (b), which activates a transcriptional inhibitor (c), and in turn inhibits the transcription of the clock gene. By the repression exerted by the inhibitor to the mRNA synthesis, the three variables build up a closed negative feedback loop.

The mathematical model for the circadian oscillator is given as follows, in which each variable is governed by a simple ordinary differential equation:

$$
\begin{cases}
\dot{a}(t) = v_1 K^n [K^n + c^n(t)]^{-1} - \delta_1 a(t), \\
\dot{b}(t) = v_2 a(t) - \delta_2 b(t), \\
\dot{c}(t) = v_3 b(t) - \delta_3 c(t),
\end{cases}
\tag{1}
$$

where $a(t)$, $b(t)$, and $c(t)$ can be interpreted as the concentrations of clock genes, clock proteins, and transcriptional inhibitors, respectively; the constants v_1, v_2, and v_3 are the dimensionless transcription rates or translation rates; the constants δ_1, δ_2, and δ_3 are the dimensionless degradation rates of the chemical molecules; and K and n are the parameters of the Hill function. The equations above describe what is probably the simplest conceivable control process consistent with certain essential features of the genetic control of enzyme synthesis [6]. For instance, by choosing $K = 1$, $n = 10$, $v_1 = v_2 = v_3 = 1$, and $\delta_1 = \delta_2 = \delta_3 = 0.1$, the system (1) produces a damped oscillator.

In order to produce physiological rhythms, many researches considered the rhythmic influence of vasoactive intestinal polypeptides (VIP). Then, a Goodwin oscillator network model with a coupling term from VIP reads

$$
\begin{cases}
\dot{a}_i(t) = v_1 K^n [K^n + c_i^n(t)]^{-1} - \delta_1 a_i(t) + \sum_{j=1}^{N} c_{ij} m_j(t), \\
\dot{b}_i(t) = v_2 a_i(t) - \delta_2 b_i(t), \\
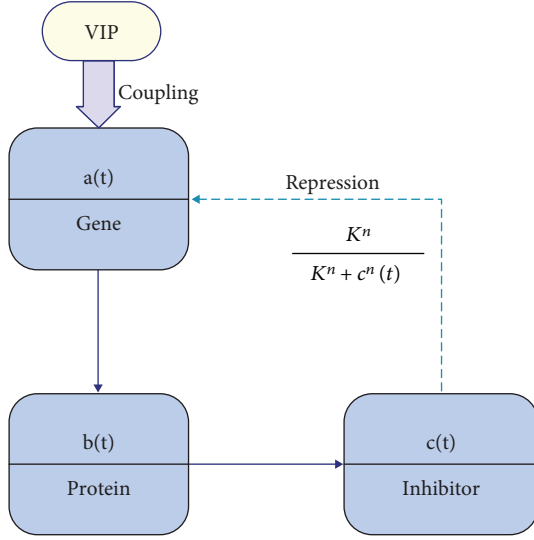\dot{c}_i(t) = v_3 b_i(t) - \delta_3 c_i(t),
\end{cases}
\tag{2}
$$

FIGURE 1: Scheme of a circadian oscillator modeled by a Goodwin oscillator. By the repression exerted by the inhibitor (c (t)) to the clock gene mRNA synthesis (a (t)), the three variables build up a closed negative feedback loop. The coupling from vasoactive intestinal polypeptide (VIP) is required to maintain circadian synchrony of the circadian oscillator.

where $(m_j(t), n_j(t))^{\mathrm{T}}$ is the concentration of VIP in the jth cell. The coupling matrix $C = (c_{ij})_{N \times N}$ represents the coupling configuration; if there is a coupling from cell i to cell j, then denote the weight of this coupling as $c_{ij} > 0$; otherwise, denote $c_{ij} = 0$. Different from most of the previous researches on complex networks, it is assumed that $c_{ii} \geq 0$ because the term $c_{ii}m_i(t)$ describes the coupling from VIP in the cell i to the Goodwin oscillator in the same cell. Throughout this paper, we further assume that the coupling matrix has equal row sums and equal column sums, i.e., there exists a nonnegative constant l such that $\sum_{i=1}^{N} c_{ij} = \sum_{j=1}^{N} c_{ij} = 2l$.

In many previous studies [11], the concentration dynamics of VIP was described by the following modified Van der Pol oscillators:

$$
\begin{cases}
\dot{m}_i(t) = \beta_1(n_i(t) - 2.5) + \beta_2(m_i(t) - 2.5) - \beta_3(m_i(t) - 2.5)^3 + ka_i(t), \\
\dot{n}_i(t) = \beta_1(m_i(t) - 2.5),
\end{cases}
\tag{3}
$$

where β_p, $p = 1,2,3$, and k are constants.

For ease of notations, we denote $x_i(t) = (\alpha_i(t), b_i(t), c_i(t))^{\mathrm{T}}$ and $y_i(t) = (m_i(t), n_i(t))^{\mathrm{T}}$ and rewrite the network (2)–(3) as follows:

$$
\begin{cases}
\dot{x}_i(t) = f_1(x_i(t))\alpha_1 + f_2(x_i(t))\alpha_2 + \displaystyle\sum_{j=1}^{N} c_{ij}\Gamma y_j(t), \\
\dot{y}_i(t) = g(y_i(t))\beta + k\Gamma^{\mathrm{T}} x_i(t),
\end{cases}
\tag{4}
$$

where $\alpha_1 = (v_1, v_2, v_3)^{\mathrm{T}}$, $\alpha_2 = (\delta_1, \delta_2, \delta_3)^{\mathrm{T}}$, and $\beta = (\beta_1, \beta_2, \beta_3)^{\mathrm{T}}$ are all real-valued vectors; the coupling component matrix

$$
\Gamma = \begin{pmatrix} 1 & 0 \\ 0 & 0 \\ 0 & 0 \end{pmatrix}.
\tag{5}
$$

The matrix functions

$$
f_1(x_i(t)) = \mathrm{diag}\left\{ K^n[K^n + c_i^n(t)]^{-1}, a_i(t), b_i(t) \right\} \in R^{3 \times 3},
$$
$$
f_2(x_i(t)) = -\mathrm{diag}\left\{ a_i(t), b_i(t), c_i(t) \right\} \in R^{3 \times 3},
$$
$$
g(y_i(t)) = \begin{pmatrix} n_i(t) - 2.5 & m_i(t) - 2.5 & (m_i(t) - 2.5)^3 \\ m_i(t) - 2.5 & 0 & 0 \end{pmatrix},
\tag{6}
$$

where $i = 1, 2, \ldots, N$. Assuming that the parameters α_1, α_2, and β, and the network topology matrices C and $\bar{C}$ are all unknown, we build the following response network:

$$
\begin{cases}
\bar{x}_i(t) = f_1(\bar{x}_i(t))\overline{\alpha}_1(t) + f_2(\bar{x}_i(t))\overline{\alpha}_2(t) + \displaystyle\sum_{j=1}^{N} \bar{c}_{ij}\Gamma \bar{y}_j(t) + \Delta_x(t) + u_{xi}(t), \\
\bar{y}_i(t) = g(\bar{y}_i(t))\overline{\beta}(t) + k\Gamma^{\mathrm{T}} \bar{x}_i(t) + \Delta_y(t) + u_{yi}(t),
\end{cases}
\tag{7}
$$

where $\bar{x}_i(t) = (\bar{a}_i(t), \bar{b}_i(t), \bar{c}_i(t))^{\mathrm{T}}$, $\bar{y}_i(t) = (\bar{m}_i(t), \bar{n}_i(t))^{\mathrm{T}}$, $\overline{\alpha}_1(t)$, $\overline{\alpha}_2(t)$, and $\overline{\beta}(t)$ are the updating laws of the unknown parameters in the network (4); $\Delta_x(t), \Delta_y(t)$ are the external disturbances such as wind and noise; and $u_{xi}(t), u_{yi}(t)$ are the adaptive controllers left to be designed in the next section, where $i = 1, 2, \ldots, N$. Network (4) and network (7) form a drive-response system; the next section will design adaptive controllers to make the drive-response system realize the outer synchronization and design parameter updating laws to identify the unknown parameters.

2. Adaptive Control Schemes for Outer Synchronization

Let us first carry out the definition of outer synchronization, two hypotheses, and a lemma to prove the effectiveness of our results.

Definition 1. The system (4)–(7) is said to achieve outer synchronization if

$$
\lim_{t \to \infty} \|e_{xi}(t)\| = 0,
$$
$$
\lim_{t \to \infty} \|e_{yi}(t)\| = 0,
\tag{8}
$$

where $e_{xi}(t) = \bar{x}_i(t) - x_i(t)$ and $e_{yi}(t) = \bar{y}_i(t) - y_i(t)$, where $i = 1, \ldots, N$.

Hypothesis 1. For any $x \in R^3$ and $y \in R^2$, denote $X = (x^T, y^T)^T \in R^5$, and

$$F(X, \alpha_1, \alpha_2, \beta) = \left[(f_1(x)\alpha_1 + f_2(x)\alpha_2)^T, (g(y)\beta + k\Gamma^T x)^T \right]^T. \tag{9}$$

Suppose that there exists a positive constant L such that

$$(Y - X)^T [F(Y, \alpha_1, \alpha_2, \beta) - F(X, \alpha_1, \alpha_2, \beta)] \leq L(Y - X)^T (Y - X) \tag{10}$$

holds for any $X, Y \in R^5$.

Since the function $F(X, \alpha_1, \alpha_2, \beta)$ of the network (4) is differentiable and the oscillator is a damped oscillator, there exists a positive constant L satisfying Hypothesis 1 in theory.

Hypothesis 2. For the disturbances $\Delta_x(t)$ and $\Delta_y(t)$, suppose that there exist two positive constants $0 \leq \rho_x, \rho_y < \infty$ such that

$$\|\Delta_x(t)\| \leq \rho_x, \|\Delta_y(t)\| \leq \rho_y. \tag{11}$$

The second hypothesis guarantees the boundedness of the disturbances, and this paper yields adaptive controllers that are robust against all possible bounded disturbances.

Lemma 1. *For any vectors $x \in R^3$ and $y \in R^2$ and the matrix Γ defined by (5), the following inequality holds:*

$$2x^T \Gamma y \leq x^T \Gamma \Gamma^T x + y^T \Gamma^T \Gamma y. \tag{12}$$

Proof. Denote $x = (a, b, c)^T$ and $y = (m, n)^T$; it follows from (5) that $\Gamma^T x = (a, 0)^T$, $\Gamma y = (m, 0, 0)^T$, and $2x^T \Gamma y = 2ma$. After a simple deduction, one gets that

$$x^T \Gamma \Gamma^T x + y^T \Gamma^T \Gamma y = a^2 + m^2. \tag{13}$$

Based on the inequality $a^2 + m^2 \geq 2am$, the lemma is proved.

Now, with the help of the preceding preliminaries and Lyapunov stability theory, we turn to prove the following theorem.

Theorem 1. *Under Hypothesis 1 and Hypothesis 2, let the parameter updating laws*

$$\begin{cases} \bar{\alpha}_p(t) = -\sum_{j=1}^{N} f_p(\bar{x}_j(t)) e_{xj}(t), & p = 1, 2, \\ \bar{\beta}(t) = -\sum_{j=1}^{N} g^T(\bar{y}_j(t)) e_{yj}(t), \end{cases} \tag{14}$$

and the adaptive controllers

$$\begin{cases} u_{xi}(t) = -\eta_{xi}(t)e_{xi}(t) - \gamma_{xi}(t) \operatorname{sign}[e_{xi}(t)] + \sum_{j=1}^{N} p_{ij}(t)\Gamma\bar{y}_j(t), \\ \dot{\eta}_{xi}(t) = k_{xi} e_{xi}^T(t) e_{xi}(t), \quad k_{xi} > 0, \\ \dot{\gamma}_{xi}(t) = \xi_{xi} \|e_{xi}(t)\|_1, \quad \xi_{xi} > 0, \\ u_{yi}(t) = -\eta_{yi}(t)e_{yi}(t) - \gamma_{yi}(t) \operatorname{sign}[e_{yi}(t)], \\ \dot{\eta}_{yi}(t) = k_{yi} e_{yi}^T(t) e_{yi}(t), \quad k_{yi} > 0, \\ \dot{\gamma}_{yi}(t) = \xi_{yi} \|e_{yi}(t)\|_1, \quad \xi_{yi} > 0, \\ \dot{p}_{ij}(t) = -e_{xi}^T(t)\Gamma\bar{y}_j(t). \end{cases} \tag{15}$$

Then, the following conclusions hold:

(i) The parameter updating laws (14) satisfy

$$\begin{aligned} \lim_{t \to \infty} \bar{\alpha}_1(t) &= \alpha_1, \\ \lim_{t \to \infty} \bar{\alpha}_2(t) &= \alpha_2, \\ \lim_{t \to \infty} \bar{\beta}(t) &= \beta \end{aligned} \tag{16}$$

(ii) There exist constants $\eta_{xi}^*, \eta_{yi}^*, \gamma_{xi}^*, \gamma_{yi}^*$ such that the adaptive controllers (15) satisfy

$$\begin{aligned} \lim_{t \to \infty} \eta_{xi}(t) &= \eta_{xi}^*, \\ \lim_{t \to \infty} \eta_{yi}(t) &= \eta_{yi}^*, \\ \lim_{t \to \infty} \gamma_{xi}(t) &= \gamma_{xi}^*, \\ \lim_{t \to \infty} \gamma_{yi}(t) &= \gamma_{yi}^*, \\ \lim_{t \to \infty} p_{ij}(t) &= c_{ij} - \bar{c}_{ij} \end{aligned} \tag{17}$$

(iii) The system (4)–(7) achieves outer synchronization, i.e.,

$$\lim_{t \to \infty} \|e_{xi}(t)\| = \lim_{t \to \infty} \|e_{yi}(t)\| = 0 \tag{18}$$

where $\|e_{xi}(t)\|_1 = e_{xi}(t) \operatorname{sign}[e_{xi}(t)]$ and $\|e_{yi}(t)\|_1 = e_{yi}(t) \operatorname{sign}[e_{yi}(t)]$, where $i, j = 1, 2, \ldots, N$.

Proof. Denote $e_i(t) = (e_{xi}^T(t), e_{yi}^T(t))^T$, $\tilde{\alpha}_p(t) = \overline{\alpha}_p(t) - \alpha_p$, $p = 1, 2$, and $\tilde{\beta}(t) = \overline{\beta}(t) - \beta$, and consider the following Lyapunov function:

$$V(t) = V_1(t) + V_2(t) + V_3(t), \tag{19}$$

where

$$V_1(t) = \frac{1}{2} \sum_{i=1}^{N} e_i^T(t) e_i(t) + \frac{1}{2} \sum_{i=1}^{N} \sum_{j=1}^{N} \left[p_{ij}(t) + \overline{c}_{ij} - c_{ij} \right]^2,$$

$$V_2(t) = \frac{1}{2} \sum_{p=1}^{2} \tilde{\alpha}_p^T(t) \tilde{\alpha}_p(t) + \frac{1}{2} \tilde{\beta}^T(t) \tilde{\beta}(t),$$

$$V_3(t) = \frac{1}{2} \sum_{i=1}^{N} \left[k_{xi}^{-1} (\eta_{xi}(t) - \eta_{xi}^*)^2 + k_{yi}^{-1} \left(\eta_{yi}(t) - \eta_{yi}^* \right)^2 \right.$$
$$\left. + \xi_{xi}^{-1} (\gamma_{xi}(t) - \gamma_{xi}^*)^2 + \xi_{yi}^{-1} \left(\gamma_{yi}(t) - \gamma_{yi}^* \right)^2 \right], \tag{20}$$

where $\eta_{xi}^*, \eta_{yi}^*, \gamma_{xi}^*, \gamma_{yi}^*$ are positive constants left to be chosen, where $i = 1, 2, \ldots, N$. The aim of the proof is to select appropriate constants to ensure that $\dot{V}(t) < 0$.

By the parameter updating laws (14) and the controllers (15), the derivative of $V_2(t)$ and $V_3(t)$ along the trajectories of (4)–(7) can be calculated as follows:

$$\dot{V}_2(t) = -\sum_{p=1}^{2} \sum_{j=1}^{N} \tilde{\alpha}_p^T(t) f_p(\overline{x}_j(t)) e_{xj}(t) - \sum_{j=1}^{N} \tilde{\beta}^T(t) g^T \left(\overline{y}_j(t) \right) e_{yj}(t), \tag{21}$$

$$\dot{V}_3(t) = \sum_{i=1}^{N} \left[(\eta_{xi}(t) - \eta_{xi}^*) e_{xi}^T(t) e_{xi}(t) \right.$$
$$+ \left(\eta_{yi}(t) - \eta_{yi}^* \right) e_{yi}^T(t) e_{yi}(t) + (\gamma_{xi}(t) - \gamma_{xi}^*) \| e_{xi}(t) \|_1$$
$$\left. + \left(\gamma_{yi}(t) - \gamma_{yi}^* \right) \| e_{yi}(t) \|_1 \right]. \tag{22}$$

It follows from Hypothesis 1 that the derivative of $V_1(t)$ can be written as

$$\dot{V}_1(t) = \sum_{i=1}^{N} e_i^T(t) \left[F\left(\overline{X}_i(t), \overline{\alpha}_1(t), \overline{\alpha}_2(t), \overline{\beta}(t) \right) \right.$$
$$\left. - F\left(X_i(t), \alpha_1, \alpha_2, \beta \right) \right]$$
$$+ \sum_{i=1}^{N} \sum_{j=1}^{N} e_{xi}^T(t) \left[\overline{c}_{ij} \Gamma \overline{y}_j(t) - c_{ij} \Gamma y_j(t) \right]$$
$$+ \sum_{i=1}^{N} \left[e_{xi}^T(t) \Delta_x(t) + e_{yi}^T(t) \Delta_y(t) + e_{xi}^T(t) u_{xi}(t) \right.$$

$$\left. + e_{yi}^T(t) u_{yi}(t) \right] - \sum_{i=1}^{N} \sum_{j=1}^{N} \left[p_{ij}(t) + \overline{c}_{ij} - c_{ij} \right] e_{xi}^T(t) \Gamma \overline{y}_j(t)$$

$$\leq \sum_{i=1}^{N} e_i^T(t) \left[F\left(\overline{X}_i(t), \overline{\alpha}_1(t), \overline{\alpha}_2(t), \overline{\beta}(t) \right) \right.$$
$$\left. - F\left(\overline{X}_i(t), \alpha_1, \alpha_2, \beta \right) + Le_i(t) \right]$$
$$+ \sum_{i=1}^{N} \sum_{j=1}^{N} \left[c_{ij} e_{xi}^T(t) \Gamma e_{yj}(t) - p_{ij}(t) e_{xi}^T(t) \Gamma \overline{y}_j(t) \right]$$
$$+ \sum_{i=1}^{N} \left[e_{xi}^T(t) \Delta_x(t) + e_{yi}^T(t) \Delta_y(t) + e_{xi}^T(t) u_{xi}(t) \right.$$
$$\left. + e_{yi}^T(t) u_{yi}(t) \right], \tag{23}$$

and then,

$$\dot{V}_1(t) \leq \sum_{i=1}^{N} e_i^T(t) \left[F\left(\overline{X}_i(t), \overline{\alpha}_1(t), \overline{\alpha}_2(t), \overline{\beta}(t) \right) \right.$$
$$\left. - F\left(\overline{X}_i(t), \alpha_1, \alpha_2, \beta \right) + Le_i(t) \right]$$
$$+ \sum_{i=1}^{N} \sum_{j=1}^{N} c_{ij} e_{xi}^T(t) \Gamma e_{yj}(t)$$
$$+ \sum_{i=1}^{N} \left[e_{xi}^T(t) \Delta_x(t) + e_{yi}^T(t) \Delta_y(t) \right]$$
$$- \sum_{i=1}^{N} \left[\eta_{xi}(t) e_{xi}^T(t) e_{xi}(t) + \gamma_{xi}(t) \| e_{xi}(t) \|_1 \right]$$
$$- \sum_{i=1}^{N} \left[\eta_{yi}(t) e_{yi}^T(t) e_{yi}(t) + \gamma_{yi}(t) \| e_{yi}(t) \|_1 \right]. \tag{24}$$

Combining the identities $\sum_{i=1}^{N} c_{ij} = \sum_{j=1}^{N} c_{ij} = 2l$,

$$F\left(\overline{X}_i(t), \overline{\alpha}_1(t), \overline{\alpha}_2(t), \overline{\beta}(t) \right) - F\left(\overline{X}_i(t), \alpha_1, \alpha_2, \beta \right)$$
$$= \left(\tilde{\alpha}_1^T(t) f_1(\overline{x}_i(t)) + \tilde{\alpha}_2^T(t) f_2(\overline{x}_i(t)), \tilde{\beta}^T(t) g^T(\overline{y}_i(t)) \right)^T, \tag{25}$$

and Lemma 1 together yields

$$\dot{V}_1(t) \leq \sum_{p=1}^{2} \sum_{i=1}^{N} \tilde{\alpha}_p^T(t) f_p(\overline{x}_i(t)) e_{xi}(t) + \sum_{i=1}^{N} \left[\tilde{\beta}^T(t) g^T(\overline{y}_i(t)) e_{yi}(t) \right]$$
$$+ L \sum_{j=1}^{N} e_i^T(t) e_i(t) + \frac{1}{2} \sum_{i=1}^{N} \sum_{j=1}^{N} c_{ij} \left[e_{xi}^T(t) \Gamma \Gamma^T e_{xi}(t) \right.$$
$$\left. + e_{yj}^T(t) \Gamma^T \Gamma e_{yj}(t) \right] + \sum_{i=1}^{N} \left[e_{xi}^T(t) \Delta_x(t) - \gamma_{xi}(t) \| e_{xi}(t) \|_1 \right.$$
$$\left. + e_{yi}^T(t) \Delta_y(t) - \gamma_{yi}(t) \| e_{yi}(t) \|_1 \right] - \sum_{i=1}^{N} \left[\eta_{xi}(t) e_{xi}^T(t) e_{xi}(t) \right.$$

$$+ \eta_{yi}(t)e_{yi}^{\mathrm{T}}(t)e_{yi}(t) \Big] \le \sum_{p=1}^{2}\sum_{j=1}^{N} \tilde{\alpha}_p^{\mathrm{T}}(t)f_p\big(\bar{x}_j(t)\big)e_{xj}(t)$$

$$+ \sum_{j=1}^{N}\Big[\tilde{\beta}^{\mathrm{T}}(t)g^{\mathrm{T}}\big(\bar{y}_j(t)\big)e_{yj}(t)\Big] + \sum_{i=1}^{N}\Big[e_{xi}^{\mathrm{T}}(t)\Delta_x(t)$$

$$- \gamma_{xi}(t)\|e_{xi}(t)\|_1 + e_{yi}^{\mathrm{T}}(t)\Delta_y(t) - \gamma_{yi}(t)\|e_{yi}(t)\|_1\Big] \quad (26)$$

$$+ \sum_{i=1}^{N}\Big[(L+l-\eta_{xi}(t))e_{xi}^{\mathrm{T}}(t)e_{xi}(t)$$

$$+ \Big(L+l-\eta_{yi}(t)\Big)e_{yi}^{\mathrm{T}}(t)e_{yi}(t)\Big].$$

Then, one concludes from the inequalities (21), (22), and (26) that

$$\dot{V}(t) \le \sum_{i=1}^{N}\Big[e_{xi}^{\mathrm{T}}(t)\Delta_x(t) - \gamma_{xi}^*\|e_{xi}(t)\|_1 + e_{yi}^{\mathrm{T}}(t)\Delta_y(t) - \gamma_{yi}^*\|e_{yi}(t)\|_1\Big]$$

$$+ \sum_{i=1}^{N}\Big[(L+l-\eta_{xi}^*)e_{xi}^{\mathrm{T}}(t)e_{xi}(t) + \Big(L+l-\eta_{yi}^*\Big)e_{yi}^{\mathrm{T}}(t)e_{yi}(t)\Big].$$

$$(27)$$

Choosing the constants $\gamma_{xi}^*, \gamma_{yi}^*, \eta_{xi}^*, \eta_{yi}^*$ large enough to ensure that

$$\rho_x - \gamma_{xi}^* < 0, \rho_y - \gamma_{yi}^* < 0, L+l-\eta_{yi}^* < 0, L+l-\eta_{yi}^* < 0, \quad (28)$$

one finally proves that $\dot{V}(t) < 0$. Based on Lyapunov stability theory, $V_2(t)$ indicates the validity of the first item, $V_3(t)$ indicates the validity of the first two equalities of the second item, the second term of $V_1(t)$ indicates that $\lim_{t\to\infty}p_{ij}(t) = c_{ij} - \bar{c}_{ij}$, and the first term of $V_1(t)$ indicates the validity of the third item. Hence, the three items are all proved.

As special cases, when some of the three unknown parameters are given and fixed, Theorem 1 remains valid. For example, assuming that the parameters α_1 and α_2 are both determined, one gets the following corollary.

Corollary 1. *Consider the system (4)–(7) with $\bar{\alpha}_1(t) = \alpha_1$ and $\bar{\alpha}_2(t) = \alpha_2$ under Hypothesis 1 and Hypothesis 2 hold. Choose the adaptive controllers (15) and the parameter updating the law*

$$\bar{\beta}(t) = -\sum_{j=1}^{N} g^{\mathrm{T}}\big(\bar{y}_j(t)\big)e_{yj}(t). \quad (29)$$

The three statements in Theorem 1 still hold.

Proof. Choose the following Lyapunov function:

$$W(t) = V_1(t) + W_2(t) + V_3(t), \quad (30)$$

where $V_1(t)$ and $V_3(t)$ are defined in the proof of Theorem 1, and

$$W_2(t) = \frac{1}{2}\tilde{\beta}^{\mathrm{T}}(t)\tilde{\beta}(t). \quad (31)$$

Analogous to the proof of Theorem 1, it follows from Lemma 1 that

$$\dot{V}_1(t) \le \sum_{i=1}^{N}\Big[e_{xi}^{\mathrm{T}}(t)\Delta_x(t) - \gamma_{xi}(t)\|e_{xi}(t)\|_1 + e_{yi}^{\mathrm{T}}(t)\Delta_y(t)$$

$$- \gamma_{yi}(t)\|e_{yi}(t)\|_1\Big] + \sum_{i=1}^{N}\Big[(L+l-\eta_{xi}(t))\|e_{xi}(t)\|^2$$

$$+ \Big(L+l-\eta_{yi}(t)\Big)\|e_{yi}(t)\|^2\Big] + \sum_{j=1}^{N}\tilde{\beta}^{\mathrm{T}}(t)g^{\mathrm{T}}\big(\bar{y}_j(t)\big)e_{yj}(t),$$

$$(32)$$

and

$$\dot{W}_2(t) = -\sum_{j=1}^{N}\tilde{\beta}^{\mathrm{T}}(t)g^{\mathrm{T}}\big(\bar{y}_j(t)\big)e_{yj}(t). \quad (33)$$

Thus, one gets

$$\dot{W}(t) \le \sum_{i=1}^{N}\Big[e_{xi}^{\mathrm{T}}(t)\Delta_x(t) - \gamma_{xi}^*\|e_{xi}(t)\|_1 + e_{yi}^{\mathrm{T}}(t)\Delta_y(t)$$

$$- \gamma_{yi}^*\|e_{yi}(t)\|_1\Big] + \sum_{i=1}^{N}\Big[(L+l-\eta_{xi}^*)e_{xi}^{\mathrm{T}}(t)e_{xi}(t)$$

$$+ \Big(L+l-\eta_{yi}^*\Big)e_{yi}^{\mathrm{T}}(t)e_{yi}(t)\Big], \quad (34)$$

which is similar to the inequality (27). The remainder of the argument is analogous to that of Theorem 1, and it is omitted here.

It follows from the proof of Theorem 1 that the functions $\gamma_{xi}(t)$ and $\gamma_{yi}(t)$ are designed for the disturbances $\Delta_x(t)$ and $\Delta_y(t)$. Therefore, we obtain the following corollary without considering the disturbances.

Corollary 2. *Consider the system (4)–(7) under Hypothesis 1. If the disturbances $\Delta_x(t) = \Delta_y(t) = 0$, choose the parameter updating laws (14) and the adaptive controllers*

$$\begin{cases} u_{xi}(t) = -\eta_{xi}(t)e_{xi}(t) + \sum_{j=1}^{N}p_{ij}(t)\Gamma\bar{y}_j(t), \\ \dot{\eta}_{xi}(t) = k_{xi}e_{xi}^{\mathrm{T}}(t)e_{xi}(t), \quad k_{xi} > 0, \\ u_{yi}(t) = -\eta_{yi}(t)e_{yi}(t), \\ \dot{\eta}_{yi}(t) = k_{yi}e_{yi}^{\mathrm{T}}(t)e_{yi}(t), \quad k_{yi} > 0, \\ \dot{p}_{ij}(t) = -e_{xi}^{\mathrm{T}}(t)\Gamma\bar{y}_j(t), \end{cases} \quad (35)$$

where $i, j = 1, 2, \ldots, N$; the three statements of Theorem 1 still hold.

Proof. Choose the following Lyapunov function:

$$W(t) = V_1(t) + V_2(t) + W_3(t), \qquad (36)$$

where $V_1(t)$ and $V_2(t)$ are defined in the proof of Theorem 1, and

$$W_3(t) = \frac{1}{2} \sum_{i=1}^{N} \left[k_{xi}^{-1} (\eta_{xi}(t) - \eta_{xi}^*)^2 + k_{yi}^{-1} \left(\eta_{yi}(t) - \eta_{yi}^* \right)^2 \right]. \qquad (37)$$

Analogous to the proof of Theorem 1, it follows from Lemma 1 that

$$\begin{aligned}
\dot{V}_1(t) \leq{}& \sum_{p=1}^{2} \sum_{j=1}^{N} \tilde{\alpha}_p^{\mathrm{T}}(t) f_p(\bar{x}_j(t)) e_{xj}(t) \\
&+ \sum_{j=1}^{N} \tilde{\beta}^{\mathrm{T}}(t) g^{\mathrm{T}}(\bar{y}_j(t)) e_{yj}(t) \\
&+ \sum_{i=1}^{N} \Big[(L + l - \eta_{xi}(t)) \|e_{xi}(t)\|^2 \\
&+ \left(L + l - \eta_{yi}(t) \right) \|e_{yi}(t)\|^2 \Big],
\end{aligned} \qquad (38)$$

and

$$\dot{W}_3(t) = \sum_{i=1}^{N} \Big[(\eta_{xi}(t) - \eta_{xi}^*) \|e_{xi}(t)\|^2 + \left(\eta_{yi}(t) - \eta_{yi}^* \right) \|e_{yi}(t)\|^2 \Big]. \qquad (39)$$

Thus, one has

$$\dot{W}(t) \leq \sum_{i=1}^{N} \Big[(L + l - \eta_{xi}^*) e_{xi}^{\mathrm{T}}(t) e_{xi}(t) + \left(L + l - \eta_{yi}^* \right) e_{yi}^{\mathrm{T}}(t) e_{yi}(t) \Big], \qquad (40)$$

which is similar to the inequality (27). The remainder of the argument is analogous to that of Theorem 1, and it is omitted here.

3. A Numerical Example

In this section, a special case of the system (4)–(7) is given to illustrate the effectiveness of the three statements of Theorem 1 one by one.

For clarity, we choose the coupling matrices as follows, the row sums of which are equal to 5:

$$C = \begin{pmatrix} 3 & 2 & 0 & 0 & 0 & 0 \\ 0 & 3 & 2 & 0 & 0 & 0 \\ 0 & 0 & 3 & 2 & 0 & 0 \\ 0 & 0 & 0 & 3 & 2 & 0 \\ 0 & 0 & 0 & 0 & 3 & 2 \\ 2 & 0 & 0 & 0 & 0 & 3 \end{pmatrix},$$

$$\bar{C} = \begin{pmatrix} 2 & 0 & 0 & 0 & 0 & 3 \\ 3 & 2 & 0 & 0 & 0 & 0 \\ 0 & 3 & 2 & 0 & 0 & 0 \\ 0 & 0 & 3 & 2 & 0 & 0 \\ 0 & 0 & 0 & 3 & 2 & 0 \\ 0 & 0 & 0 & 0 & 3 & 2 \end{pmatrix}. \qquad (41)$$

The topology structure corresponding to the above coupling matrices is shown in Figure 2. For instance, the element $\bar{c}_{21} = 3$ implies that there is a coupling from the oscillator $\bar{y}_2$ to the oscillator $\bar{x}_1$, and the weight of this coupling is 3; the element $c_{11} = 3$ implies that there is a coupling from the oscillator y_1 to the oscillator x_1, and the weight of this coupling is 3.

Based on the previous results [6], we set the parameters of the drive network (4) as $K = 1$, $n = 4$, $k = 1$, $\alpha_1 = (v_1, v_2, v_3)^{\mathrm{T}} = (0.1, 0.1, 0.1)^{\mathrm{T}}$, $\alpha_2 = (\delta_1, \delta_2, \delta_3)^{\mathrm{T}} = (0.35, 0.35, 0.35)^{\mathrm{T}}$, and $\beta = (\beta_1, \beta_2, \beta_3)^{\mathrm{T}} = (0.28, 1, 0.2)^{\mathrm{T}}$. The initial values $\bar{\alpha}_1(0)$, $\bar{\alpha}_2(0)$, and $\bar{\beta}(0)$ are selected randomly in $[0, 1] \times [0, 1] \times [0, 1]$, the initial values $x_i(0)$ and $\bar{x}_i(0)$ are selected randomly in $[0, 1] \times [0, 1] \times [0, 1]$, the initial values $y_i(0)$ and $\bar{y}_i(0)$ are selected randomly in $[0, 1] \times [0, 1]$, and the disturbances $\Delta_x(t) = (\cos t, -\sin t, \sin t)^{\mathrm{T}}$ and $\Delta_y(t) = (-\cos t, 2 \sin t, -3 \sin t)^{\mathrm{T}}$. Then, with the help of Matlab, the following figures are provided to verify the effectiveness of the obtained theoretical results.

Figures 3 and 4 are presented to verify the validity of the parameter laws (14). As can be seen, the parameter updating laws (14) are in a good agreement with the actual value of the corresponding parameters; i.e.,

$$\begin{aligned}
& \lim_{t \to \infty} \bar{v}_1(t) = \lim_{t \to \infty} \bar{v}_2(t) = \lim_{t \to \infty} \bar{v}_3(t) = 0.1, \\
& \lim_{t \to \infty} \bar{\delta}_1(t) = \lim_{t \to \infty} \bar{\delta}_2(t) = \lim_{t \to \infty} \bar{\delta}_3(t) = 0.1, \\
& \lim_{t \to \infty} \bar{\beta}_1(t) = 0.28, \\
& \lim_{t \to \infty} \bar{\beta}_2(t) = 1, \\
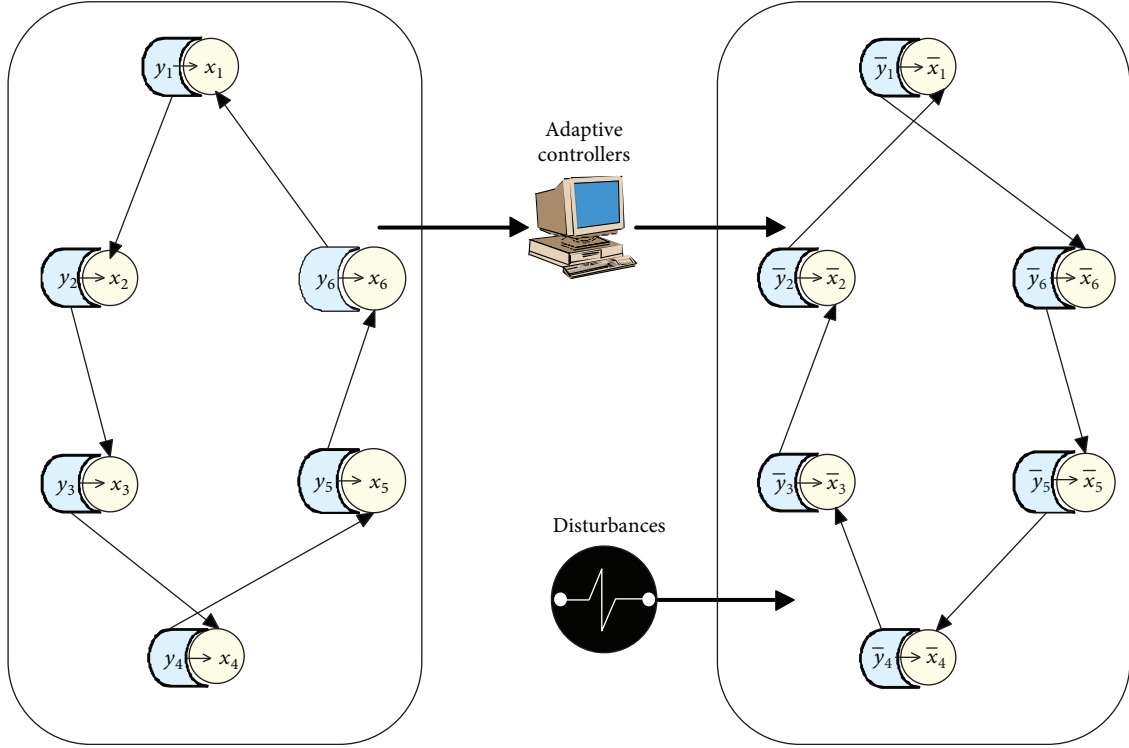& \lim_{t \to \infty} \bar{\beta}_3(t) = 0.2.
\end{aligned} \qquad (42)$$

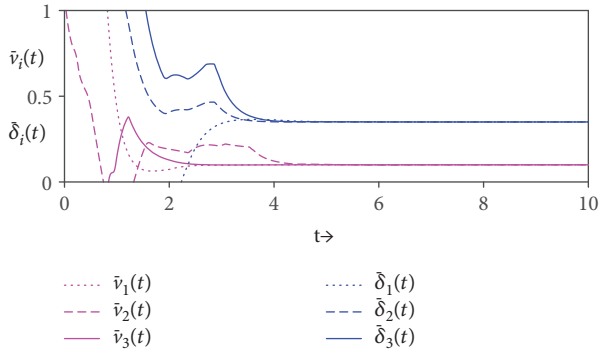FIGURE 2: The topology structure of a special case of the network (4)–(7) with $N = 6$.

FIGURE 3: Parameter identification of the system (4)–(7): $\lim_{t\to\infty} \bar{\alpha}_1(t) = \alpha_1$ and $\lim_{t\to\infty} \bar{\alpha}_2(t) = \alpha_2$.
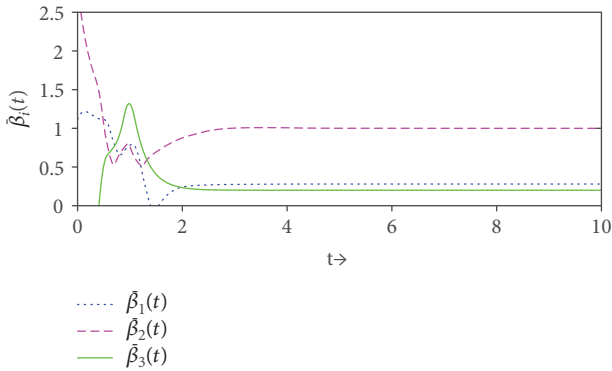

FIGURE 4: Parameter identification of the system (4)–(7): $\lim_{t\to\infty} \bar{\beta}(t) = \beta$.

Therefore, the first item of Theorem 1 is verified by Figures 3 and 4.

Figure 5 depicts the time evolutions of the control gains $\eta_{xi}(t)$ of the adaptive controllers (15). As can be seen, for each adaptive control gain $\eta_{xi}(t)$, there exists a positive constant η_{xi}^* such that

$$\lim_{t\to\infty} \eta_{xi}(t) = \eta_{xi}^*, i = 1, 2, \ldots, 6. \tag{43}$$

The time evolutions of $\eta_{yi}(t), \gamma_{xi}(t), \gamma_{yi}(t)$ are all similar to those of $\eta_{xi}(t), i = 1, 2 \cdots, 6$, and we omitted them here. The time evolutions of the topology updating laws $p_{ij}(t)$ in the adaptive controllers (15) are plotted in Figure 6, which verifies that

$$\lim_{t\to\infty} \left(p_{ij}(t)\right)_{6\times6} = \left(c_{ij} - \bar{c}_{ij}\right)_{6\times6}$$

$$= \begin{pmatrix} 1 & 2 & 0 & 0 & 0 & -3 \\ -3 & 1 & 2 & 0 & 0 & 0 \\ 0 & -3 & 1 & 2 & 0 & 0 \\ 0 & 0 & -3 & 1 & 2 & 0 \\ 0 & 0 & 0 & -3 & 1 & 2 \\ 2 & 0 & 0 & 0 & -3 & 1 \end{pmatrix}. \tag{44}$$
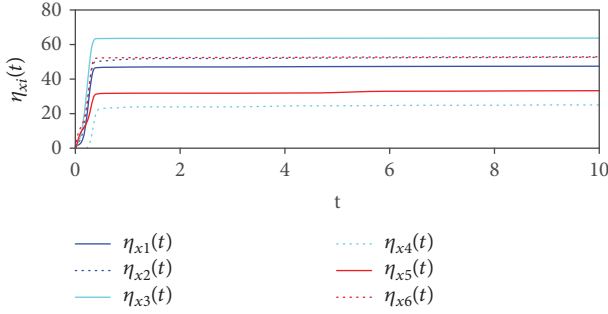
FIGURE 5: The convergence of the control gains $\eta_{xi}(t)$ of the adaptive controllers (15): $\lim_{t \to \infty} \eta_{xi}(t) = \eta_{xi}^*$.
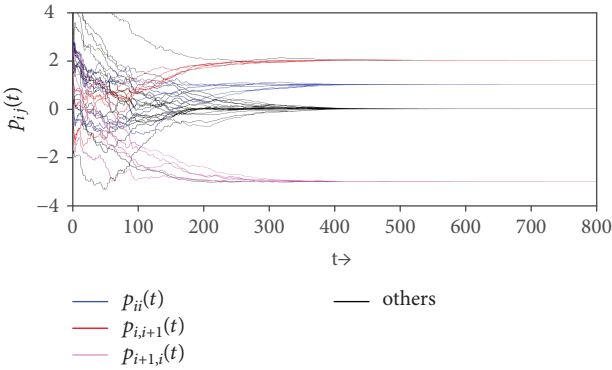

FIGURE 6: The convergence of the topology updating laws $p_{ij}(t)$ in the adaptive controllers (15): $\lim_{t \to \infty} p_{ij}(t) = c_{ij} - \bar{c}_{ij}$.

In particular, the blue lines indicate that $\lim_{t \to \infty} p_{ii}(t) = 1$, the red lines indicate that $\lim_{t \to \infty} p_{i,i+1}(t) = 2$, the magenta lines indicate that $\lim_{t \to \infty} p_{i+1,i}(t) = -3$, and the black lines indicate that $\lim_{t \to \infty} p_{61}(t) = 2$, $\lim_{t \to \infty} p_{16}(t) = -3$, and $\lim_{t \to \infty} p_{ij}(t) = 0$ for other elements. Therefore, the second item of Theorem 1 is verified by Figures 5 and 6.

Finally, the time evolutions of the outer synchronization errors $e_i(t) = \|e_{xi}(t)\| + \|e_{yi}(t)\|$, where $i = 1, 2, \ldots, 6$ are shown in Figure 7, which shows that the errors converge to zero and outer synchronization is achieved under the adaptive control schemes.

4. Conclusions

Based on Lyapunov stability theory, this paper has discussed the dynamic principles of mammals' circadian rhythms, where the suprachiasmatic nucleus (SCN) of the hypothalamus was modeled by a Goodwin oscillator and the vasoactive intestinal polypeptides (VIP) was modeled by a Van der Pol oscillator. Considering that it is very difficult to get the exact values of the system parameters, this paper has proposed effective parameter updating laws to identify the unknown parameters. The result has been proved based on strict theoretical reduction, and it should have a theoretical advantage over the previous results, which were based on the statistical method or experimental data. Another contribution of this paper is the problem of outer synchronization under adaptive
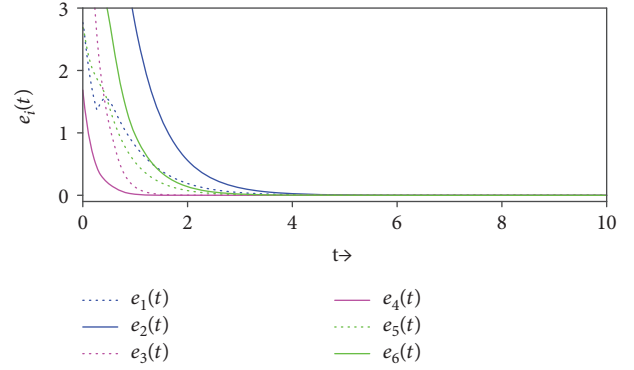

FIGURE 7: Time evolutions of the outer synchronization errors $e_i(t) = \|e_{xi}(t)\| + \|e_{yi}(t)\|$: $\lim_{t \to \infty} \|e_{xi}(t)\| = \lim_{t \to \infty} \|e_{yi}(t)\| = 0$, $i = 1, 2, \ldots, 6$.

control. Noticing that the coupling manner is different from the widely accepted coupling of the classical complex network, this paper has designed targeted adaptive controllers to synchronize the drive Goodwin oscillator network and the response one. The effectiveness of the obtained results has been verified both theoretically and numerically.

We hope that the results can provide theoretical guidance for biology experiments in spite of the confusing biological applications, and we will continue to study the context of the biological interpretation later. Another possible further work is the identification of unknown time-varying parameters since this paper is only applicable to the identification of given and fixed parameters.

Data Availability

The authors affirm that all data necessary for confirming the conclusions of the article are present in the article.

Conflicts of Interest

The authors declare that there is no conflict of interests regarding the publication of this article.

Acknowledgments

References

[1] M. Ukai-Tadenuma, R. G. Yamada, H. Xu, J. A. Ripperger, A. C. Liu, and H. R. Ueda, "Delay in feedback repression by cryptochrome 1 is required for circadian clock function," *Cell*, vol. 144, no. 2, pp. 268–281, 2011.

[2] H. R. Ueda, W. Chen, A. Adachi et al., "A transcription factor response element for gene expression during circadian night," *Nature*, vol. 418, no. 6897, pp. 534–539, 2002.

[3] J. C. Leloup, D. Gonze, and A. Goldbeter, "Limit cycle models for circadian rhythms based on transcriptional regulation in

Drosophila and *Neurospora*," *Journal of Biological Rhythms*, vol. 14, no. 6, pp. 433–448, 1999.

[4] T. Saithong, K. J. Painter, and A. J. Millar, "The contributions of interlocking loops and extensive nonlinearity to the properties of circadian clock models," *PLoS One*, vol. 5, no. 11, article e13867, 2010.

[5] S. M. Reppert and D. R. Weaver, "Coordination of circadian timing in mammals," *Nature*, vol. 418, no. 6901, pp. 935–941, 2002.

[6] B. C. Goodwin, "Oscillatory behavior in enzymatic control processes," *Advances in Enzyme Regulation*, vol. 3, pp. 425–437, 1965.

[7] D. Gonze and W. Abou-Jaoude, "The Goodwin model: behind the hill function," *PLoS One*, vol. 8, no. 8, article e69573, 2013.

[8] D. Gonze, S. Bernard, C. Waltermann, A. Kramer, and H. Herzel, "Spontaneous synchronization of coupled circadian oscillators," *Biophysical Journal*, vol. 89, no. 1, pp. 120–129, 2005.

[9] R. Y. Moore, "Chapter 8 Entrainment pathways and the functional organization of the circadian system," *Progress in Brain Research*, vol. 111, pp. 103–119, 1996.

[10] E. S. Maywood, A. B. Reddy, G. K. Y. Wong et al., "Synchronization and maintenance of timekeeping in suprachiasmatic circadian clock cells by neuropeptidergic signaling," *Current Biology*, vol. 16, no. 6, pp. 599–605, 2006.

[11] Y. Li and Z. Liu, "Coupling mechanism in the gate and oscillator model of the SCN," *Physica A*, vol. 457, pp. 62–72, 2016.

[12] C. Yang, J. Qiu, and H. He, "Exponential synchronization for a class of complex spatio-temporal networks with space-varying coefficients," *Neurocomputing*, vol. 151, pp. 401–407, 2015.

[13] P. Zhou, S. Cai, J. Shen, and Z. Liu, "Adaptive exponential cluster synchronization in colored community networks via aperiodically intermittent pinning control," *Nonlinear Dynamics*, vol. 92, no. 3, pp. 905–921, 2018.

[14] Y. Guo, "Exponential stability analysis of travelling waves solutions for nonlinear delayed cellular neural networks," *Dynamical Systems*, vol. 32, no. 4, pp. 490–503, 2017.

[15] M. Li and J. Wang, "Exploring delayed Mittag-Leffler type matrix functions to study finite time stability of fractional delay differential equations," *Applied Mathematics and Computation*, vol. 324, pp. 254–265, 2018.

[16] Y. Li, Y. Sun, and F. Meng, "New criteria for exponential stability of switched time-varying systems with delays and nonlinear disturbances," *Nonlinear Analysis: Hybrid Systems*, vol. 26, pp. 284–291, 2017.

[17] L. M. Pecora and T. L. Carroll, "Master stability functions for synchronized coupled systems," *Physical Review Letters*, vol. 80, no. 10, pp. 2109–2112, 1998.

[18] J. Zhang, Z. Ma, and G. Chen, "Robustness of cluster synchronous patterns in small-world networks with inter-cluster co-competition balance," *Chaos*, vol. 24, no. 2, article 023111, 2014.

[19] X. Lv, X. Li, J. Cao, and P. Duan, "Exponential synchronization of neural networks via feedback control in complex environment," *Complexity*, vol. 2018, Article ID 4352714, 13 pages, 2018.

[20] W. Sun and L. Peng, "Observer-based robust adaptive control for uncertain stochastic Hamiltonian systems with state and input delays," *Nonlinear Analysis: Modelling and Control*, vol. 19, no. 4, pp. 626–645, 2014.

[21] J. Zhang, Y. Wang, Z. Ma, J. Qiu, and F. Alsaadi, "Intermittent control for cluster-delay synchronization in directed networks," *Complexity*, vol. 2018, Article ID 1069839, 9 pages, 2018.

[22] C. Yang, T. Huang, Z. Li, J. Zhang, J. Qiu, and F. E. Alsaadi, "Synchronization of nonlinear complex spatio-temporal networks using adaptive boundary control and pinning adaptive boundary control," *IEEE Access*, vol. 6, pp. 38216–38224, 2018.

[23] S. Cai, Q. Jia, and Z. Liu, "Cluster synchronization for directed heterogeneous dynamical networks via decentralized adaptive intermittent pinning control," *Nonlinear Dynamics*, vol. 82, no. 1-2, pp. 689–702, 2015.

[24] X. Chen, J. H. Park, J. Cao, and J. Qiu, "Adaptive synchronization of multiple uncertain coupled chaotic systems via sliding mode control," *Neurocomputing*, vol. 273, pp. 9–21, 2018.

[25] J. Guan and K. Wang, "Sliding mode control and modified generalized projective synchronization of a new fractional-order chaotic system," *Mathematical Problems in Engineering*, vol. 2015, Article ID 941654, 9 pages, 2015.

[26] K. Li, W. Yu, and Y. Ding, "Successive lag synchronization on nonlinear dynamical networks via linear feedback control," *Nonlinear Dynamics*, vol. 80, no. 1-2, pp. 421–430, 2015.

[27] X. J. Xie and M. M. Jiang, "Output feedback stabilization of stochastic feedforward nonlinear time-delay systems with unknown output function," *International Journal of Robust and Nonlinear Control*, vol. 28, no. 1, pp. 266–280, 2018.

[28] S. A. Soldatenko, "Weather and climate manipulation as an optimal control for adaptive dynamical systems," *Complexity*, vol. 2017, Article ID 4615072, 12 pages, 2017.

[29] L. Wang, J. Zhang, and W. Sun, "Adaptive outer synchronization and topology identification between two complex dynamical networks with time-varying delay and disturbance," *IMA Journal of Mathematical Control and Information*, 2018.

[30] J. Zhang, W. Zhang, D. Zhang, C. Yang, K. Zhu, and J. Qiu, "Outer synchronization of a modified quorum-sensing network via adaptive control," *Mathematical Problems in Engineering*, vol. 2018, Article ID 2801896, 8 pages, 2018.

[31] H. Liu, W. Sun, and G. Al-mahbashi, "Parameter identification based on lag synchronization via hybrid feedback control in uncertain drive-response dynamical networks," *Advances in Difference Equations*, vol. 2017, no. 1, 2017.

[32] Y. L. Tong, "Parameter estimation in studying circadian rhythms," *Biometrics*, vol. 32, no. 1, pp. 85–94, 1976.

[33] G. J. Dörrscheidt and L. Beck, "Advanced methods for evaluating characteristic parameters (τ, α, ϱ) of circadian rhythms," *Journal of Mathematical Biology*, vol. 2, no. 2, pp. 107–121, 1975.

[34] M. R. Marler, P. Gehrman, J. L. Martin, and S. Ancoli-Israel, "The sigmoidally transformed cosine curve: a mathematical model for circadian rhythms with symmetric nonsinusoidal shapes," *Statistics in Medicine*, vol. 25, no. 22, pp. 3893–3904, 2006.

[35] B. Martinez-Tellez, G. Sanchez-Delgado, F. M. Acosta et al., "Differences between the most used equations in BAT-human studies to estimate parameters of skin temperature in young lean men," *Scientific Reports*, vol. 7, no. 1, article 10530, 2017.